

15

AD695929

FOREIGN TECHNOLOGY DIVISION



LIQUID FUEL ROCKET ENGINES —
DESIGN FUNDAMENTALS

by

M. V. Dobrovolskiy



U.S. GOVERNMENT
NOV 6 1969
REGISTERED

Distribution of this document is unlimited. It may be released to the Clearinghouse, Department of Commerce, for sale to the general public.

Reproduced by the
CLEARINGHOUSE
for Federal Scientific & Technical
Information Springfield Va. 22151

EDITED MACHINE TRANSLATION

LIQUID FUEL ROCKET ENGINES — DESIGN FUNDAMENTALS

By: M. V. Dobrovolskiy

English pages: Cover to 301

Source: Zhidkostnyye Raketnyye Dvigateli.
Osnovy Proyektirovaniya Moskva,
Izdatel'stvo "Mashinostroyeniye,"
1968, pp. 1-396.

THIS TRANSLATION IS A RENDITION OF THE ORIGINAL FOREIGN TEXT WITHOUT ANY ANALYTICAL OR EDITORIAL COMMENT. STATEMENTS OR THEORIES ADVOCATED OR IMPLIED ARE THOSE OF THE SOURCE AND DO NOT NECESSARILY REFLECT THE POSITION OR OPINION OF THE FOREIGN TECHNOLOGY DIVISION.

PREPARED BY:

**TRANSLATION DIVISION
FOREIGN TECHNOLOGY DIVISION
WP-AFB, OHIO.**

DATA HANDLING PAGE

61-ACCESSION NO. 98-DOCUMENT LOC TM9500997		39-TOPIC TAGS spacecraft propulsion equipment, liquid propellant engine, nozzle flow, combustion chamber, liquid rocket fuel, combustion kinetics, fuel injector		
66-TITLE LIQUID FUEL ROCKET ENGINES-DESIGN FUNDAMENTALS				
47-SUBJECT AREA 21				
12-AUTHOR/CO-AUTHORS DOBROVOL'SKIY, M. V.				10-DATE OF INFO -----68
43-SOURCE ZHIDKOSTNYYE RAKETNYYE DVIGATELLI. OSNOVY PROYEKTIROVANIYA (RUSSIAN)				68-DOCUMENT NO. MT-24-135-69
				69-PROJECT NO. 60401
63-SECURITY AND DOWNGRADING INFORMATION UNCL. O		64-CONTROL MARKINGS NONE		97-HEADER CLASH UNCL
76-REEL FRAME NO. 1889 0850	77-SUPERSEDES	78-CHANGES	48-GEOGRAPHICAL AREA UR	NO OF PAGES 615
CONTRACT NO.	X REF ACC. NO. 65-	PUBLISHING DATE 94-00	TYPE PRODUCT TRANSLATION	REVISION FREQ NONE
STEP NO. 02-UR/0000/68/000/000/0001/0396			ACCESSION NO.	

ABSTRACT

(U) This book presents design fundamentals of liquid fuel rocket engines (ZhRD). It considers questions of design of the engine chamber and the propulsion system on the whole. Basic statements of the theory, methods of calculation and description of sub-assemblies and units of devices with liquid fuel rocket engine are given. Processes of expansion of gases in nozzles, carburetion and heat exchange are expounded, as well methods of profiling nozzles, calculation of injectors, determination of forms and volumes of combustion chambers. An analysis of work of installations with open and closed circuits is given. Supply systems with turbopump assemblies and pressure feed systems with gas, powder, and liquid pressure generators are considered. Much attention is allotted to work of installations with closed circuits and methods of power coordination of such circuits. Examples of propulsion systems were given, in particular, a description of the propulsion system of the rocket "Vostok." The book gives actual data on structures, fuels and materials and their characteristics on the basis of foreign and domestic publications. Examples of designs are purely methodical and do not pertain to any defined type of engine. The book is a textbook for students of higher educational institutions and can also be useful to engineers and graduate students specializing in rocket technology.

TABLE OF CONTENTS

U. S. Board on Geographic Names Transliteration System.....	v
Designations of the Trigonometric Functions.....	vi
List of Acronyms.....	vii
Preface.....	ix
Chapter I. General Remarks.....	1
1.1. Classification of ZhRD Fuel.....	1
1.2. Basic Parameters of ZhRD.....	12
1.3. Systems of Loss Coefficients. Expenditure of Fuel and Basic Dimensions of Nozzles.....	20
Chapter II. Nozzles of a Liquid Fuel Rocket Engine.....	26
2.1. Types of Nozzles and Basic Requirements of Them....	26
2.2. Losses in the Nozzle of a Liquid Fuel Rocket Engine.....	29
2.3. Designing of Conical Nozzles.....	42
2.4. Basic Initial Positions in the Construction of a Profiled Nozzle.....	43
2.5. Shortened and Optimum Nozzles.....	48
2.6. Approximate Method of Construction of a Contour of an Optimum Nozzle.....	54
2.7. Operation of the Nozzle in Off-Design Conditions with High Counterpressure.....	60
2.8. Work and Characteristic of Nozzles with a Central Body.....	64
2.9. Calculation of Nozzles with a Central Body.....	73
Chapter III. Carburetor and Chamber Heads of ZhRD.....	86
3.1. Basic Elements of Carburetion and Combustion Processes.....	86
3.2. Spray Injectors.....	102
3.3. Centrifugal Injectors.....	112
3.4. Two-Component Injectors.....	132

3.5.	Chamber Heads for the ZhRD.....	137
3.6.	Influence of the Head on Carburetion and Specific Thrust.....	145
Chapter IV.	Cooling of ZhRD.....	165
4.1	Heat Exchange in ZhRD.....	165
4.2.	Methods of Cooling the ZhRD.....	174
4.3.	Process of Convection Heat Transfer from the Gas to the Wall.....	187
4.4.	Internal Relations of Energy and Impulses for the Boundary Layer.....	196
4.5.	Solution of the Integral Relation of Energy.....	212
4.6.	Calculation of Convection Heat Exchange in a ZhRD.....	220
4.7.	Conversion of Convection Thermal Flows.....	235
4.8.	Determination of Radiant Heat Flows.....	238
4.9.	Determination of Heat Transfer from the Wall to the Cooling Liquid.....	248
4.10.	Forms of Coolant Passages of Chambers of a ZhRD.....	251
4.11.	Calculation of Heat Transfer in a Ribbed Coolant Passage.....	261
4.12.	Calculation of Cooling of a ZhRD.....	272
4.13.	Certain Special Cases of Cooling ZhRD.....	283
Chapter V.	Chambers of Liquid Propellant Rocket Engines.....	302
5.1.	Shapes and Examples of Existing Chambers of Liquid Propellant Rocket Engines.....	302
5.2.	Determining the Volume of the Combustion Chamber...	310
5.3.	Unstable Burning.....	314
5.4.	Start and Shutdown of Engine.....	321
5.5.	Aftereffect Impulse.....	329
5.6.	Engine Chamber Strength Calculation.....	336
5.7.	Additional Remarks.....	342

Chapter VI. Propulsion Systems.....	345
6.1. Feed Systems.....	345
6.2. Propulsion Systems with a Turbopump Feeding System.....	348
6.3. Thrust and Specific Thrust of a Propulsion System.....	358
6.4. Fuel Tanks.....	361
6.5. Feed System Equipment.....	370
6.6. Determination of Feed Pressure and Hydraulic Characteristics of the Feed System.....	381
6.7. Systems of Control and Adjustment of a ZhRD.....	388
6.8. Examples of Systems Carried Out with Turbopump Feed.....	397
Chapter VII. Turbopump Units.....	412
7.1. Pumps for Feeding Components to ZhRD.....	413
7.2. Calculation and Characteristics of ZhRD Pumps.....	433
7.3. TNA Turbines.....	446
7.4. Joint Operation of Turbine and Pumps.....	465
7.5. Gas Generators.....	479
Chapter VIII. Closed-Circuit Propulsion Systems.....	496
8.1. "Gas + Liquid" Closed Circuit.....	498
8.2. Closed "Gas + Liquid" Circuit Without ZhGG.....	514
8.3. Closed "Gas + Gas" Circuit.....	520
Chapter IX. Propulsion Systems with a Pressurized Feed System.....	525
9.1. Gas Cylinder Feed System.....	527
9.2. Examples of Propulsion Systems with Gas-Pressurized Feed.....	537
9.3. Reduction Valves of Gas Pressure.....	547
9.4. Characteristics of Reduction Valves.....	554
9.5. Design of Reducing Valve.....	570

9.6.	Displacement Supply Systems with PAD and ZhAD.....	579
9.7.	Propulsion Systems with Preliminary Fueling and Hybrid Engines [149[, [150], [151].....	595
	Appendex.....	601
	Bibliography.....	605

U. S. BOARD ON GEOGRAPHIC NAMES TRANSLITERATION SYSTEM

Block	Italic	Transliteration	Block	Italic	Transliteration
А а	<i>А а</i>	A, a	Р р	<i>Р р</i>	R, r
Б б	<i>Б б</i>	B, b	С с	<i>С с</i>	S, s
В в	<i>В в</i>	V, v	Т т	<i>Т т</i>	T, t
Г г	<i>Г г</i>	G, g	У у	<i>У у</i>	U, u
Д д	<i>Д д</i>	D, d	Ф ф	<i>Ф ф</i>	F, f
Е е	<i>Е е</i>	Ye, ye; E, e*	Х х	<i>Х х</i>	Kh, kh
Ж ж	<i>Ж ж</i>	Zh, zh	Ц ц	<i>Ц ц</i>	Ts, ts
З з	<i>З з</i>	Z, z	Ч ч	<i>Ч ч</i>	Ch, ch
И и	<i>И и</i>	I, i	Ш ш	<i>Ш ш</i>	Sh, sh
Й я	<i>Й я</i>	Y, y	Щ щ	<i>Щ щ</i>	Shch, shch
К к	<i>К к</i>	K, k	Ъ ъ	<i>Ъ ъ</i>	"
Л л	<i>Л л</i>	L, l	Ы ы	<i>Ы ы</i>	Y, y
М м	<i>М м</i>	M, m	Ь ь	<i>Ь ь</i>	'
Н н	<i>Н н</i>	N, n	Э э	<i>Э э</i>	E, e
О о	<i>О о</i>	O, o	Ю ю	<i>Ю ю</i>	Yu, yu
П п	<i>П п</i>	P, p	Я я	<i>Я я</i>	Ya, ya

* ye initially, after vowels, and after ъ, ь; e elsewhere.
 When written as ѣ in Russian, transliterate as yě or ѣ.
 The use of diacritical marks is preferred, but such marks
 may be omitted when expediency dictates.

**FOLLOWING ARE THE CORRESPONDING RUSSIAN AND ENGLISH
DESIGNATIONS OF THE TRIGONOMETRIC FUNCTIONS**

Russian	English
sin	sin
cos	cos
tg	tan
ctg	cot
sec	sec
cosec	csc
sh	sinh
ch	cosh
th	tanh
cth	coth
sch	sech
csch	csch
arc sin	sin ⁻¹
arc cos	cos ⁻¹
arc tg	tan ⁻¹
arc ctg	cot ⁻¹
arc sec	sec ⁻¹
arc cosec	csc ⁻¹
arc sh	sinh ⁻¹
arc ch	cosh ⁻¹
arc th	tanh ⁻¹
arc cth	coth ⁻¹
arc sch	sech ⁻¹
arc csch	csch ⁻¹
—	
rot	curl
lg	log

List of Acronyms

Following is a list of conventional acronyms utilized in the translation of this document.

BRDD (БРДД) - long range ballistic missile
EPK (ЭРК) - electropneumatic valve
GRD (ГРД) - hybrid engine
LM (English only) - lunar module
LPRE (English only) - liquid fuel rocket engine
NDMG (НДМГ) - nonsymmetric dimethylhydrazine
PAD (ПАД) - powder pressure accumulator
PGG (ПГГ) - steam-gas generator
RDTT (РДТТ) - solid propellant rocket motor
SAS (САС) - emergency rescue system
TNA (ТНА) - turbopump assembly
VRD (ВРД) - jet engine
ZhAD (ЖАД) - liquid fuel pressure accumulator
ZhGG (ЖГГ) - liquid-gas generator
ZhRD (ЖРД) - liquid fuel rocket engine
ZUR (ЗУР) - SAM

This book presents design fundamentals of liquid fuel rocket engines (ZhRD). We consider questions of design of the engine chamber and the propulsion system on the whole. Basic statements of the theory, methods of calculation and description of subassemblies and units of devices with liquid fuel rocket engine are given.

Processes of expansion of gases in nozzles, carburetion and heat exchange are expounded, as well methods of profiling nozzles, calculation of injectors, determination of forms and volumes of combustion chambers. An analysis of work of installations with open and closed circuits is given. Supply systems with turbopump assemblies and pressure feed systems with gas, powder, and liquid pressure generators are considered.

Much attention is allotted to work of installations with closed circuits and methods of power coordination of such circuits. Examples of propulsion systems were given, in particular, a description of the propulsion system of the rocket "Vostok."

The book gives actual data on structures, fuels and materials and their characteristics on the basis of foreign and domestic publications. Examples of designs are purely methodical and do not pertain to any defined type of engine.

The book is a textbook for students of higher educational institutions and can also be useful to engineers and graduate students specializing in rocket technology.

PREFACE

More than ten years have passed since the first Soviet artificial earth satellite opened the era of conquest of outer space. The most important elements in space rocket systems are propulsion systems with liquid fuel rocket engines (ZhRD) which ensures only flights at earlier unattainable velocities within limits of earth's atmosphere, but also the possibility of flight in outer space. The apparent simplicity of ZhRD, the very idea of which was expressed by K. E. Tsiolkovskiy over 70 years ago, the creation of such engines has required knowledge and experience corresponding to the present level of science and technology, wide introduction of methods of hydrodynamics, gas dynamics and heat exchange to engineering designs.

A contemporary propulsion system with a ZhRD constitutes a complicated system, the work of subassemblies and units of which is interconnected. Therefore, design of one or another unit is impossible to conduct separately, neglecting the construction and work of remaining elements of the installation, which creates definite difficulties in the presentation of corresponding material.

In the present textbook we have attempted a systematic account of design fundamentals of chambers of the engine and the propulsion system on the whole. By contents it is possible to divide the book into two parts: Chapters I-V, which expound basic questions of design of engine chambers, and Chapters VI-IX, which examine basic questions of design of the propulsion system on the whole.

It is assumed that students in the present course are familiar with fundamentals of rocket technology and the theory of working processes in ZhRD. However, for convenience the first chapter presents briefly the basic ideas which are used in examining the various questions in designing ZhRD. For a best understanding of working processes and peculiarities of design of elements of these engines the basic design methods are illustrated by examples.

In view of the limited volume of this book, certain questions (turbopump assemblies, control, etc.), examined in special textbooks or aids are given in compressed form. Moreover, only the basic information necessary for a correct approach to designing installations on the whole are given. The author has tried to avoid mathematical computations in cases when they cannot be used for a direct calculation of the various elements of a propulsion system.

When writing the textbook we systematized information published in periodicals and books and also made use of earlier published works of the author.

We express our deep gratitude to Professors S. D. Grishin, F. L. Yakaytis, and Docent Yu. V. Krylov for valuable remarks and recommendations made in reviewing the book, and also Professor G. B. Sinyarev for his valuable advice, given during a joint discussion of the book.

The author requests that readers send their opinions and critical remarks to the following address: Moskva, K-51, Petrovka, 24, Izdatel'stvo "Mashinostroyeniye" [Москва, К-51, Петровка, 24, издательство "Машиностроение]."

CHAPTER I

GENERAL REMARKS

The present chapter gives basic ideas and relationship between parameters which must be known for studying design fundamentals of ZhRD. Moreover, it is assumed that the reader is acquainted with fundamentals of rocket technology and the theory of working processes in chambers of ZhRD, in consequence of which ideas and relationships to be mentioned later are given in concise form without proof. Those who are interested can find greater detail on proofs and analysis of these relationships in works [25], [14], and [2].

1.1. Classification of ZhRD Fuel

Liquid-propellant rocket engine is the name of rocket engines which use liquid fuel.

Liquid fuel and liquid oxidizer move from tanks to the engine chamber where, as a result of fuel combustion, high-temperature gaseous products are formed (Fig. 1.1). In the nozzle they are expanded from the chamber pressure to the nozzle section pressure and flow into the surrounding air at high speed. The outflow of gases from the nozzle is the cause of the reactive force of the engine.

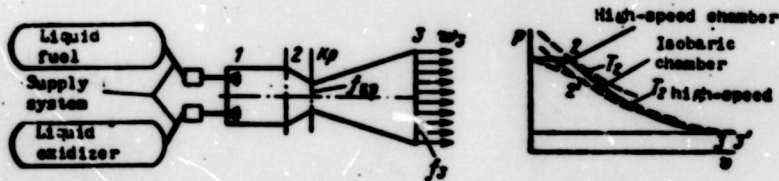


Fig. 1.1. Diagram and cycle of ZhRD.

Classification of ZhRD

The type of ZhRD is determined by some characteristic criterion (fuel, circuit, method of supply, assignment, etc.). Figure 1.2 gives a diagram of classification of ZhRD in terms of basic characteristic criteria. Work of ZhRD with the different circuits, methods of supply, structural elements, conditions of operation and also basic properties and types of fuels used are explained in subsequent sections of the book. Therefore we will not describe a given circuit in terms of noted criteria. Let us consider only the area of application of ZhRD.

Area of Application of ZhRD

The basic application of ZhRD is as the engine of rockets, whence the name liquid propellant rocket engines.

They are the basic type of engine of launch rockets of satellites or spaceships. Figure 1.3 shows the three-stage rocket "Vostok," which was used for orbiting the spaceship with astronaut Yu. A. Gagarin. Figure 4.29 shows the propulsion system of the first stage of "Vostok" liquid propellant rocket engine RD-107. Figure 6.7 shows liquid propellant rocket engine "Cosmos" RD-119 for the second stage of "Cosmos" rockets launch. Figure 1.4 shows a diagram of the three-stage launch rocket "Saturn-V" with the "Apollo" intended for flight to the moon. Thrust of the propulsion system of the first stage is 3400 t (~ 3.4 MN). Figure 6.32 gives an assembly diagram of the propulsion system of the first stage of the launch rocket.

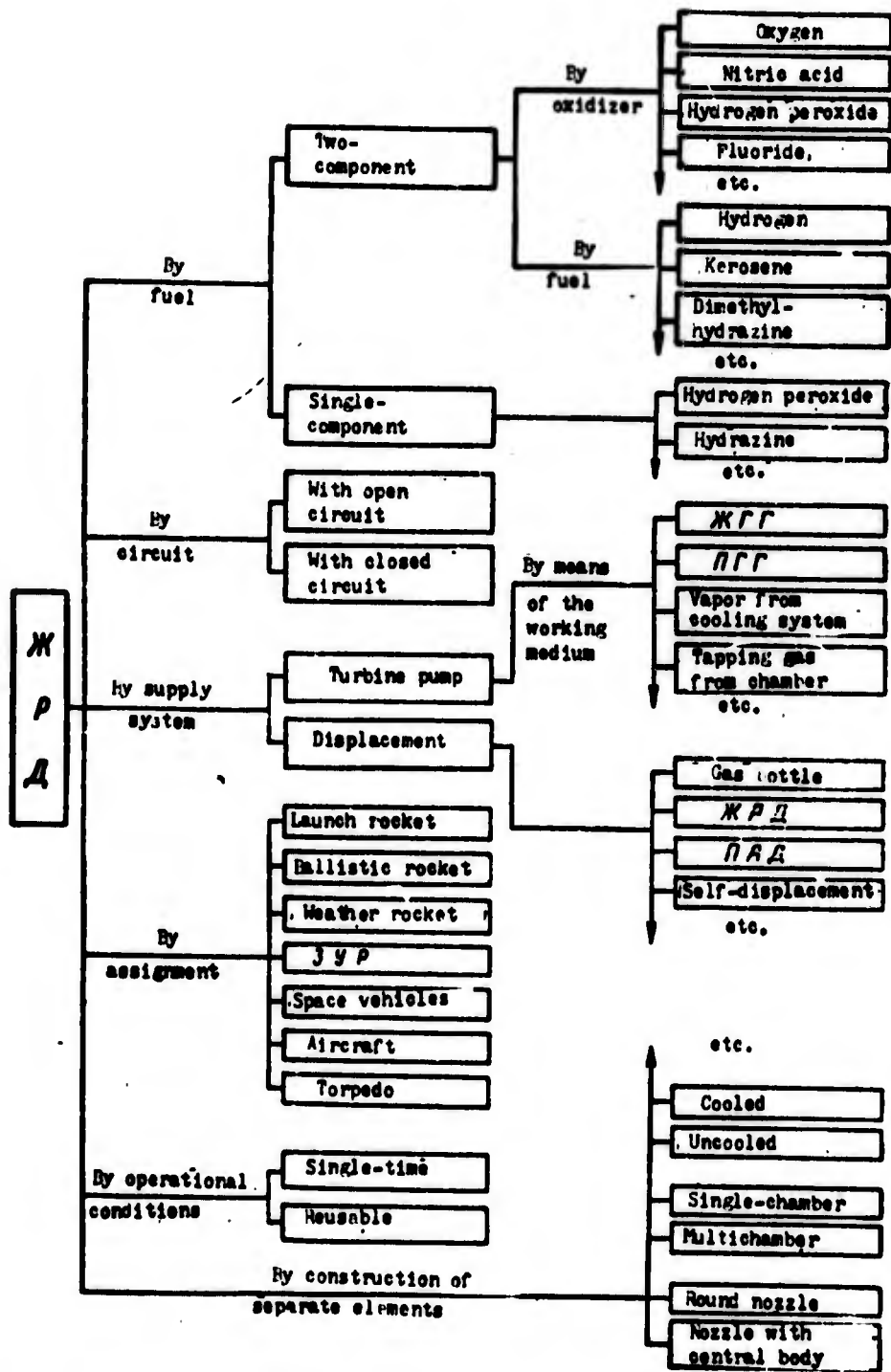
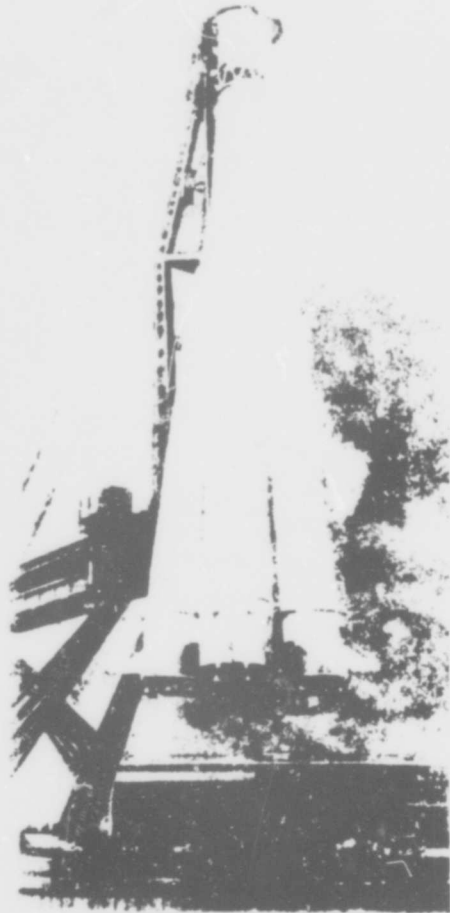


Fig. 1.2. Classification of ZhRD.

Fig. 1.3. "Vostok."



Liquid fuel rocket engines are widely used in long-range ballistic missiles (BRDD) and those of medium range of operation, ABM, SAM, and also in meteorological rockets. Figure 6.31 shows the assembly diagram of the propulsion system of the "Atlas" BRDD.

Liquid fuel rocket engines are also one of the basic types of engine utilized in spaceships for braking and in orientation system (Fig. 1.5). Figure 9.6 shows a diagram of an installation for correcting the speed of a spaceship.

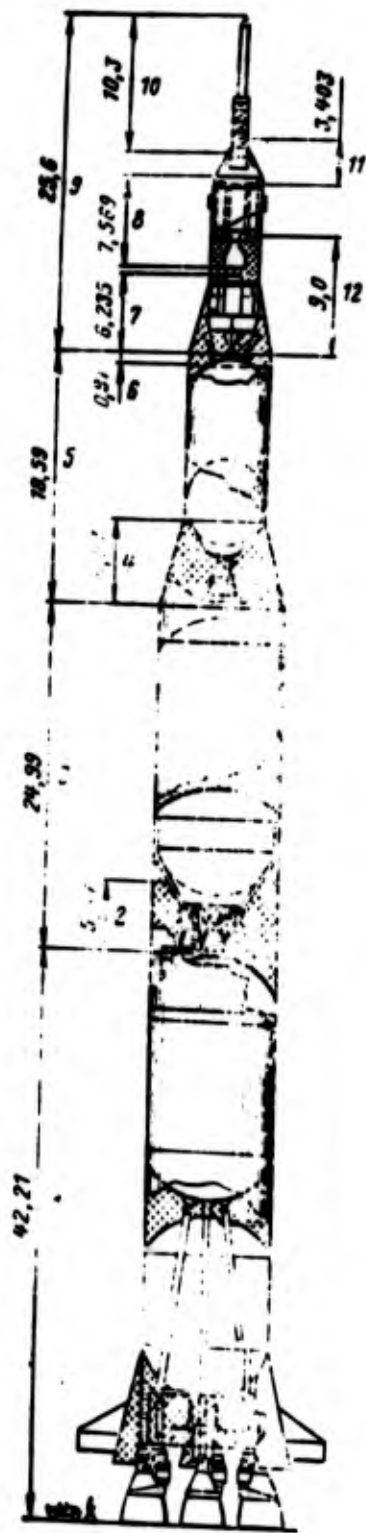


Fig. 1.4. Diagram of "Saturn" launch rocket with "Apollo" and emergency rescue system (SAS): 1 - first stage; 2 - adapter between first and second stages; 3 - second stage; 4 - adapter between second and third stages; 5 - third stage; 6 - instrument section; 7 - LM; 8 - engine section; 9 - "Apollo" command module; 10 - SAS; 11 - crew section; 12 - adapter between launch rocket and spaceship.

Besides use in rocket systems, ZhRD have found application as the engine of other than rocket systems. Liquid fuel rocket engines are set on aircraft as a basic engine as well as for start boosters (Fig. 1.6). They are also known to be used as the engine of torpedoes.

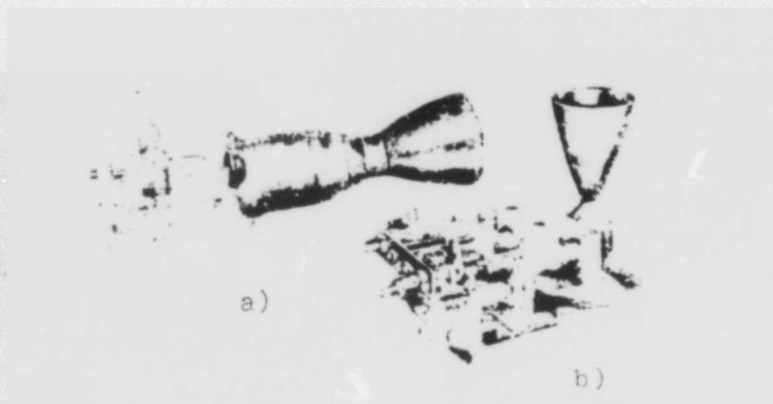


Fig. 1.5. ZhRD for orientation system:
 a) 90 kg (883 N) thrust; b) 7.2 kg
 (70.6 N) thrust.

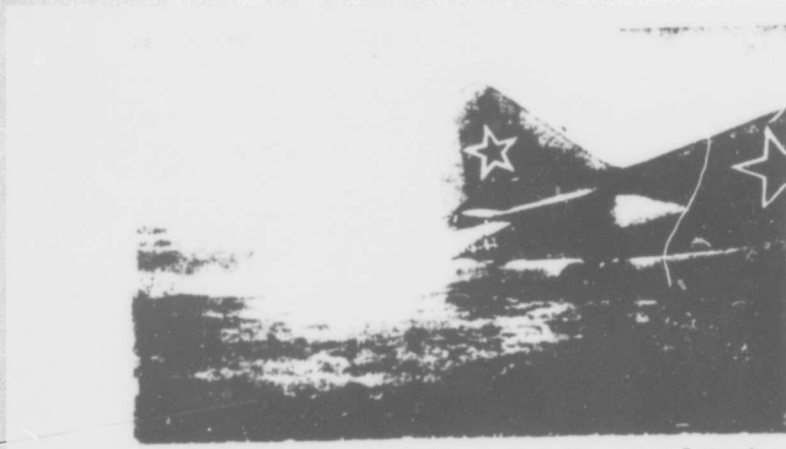


Fig. 1.6. RD-1-Kh3 aircraft accelerator.

Fuel

In contrast to usual thermal machines where fuel is actually fuel, in ZhRD the fuel is oxidizer + fuel.

For a given oxidizer and fuel, properties of the fuel are determined by their relationship, which is characterized by excess oxidant ratio

$$\alpha = \frac{\nu}{\nu_0}$$

where ν_0 and ν - stoichiometrical and real ratio of expenditure of oxidizer to expended combustible respectively. Value α essentially affects the basic propellant properties.

In ZhRD we distinguish fuel which is spontaneously inflammable, i.e., inflammable upon contact of oxidizer with fuel, and non-self-igniting, i.e., requiring an outside source of ignition. We also distinguish two-component and single-component (unitary) fuels.

Liquid fuel rocket engines almost exclusively are bi-propellants. Monopropellants are used mainly to drive to turbopump assemblies (TNA) (in systems with PGG) and in certain low thrust engines [for example, engines of orientation systems of spaceships (see Fig. 9.1)].

According to conditions of exploitation fuels are divided into high-boiling and low-boiling (cryogenic) fuels, the components of which under normal conditions are liquified gases (for example, oxygen, hydrogen, fluorine).

Requirements on fuels of ZhRD can be divided into three groups: a) basic, b) structural, c) operational.

Basic requirements are determined by the main problem - obtaining the greatest specific thrust with the smallest possible mass of the propulsion system. Finally they are formulated so: the fuel should possess a large reserve of chemical energy and high density, and combustion products of the fuel should possess good thermodynamic properties (value of gas constant, isentrope index, etc.).

Structural and operational requirements are determined by the problem of creating a propulsion system which is reliable, convenient in operation, and as cheap as possible. In accordance with these requirements one evaluates the physical properties of the fuel, cooling properties, ability to self-ignite and limits of inflammability, chemical stability, explosiveness, aggressiveness with respect to metals, toxicity, boiling point and fusion point, and, finally, cost of the fuel.

Thus, components of fuel have numerous and various requirements which simultaneously can not be satisfied by one of the components,

although the possibility of use in fuels of almost all elements of the periodic system of Mendeleev has been investigated [23].

In ZhRD the basic components of fuels are oxidizers on the basis of oxygen (pure oxygen or its compounds) and fuels on the basis of hydrogen and carbon (hydrocarbons, hydrazoic compounds, pure hydrogen). In the very near future it is possible to expect the use of fluorine and its compounds as oxidizer and compounds of boron, beryllium, and lithium as fuels.

Tables 1.1, 1.2, and 1.3 give certain basic properties of oxidizers, combustibles, and fuels.

Table 1.1. Basic physicochemical properties of certain oxidizers used in liquid fuel rocket engines.

Oxidizer	Chemical formula	Molecular weight	Full heat content			Density, kg/m ³	T _{liq} , °K	T _{sub} , °K	Cost of 1 kg (dollars)
			kcal/kg	kcal/mole	kJ/kg				
Oxygen, liquid	O ₂	32	-95.9	-3100	-402	1140	54.3	90.16	0.11
Fluorine, liquid	F ₂	38	-79	-3000	-331	1510	55.16	85.16	13.2
Nitric acid	HNO ₃	63.016	-57	-11404	-2780	1510	231.3	359.16	0.26
Nitrogen tetroxide	N ₂ O ₄	92.016	-73.3	-6740	-303	1450	261.9	294.3	0.18
Hydrogen peroxide	H ₂ O ₂	34.016	-1310	-11500	-5180	1440	272.26	423 (var.)	1.1
Ozone	O ₃	48	+629	+30200	+2635	1700	21.76	161.66	-
Fluorine monoxide	OF ₂	54	+53	+2860	+222	1520	49	128	-
Water	H ₂ O	18.016	-3786	-68370	-15890	1000	273.16	373.16	-

Table 1.2. Physicochemical properties of certain combustibles of ZHRD.

Fuel	Chemical formula	Molecular weight	Ball heat content				Density, kg/m ³	T _g , °C	T _m , °C	Cost of 1 kg (dollars)
			ball/kg	ball/mole	kJ/kg	kJ/mole				
Kerosene	C ₁₂ H ₂₆	170 (year)	-607.5	-63760	-1600	804.7	213	420-500	0.000	
Ethylene	H ₂	2.016	-610	-1000	-3000	71	13.70	30.45	-	
Acetylene	C ₂ H ₂	26.038	+60.8	+6450	+300	1022	200.00	457.30	-	
Triethylamine	(C ₂ H ₅) ₃ N	101.104	-145.7	-14,717	-610	720	100.30	302.05	-	
Xylylene	C ₈ H ₁₀ (C ₆ H ₄) ₂	121.164	-60.5	-6020	-202	970	210	400	-	
Aniline	NH ₂	17.032	-1004.5	-17000	-4100	600	105.30	220.70	0.00	
Ethanol	H ₂ H ₂	28.060	+300.1	+12000	+1570	1010	374.00	300.00	4.4	
Hydrazine hydrate	(NH ₂) ₂ H ₂ O	50.00	-13.15	-1200	-305	1000	203	301.00	-	
Asymmetric dimethylhydrazine (ADMH)	(C ₂ H ₅) ₂ NNH ₂	60.102	+105	+11120	+774	705	215	305	3.3	
Pentaborane	B ₅ H ₉	63.172	+120	+7000	+515	630	225.00	321	-	
Methylhydrazine	CH ₃ NHNH ₂	46.074	+202	+13040	+1220	800	220.70	300	-	

T_M = melting point; T_{BP} = boiling point.

Table 1.3. Basic properties of certain fuels of ZHRD ($p_2/p_3 = 70$) [2], [8], [25], [32], [35].

Liquid oxygen	Fuel	γ kg/kg	T_2 °K	P_{ya} (equilibrium expansion for v_{exp})				β		
				kg·s/kg	N·s/kg	kg·s/l	N·s/l	s	m/s	
										kg·s/kg
Liquid oxygen	Ethyl alcohol	1,48-1,8	3300-3400	287	2820	285	2800	170-175	1660-1716	
	Kerosene	2,24-2,73	3550-3700	298	2930	308	3020	180-185	1765-1815	
	NDMG	1,30-1,83	3450-3720	310	3040	304	2980	185-190	1815-1864	
	Ammonia	1,3-1,4	3050-3100	294	2890	281	2560	179-183	1756-1795	
	Hydrazine	0,74-0,90	3370-3400	313	3080	335	3290	190-194	1864-1904	
	Aerazine*	1,07-1,37	3380-3500	312	3070	319	3130	189-193	1853-1893	
	Hydrene*	1-50-1,80	3490-3500	305	3000	312	3070	185-187	1815-1835	
	Hydrogen	3,40-4,02	2700-3100	391	3840	172	1690	245-165	2405-1619	
	Liquid fluorine	Hydrogen	4,54-23,7	4000-4830	410	4020	305	2990	258-234	2530-2295
		Hydrazine	1,83-2,40	4490-4630	383	3560	478	4630	218-225	2140-2220
Ammonia		2,80-3,40	4400-4560	357	3400	422	4140	215-220	2120-2160	
NDMG				315	3390					
Chlorine trifluoride	Hydrazine	2,16-2,94	3670-3820	294	2830	414	4300	180-185	1715-1815	
	Aerazine*	2,27-3,11	3610-3820	287	2820	417	4020	170-179	1570-1756	
	Hydrene*	2,62-3,20	3620-3730	276	2710	395	3670	168-173	1648-1694	
	Kerosene	3,11-12,8	3540-3110	258	2530	386	3790	158-145	1550-1423	
	NDMG	2,53-3,28	3620-3770	290	2770	388	3900	170-175	1669-1716	

(Table 1.3 Cont'd.)

Liquid oxygen	Fuel	$v \frac{kg}{m^3}$	T_0 °K	P_{ya} (equilibrium expansion: for V_{0y0})				β	
				$kg \cdot s / kg$	$m \cdot s / kg$	$kg \cdot s / l$	$m \cdot s / l$	α	m/s
Nitric acid (7%)	Kerosene	5.0-5.80	2900-3000	235	2310	310	3040	155-157	1522-1541
	Tonka 250**	4.50-4.60	2850-3000	240	2360	315	3090	155-160	1522-1570
	Aniline (8%) - furfuryl alcohol (20%)	3.80-3.90	3000-3050	230	2250	315	3090	155-158	1522-1530
Nitrogen tetroxide	Kerosene	3.46-4.50	3350-3450	276	2710	348	3420	165-168	1619-1648
	NDMG	2.12-2.95	3250-3410	265	2600	339	3330	173-170	1694-1699
	Aerozine*	1.62-2.15	3250-3350	268	2630	348	3420	178-175	1726-1716
	Hydrazine**	2.20-2.95	3270-3400	262	2770	347	3410	172-174	1689-1707
	Methylhydrazine	2.0-2.50	3050-3370	287	2820	347	3410	178-173	1746-1694
	Hydrazine	1.08-1.42	3130-3250	292	2850	357	3500	180-183	1765-1795
Hydrogen peroxide (95%)	Kerosene	6.36-7.58	2900-3050	273	2690	355	3480	167-170	1639-1669
	Hydrazine	1.84-2.20	2850-3050	282	2770	355	3480	174-176	1707-1726

*Aerozine - a mixture of 50% NDMG and 50% hydrazine.

**Hydrazine - mixture of 60% NDMG and 40% hydrazine.

***Tonka 250 - mixture of 50% xyllicene and 50% triethylamine, [German brand].
[NDMG - asymmetric dimethylhydrazine].

1.2. Basic Parameters of ZhRD

Here and below the parameters related to the chamber of ZhRD will be designated in accordance with flow of the cycle of a ZhRD and characteristic sections (see Fig. 1.1). We will relate all parameters of a combustion chamber to section "2," i.e., pressure in the combustion chamber, temperature, density, etc., will be designated p_2 ; T_2 ; ρ_2 , etc. In cases when we consider acceleration of gas in the chamber, we will use parameters of braked flow.

Thrust and Specific Thrust

Thrust and specific thrust are important parameters of ZhRD. The formula for thrust traction assuming one-dimensional flow of gas through the nozzle of ZhRD has the form

$$P = \frac{w_3}{g} G + f_3 (p_3 - p_H) \quad (1.1)$$

where P - thrust; G - fuel consumption; p_3 ; w_3 ; f_3 - pressure, speed, and area of cross section on nozzle section; p_H - ambient pressure.

When $p_3 = p_H$ the engine works in design conditions so design thrust

$$P = \frac{w_3}{g} G \quad (1.2)$$

If $p_H = 0$, i.e., when the engine works in a vacuum, thrust in a vacuum

$$P_v = \frac{w_3}{g} G + f_3 p_3 \quad (1.3)$$

When $p_3 > p_H$ or $p_3 < p_H$ of the engine works in conditions of under-expansion and overexpansion respectively.

Specific thrust, i.e., thrust referred to flow rate per second of fuel

$$P_{sp} = \frac{P}{G}$$

[уд - specific]

or

$$P_{ya} = \frac{w_1}{g} + \frac{f_1}{g} (p_2 - p_0). \quad (1.4)$$

In design conditions

$$P_{ya} = \frac{w_1}{g}. \quad (1.5)$$

By introducing the idea of effective exit velocity w_e , specific thrust in any conditions can be expressed analogously to formula (1.5)

$$P_{ya} = \frac{w_e}{g}. \quad (1.6)$$

where

$$w_e = w_1 + \frac{f_1}{g} (p_2 - p_0). \quad (1.7)$$

Specific thrust is one of the most important parameters of work of ZhRD since on its value, in the end, depends the loading factor of the rocket system (ratio of payload to starting load) Figure 1.7 gives a calculation graph of change of initial mass of system for launching satellite with a mass of 5.5 t depending on specific thrust.

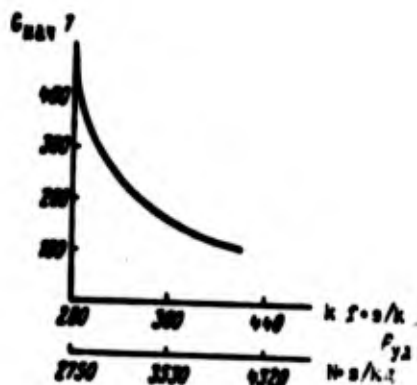


Fig. 1.7. Influence of specific thrust on initial mass of the system.

In heat engines one frequently meets the idea of specific fuel consumption, i.e., fuel consumption per unit of time for a thrust of 1 kgf.

$$G_{ya} = \frac{Q}{P} = \frac{1}{P_{ya}} = \frac{3000}{P_{ya}} \frac{\text{kg/n}}{\text{kgf}}. \quad (1.8)$$

Inasmuch as specific consumption in ZhRD is simply connected with specific thrust, the concept of $G_{y\Delta}$ is rarely used.

Basic Relationships of ZhRD

The basic relationships characterizing work of ZhRD and defining its characteristics are: specific impulse β , thrust coefficients K and K_{Π} and expansion ratio of the nozzle f_3/f_{kp} . [k_p - critical].

Specific impulse β (or complex β) of pressure in a combustion chamber is

$$\beta = \frac{I_{sp} p_2}{\sigma} \quad (1.9)$$

If one were to express β as the ratio of $f_{kp} p_2$ to mass flow rate, then β has the dimension of speed m·s. Therefore in Western literature specific impulse is usually called characteristic speed and is designated by c^* .

The theoretical value of β is calculated by the expression obtained from the equation of consumption

$$\beta = \frac{\sqrt{R_2 T_2}}{A_n} \quad (1.10)$$

Here

$$A_n = \sqrt{g n} \left(\frac{2}{n+1} \right)^{\frac{n+1}{2(n-1)}}; \quad (1.11)$$

n - polytropic index of expansion of combustion products from p_2 to p_{kp} .

Values $\sqrt{R_2 T_2}$ and A_n depend on the kind of fuel and barely depend on other parameters of work of an engine (within limits of 1-2%). Therefore we approximately consider that theoretically β depends only on the kind of fuel and is a constant thermodynamic characteristic of a given fuel. For a given fuel the value of the β complex depends only on the quality of the flow of processes

in the combustion chamber and does not depend on processes in the nozzle. Thus, for a given fuel κ is a characteristic determining the work of only the combustion chamber.

Nozzle thrust coefficient K (or thrust coefficient)

$$K = \frac{P}{f_{sp} p_2} \quad (1.12)$$

The thrust coefficient shows how many times engine thrust exceeds the basic component force of thrust $f_{sp} p_2$. Therefore, sometimes K is called dimensionless thrust. The theoretical value of K is calculated by the expression obtained from the formula of thrust

$$K = 2 \frac{n_{sp}}{\sqrt{n_{sp}^2 - 1}} \left(\frac{2}{n_{sp} + 1} \right)^{\frac{1}{n_{sp} - 1}} \sqrt{1 - \left(\frac{p_1}{p_2} \right)^{\frac{n_{sp} - 1}{n_{sp}}}} \times \\ \times \left[1 + \frac{n_{sp} - 1}{2n_{sp}} \frac{\frac{p_2 - p_1}{p_2}}{\left(\frac{p_2}{p_1} \right)^{\frac{1}{n_{sp}}} \left[1 - \left(\frac{p_1}{p_2} \right)^{\frac{n_{sp} - 1}{n_{sp}}} \right]} \right] \quad (1.13)$$

where n_{sp} - mean index of isentrope of expansion. It is more convenient to use the thrust coefficient in a vacuum K_v :

$$K_v = \frac{P_v}{f_{sp} p_2} \quad (1.14)$$

When $p_1 = 0$ the calculation expression for K_v is obtained from equation (1.13):

$$K_v = 2 \frac{n_{sp}}{\sqrt{n_{sp}^2 - 1}} \left(\frac{2}{n_{sp} + 1} \right)^{\frac{1}{n_{sp} - 1}} \sqrt{1 - \left(\frac{p_1}{p_2} \right)^{\frac{n_{sp} - 1}{n_{sp}}}} \times \\ \times \left[1 + \frac{n_{sp} - 1}{2n_{sp}} \frac{\left(\frac{p_1}{p_2} \right)^{\frac{n_{sp} - 1}{n_{sp}}}}{1 - \left(\frac{p_1}{p_2} \right)^{\frac{n_{sp} - 1}{n_{sp}}}} \right] \quad (1.15)$$

As we see, K_n does not depend either on work of the combustion chamber or on external conditions (p_{ext}) and is a characteristic determining work of the nozzle of the chamber only.

In accordance with formulas (1.1) and (1.3) K and K_n are connected by

$$K = K_n - \frac{f_3}{f_{\text{sp}}} \frac{P_n}{P_2}, \quad (1.16)$$

whence taking into account equality (1.12) we obtain the expression for determination of empirical

$$K_{n,1} = \frac{P_{1,1} + f_3 P_n}{f_{\text{sp}} P_2}, \quad (1.17)$$

where $P_{1,1}$ - measured real thrust of engine. Comparing expressions (1.9), (1.12) and (1.14), we obtain the formula for determination $P_{1,1}$ and $P_{1,2}$:

$$P_{1,1} = \beta K; \quad P_{1,2} = \beta K_n. \quad (1.18)$$

Expansion ratio of the nozzle \bar{r}_3 (or simply broadening) is defined as the ratio

$$\bar{r}_3 = \frac{f_3}{f_{\text{sp}}}. \quad (1.19)$$

This value not only determines nozzle dimensions but also characterizes basic parameters of work of the nozzle p_2^*/p_3 , M_3 (or speed w_3), ρ_2^*/ρ_3 . (Here and below the asterisks "*" designate parameters of braked flow).

$$\bar{r}_3 = \frac{\left(\frac{2}{n_{n3}+1}\right)^{\frac{1}{n_{n3}-1}} \sqrt{\frac{n_{n3}-1}{n_{n3}+1}}}{\left(\frac{P_2}{P_3}\right)^{\frac{1}{n_{n3}}} \sqrt{1 - \left(\frac{P_2}{P_3}\right)^{\frac{n_{n3}-1}{n_{n3}}}}}, \quad (1.20)$$

or

$$\bar{f}_3 = \frac{1}{M_3} \left[\frac{2}{n_{n3}+1} \left(1 + \frac{n_{n3}-1}{2} M_3^2 \right) \right]^{\frac{n_{n3}+1}{n_{n3}-1}}; \quad (1.21)$$

$$w_3 = \sqrt{2g \frac{n_{n3}}{n_{n3}-1} RT_2 \left[1 - \left(\frac{p_3}{p_2} \right)^{\frac{n_{n3}-1}{n_{n3}}} \right]}; \quad (1.22)$$

$$\frac{p_3^*}{p_2} = \left(1 + \frac{n_{n3}-1}{2} M_3^2 \right)^{\frac{n_{n3}}{n_{n3}-1}}; \quad (1.23)$$

$$\frac{T_3^*}{T_2} = 1 + \frac{n_{n3}-1}{2} M_3^2; \quad (1.24)$$

$$\frac{u_3^*}{a_3} = \left(1 + \frac{n_{n3}-1}{2} M_3^2 \right)^{\frac{1}{n_{n3}-1}}. \quad (1.25)$$

Comparing resulting expression, we see that broadening of the nozzle is simply defined by any of the basic parameters of work of a nozzle. Relation

$$\delta = \frac{p_3}{p_2} \quad (1.26)$$

is called the expansion area ratio of a nozzle. As we see from expression (1.20), expansion ratio δ for an assigned fuel, (i.e., n_{n3}) and broadening of the nozzle \bar{f}_3 do not depend on a change of pressure in the combustion chamber.

Relationships (1.20)-(1.25) are obviously valid not only for determination of parameters on the nozzle section, but also permit determining p_2^*/p , M (or w), ρ_2^*/ρ in any section of the nozzle with $\bar{f} = f/f_{it}$. Using the shown relationships, one can determine the change in p , w , ρ , T over the length of the nozzle. Figure 1.8 gives a graph of the change of broadening depending on ratio p_2^*/p and the isentrope of expansion n_{n3} .

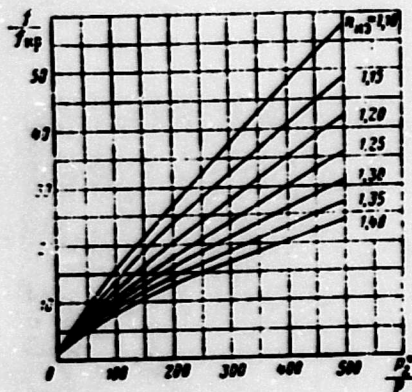


Fig. 1.8. Dependence $f/f_{sp} =$

$$= f\left(\frac{p_2}{p_1}, n_{sp}\right)$$

Characteristics of ZhRD

In ZhRD we distinguish two basic types of characteristics: throttle and altitude.

The throttle (or consumption) characteristic is the name of the dependence of thrust P or specific thrust P_{yH} on consumption of components G at constant altitude.

The altitude characteristic is the name of the change in thrust P or specific thrust P_{yH} depending on altitude of work of the engine H (or an ambient pressure p_{H1}) during constant consumption.

The equation of the throttle characteristic $P = f(G)$ is obtained from the formula of thrust (1.1) converted taking into account relationships (1.9) and (1.26) and taking $p_2 = p_2^*$:

$$P = G \left(\frac{D_1}{G} + \frac{f_1}{f_{sp}} \right) - f_3 p_{H1} \quad (1.27)$$

Inasmuch as the sum in parentheses and member $f_3 p_{H1}$ do not depend on consumption, the equation of the characteristic has the form of an equation of a straight line

$$P = AG - B.$$

On Fig. 1.9a are represented throttle characteristics plotted from equation (1.27) for an engine with different expansion ratio, and

on Fig. 1.9b for an engine working on land ($P_a = P_0$) and in a vacuum ($P_a = 0$). If there is a considerable decrease of consumption as compared to calculation conditions separation of flow from walls of the nozzle will occur (see section 2.7). In this case equation (1.27) will not be valid and the real characteristic will go through the origin of coordinates as shown by the dotted line.

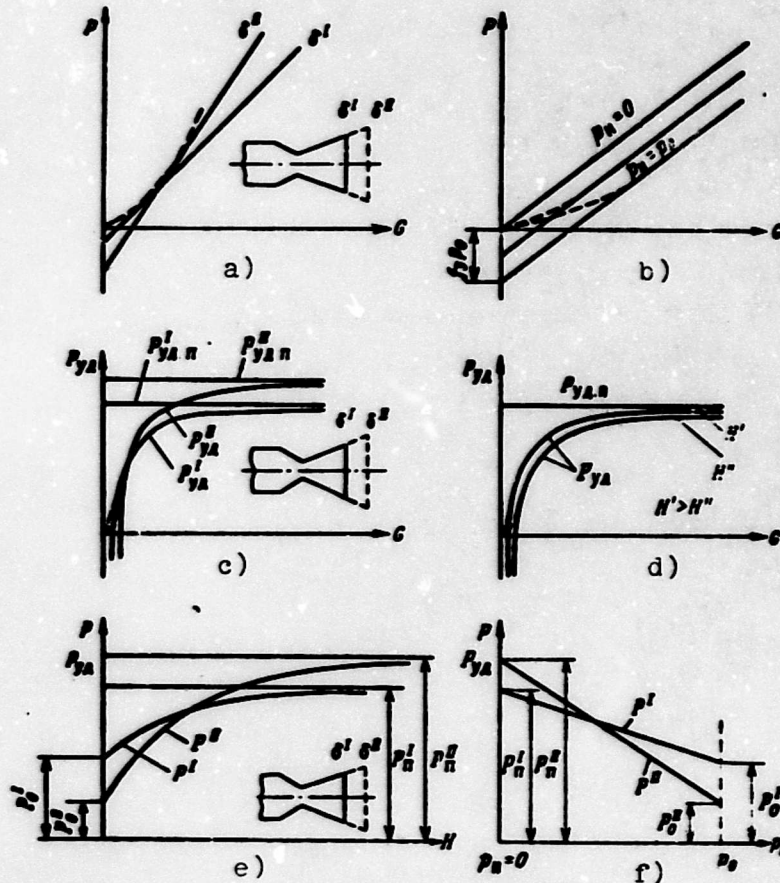


Fig. 1.9. Characteristics of ZhRD: a, b) throttle characteristic of thrust ($P = f(G)$); c, d) throttle characteristic of specific thrust ($P_{ya} = f(G)$); e, f) altitude characteristic.

The throttle characteristic of change of specific thrust is obtained from formula (1.27):

$$P_{ya} = \frac{w_2}{g} + \frac{f_3}{f_{sp}} \delta_2^2 - \frac{f_3 P_a}{G} \quad (1.28)$$

During work of the engine in a vacuum ($P_{11} = 0$)

$$P_{ya.0} = \frac{v_1}{g} + \frac{f_1}{f_{sp}} \cdot g. \quad (1.29)$$

i.e., specific thrust in a vacuum does not depend on consumption.

On Fig. 1.9c, d are shown throttle characteristics $P_{y11} = f(G)$ and $P_{ya.11} = f(G)$ for engines with different expansion ratios and for engines working at various altitudes.

Dependences of thrust or specific thrust on flight altitudes (altitude characteristic) are determined directly by formulas (1.1) or (1.4), in which with a change of height only p_{11} is changed. From a comparison of these formulas it is clear that the characteristic of thrust and specific thrust differ in altitude only by scale (Fig. 1.9f). The altitude characteristic of thrust or specific thrust in terms of altitude of work for engines with different broadenings are shown in Fig. 1.9e.

1.3. Systems of Loss Coefficients. Expenditure of Fuel and Basic Dimensions of Nozzles

System of Coefficients for Evaluating the Quality of Processes in ZhRD

For evaluating the quality of flow of processes in ZhRD it is possible to use either efficiencies, which estimate the perfection of conversion of initial energy into effective work, or coefficients, which estimate the loss of specific thrust (impulse) due to a low-quality flow of processes of conversion of energy.

In the first case there will be the so-called power coefficients (efficiency), in the second, impulse coefficients.

In ZhRD the more commonly used are impulse coefficients, examined below. Power coefficients are detailed in [14] and [25].

If one were to designate ϕ on the loss factor of specific thrust then specific real thrust could be defined as

$$P_{yA-A} = \phi P_{yA} \quad (1.30)$$

losses of specific thrust in general are determined by losses in the chamber, in the nozzle and on thermal resistance, which we will estimate accordingly loss factor in the chamber ϕ_K , nozzle coefficient ϕ_C and loss factor on thermal resistance ϕ_{thermal} , so that

$$\eta = \eta_K \eta_C \eta_{\text{thermal}} \quad (1.31)$$

Above we noted two basic parameters, determining processes in a combustion chamber and in a nozzle: complex β and K_{ch} . The distinction in the real value of complex β , obtained on the basis of experimental data by formula (1.9) from the value calculated by equation (1.10) testifies to the low-quality of organization and flow of processes in the combustion chamber, i.e., losses in the combustion chamber (for detail see section 3.6). Thus

$$\eta_K = \frac{f_{K1}}{\beta} \quad (1.32)$$

If, during a comparison of calculation and real values of complex β , real expenditure is set equal to calculation and the calculation of β is conducted at real value f_{K1} , i.e., $G_{\text{ch}} = G$ and $f_{K1, \text{calc}} = f_{K1}$, then

$$\eta_K = \frac{f_{K1}}{\beta} = \frac{f_{K1}}{\beta} \quad (1.33)$$

Thus, ϕ_K characterizes the value of losses of pressure due to the low-quality of processes. Therefore ϕ_K is frequently called the coefficient of fullness of pressure.

Placing in equation (1.32) the value of β from formula (1.10), we obtain

$$\eta_K = \frac{(\sqrt{R_2 T_2})_1}{\sqrt{R_2 T_2}}$$

whence, taking $R_{2H} = R_2$,

$$\frac{T_{2H}}{T_2} = \eta_K^2 \quad (1.34)$$

Formula (1.34) permits for known or assigned η_K approximately estimating the decrease in design temperature in the combustion chamber due to losses in it.

Losses in the chamber are made up of two forms of losses: losses on incompleteness of combustion due to the low-quality flow of processes of conversion of fuel into combustion products (see section 3.1) these losses do not yield to exact calculation, are usually determined experimentally, and are characterized by the coefficient of incompleteness of combustion ϕ_{pr} ; and losses on irregularity of distribution over the section of the chamber of the ratio of components and specific weight flow, expressed by variation factor ϕ_{r} . Thus,

$$\eta_K = \eta_{\text{cr}} \eta_{\text{r}} \quad (1.35)$$

Total losses in the combustion chamber are within limits $\eta_K = 0.95 - 0.99$.

Losses in the nozzle are defined as the ratio of the real value of the thrust coefficient in a vacuum $K_{\text{ил.вл}}$ defined on the basis of results of experimental data by formula (1.17), to its theoretical value calculated by formula (1.15):

$$\eta_c = \frac{K_{\text{ил.вл}}}{K_n} \quad (1.36)$$

In general they are composed on losses on dispersion of flow (ϕ_{pac}), on friction (ϕ_{fr}), inlet (ϕ_{BX}), on nonequilibrium of the process of expansion ($\phi_{\text{неп.р.}}$), on nonadiabaticness ($\phi_{\text{CХЛ}}$), and also of losses connected with the presence of a boundary layer ($\phi_{\text{CУЖ}}$), and losses during expansion of a two-phase flow ($\phi_{\text{ф}}$). Thus,

$$\eta_c = \eta_{\text{pac}} \eta_{\text{fr}} \eta_{\text{BX}} \eta_{\text{неп.р.}} \eta_{\text{CХЛ}} \eta_{\text{CУЖ}} \eta_{\text{ф}} \quad (1.37)$$

(For detail see section 2.2).

Losses on thermal resistance take place only in a high-speed combustion chamber. Then calculation is given in works [2] and [110]. For an isobaric combustion chamber $\phi_{\text{ТОНН}} = 1$, and then expression (1.31) takes the form

$$\eta = \eta_n \eta_c. \quad (1.38)$$

Determination of Fuel Consumption and Areas of Nozzle Sections f_{H1} and f_3

Let us examine how we determine taking losses into account, fuel consumption and areas of the critical and nozzle exit section (f_{H1} and f_3) for an assigned thrust known from thermal calculation of specific thrust P_{sp} and assigned or known loss factors ϕ_{H} and ϕ_c .

Theoretical fuel consumption, i.e., neglecting losses

$$G = \frac{P}{P_{\text{H1}}}. \quad (1.39)$$

Real fuel consumption, i.e., taking losses into account, is necessary to ensure assigned thrust

$$G_{\text{a}} = \frac{P}{\eta P_{\text{H1}}}. \quad (1.40)$$

From expressions (1.39) and (1.40) we obtain the relationship between real and theoretical expenditures of fuel:

$$G_{\text{a}} = \frac{G}{\eta}. \quad (1.41)$$

i.e., for production of assigned thrust it is necessary to pass more fuel in order to compensate for losses.

Theoretical area of critical section f_{H1} is determined from formula (1.19)

$$f_{up} = \frac{G_3}{P_2} \quad (1.42)$$

Real area of critical section f_{K1} taking equations (1.32) and (1.41) into account

$$f_{up,1} = \frac{G_3 \gamma_1}{P_2} = \frac{G_3 \gamma_k}{\gamma P_2} = \frac{G_3}{P_2} \frac{\gamma_k}{\gamma \gamma_c}$$

or

$$f_{up,1} = f_{up} \frac{1}{\gamma_c} \quad (1.43)$$

This means that the area of the critical section must be increased only in order to pass through it the additional fuel consumption for compensating losses in the nozzle, this additional fuel consumption for compensation of losses in the chamber, not requiring an increase in f_{K1} .

Let us define the area of nozzle section in a cut. According to the equation of expenditure theoretical f_3 and real f_{31} will accordingly be equal to

$$f_3 = \frac{G}{w_3 \gamma_3} \quad (1.44)$$

$$f_{31} = \frac{G_1}{w_{31} \gamma_{31}} \quad (1.45)$$

Let us find the approximate connection between f_{31} and f_3 . According to equation (1.30)

$$w_{31} = \gamma w_3 \quad (1.46)$$

On the basis of the equation of state

$$\frac{\gamma_{31}}{\gamma_3} = \frac{R_p T_3}{(R_p T_3)_1} \approx \frac{T_3}{T_{31}} \quad (1.47)$$

Since

$$T_3 = T_2 \left(\frac{P_3}{P_2} \right)^{\frac{\alpha_{32}-1}{\alpha_{32}}}; \quad T_{3n} = T_{2n} \left(\frac{P_3}{P_2} \right)^{\frac{\alpha_{32}-1}{\alpha_{32}}},$$

then in accordance with equality (1.34)

$$\frac{T_{3n}}{T_3} = \frac{T_{2n}}{T_2} \approx \eta_r^2. \quad (1.48)$$

Putting in expression (1.45) the values G_{3n} , w_{3n} and γ_{3n} from relationships (1.41), (1.45) and (1.47), taking into account equality (1.48), we obtain

$$f_{3n} \approx \frac{G_{\eta_r^2}}{\eta_r^2 w_{3n} \gamma_{3n}} \approx f_3 \frac{\eta_r^2}{(\eta_r \eta_r)^2} \approx f_3 \frac{1}{\eta_r^2}. \quad (1.49)$$

We see that the influence of losses shows up on a sharper increase in f_{3n} than in f_{3n}^* . The cause of this is that the value of f_{3n} , besides the increase of expenditure, is influenced also by the decrease of real speed w_{3n} as compared to w_3 .

CHAPTER II

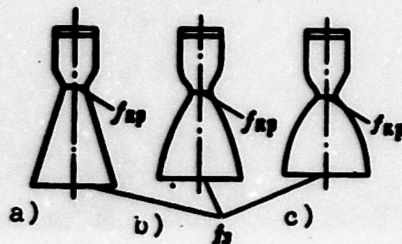
NOZZLES OF A LIQUID FUEL ROCKET ENGINE

In the nozzle of the chamber of the engine there occurs expansion and acceleration of products of combustion, i.e., the transformation of thermal energy obtained in the combustion chamber into kinetic energy of the motion of gases. The quality and weight of the whole propulsion system depend on the quality of operation of the nozzle, its economy and weight.

2.1. Types of Nozzles and Basic Requirements of Them

At present there are used or there is investigated the possibility of using the following basic types of nozzles (Fig. 2.1): conical, profiled and nozzles with a central body.

Round nozzles



Nozzles with a central body

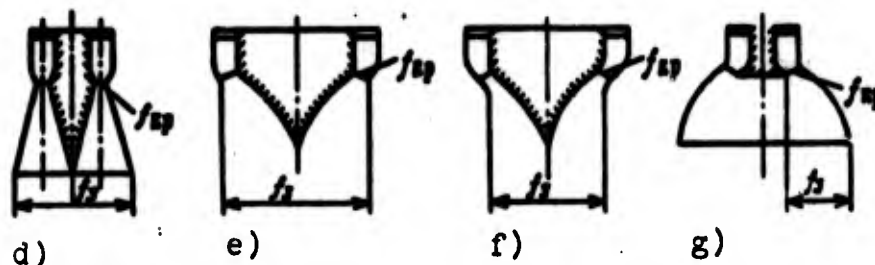


Fig. 2.1. Types of nozzles of the liquid-fuel rocket engine: a - conical; b - profiled; c - with an angular entrance; d - annular; e - with full external expansion; f - with partial internal expansion; g - plate with free internal expansion.

Conical and Profiled Nozzles

Conical nozzles have the supercritical section in the form of a cone with a direct generatrix (Fig. 2.1a). They are the simplest to manufacture and have been widely in rocket engines.

With respect to economy of the operation, i.e., with respect to the magnitude of losses, and weight characteristics, they yield to profiled nozzles and at present are almost completely displaced by them, finding application only in certain engines of low thrust.

Profiled nozzles have the generatrix of the supercritical section made in a curve, which coincides with the streamline (Fig. 2.1b, c). At present this is the most widespread type of nozzles of a liquid fuel rocket engine [ZhRD]. There are nozzles with a smooth entrance into the supercritical section of the nozzle (Fig. 2.1b) and nozzles having a break of the generatrix in the throat. The latter type of nozzle is called a nozzle with angular entrance into the supersonic section or, simply, nozzle with angular entrance (Fig. 2.1c).

Sometimes nozzles whose throat has the form of a circle, in contrast to nozzles with a central body, are called ordinary or

round nozzles. But usually by conical or profiled nozzles round nozzles are implied.

Nozzles with a Central Body

In recent years there has been intensively investigated the possibility of the application in a ZhRD of nozzles with a central body similar in principle to the type of nozzles successfully used in a jet engine [VRD].

Here are the following types of nozzles with a central body.

Ring nozzles (Fig. 2.1d), the expansion of flow in which is limited by an annular channel with solid walls. In principle the operation of annular nozzles does not differ from the operation of round nozzles.

Nozzles with full external expansion (Fig. 2.1e), not having an external wall forming the flow after the throat. Frequently this type of nozzle is simply called nozzle with a central body.

Nozzles with partial internal expansion (Fig. 2.1f) where the external wall determines expansion only up to a definite pressure. Such type of nozzle is intermediate between nozzles shown on Fig. 2.1d and 2.1e. The application of these nozzles can appear expedient with the necessity of deep expansion and the acceleration of gas up to great M values.

Plate nozzles (see Fig. 2.1g), thus called because of the plate form of the central body with a free internal surface of expansion, since after the critical section they do not have an internal wall.

Problem of the Designing of Nozzles and Requirements for Them

From a thermal calculation of the engine there are known only dimensions of the throat of the nozzle f_{np} . nozzle exit section

f_3 (or the pressure is assigned on nozzle p_3). In the designing of the combustion chamber we also determine dimensions of the entrance into the nozzle section. However, other important dimensions of the nozzle determining its form and design dimensions (in particular, the length of the nozzle and angles of inclination of walls of the nozzle in the entrance and outlet sections) are unknown to us.

The problem of designing the nozzle consists in the determination of such a contour of walls of the nozzle with which the following basic requirements for the nozzles would be satisfied.

1. The nozzle should have losses of thrust as small as possible, i.e., as large a value of the coefficient of the nozzle ϕ_c is possible.

2. The surface of the walls of the nozzle at assigned f_m and f_3 should be the least, which decreases the weight of the nozzle and facilitates its cooling.

3. The construction and technology of manufacture of the nozzle should be as simple as possible.

As frequently happens in technology, the indicated requirements are to a certain degree contradictory, and the full satisfaction one of them leads to a certain impairment of other properties of the nozzle. Therefore, in the designing of the nozzle depending upon the assignment of the engine, we take a certain compromise solution.

2.2. Losses in the Nozzle of a Liquid Fuel Rocket Engine

Classification and Estimate of Losses

As was already indicated (see section 1.3), losses in the nozzle of a liquid fuel rocket engine are estimated by the coefficient

$$\varphi_c = \frac{K_{n,d}}{K_n}$$

Quantity φ_c depends on various kinds of losses in the nozzle, the basic of which are the following:

1. Losses to the dispersion of speed at the outlet of the nozzle φ_{pac} .
2. Frictional losses of gas on walls of the nozzle φ_{TP} .
3. Losses at the entrance into the nozzle φ_{ax} .
4. Losses to the nonequilibrium of the process of expansion φ_{nep} .
5. Losses connected with the nonadiabatic flow of products of combustion along the nozzle. Sometimes they are called cooling losses φ_{oxa} .
6. Losses to the narrowing of the section of the flow φ_{cym} .
7. Losses taking place with the outflow of two-phase working substances φ_{ϕ} .

In certain cases losses in the nozzle are conditionally attributed to losses in thrust appearing due to the off-design nature of the operating conditions of the nozzle $\varphi_{n.p.}$. This is inadmissible since losses of thrust due to the off-design nature of operating conditions do not depend on the quality of the flow of processes in the nozzle. However, sometimes in the comparative estimate of different contours of shortened nozzles, it is convenient to consider these losses by introduction of the coefficient $\varphi_{n.p.}$ referred to the nozzle.

Each of the indicated kinds of losses is estimated the appropriate coefficient φ_i (φ_{pac} , φ_{TP} , etc.) expressed as

$$\varphi_i = \frac{P_n - \Delta P_i}{P_n}, \quad (2.1)$$

where ΔP_i - decrease in thrust from a given type of loss. Knowing for every kind of loss ϕ_i , we can determine ϕ_c :

$$\begin{aligned} \varphi_c &= \frac{P_{n1}}{P_n} = \frac{P_n - \sum_{i=1}^n \Delta P_i}{P_n} = 1 - \frac{\sum_{i=1}^n \Delta P_i}{P_n} = \\ &= \sum_{i=1}^n \left(1 - \frac{\Delta P_i}{P_n}\right) - (n-1). \end{aligned} \quad (2.2)$$

Taking into account equation (2.1), we will obtain

$$\varphi_c = \sum_{i=1}^n \varphi_i - (n-1). \quad (2.3)$$

It is more convenient (and more usual) to determine ϕ_c not as the sum ϕ_i but as the product

$$\varphi_c = \varphi_{pac} \varphi_{rp} \varphi_{\alpha} \varphi_{dep} \varphi_{\omega} \varphi_{\omega n} \varphi_{\gamma n} \varphi_{\phi}. \quad (2.4)$$

The difference in the quantity ϕ_c determined by formulas (2.3) or (2.4) is small.

According to results of experimental data, the total magnitude of losses in the nozzle is determined by the formula (1.36): $\varphi_c = K_{n1}/K_n$.

Let us examine the components of losses entering into expression (2.4).

Losses to the Dispersion of Speed at the Outlet of the Nozzle

In deriving the equation of thrust we considered that the direction of the flow of masses passing from the nozzle is

in parallel to the axis of the nozzle. In reality, if in section f_3 the direction of the wall of the nozzle is not in parallel to the axis, then the velocity of the flow directed along the wall is deflected from the direction of the action of the tractive force (Fig. 2.2). The traction of the nozzle is determined only by the component of speed parallel to the axis w_3' .

Since $w_3' < w_3$, then the thrust of the nozzle is smaller than the design thrust, which corresponds to speed w_3 . Let us determine the magnitude of losses to dispersion. With quite small values of β_3 and with the ratio $l_3/l_{np} > 3$ it is possible to assume that in the nozzle exit section radial flow takes place, and the surface $p_3 = \text{const}$ has the form of a sphere of radius ρ with surface f_3' .

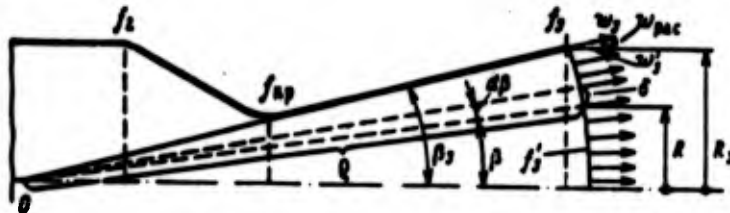


Fig. 2.2. Determination of φ_{pac} .

To determine the thrust let us separate on surface f_3' the annular element with arc δ included between angles β and $\beta + d\beta$, and let us find the thrust of the element. The axial component of the thrust of the element in a vacuum

$$dP_{n.a} = w_3' \frac{\gamma_3 w_3^2 2\pi R^3}{g} + p_3 2\pi R \delta \cos \beta. \quad (2.5)$$

Considering, that

$$\left. \begin{aligned} w_3' &= w_3 \cos \beta; \\ \delta &= \rho d\beta = \frac{R}{\sin \beta} d\beta; \\ R &= R_3 \frac{\sin \beta}{\sin \beta_3}, \end{aligned} \right\} \quad (2.6)$$

and substituting expressions (2.6) into equation (2.5), we will obtain

$$dP_{n,1} = \frac{\gamma_3 w_3^2}{g} 2\pi \frac{R_3^2}{\sin^2 \beta_3} \sin \beta \cos \beta \cdot d\beta + p_3 2\pi \frac{R_3^2}{\sin^2 \beta_3} \sin \beta \cos \beta \cdot d\beta.$$

Integrating this expression within limits from 0 to β_3 , we obtain

$$\begin{aligned} P_{n,1} &= 2\pi \frac{R_3^2}{\sin^2 \beta_3} \int_0^{\beta_3} \left(\frac{\gamma_3 w_3^2}{g} \sin \beta \cos \beta + p_3 \sin \beta \cos \beta \right) d\beta = \\ &= 2\pi \frac{R_3^2}{\sin^2 \beta_3} \left[\frac{\gamma_3 w_3^2}{g} \frac{(1 - \cos^2 \beta_3)}{2} + p_3 \frac{(1 - \cos^2 \beta_3)}{2} \right]. \end{aligned} \quad (2.7)$$

The flow rate through surface f'_3

$$G = \int_0^{\beta_3} \gamma_3 w_3 df.$$

In accordance with equations (2.6) the surface of the element

$$df = 2\pi R^2 = 2\pi R \frac{R}{\sin \beta} d\beta = 2\pi \frac{R_3^2}{\sin^2 \beta_3} \sin \beta \cdot d\beta, \quad (2.8)$$

and then

$$G = 2\pi \gamma_3 w_3 \frac{R_3^2}{\sin^2 \beta_3} \int_0^{\beta_3} \sin \beta \cdot d\beta = 2\pi \gamma_3 w_3 \frac{R_3^2}{\sin^2 \beta_3} (1 - \cos \beta_3).$$

The surface area of the segment

$$f'_3 = 2\pi \frac{R_3^2}{\sin^2 \beta_3} (1 - \cos \beta_3). \quad (2.9)$$

Substituting values (2.2) and (2.9) into expression (2.7), we will obtain

$$P_{r,2} = \frac{1 + \cos 2\beta_3}{2} \left(\frac{w_3}{g} G + P_2 f_3' \right). \quad (2.10)$$

Comparing the expression in parentheses with the equation of thrust (1.3), we see that this value is the rocket engine thrust in a vacuum with parallel outflow, for which the area at the exit is equal to f_3' .

If in view of the smallness of angle β_3 we take the surface area f_3' equal to the area of nozzle section f_3 , then the value in parentheses will be equal to the rocket engine thrust with parallel outflow. Designating

$$\frac{1 + \cos 2\beta_3}{2} = \varphi_{pec} \quad (2.11)$$

we finally copy equation (2.10) in the form

$$P_{r,2} = \varphi_{pec} P_{r0} \quad (2.12)$$

where φ_{pec} - loss factor of thrust to the dispersion of flow in view of the nonparallelism of the outflow. The dependence of φ_{pec} on angle β_3 is given in Table 2.1.

Table 2.1

$2\beta_3$	0	4	8	12	16	20	24	28	32	36	40
φ_{pec}	1.000	0.9997	0.9988	0.9972	0.9951	0.9924	0.9890	0.9851	0.9806	0.9755	0.9698

From the table it is clear that for the nozzle with an opening of $2\beta_3 = 28^\circ$ thrust P will be 98.5% of the thrust determined by

the formula (1.3), and at angle $2\beta_3 = 12^\circ$ losses to dispersion will be a total of 0.3%. Although the given deduction is correct only for the radial flow of gases over the nozzle, formula (2.11) with a sufficient degree of accuracy permits estimating losses to dispersion also for profiled nozzles.

For a decrease in losses to dispersion it is desirable to have angle β_3 as small as possible, and when $\beta_3 = 0$ it will be $\Phi_{pac} = 1$. However, as we will subsequently see (see section 2.5), in nozzles of rocket engines it is inexpedient to reduce angle β_3 to zero, since with this frictional losses and weight of the nozzle greatly increase. For the usually applied or conical nozzles the angle at exit $2\beta_3$ is within limits 10-30°, and losses of thrust to dispersion are 0.3-1.5%.

Frictional Losses in the Nozzle

As a result of the friction of gas on the walls, there appears a force acting on the wall of the nozzle in a direction opposite to the tractive force ("pulling" force). The value of frictional force acting on the annular section of the wall of the nozzle dF_{f1} (Fig. 2.3),

$$dP_{r1} = C_{f1} \frac{\rho_1 w_1^2}{2} \cos \beta \cdot dF_{f1} \quad (2.13)$$

where ρ_1 and w_1 - density and flow rate in the 1-th section; C_{f1} - coefficient of skin friction.

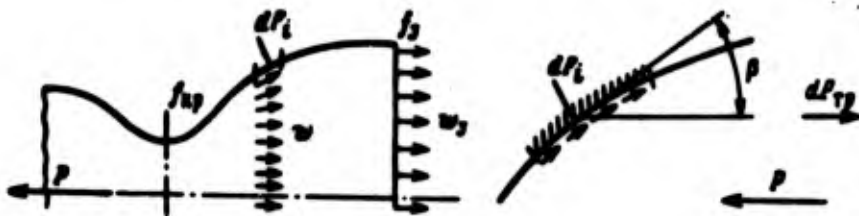


Fig. 2.3. Determination of frictional losses.

The coefficient of skin friction C_f , taking into account the compressibility and heat exchange, can be calculated on the basis of the theory of the boundary layer. Approximate values of C_f can be obtained by using the semi-empirical formula

$$C_f = C_{f_0} \left(1 + r \frac{\lambda - 1}{2} M^2\right)^{-0.5}, \quad (2.14)$$

where C_{f_0} - coefficient of friction of the incompressible liquid; r - recovery factor. For tentative calculations frictional losses can be taken as

$$r = 0.88; C_{f_0} = 0.003 - 0.006.$$

The total frictional force acting on the wall of the nozzle is equal to

$$\Delta P_{fr} = \int dP_{fr}. \quad (2.15)$$

The thrust in a vacuum, taking into account the action of frictional forces,

$$P_{z,0} = P_0 - \Delta P_{fr} = \varphi_{fr} P_0 \quad (2.16)$$

where φ_{fr} - frictional loss factor

$$\varphi_{fr} = \frac{P_0 - \Delta P_{fr}}{P_0} = 1 - \frac{\Delta P_{fr}}{P_0}. \quad (2.17)$$

For nozzles of a ZhRD values of the frictional loss factor lie within 0.98-0.995.

Example. Determine frictional losses in a nozzle and frictional loss factors φ_{fr} and losses to dispersion φ_{dis} , neglecting the friction on the section of chamber prior to the throat.

The basic parameters of operation of the engine and dimensions of the nozzle

$$p_0^* = 70 \text{ kgf/cm}^2 (0.67 \text{ MN/m}^2); G = 12.5 \text{ kg/s};$$

$$T_0 = 3010^\circ \text{K}; n_{no} = 1.2;$$

$$R = 34.3 \text{ kgf}\cdot\text{m/kg}\cdot\text{deg} (337 \text{ J/kg}\cdot\text{deg}); R_{no} = 30 \text{ mm};$$

$$p_0 - p_a = 0.7 \text{ kgf/cm}^2 (0.069 \text{ MN/m}^2);$$

$$R_0 = 103.8 \text{ mm};$$

$$L_0 = L_1/R_{no} = 10; \beta_1 = 4^\circ.$$

The contour of the nozzle is shown in Fig. 2.4.

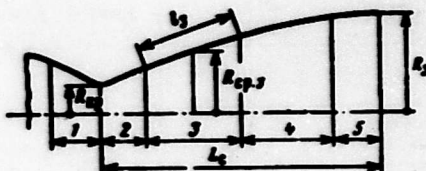


Fig. 2.4. To determination ΔP_{fp} ; division on sections.

Solution. To determine frictional losses let us divide the nozzle lengthwise into five sections and determine frictional losses according to parameters referred to the middle of the section. The coefficient of friction is determined approximately by formula (2.14).

Let us consider $C_f = 0.003$ and $r = 0.69$. By knowing the mean values of M_{no} , let us determine quantities $p/p_0, M, q, w$ by the well-known relationships of gas dynamics. Data of the calculation are given in Table 2.2. The total frictional force:

$$\Delta P_{fp} = \sum_{i=1}^5 \Delta P_{fp,i} \approx 31.7 \text{ kgf} (311 \text{ N}).$$

Let us define loss factors φ_{fp} and φ_{pa} . The thrust in a vacuum

$$P_a = \frac{w_1}{g} G + f_{pa} p_0 = \frac{2550}{9.81} \cdot 12.5 + 3.36 \cdot 10^{-4} \cdot 0.7 \cdot 10^4 = 3487 \text{ kgf} (34200 \text{ N}).$$

The frictional loss factor

$$\eta_{fp} = \frac{P_n - \Delta P_{fp}}{P_n} = \frac{3487 - 31.7}{3487} = 0.991.$$

The loss factor to dispersion

$$\eta_{pdc} = \frac{1 + \cos \beta}{2} = \frac{1 + \cos 4^\circ}{2} = 0.9988.$$

Table 2.2.

Number of sections	1	2	3	4	5
Angle of inclination of contour β in deg.	30	21,5	16	11	4
$\cos \beta$	0,864	0,980	0,990	0,995	0,999
Average radius $R_{cp} \cdot 10^3$ in m	37,5	38,5	64,5	91	102
Surface of the section $\Delta F_i = 2\pi R_{cp} l \cdot 10^6$ in m ²	13,9	13,0	41,8	58,2	32,9
l/l_{cp}	1,56	1,65	4,62	9,20	11,6
P/P_n^2	0,901	0,165	0,0336	0,0140	0,0104
M^2	0,174	3,50	7,40	10,36	11,3
$\left(1 + \frac{M^2 - 1}{2} r M^2\right)^{0,66}$	1,01	1,16	1,32	1,43	1,47
$C_f \cdot 10^6$	0,267	0,258	0,227	0,21	0,204
$w^2 \cdot 10^{-4}$ m ² /s ²	20,9	314	517	617	643
q in kgf·g ² /m ⁴ in kg/m ³	0,634 6,22	0,154 1,51	0,0432 0,424	0,0197 0,193	0,0158 0,155
$\frac{qw^2}{2} \cdot 10^{-4}$	6,63	24,2	11,2	6,08	5,08
$C_f \frac{qw^2}{2}$	198	624	254	128	104
Frictional force on the section in kgf	2,38	7,95	10,5	7,4	3,41
$\Delta P_{fp} = C_f \frac{qw^2}{2} \Delta F_i \cos \beta$ in H	23,4	78,0	103	72,6	33,4

Losses at the Entrance Into the Nozzle

With gas flow in the subcritical part of the nozzle with a steep turn of peripheral flow streams in a direction toward the axis of the nozzle, compression of gas streams flowing near the axis of the nozzle occurs. As a result of this the pressure in the central streams is set higher than the pressure around the wall of the nozzle. Fig. 2.5a shows a diagram of the distribution of pressure in the section I-I. In conformity with such a distribution of pressures along the section in a peripheral region the flow rate is set higher than that near the axis. Therefore, at the entrance into the region of the throat the peripheral flow accelerates earlier up to the critical speed than does the flow near the axis. The surface of the critical speed AO is deformed, obtaining a convex form. With great curvature of the entrance section the formation of compression shocks and also the separation of flow is possible. Furthermore, since the exact form of the surface of the critical speed is unknown, losses can appear due to the noncorrespondence of the real character of the flow in the entrance part of accepted design scheme.

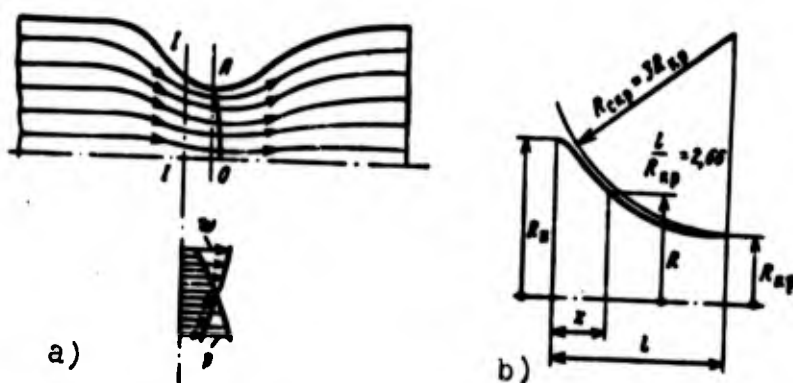


Fig. 2.5. Explanation of entrance losses: a) appearance of losses at the entrance; b) Vitoshinskiy profile.

All these losses are connected with the organization of the flow in the entrance part of the nozzle and therefore they are called entrance losses in the nozzle. The magnitude of the losses is estimated by coefficient φ_{ex} .

The smooth entrance into the nozzle at which the surface of the stalling speed can be considered flat provides a contour of the subsonic part constructed by the formula of Vitoshinskiy (Fig. 2.5b):

$$\frac{R}{R_{\text{sp}}} = \frac{1}{\sqrt{1 - \left[1 - \left(\frac{R_{\text{sp}}}{R}\right)^3\right] \frac{1 - (x/D_{\text{sp}})}{1 + 3(x/D_{\text{sp}})}}}} \quad (2.18)$$

The surface of the critical speed will be obtained quite close to a flat surface if we profile the entrance part by an arc of a circle with a radius $R_{\text{exp}} = 3R_{\text{sp}}$. The flat surface of the stalling speed is frequently taken as the initial with calculation of the profile of the supercritical part [43]. However, with such a construction a relatively long entrance part of the nozzle is obtained, i.e., the dimensions and weight of the nozzle increase.

Experiments on the determination of the entrance losses in nozzles distinguished by a radius of curvature of the nozzle in the region of the critical section showed that when $R_{\text{exp}} > 0.65D_{\text{sp}}$ entrance losses are practically absent. Therefore, in the profiling of nozzles of a ZhRD, depending upon the accepted design scheme, the entrance part of the nozzle in the region of the throat is constructed on an arc of a circle with the following radius of curvature [8]:

$$R_{\text{exp}} = (0.65 - 1.5)D_{\text{sp}} \quad (2.19)$$

Entrance losses here are taken equal to zero, i.e., $\varphi_{\text{ex}} = 1$.

Other Losses

Losses to the nonequilibrium of the process of expansion (Φ_{nep}).

With very great broadenings, when the thermodynamic temperature of products of combustion in the nozzle decreases down to values of 1000-1700°K, or with the reduction of the time of stay of gases in the nozzle (for example, in microengines), the process of expansion of gases can flow partially or completely unbalanced (in detail see work [25]). With this the magnitude of specific thrust drops as compared to the specific thrust determined with equilibrium expansion. Losses to nonequilibrium can reach 5-10%. Quantity Φ_{nep} can be determined by estimating the degree of nonequilibrium.

Losses due to the nondiabatic nature of the process of expansion

(Φ_{ozn}). The cause of these losses (also called cooling losses) is the heat removal from the flow into the wall. With this if the heat is removed irrevocably (for example, with cooling by a special component not utilized as fuel, or in the case of uncooled chamber) the specific thrust decreases as compared to specific thrust determined with adiabatic expansion. The magnitude of these losses with intense cooling can reach 3-5%. If, however, there is used regenerative cooling, at which the heat, tapped by the coolant, returns back into the chamber, then there will be no losses of specific thrust due to heat removal from the flow. Conversely, there will occur a certain increase in P_{yn} since in the nozzle heat from the flow is removed at lower pressure than the pressure at which this heat returns into the chamber. However, an increase in P_{yn} here is a fraction of a percent and therefore in calculations is not considered. Calculation of the influence of the nonadiabatic state on P_{yn} is examined in work [2].

Losses to the narrowing of the flow owing the boundary layer

(Φ_{ryn}). Due to the presence of the boundary layer, and also the formation at the wall of a special wall layer, for internal cooling real areas of the cross section decrease and the character of flow in the nozzle

is distorted, which in the end can lead to a loss in speed and thrust. The magnitude of these losses is small and is considered in the total estimate ϕ_c .

Losses with expansion of two-phase flow (ϕ_e). In the use of certain forms of high-calorie fuels (for example, metallized fuels) in products of combustion small particles (for example, condensed oxides) can be formed. In this case in the nozzle there occurs expansion of not a uniform but a two-phase gas flow (heterogeneous). With the expansion in the nozzle the drop in temperature and increase in velocity of the particles attracted by the gas flow occur more slowly as compared to the change in corresponding parameters of the gas. This leads to a lowering of the specific thrust. Losses in specific thrust with expansion in the nozzle of a two-phase flow can reach considerable values, of the order of 3-10 and more percents, and sharply reduce the effectiveness of the application of high-calorie fuels.

2.3. Designing of Conical Nozzles

Considering the dependence of losses at the entrance, to dispersion and to friction on form and dimensions of the nozzle, in the designing of conical nozzles it is possible to recommend the following values of the basic geometric dimensions of the nozzle (Fig. 2.6). The entrance part is designed from the condition of providing the absence of entrance losses.

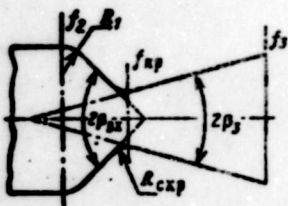


Fig. 2.6. Designing of conical nozzles.

The angle of entrance into the nozzle part

$$2\beta_{nz} = 45-80^\circ.$$

$$(2.20)$$

The radius of curvature of the critical part of the nozzle

$$R_{\text{кр}} = (0,65-1)D_{\text{кр}}$$

The radius of curvature of the entrance part of the nozzle

$$R_1 = (0,35-0,5)D_{\text{кр}} \quad (2.21)$$

The angle of the outlet part of the nozzle $2\beta_3$ is selected on the basis of experimental data concerning the dependence of the product $\Psi_{\text{pac}}\Psi_{\text{тр}}$ on the aperture angle of the supercritical part of the nozzle $2\beta_3$. A typical graph of such a dependence is shown on Fig. 2.7. Usually

$$2\beta_3 = 25-30^\circ \quad (2.22)$$

A certain impairment of quantity $\Psi_{\text{pac}}\Psi_{\text{тр}}$ when $2\beta_3 = 30^\circ$ is compensated by a decrease in length and, consequently, weight of the nozzle. The main deficiency in conical nozzles is that even with the most acceptable angles $2\beta_3$ the nozzle is obtained relatively long, heavy and has comparatively great losses to dispersion and friction.

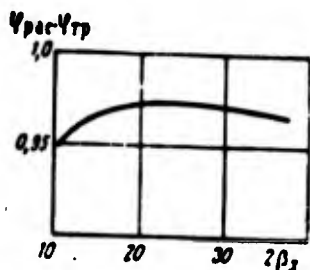


Fig. 2.7. Dependence of $\Psi_{\text{pac}}\Psi_{\text{тр}}$ on angle $2\beta_3$.

Profiling the contour of the nozzle permits making it shorter and lighter with a simultaneous decrease in losses.

2.4. Basic Initial Positions in the Construction of a Profiled Nozzle

Let us examine the basic positions from which one proceeds in the construction of the contour of the supersonic part of a profiled nozzle.

I. Region on the left of surface AOA' - region of subsonic gas flow. In it the acceleration of the subsonic gas flow up to a stalling speed occurs. The contour of the subsonic part of the nozzle is profiled proceeding from the condition of providing the absence of entrance losses in the nozzle (see section 2.2).

II. Surface AOA' - surface on which the speed of gas reaches the speed of sound at a given point, i.e., the surface of the stalling speed. The form of it in general can be both flat and convex and is determined by the contour of a subsonic part of the nozzle. As yet there is no accurate solution to problem of the determination of the form of the surface of stalling speed. With different methods of profiling the nozzle we proceed from different forms of the surface AOA' . The most widespread assumptions are about its flat or spheric form.

III. Region $AA_n O_n A_n' A'$ - region of preliminary expansion. Here the expansion and acceleration of gas occurs. On the section of nozzle AA_n there appears an infinite quantity of weak rarefaction waves $A_1 C_1'; A_2 C_2' \dots A_n C_n'$, which are characteristics. With transition through the rarefaction waves a decrease in pressure and acceleration of supersonic flow occurs. In the calculation of the contour of the nozzle the curvilinear section AA_n is replaced by a finite number of chords $AA_1; A_1 A_2; A_2 A_3 \dots$. With this the broken line $AA_1 \dots A_n$ is selected in such a manner so that the direction of the characteristics is changed by an infinite number (for example, 2°). Thus, the infinite number of rarefaction waves of infinitesimal intensity is replaced by a series of rarefaction waves outgoing from points of the turn of the broken line. This replacement is equivalent to the assumption that expansion occurs not continuously but at small finite distances.

The angle of inclination of the velocity vector at the wall AA_n with respect to the axis of the nozzle continuously increases up to point A_n . At point O_n the flow rate reaches the assigned speed.

IV. Region $A_n O_n C_n$ - region of levelling off of the flow.

In this region there occurs further acceleration of gas up to the assigned speed and levelling off of the direction of the motion of gas. The contour of the nozzle in this region is profiled from the condition that at points C_1, C_2, C_3 , etc. reflection of rarefaction waves $A_1'C_1, A_2'C_2, A_3'C_3$, the direction of the wall coincides with the direction of the speed. Therefore, at these points the angle of inclination of the wall $A_n C_n$ is changed by an angle equal to the angle of rotation of the flow with passage through the rarefaction wave $A_1'C_1, A_2'C_2, A_3'C_3$, etc. The angle of inclination of the velocity vector of the flow at the wall $A_n C_n$ from point A_n up to point C_n continuously decreases. With the attenuation of all rarefaction $A_1'C_1, A_2'C_2, \dots$ walls of the nozzle will be parallel to the axis of the nozzle (for an ideal nozzle). Thus, starting from point A_n of the angle of inclination of the contour of the wall to the axis of the nozzle continuously decreases. Point A_n is the inflection point.

On section AA_n the angle of inclination of the contour continuously increases. With the construction of the profile on this section, depending upon the streamline according to which the profile of the nozzle is constructed, there can be obtained a larger or smaller length of the generatrix AA_n , and with the construction of the profile along the limiting streamline the section will reduce to a point. Region IV will start directly from the critical section of the nozzle in which the contour of the nozzle will have a break (Fig. 2.9a). Therefore, such a nozzle is called a nozzle with an angular entry. Other things being equal, the length of the supersonic part of the nozzle with angular entry will be least. Therefore, in a ZNRD the application of nozzles with angular entry is expedient.

V. Region $C_n O_n C_n'$ - region of uniform gas flow. For an ideal nozzle the direction of the motion of flow in this region is in parallel to the axis. The flow rate is equal to that assigned.

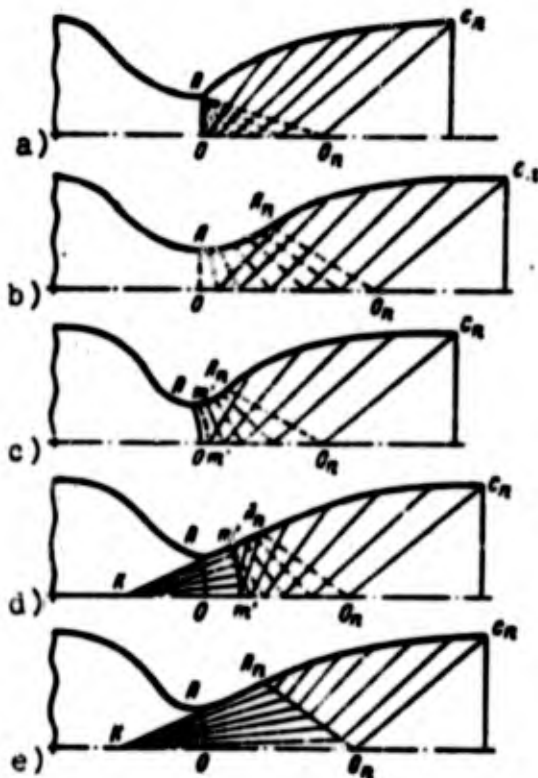


Fig. 2.9. Different initial conditions for the construction of a grid of characteristics and profile of a nozzle: a) flat surface, angular entry; b) flat surface AO, smooth entry; c) $m'm'$ -- calculated surface, rounded entry; d) radial flow up to surface $m'm'$; e) radial flow up to surface A_1O_1 ; conical entry.

To construct the grid of characteristics, it is necessary to know the initial velocity distribution in some section of the supersonic part of the nozzle. If the form and position of the surface of the critical speed AOA' are known, then construction of characteristics can be conducted from it. Here it is necessary to consider that near the surface the speed of flow insignificantly exceeds the critical speed, in consequence of which the accuracy of the construction of characteristics is not great. Therefore, sometimes characteristics are constructed starting from a certain section where the flow already possesses supersonic speed. Here the velocity distribution on this section is considered known.

With the profiling of nozzles of a ZHRD, several procedures of the construction of characteristics and profile have been used.

Frequently we proceed from the assumption that with a sufficiently smooth profile of the subsonic part (large value of $R_{\text{ср.}}$), in the narrow section will be formed flat surface of the critical speed.

Here the grid of the characteristics will have the form shown on Fig. 2.9a, b. The profile of the nozzle shown on Fig. 2.9a has an angular entry into the supercritical part (nozzle with angular entry). The profile on Fig. 2.9b has a smooth entry. Here the length of the critical part of the nozzle will be greater than that in the case of angular entry. In the construction of the entry part, which provides a flat surface of critical speed for profiling the supercritical part of the nozzle both with angular entry and in terms of the intermediate streamline, it is possible to use tables of parameters of the supersonic flow of gases compiled by O. H. Katskova and Yu. D. Shnyglevskiy [44].

The characteristics can be constructed as is shown on Fig. 2.9c, i.e., from the convex surface $m'm'$ in the region of the critical section [56] calculated by the Zauer method [42].

In certain works it is proposed to make the initial section of the supersonic part of the nozzle conical. Here the flow in the critical section actually is not examined and it is taken that the supersonic flow starts from the source at point K (Fig. 2.9d, e). On the initial section the flow is taken radial and known either up to section $m'm'$ in the supersonic part (Fig. 2.9d) or up to the characteristic $A_n O_n$ (Fig. 2.9c). Construction of characteristics starts either from surface $m'm'$ or from characteristic $A_n O_n$, which is known in this case. However, an investigation of the field of flow in conical nozzles showed that the coincidence with the flow from the source takes place only on very distant sections of the supersonic flow. Furthermore, the supersonic part of the nozzle, constructed on the assumption of radial flow on its initial section, has a smooth entry and is obtained longer than for nozzles with an angle entry.

2.5. Shortened and Optimum Nozzles

Shortened Nozzles

Being based on the method of characteristics well-known from gas dynamics, we can profile an ideal nozzle with uniform and

parallel flow on the section.

If one were not to consider frictional losses of thrust then such a nozzle will give the greatest thrust. Let us consider, however, whether the application of ideal nozzles in a ZhRD is expedient.

The end section BC of an ideal nozzle, represented on Fig. 2.10, gives a very small increase in thrust, since on this section the generatrix of the surface of the nozzle is almost parallel to the axis. By shortening the nozzle, it is possible to obtain a considerable decrease in dimensions and weight of the nozzle, which is very important for rocket engines. Furthermore, it appears that on the extreme section BC frictional losses of thrust exceed the increase in thrust on this section. Thus, with a definite decrease in length of the ideal nozzle we gain not only in weight of the nozzle and its dimensions but even in thrust. Such nozzles obtained by means of decreasing the length of the ideal nozzle are called shortened nozzles.

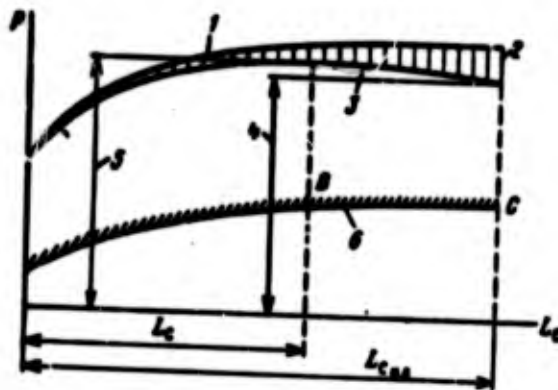


Fig. 2.10. Comparison of an ideal nozzle with a shortened nozzle: 1 - thrust neglecting frictional losses; 2 - frictional; 3 - thrust taking into account frictional losses; 4 - thrust of an ideal nozzle; 5 - thrust of a shortened nozzle; 6 - contour of an ideal nozzle.

Optimization of the Nozzles

An ideal nozzle from which a shortened one is obtained is called an initial nozzle. It is obvious that for obtaining a shortened nozzle, which provides, for example, the assigned speed (i.e., having assigned f_{opt}), the initial nozzle should be calculated at some large Mach number unknown to us. Therefore, it is necessary to construct a family of initial nozzles with different M and to select from it an optimum shortened nozzle providing the assigned f_{opt} with the least losses of thrust. It is possible also, having shortened, for example, all the initial nozzles of the given family up to some assigned length l_c , to find the nozzle of assigned length giving the greatest thrust taking into account all losses.

It is possible, finally, to find the nozzle of the assigned surface most advantageous in thrust, (i.e., in practice, assigned weight), cutting off nozzles of equal surface from the initial nozzles.

Nozzles providing the greatest thrust of the propulsion system at definite assigned conditions (f_{opt} , length, surface, etc.), are called optimum nozzles. Obviously, in a ZHRD the most expedient is the application of optimum nozzles which provide, depending upon requirements for the installation, the greatest thrust at the assigned length or weight, or area f_3 , etc.

Fig. 2.11 gives a family of contours of initial nozzles with angular entry on which there are plotted curves of constant thrust coefficient in a vacuum which is determined into account frictional losses. Such graphs are used for the analysis and selection of different types optimum nozzles. On them the contour of the optimum nozzle of assigned length is determined by the point of tangency of the vertical line, corresponding to the assigned length, to the curve of constant thrust. The contour of optimum nozzle of assigned surface will be determined by the point of tangency of the line of constant surface to the curve of constant thrust. On Fig. 2.11

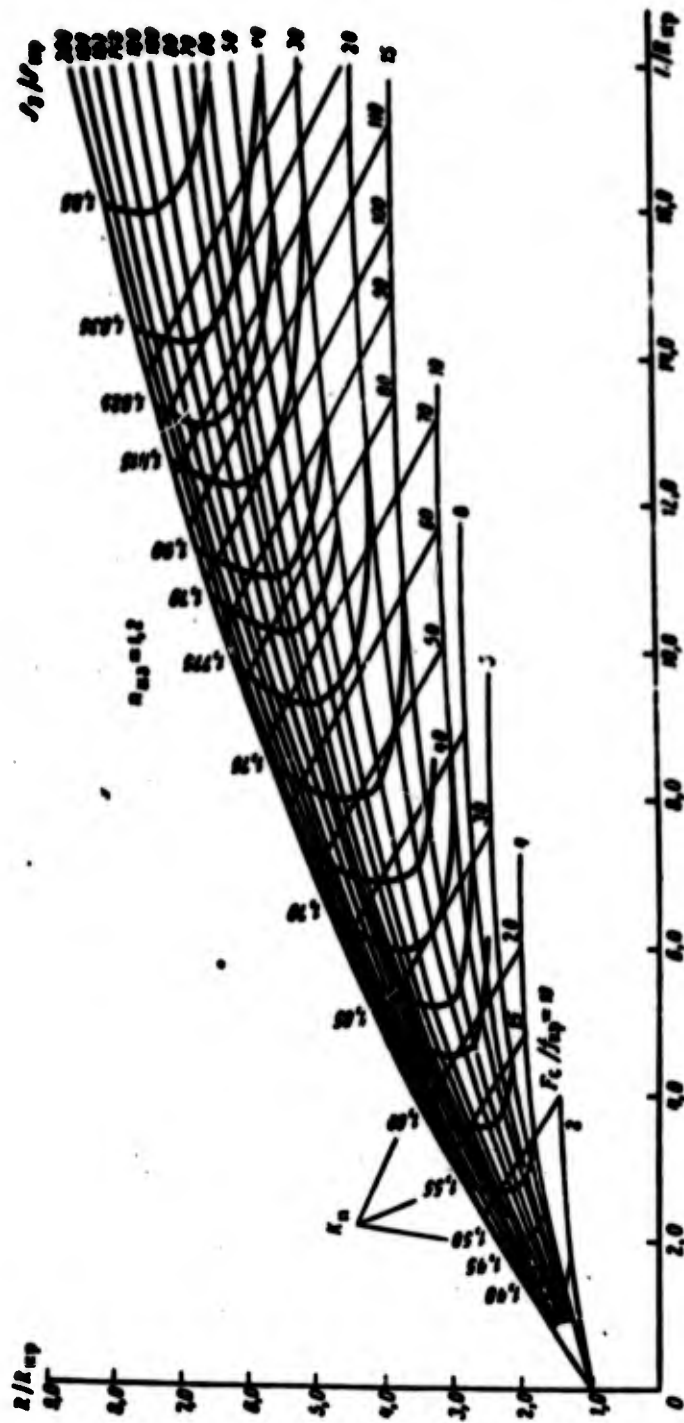


FIG. 2.11. Selection of the profile of the optimum nozzle.

it is clear that with the assigned thrust the contour of the nozzle of least surface. The contour of the optimum nozzle with assigned area f_3 will be determined by the point of tangency of the horizontal line corresponding to area f_3 with the curve of constant thrust.

The application of optimum nozzles gives high gain not only in thrust but also in dimensions of the nozzle. Figure 2.12 gives a comparison of lengths and contours of different types of nozzles.

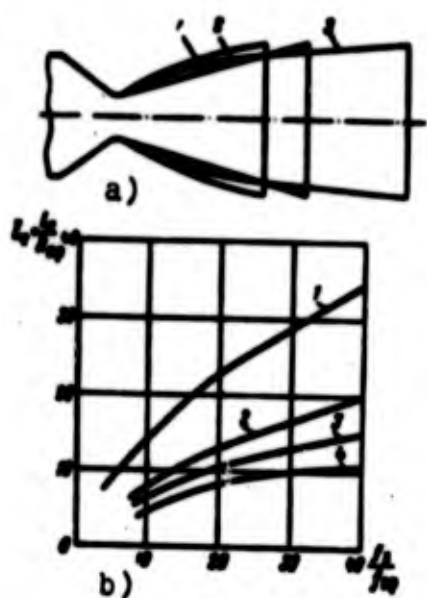


Fig. 2.12. Comparison of nozzles of different types: a) by contours; b) by lengths; 1 - ideal; 2 - conical; 3 - optimum; 4 - with a central body.

The optimum nozzle with the least length of the supersonic part will be obtained with the fulfillment of the contour with angular entry. For a ZhRD such a nozzle is most profitable, but technological difficulties and the danger of flow separation near the angular edge lead in a number of cases to the necessity of making the entry with small rounding.

In this case we found the optimum nozzle from a number of shortened ones obtained by cutting part of the initial nozzle. The contour of the optimum nozzle may also be obtained directly as a result of the solution of the variational problem on the finding of the contour of the nozzle of the greatest thrust under certain assigned conditions. Thus, in works [40], [52], [56] the problem

of determination of profile of the optimum nozzle is solved, which provides the greatest thrust at the assigned length of the nozzle L_0 , pressure in the combustion chamber p_2 and ambient pressure p_a ; in work [50] the variational problem of finding the optimum nozzle of least weight is examined. In the indicated works losses of thrust to dispersion and to the off-design state of operating conditions of the nozzle are considered; the remaining forms of losses (including frictional losses) are not considered.

Having determined the optimum contour of the nozzle with the assigned length (or other parameter), we can construct a family of optimum nozzles and from this family select the nozzle which satisfies us the most with respect to other conditions (weight, midsection, frictional losses, etc.). Here frictional losses can be found by direct calculation.

Losses of thrust of optimum nozzles both obtained by means of shortening the initial nozzles and constructed from results of the solution of the variational problem, are practically identical.

In work [56] on the basis of the solution of the variational problem the connection between the magnitude of underexpansion $(p_2 - p_a)$ and angle β_3 for nozzles of assigned length is found:

$$\sin 2\beta_3 = \frac{p_2 - p_a}{\frac{1}{2} \rho_2 v_2^2} \operatorname{ctg} \alpha_3. \quad (2.23)$$

Here α_3 - Mach angle;

$$\sin \alpha_3 = \frac{1}{M_3}. \quad (2.24)$$

This dependence can be used in the calculation of nozzles of engines operating in a vacuum.

2.6. Approximate Method of Construction of a Contour of an Optimum Nozzle

Order of Construction

In the fulfillment of a sketch project for the possibility of the approximate calculation of thrust characteristics of an engine, the calculation of cooling, and also for the estimate of the weight of engine, it is frequently sufficient to know the approximate contour of the nozzle, the dimensions of which insignificantly differ from dimensions of the exact contour.

In this case it is possible to use methods of approximation of the construction, which permit rapidly finding the optimum contour. Below there is given one of such methods founded on results of the solution of the variational problem about finding the contour of the optimum nozzle of assigned length and further analysis of the family of found contours [56].

Calculations were conducted with a constant index of the isentrope $\kappa_{\text{opt}} = 1.23$. In the construction of the grid of the characteristics for finding the contour, the region of the critical section was constructed by arcs of a circle (see Fig. 2.14). The radius of curvature of entry part on the section prior to the critical section $R_{\text{crit}} = 0.75D_{\text{opt}}$; the radius of curvature of the generatrix at the entrance into the supercritical part $r_{\text{sup}} = 0.225D_{\text{opt}}$. The surface of the critical speed was taken to be convex (see Fig. 2.9c).

On the basis of the analysis of the family of contours of optimum nozzles are curves of the dependence of angle β_m of inclination of the contour at the point of contact to the generatrix AA_n at the entrance into the supercritical part and angle of inclination of the contour on section β_3 on the dimensionless length of the nozzle $L_c = L_c/R_{\text{opt}}$ and dimensionless radius of the nozzle on section R_n/R_{opt} (Fig. 2.13). The supercritical part of the contour on section A_nC is approximately approximated by a parabola.

Calculations showed that replacement of the exact contour by a parabolic contour leads to a divergence in radial dimensions of the nozzle within 1-3% [56].

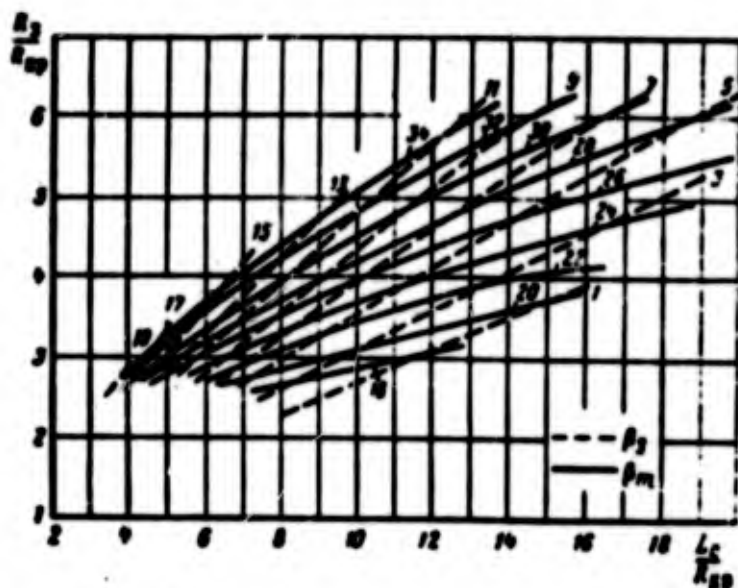


Fig. 2.13. Dependence β_m and β_3 on the length L_c/R_{cp} and radius of the nozzle on section R_3/R_{cp} .

The construction of a contour is produced in the following order (Fig. 2.14). According to the known R_{cp} we construct a contour of the nozzle in the region of the critical section, assuming $R_{cp} = 1.5R_{cp}$ and $r_{cp} = 0.45R_{cp}$. According to the known (by assigned or defined calculation) two parameters of the four (L_c/R_{cp} ; R_3/R_{cp} ; β_m ; β_3) with the help of the grid of Fig. 2.13 two other parameters are

determined. Usually $\frac{R_3}{R_{cp}} = \sqrt{\frac{I_3}{I_{cp}}}$ (or which is the same, p_2/p_3^* , or M_3) and the angle of inclination of the contour on section β_3 . Typical values of β_3 for nozzles of a ZHRD are within 10-14°. Sometimes β_3 can be determined by the relation (2.23).

By knowing L_c , R_{cp} , β_m and β_3 the find point A_{11} , drawing at angle β_m a tangent to arc AA_{11} and point C - according to the known

L_c and R_3 . To construct a parabola we conduct from point C at angle β_3 straight line Cf up to the crossing with tangent $A_n f$. Dividing segments $A_n f$ and Cf into 5-7 parts and connecting the corresponding points 1, 2, 3, etc. by straight lines, we construct an enveloping parabola $A_n C$. Line $A A_n C$ will be the unknown contour of the supersonic part of the nozzle.



Fig. 2.14. Construction of the contour of the nozzle.

In the work [8] of V. D. Kurpatenkov there is given in detail a discussion of the method of constructing the contour of the nozzle.

Examples of Constructing a Contour of the Profiled Nozzle

Example 1. Find the profile of a high-altitude nozzle of an engine operating in a vacuum ($p_3 = 0$).

Pressure in the chamber $p_2 = 30 \text{ kgf/cm}^2$ (2.96 MN/m^2); area of the critical section $f_{*} = 100 \text{ cm}^2$; ($R_{*} = 56.4 \text{ mm}$); $\kappa = 1.2$; $R = 37 \text{ kgf}\cdot\text{m}\cdot\text{deg}$ ($360 \text{ J/kg}\cdot\text{deg}$); $T_2 = 3650^\circ\text{K}$.

Solution. Let us set the pressure on the section $p_3 = 0.075 \text{ kgf/cm}^2$ (7350 N/m^2).

1. Let us determine the area of the section of the nozzle f_3 and also speed w_3 and density of products of combustion on the section p_3 . According to formula (1.20) or the graph of Fig. 1.8.

$$\frac{f_2}{f_{op}} = \frac{\left(\frac{2}{\rho_{op}+1}\right)^{\frac{1}{\gamma-1}} \sqrt{\frac{\rho_{op}-1}{\rho_{op}+1}}}{\sqrt{\left(\frac{\rho_2}{\rho_1}\right)^{\frac{2}{\gamma}} - \left(\frac{\rho_2}{\rho_1}\right)^{\frac{2\gamma}{\gamma-1}}} - \frac{\left(\frac{2}{1.2+1}\right)^{\frac{1}{1.2-1}} \sqrt{\frac{1.2-1}{1.2+1}}}{\sqrt{\left(\frac{0.075}{20}\right)^{\frac{2}{1.2}} - \left(\frac{0.075}{20}\right)^{\frac{2.4}{1.2}}}} = 24.7;$$

$$f_2 = 24.7 f_{op} = 2170 \text{ cm}^2;$$

$$A_2 = 212 \text{ mm}; \quad A_2/R_{op} = 5.001.$$

$$c_2 = \sqrt{2g \left(\frac{\rho_2}{\rho_{op}-1}\right) \left[1 - \left(\frac{\rho_2}{\rho_1}\right)^{\frac{2\gamma-1}{\gamma}}\right]} =$$

$$= \sqrt{2 \cdot 9.81 \frac{1.2}{1.2-1} \cdot 27.3200 \left[1 - \left(\frac{0.075}{20}\right)^{\frac{2.4-1}{1.2}}\right]} = 2170 \text{ m/s}.$$

According to formula (1.23)

$$M_2 = \sqrt{\frac{2}{\rho_{op}-1} \left[\left(\frac{\rho_2}{\rho_1}\right)^{\frac{2\gamma-1}{\gamma}} - 1 \right]} = \sqrt{\frac{2}{1.2-1} \left[\left(\frac{0.075}{20}\right)^{\frac{2.4-1}{1.2}} - 1 \right]} = 4.14.$$

Let us define ρ_2 and ρ_3 :

$$\rho_2 = \frac{p_2}{gRT_2} = \frac{20 \cdot 10^4}{9.81 \cdot 27.3200} = 0.227 \text{ kg} \cdot \text{m}^3/\text{m}^3 \quad (2.23 \text{ kg/m}^3);$$

$$\rho_3 = \rho_2 \left(\frac{\rho_2}{\rho_1}\right)^{\frac{1}{\gamma}} = 0.227 \left(\frac{0.075}{20}\right)^{\frac{1}{1.2}} = 1.54 \cdot 10^{-3} \text{ kg} \cdot \text{m}^3/\text{m}^3 \quad (0.0151 \text{ kg/m}^3).$$

2. Let us determine the angle of inclination of the contour on the nozzle section β_3 , which provides the assigned p_3 and p_H the optimum contour of the nozzle. According to formula (2.23)

$$\sin \beta_3 = \frac{p_3 - p_2}{\frac{1}{2} \rho c^2} \sqrt{M_3^2 - 1} = \frac{0.075 \cdot 10^4 - 0}{\frac{1}{2} \cdot 1.54 \cdot 10^{-3} \cdot 2170^2} \sqrt{4.14^2 - 1} = 0.260,$$

whence $\beta_3 = 27^\circ 30'$; $\beta_2 = 17^\circ 15'$.

3. Knowing β_3 and R_3 and using graphs of Fig. 2.13, let us determine angle β_n and the length of the nozzle L_c :

$$\beta_n = 37^\circ 15'; \quad L_c = 12.4 R_3 = 600 \text{ mm}.$$

4. Let us determine the radii of curvature of the entry part of the nozzle:

$$R_{\text{exp}} = 1.5 R_{\text{sp}} = 1.5 \cdot 22.4 = 33.6 \text{ mm};$$

$$r_{\text{exp}} = 0.45 R_{\text{sp}} = 10.1 \text{ mm}.$$

5. According to β_m , β_3 and dimensions, let us determine the profile of the nozzle, approximating by the parabola the contour of the nozzle (see Fig. 2.15).

Example 2. Determine the profile of the chamber nozzle of an engine operating with the following parameters.

The pressure in the combustion chamber $p_2 = 60 \text{ kgf/cm}^2$ (5.92 MN/m^2); pressure on section $p_3 = 0.6 \text{ kgf/cm}^2$ (0.059 MN/m^2); area of critical section $f_{\text{sp}} = 100 \text{ cm}^2$, $R_{\text{sp}} = 22.4 \text{ mm}$; $n_{\text{ex}} = 1.2$; $R_2 = 37 \text{ kgf} \cdot \text{m/kg} \cdot \text{deg}$ ($363 \text{ J/kg} \cdot \text{deg}$); $T_2 = 3650^\circ \text{K}$.

Solution 1. Since the ambient pressure p_n is not assigned, we assume that the optimum contour of the nozzle providing the least losses of thrust to friction and dispersion will be at the value $\varphi_{\text{opt}} = 0.992$. We determine the value of β_3 , which corresponds to

$$\varphi_{\text{opt}} = \frac{1 + \cos \beta_3}{2} = 0.992,$$

whence $\beta_3 \approx 10^\circ$ (it would be possible simply to assign angle $\beta_3 = 10^\circ$).

2. According to formula (1.20) or the graph of Fig. 1.8, let us determine f_2/f_{sp} :

$$\frac{f_2}{f_{\text{sp}}} = \frac{\left(\frac{2}{1.2+1}\right)^{\frac{1}{1.2-1}} \sqrt{\frac{1.2-1}{1.2+1}}}{\left(\frac{0.6}{60}\right)^{\frac{1}{1.2}} \sqrt{1 - \left(\frac{0.6}{60}\right)^{\frac{1.2}{1.2}}}} = 11.86; \quad R_2/R_{\text{sp}} = 3.44; \quad R_2 = 194 \text{ mm}.$$

3. From the known R_2/R_{sp} and β_3 let us determine with the help of graphs of Fig. 2.13 β_m and L_c .

4. We construct the contour of the nozzle (Fig. 2.15).

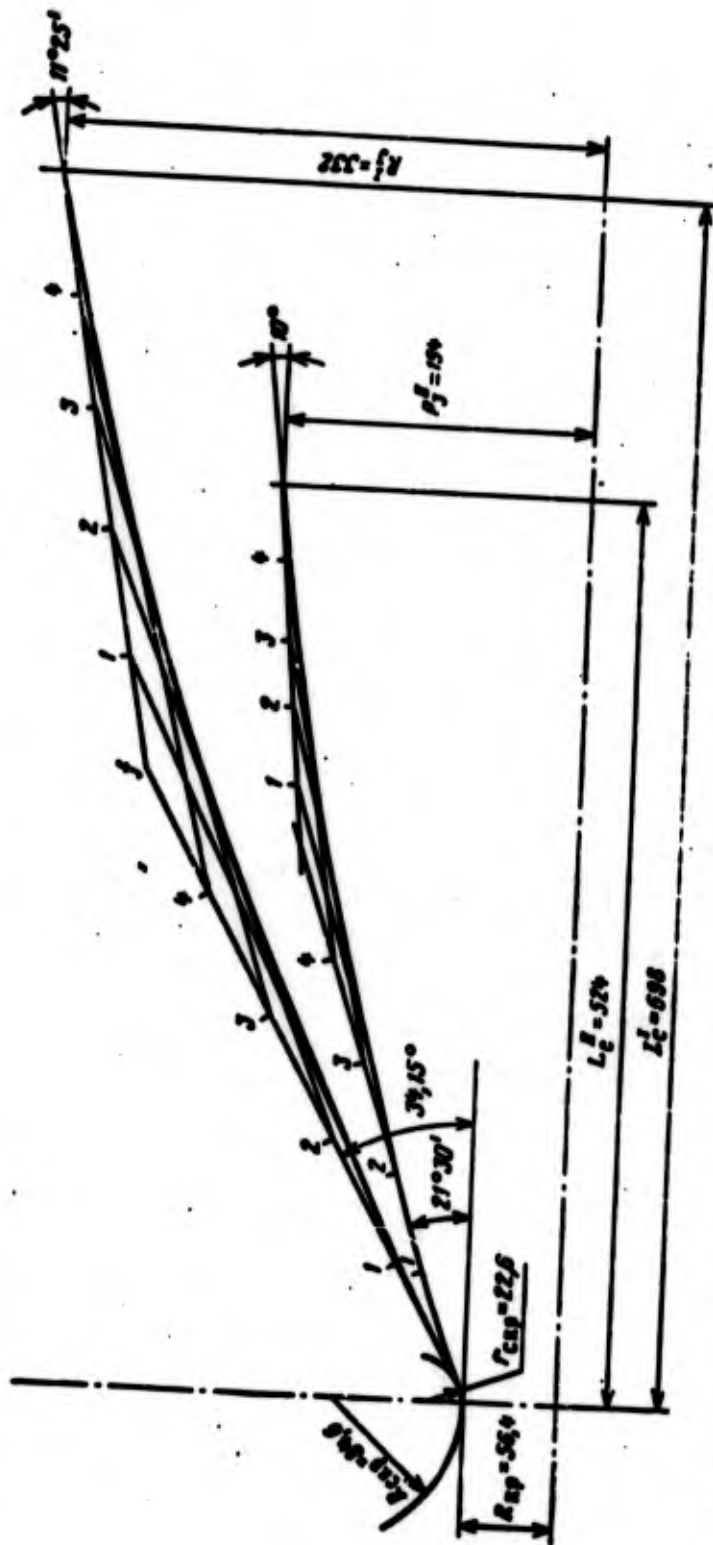


FIG. 2.15. Solution to the examples.

2.7. Operation of the Nozzle in Off-Design Conditions with High Counterpressures

It is known that with an excess of ambient pressure p_n over the design pressure on section p_3 the nozzle operates in conditions of overexpansion.

In practice gases are frequently possible when the rocket engine must operate considerable counterpressures of the environment 5-10 and more times exceeding the design pressure on section p_3 , as, for example, with the underwater launching of a rocket or with the operation near land of an engine designed for high-altitude operation. It was determined that with the operation of a ZhRD under conditions of high counterpressures, there occurs flow separation from walls of the nozzle (Fig. 2.16) and after the separation point a complicated system of shock waves appears. The intensity of the shock and place of flow separation to a considerable degree depend on the development of the boundary layer at the wall of the nozzle.



Fig. 2.16. Flow separation from wall at high counterpressures.

The typical pattern of the distribution of pressures along the nozzle with flow separation is shown on Fig. 2.17.

To determine the thrust of the ZhRD, it is important to know the section in which flow separation occurs in nozzle (i.e., the pressure at which separation occurs - p_{sep}).

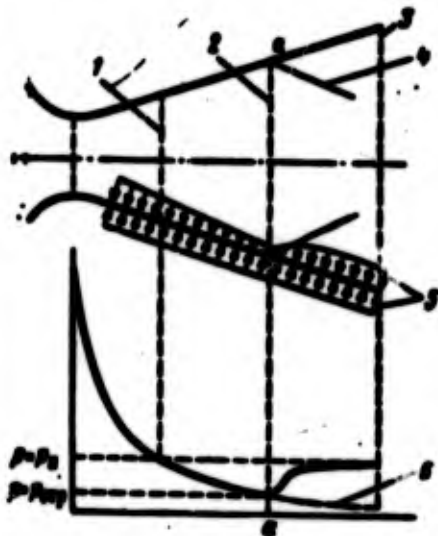


Fig. 2.17. Change in pressure in the nozzle with flow separation: 1 - reference plane; 2 - section of separation; 3 - nozzle section; 4 - oblique shock wave; 5 - pressure diagram; 6 - change in pressures with continuous flow.

Figure 2.18 gives experimental curves of the change in pressure p/p_{0exp} of the air flow depending upon quantity p_2^*/p_0 and the profile form of the nozzle [45].

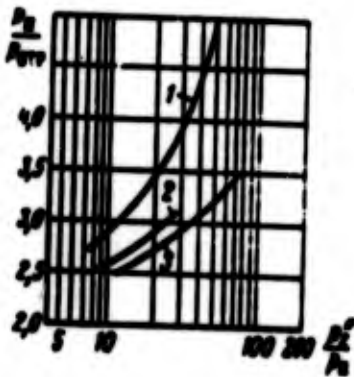


Fig. 2.18. Dependence of p_2/p_{0exp} on p_2^*/p_0 and the form of the nozzle with air flow: 1, 2 - profiled nozzles $\beta_3 < \beta_3$; 3 - conical nozzle $\beta_3 = 15^\circ$.

As can be seen from the given graphs, with the same ratio p_2^*/p_0 in nozzles having a smaller angle of inclination of the contour β_3 , flow separation occurs at large values of p_2/p_{0exp} i.e., with a decrease in angle β_3 great overexpansion of the flow in the nozzle is possible.

Qualitatively analogous dependences take place with flow through the nozzle of products of combustion of a liquid fuel rocket engine.

Figure 2.19 gives a curve of the dependence of the characteristic of flow separation with expansion on P_2^*/P_{2*} , obtained as a result of an analysis of the outflow of products of combustion of different fuels of a ZhRD through a conical nozzle with angle $2\beta_3 = 30^\circ$.

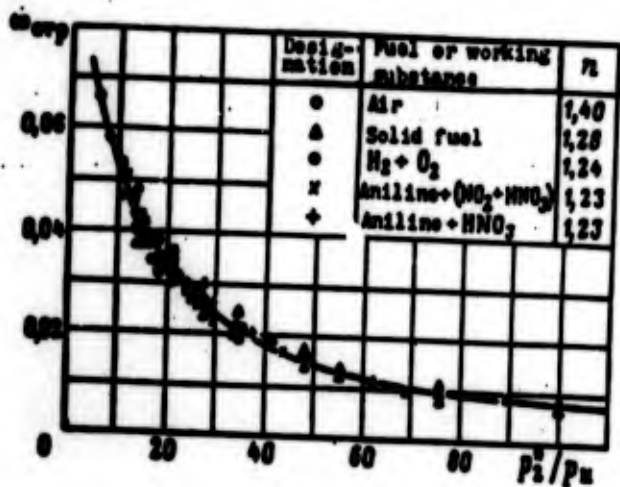


Fig. 2.19. Dependence on the ratio of pressure P_2^*/P_{2*} .

The characteristic of flow separation:

$$\alpha_{\text{sep}} = \frac{P_2 - P_{\text{sep}}}{P_2} \quad (2.25)$$

Knowing α_{sep} , the pressure of separation can be found:

$$\frac{P_{\text{sep}}}{P_2} = 1 - \alpha_{\text{sep}} \quad (2.26)$$

For profiled nozzles having a smaller angle than β_3 , quantity P_{sep}/P_{2*} apparently, will be somewhat smaller.

In the absence of special data expression (2.26) can be used for the determination of values P_{sep} in the nozzle of a ZhRD.¹

¹Investigations showed that considerable divergences between experimental and calculation data, obtained by α_{sep} frequently take place. Therefore, one should approach the use of α_{sep} with great caution.

With the known value of p_{0np} from elementary considerations we obtain the following formula of thrust of ZhRD:

$$P_{0np} = P_a + \Delta P(f_{0np} - f_a) \quad (2.27)$$

where P_a - thrust created by the part of the nozzle of the engine up to section a-a and determined by the usual thrust formula.

$$P_a = \frac{w_{0np}}{g} G + f_{0np}(p_{0np} - p_a) \quad (2.28)$$

where f_{0np} - area of section a-a; $\Delta P(f_{0np} - f_a)$ - force acting on the section of wall of the nozzle; it characterizes the difference in forces of external and internal pressure on the section of the nozzle a-3. Obviously, the direction of action of this force is opposite to the direction of the tractive force.

Here

$$\Delta P = \xi_0(p_a - p_{0np}) \quad (2.29)$$

Coefficient ξ_0 allows for the degree of restoration of pressure on the internal wall after the separation point. It should be estimated depending upon the length of section a-3. It is possible to consider approximately $\xi_0 = 0.1-0.5$. With an increase in the length of the wall of the nozzle after the separation point, the effect of the difference between the external and internal pressure in the environment of the point of separation is affected less and ξ_0 should be taken nearer to the lower limit.

In conclusion let us note that in determining the thrust of an engine in conditions of flow separation, the main question is the finding of the flow separation point a. The position of it depends on many factors, in the first place, on flow rate (M number), profile of the nozzle, fuel, and state of the surface of the nozzle. Although there has been conducted a large quantity of experimental

works by definition of the point of separation a strict analytic solution to the problem under assumptions acceptable under conditions of work of a ZhrD has not as yet been found.

2.8. Work and Characteristic of Nozzles with a Central Body

In section 2.1 the definition and basic diagrams of nozzles with a central body are given. Let us consider peculiarities of the operation of such nozzles.

Ring nozzles with a central body (see Fig. 2.1d). The throat of the nozzle has the form of a ring so that the gas flow is expanded in the annular channel formed by the contour of the central body and external contour. In ring nozzles just as in standard nozzles, the formation of the flow is determined by the contour of walls of the nozzle. Losses of thrust to dispersion in the annular nozzle formed by the conical internal and external contours can be determined by conducting calculations analogous to those examined above in section 2.2. The final expression of φ_{pac} for the ring nozzle has the form

$$\varphi_{pac} = \frac{\frac{1}{2} (\sin \alpha_c + \sin \beta)^2}{(\alpha_c + \beta) \sin \alpha_c + \cos \alpha_c - \cos \beta} \quad (2.30)$$

where α_c - angle of inclination of the internal contour of the nozzle, β - angle of inclination of the external contour of the nozzle. Obviously, when $\beta = \alpha_c = 0$ the ring nozzle will be turned into a round one, and from formula (2.30) we will obtain the formula of losses in a round nozzle (2.11). In article [48] the work of ring nozzles with two angle points is investigated, and it is shown that ring nozzles provide gain in the length of the nozzle.

Characteristics of the operation of ring nozzle essentially do not differ from characteristics of a round nozzle, and therefore,

subsequently, in speaking of nozzles with a central body we will imply only nozzles with a central body having a free limit of flow.

For a ZhRD nozzles with central body are of great interest, and diagrams of them are shown on Fig. 2.1e, f, and g.

In contrast to the standard supersonic nozzles, in which the flow is formed by walls of the nozzle, in nozzles with a central body the expansion of flow is not limited completely by solid walls.

In nozzles the diagram of which is shown on Fig. 2.1e and f the external boundary of the stream is a free surface. In plate nozzles (see Fig. 2.1g) the free surface is the internal boundary of stream.

Nozzle with External Expansion.

Let us examine the operation of a nozzle with a central body with a free external boundary of the stream (see Fig. 2.1e). A typical shadow photograph of a nozzle with a central body operating in design conditions is shown on Fig. 2.20a, and with an expansion ratio corresponding to conditions of overexpansion (in the concept accepted for standard nozzles), i.e., when $p_2^*/p_n < (p_2^*/p_n)_{\text{расч}}$ — on Fig. 2.20b.

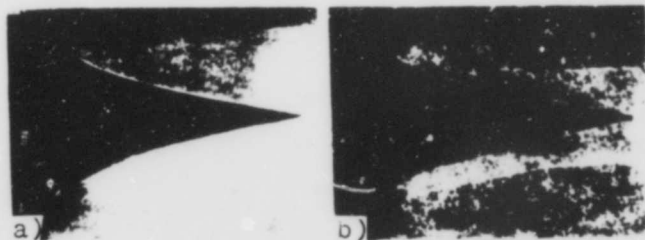


Fig. 2.20. Shadow photographs of the flow in a nozzle with central body: a) design operating conditions; b) ratio p_2^*/p_n is less than the design.

The expansion and acceleration of flow in the operation of a nozzle with a free external boundary of the stream occurs in the following way (Fig. 2.21a).

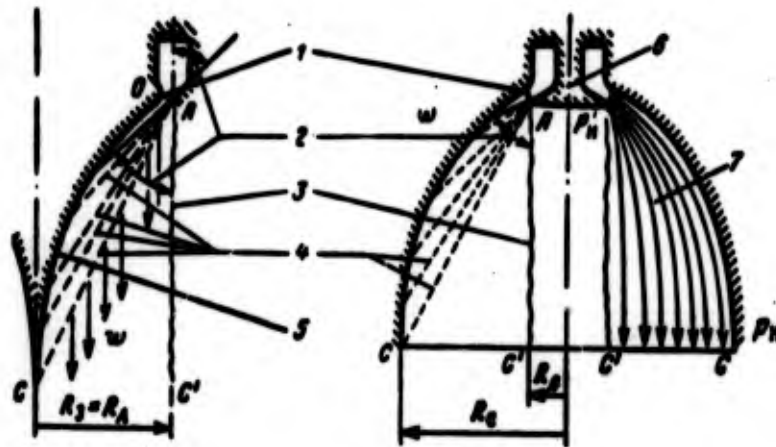


Fig. 2.21. Expansion of flow in a nozzle with a central body: a) nozzle with external expansion; b) plate nozzle, 1 - surface of critical speed; 2 - angle of rotation of the flow ω ; 3 - free surface of the flow; 4 - rarefaction wave; 5 - contour of the central body; 6 - plate central body; 7 - flow line.

The flow of products of combustion accelerates in the convergent ring nozzle up to a critical speed, which is reached in the annular section OA. For a nozzle with full external expansion, further expansion of the gas occurs with the flowing around of the extreme edge at point A where there appears a fan of rarefaction waves and in passing through which the flow accelerates up to speed w and turns at angle ω . Quantities w and ω are determined by the pressure drop p_3^*/p_n and for the plane flow by formulas (2.37) and (2.38).

With the operation of the nozzle in design conditions ($p_3 = p_n$) the external boundary of stream AC' is directed in parallel to the axis of the nozzle. The area of the outlet section f_3 is equal

to the area of a circle with radius $R_3 = R_A$. With an increase in the pressure ratio up to $(p_2^*/p_2)^* > (p_2^*/p_2)_{max}$ the nozzle operates in conditions of underexpansion. Here due to the increase in p_2^*/p_2 the angle of rotation of the flow α will be increased, and the external boundary of the flow will pass along AC" (Fig. 2.22). A change in pressure along the contour of the central body will occur just as in a standard round nozzle (i.e., in the case of a decrease in p_2 it will remain constant, and in the case of an increase in p_2 it will increase proportionally).

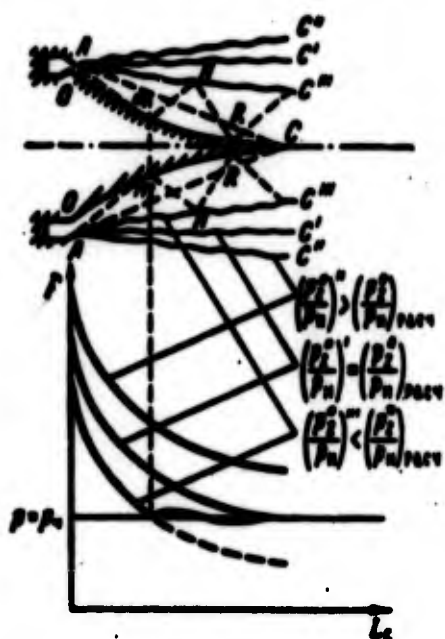


Fig. 2.22. Change in free surface of expansion and pressure along contour "OmC" under different operating conditions of nozzle.

The equation of thrust of a nozzle with a central body when operating in conditions of underexpansion will have the same form as that for a round nozzle:

$$P^* = \frac{G}{c} + f_2(p_2 - p_2) \quad (2.31)$$

The characteristic of the change in thrust of a nozzle with a central body when operating in conditions of underexpansion will coincide with the characteristic obtained for a standard nozzle (Fig. 2.23).



Fig. 2.23. Characteristic of the change in thrust for different types of nozzles: 1 - ideally variable-area nozzle; 2 - nozzle with a central body; 3 - round nozzle with flow separation; 4 - round nozzle without flow separation; 5 - design conditions.

With values of p_2^*/p_{2a} smaller than the design values, the flow in the nozzle with a central body is different from the flow in a standard nozzle: expansion on the edge at point A occurs only up to the ambient pressure p_a . The extreme rarefaction wave from point A enters into the contour OC at point m, and further expansion (overexpansion) up to pressures less than p_a , does not occur so that the external boundary of the flow formed by the external pressure will pass along the line AC''' (this is well evident on the shadow photograph of Fig. 2.20b). The expansion of flow along contour OC up to section m-m occurs just as in the standard nozzle, and the pressure at point m can be considered equal to the ambient pressure p_a . With the flow below point m along the contour mC flow turns and is somewhat compressed (as with the flowing around of a concave surface by supersonic flow). At point m (see Fig. 2.22) the rarefaction wave Am is reflected from the wall. The reflected shock wave mN at point N is again reflected from the external free boundary on the surface, and the rarefaction wave, entering into point R of the contour of the central body will again be reflected and so on. With passage through the shock wave mN the pressure is somewhat increased, in consequence of which on the section of the wall mR the pressure on the wall in general can even increase somewhat. Then with passage through the rarefaction wave NR the pressure again drops, and up to the line of the end of the nozzle CC'' the flow will pass consecutively through a system of several waves of rarefaction and compression. Therefore, below point m the pressure along contour mC can be considered constant and equal to the ambient pressure, as is shown on Fig. 2.22. Thus in conditions corresponding to conditions of overexpansion

for the standard nozzle with operation of a nozzle with a central body, overexpansion does not occur. The flow will be expanded only up to a pressure equal to the ambient pressure. The area of the outlet section of the flow with operation with $(p_2^*/p_n)^{**} < (p_2^*/p_n)_{\text{design}}$ will decrease and will be equal to the area of flow in section m-m.

The thrust of an engine having a nozzle with a central body operation at a pressure ratio $(p_2^*/p_n)^{**} < (p_2^*/p_n)_{\text{design}}$ will correspond to design conditions of an engine operating with expansion ratio $(p_2^*/p_n)^{**}$ i.e.,

$$P^* = \frac{w_{2m}}{g} G, \quad (2.32)$$

where w_{2m} - speed corresponding to the given ratio $(p_2^*/p_n)^{**}$.

Thus, with a decrease in the pressure ratio p_2^*/p_n lower than the design ratio, the thrust of an engine with a nozzle with a central body will correspond to the thrust of an engine with a round ideally variable-area nozzle. Therefore, nozzles with a central body with a free surface of expansion are frequently called self-adjusting nozzles.

The characteristic of the change in thrust of the nozzle with a central body with the operation with $(p_2^*/p_n)^{**} < (p_2^*/p_n)_{\text{design}}$ in accordance with equation (2.32) will pass higher than the characteristic of the standard nozzle, in which because of the overexpansion of flow the thrust will decrease sharply.

It is necessary to note that under off-design conditions of the operation of the engine with a nozzle with a central body, besides a change in speed (because of the change in p_2^*/p_n) there also occurs a deviation of the directions of motion of the flow from the axial. This leads to certain losses in thrust to dispersion, in consequence of which the characteristic of the nozzle with a central body will pass below the characteristic of a round ideally variable-area nozzle.

Nozzle with Partial Internal Expansion

Figure 2.1d gives a diagram of a nozzle with a central body with partial internal expansion. Such nozzles are an intermediate type between the ring nozzle and a nozzle with a central body and external expansion. The application of them is expedient in those cases when the nozzle with a central body should provide acceleration of flow up to high M numbers, i.e., with a large ratio p_2^*/p_n . The fact is that in a nozzle with full external expansion with an increase in p_2^*/p_n angle of rotation of the flow ω is increased. At values of p_2^*/p_n corresponding to values of M of the order of 3.6-4.2 (depending upon the index n_m), the angle of rotation of the flow reaches 90° and grows with a further increase in p_2^*/p_n (Fig. 2.24).

Since it is necessary to provide a sufficiently smooth acceleration of products of combustion up to the speed of sound, it is obvious that with an increase in the angle of rotation of the flow there will be an increase in the diameter of the annular combustion chamber, i.e., dimensions and weight of the entire engine. Therefore, at p_2^*/p_n for a decrease in the angle of rotation of the flow (and consequently, dimensions of the engine), it is expedient to use the preliminary expansion in the ring nozzle up to a certain speed M_0 ($1 < M_0 < M_0$).

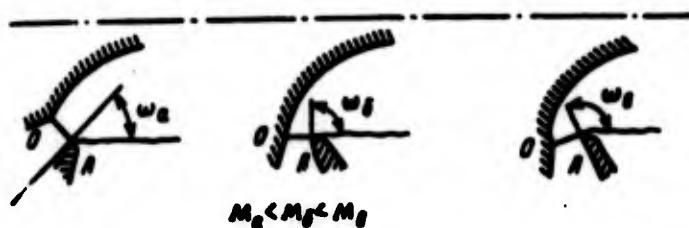


Fig. 2.24. Change in the angle of rotation of the flow and position of the surface of critical speed OA depending upon the M number.

Let us consider how the characteristic of the change in thrust for a nozzle with partial internal expansion will pass (Fig. 2.25).

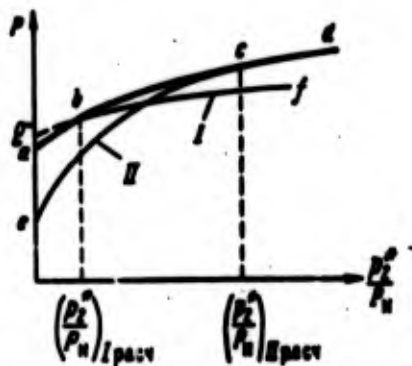


Fig. 2.25. Characteristic of a nozzle with incomplete internal expansion.

For a nozzle with a design relationship of pressures equal to $(p_2^*/p_n)_{II_{pacv}}$, the characteristic II with full internal expansion (standard round nozzle) will pass along curve ecd and with full external expansion — along $gbcd$. For a nozzle with full internal expansion designed on $(p_2^*/p_n)_{I_{pacv}}$, characteristic I will pass along curve abf . With the application of a nozzle with partial internal and further external expansion the change in thrust with an increase in p_2^*/p_n to $(p_2^*/p_n)_{I_{pacv}}$ will pass along characteristic I. However, with a further increase in p_2^*/p_n the nozzle will operate as a nozzle with external expansion, and the characteristic will pass along the line bcd .

Thus, curve $abcd$ will be the characteristic of the change in thrust of the nozzle with partial internal expansion.

Plate Nozzle

In a plate nozzle (see Fig. 2.1g, 2.21 and 2.26) the annular critical section of the nozzle is located nearer to the axis of the nozzle, which permits decreasing the dimensions of the combustion chamber. Products of combustion flow out from the throat, parting in a direction from the axis. With flow along the external contour of nozzle OC the flow turns in a direction along the axis. Gas expansion occurs with the flowing around of edge A of the plate central body. The free surface is the internal border of the flow whose contour is determined by pressure p_n' at the end of the plate of the central body. In general this pressure is somewhat less

than the ambient pressure p_n in connection with the ejection of flow from the central region of the nozzle.

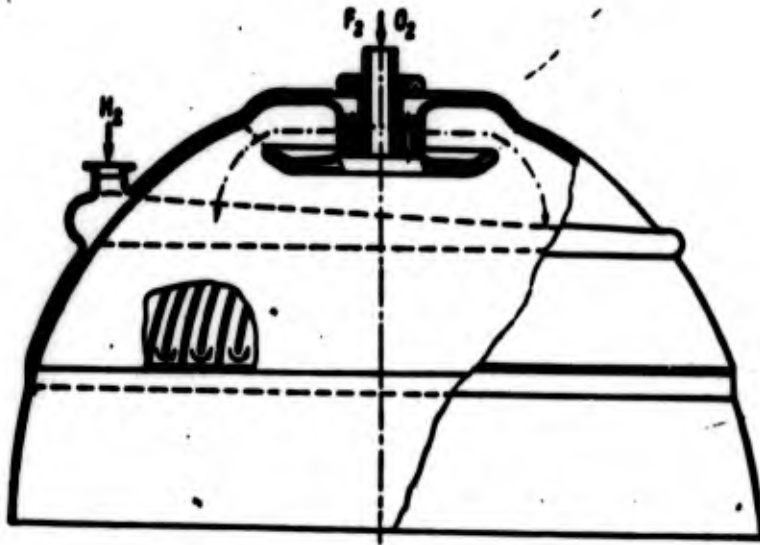


Fig. 2.26. Engine with a plate nozzle [55].

The area of the outlet section of the plate nozzle operating in design conditions is equal to

$$f_2 = \pi (R_2^2 - R_1^2). \quad (2.33)$$

Figure 2.27 shows the location of a free internal surface of flow in the plate nozzle for different relationships of p_2^*/p_n' : a) design relationship; b) underexpansion; c) conditions corresponding to conditions of overexpansion.

When $(p_2^*/p_n')^{**} < (p_2^*/p_n')_{\text{design}}$ just as in the case of the nozzle with a central body, on section mC the pressure on the wall of the nozzle with transition through the system of reflected waves can increase somewhat.

In contrast to the nozzle with a central body and external free surface in the plate nozzle in connection with the fact that $p_n' < p_n$

a certain overexpansion of flow at the wall of the nozzle up to pressure $p_2' < p_2$ is possible, i.e., in the plate nozzle a negative component of thrust owing to overexpansion can appear.

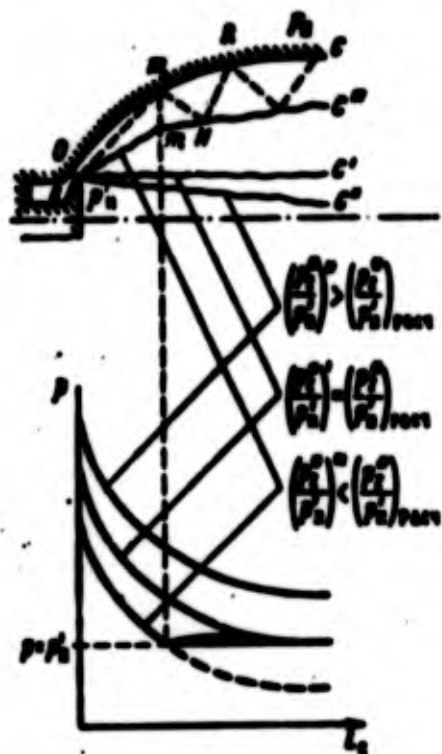


Fig. 2.27. Change in free surface of expansion and pressure along contour OmC under different operating conditions of the plate nozzle.

However, the magnitude of such overexpansion is small, and in the first approximation it is possible to assume that in the plate nozzle overexpansion is absent. In this case the characteristic of the change in thrust depending upon p_2'/p_2 for the plate nozzle, will be determined by the same equations as for the nozzle with a central body and will pass as is shown on Fig. 2.23.

2.9. Calculation of Nozzles with a Central Body

Let us examine the approximate method of the construction of a contour of nozzles with a central body. For simplification of calculation let us assume that the expansion of flow in a nozzle occurs just as with the Prandtl-Mayer plane flow. Therefore, in the calculation of the expansion of flow after edge A, we will consider the dependences obtained for the plane flow applicable.

The distance of edge A from the axis of the nozzle is equal to the radius of the outlet section R_3 and is determined by formula (1.21),

$$\frac{f_3}{f_{sp}} = \frac{1}{M_3} \sqrt{\left[\frac{2}{n_{33}+1} \left(1 + \frac{n_{33}-1}{2} M_3^2 \right) \right]^{\frac{n_{33}+1}{n_{33}-1}}}, \quad (2.35)$$

where

$$f_3 = \pi R_3^2 \quad (2.36)$$

and f_{sp} is determined by the relation (1.42).

To construct a contour of a central body OC, let us find the position of the arbitrary point B on the contour of the central body. Entering into point B will be the intermediate rarefaction wave AB. The flow rate w (or M) along the rarefaction wave (characteristic) AB is constant. The section of the flow f in which the speed is equal to w will be defined as the projection of the lateral surface of a frustum of a cone formed by the rotation of segment AB around the axis of the nozzle on the plane normal to the speed. The area of the section of flow f and angle α between the direction of flow and tangent AE are determined by relations

$$\frac{f}{f_{sp}} = \frac{1}{M} \sqrt{\left[\frac{2}{n_{33}+1} \left(1 + \frac{n_{33}-1}{2} M^2 \right) \right]^{\frac{n_{33}+1}{n_{33}-1}}}, \quad (2.37)$$

$$\alpha = \sqrt{\frac{n_{33}+1}{n_{33}-1}} \operatorname{arctg} \sqrt{\frac{n_{33}-1}{n_{33}+1} (M^2-1)} - \operatorname{arctg} \sqrt{M^2-1}. \quad (2.38)$$

Angle α between directions of characteristic AB and speed w (Mach angle) will be determined by the relation

$$\sin \alpha = \frac{1}{M}. \quad (2.39)$$

If R is the distance from point B to the axis, and length AB is equal to L , then

$$f = \pi L (R + R_3) \sin \alpha. \quad (2.40)$$

Designating ψ the angle between the direction of tangent A_3 and normal to the axis, from geometric relationships we can write

$$\begin{aligned} \alpha_3 &= 90^\circ - \psi; \\ \angle BAC' &= (\alpha - \omega) + \alpha_3 = \alpha - (\omega + \psi) + 90^\circ. \end{aligned} \quad (2.41)$$

Designating $\angle BAC' = \theta$, we obtain

$$\begin{aligned} \theta &= 90^\circ + \alpha - (\omega + \psi); \\ \angle DBA &= 90^\circ - \theta = -\alpha + (\omega + \psi). \end{aligned} \quad (2.42)$$

Since $BD = R_3 - R$, then

$$L = \frac{R_3 - R}{\cos [\alpha - (\omega + \psi)]}. \quad (2.43)$$

Substituting expressions (2.43) and (2.39) into equation (2.40), we obtain

$$f = \frac{\pi (R_3^2 - R^2)}{M \cos [\alpha - (\omega + \psi)]}. \quad (2.44)$$

whence, taking into account relation (2.36),

$$R = R_3 \sqrt{1 - \frac{f}{f_3} M \cos [\alpha - (\omega + \psi)]}. \quad (2.45)$$

Substituting equality (2.45) into formula (2.43), we obtain

$$L = \frac{R_3}{\cos [\alpha - (\omega + \psi)]} \left[1 - \sqrt{1 - \frac{f}{f_3} M \cos [\alpha - (\omega + \psi)]} \right]. \quad (2.46)$$

or

$$L = \frac{L}{R_0} = \frac{1}{\cos[\alpha - (\alpha + \psi)]} \left[1 - \sqrt{1 - \frac{f}{f_0} M \cos[\alpha - (\alpha + \psi)]} \right]. \quad (2.47)$$

Equations (2.42) and (2.47) are design equations for the construction of the contour of a central body.

The position of extreme points of the contour C and O can be determined immediately. At point C

$$\left. \begin{aligned} \alpha = \alpha_2; \quad M = M_2; \quad \alpha = \alpha_2; \quad f = f_2; \\ \cos[\alpha - (\alpha + \psi)] = \cos[\alpha_2 - (\alpha_2 + 90^\circ - \alpha_2)] = \sin \alpha_2. \end{aligned} \right\} \quad (2.48)$$

Substituting (2.48) into (2.42) and (2.47) we obtain

$$\theta_2 = \alpha_2; \quad L_2 = \frac{1}{\sin \alpha_2} = M_2. \quad (2.49)$$

At point O

$$\alpha = 0; \quad \alpha = 90^\circ; \quad M = 1; \quad f = f_{sp}. \quad (2.50)$$

Let us substitute equality (2.50) into expressions (2.42) and (2.47). Then

$$\left. \begin{aligned} \theta_{sp} = 180^\circ - \psi; \\ L_{sp} = \frac{1}{(\cos 90^\circ - \psi)} \left[1 - \sqrt{1 - \frac{f_{sp}}{f_0} \cos(90^\circ - \psi)} \right]; \\ L_{sp} = OA = L_{sp} R_0. \end{aligned} \right\} \quad (2.51)$$

To construct a contour of a central body having assigned a series of M values from $M = 1$ to $M = M_2$ it is convenient to reduce the calculations by definitions of θ and L to a table (see Table 2.3).

Shortened Nozzles with a Central Body

As a result of the calculation we obtain a contour of a central body of an ideal nozzle, i.e., a nozzle providing on the

section a flow which is uniform and parallel to the axis of the nozzle. Thus, just as in the case of round nozzles, an ideal nozzle with a central body has very great length. Therefore, here for a decrease in dimensions and weight it is expedient to use shortened nozzles. Experiments show that the shortening of a central body by means of replacement of the profiled contour of a cone leads to very small losses of thrust [55].

A comparison of profiles of the central body of an ideal and shortened nozzles, bounded by conical contours with different half-angles of opening of the cone, is given on Fig. 2.29a, from which it is clear that replacement of the end part of the contour by a cone with an angle of opening of $20-30^\circ$ permits decreasing the length of the nozzle by 40-60%.

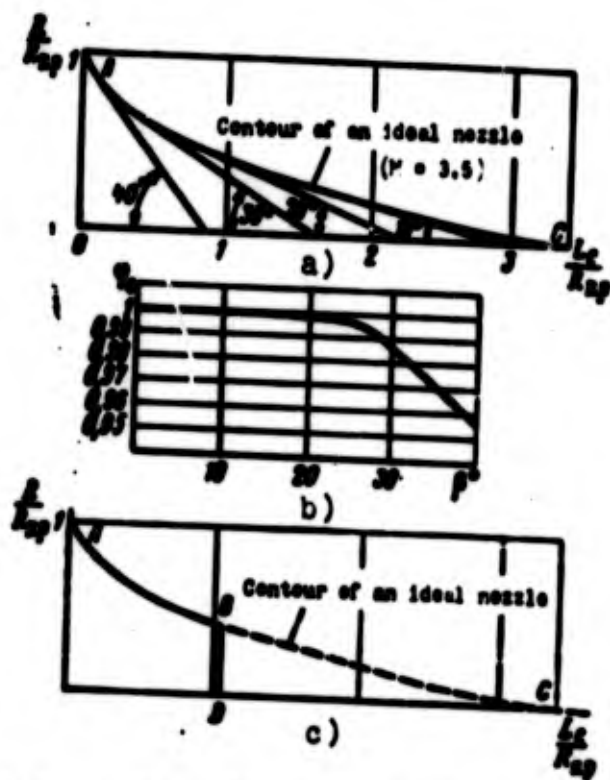


Fig. 2.29. Shortening of nozzles with a central body: a) replacement of part of the contour by a cone; b) change in ϕ_c depending upon the half-angle δ of the central body; c) segment of the part of the contour.

Figure 2.29b shows the change in the coefficient of the nozzle ϕ_c depending upon the half-angle β of opening of the cone. From the graph it is clear that even when $\beta = 30^\circ$ losses of thrust are about 1%.

The central body can be shortened also by cutting its end part and replacing contour ABC by contour ABD (Fig. 2.29c).

A shortened contour of the nozzle with a central body can also be constructed by solving the variational problem on the detecting of the optimum contour.

Calculation of Plate Nozzles

Having taken for the plate nozzle the assumption about the plane flow of gas with the flowing around of edge A, the aforementioned method can be used for an approximate calculation of the plate nozzle (Fig. 2.30).

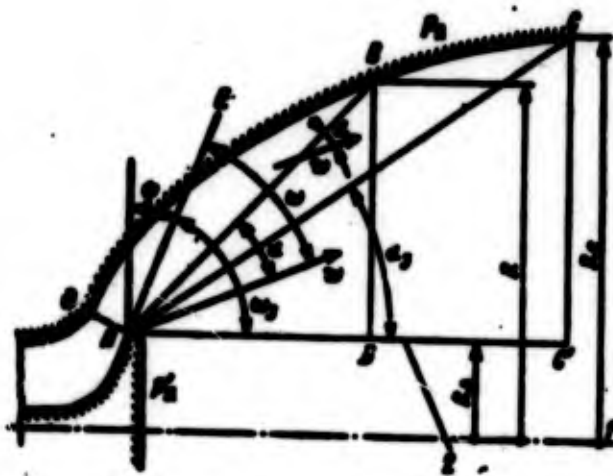


Fig. 2.30. Calculation of the contour of a plate nozzle: 1 - axis of the nozzle; 2 - free surface.

Initial data for the calculation of the plate nozzle are the same as in the calculation of a nozzle with external expansion.

Let us designate: R_A - radius of the plate central body from the axis to edge A (this radius is assigned from design considerations); R_c - radius of the contour of the nozzle section. Then

$$f_0 = \pi(R_c^2 - R_A^2). \quad (2.52)$$

For the arbitrary point B the contour of the nozzle area of the section of flow with speed w (or M) will be defined as the projection of the lateral surface of the frustum of a cone formed by the rotation of segment $AB = L$ around the axis on the surface normal to the direction of the flow rate w :

$$f = \pi L(R + R_A) \sin \alpha. \quad (2.53)$$

Since in this case relation (2.42) are real, then

$$L = \frac{R - R_A}{\cos[\alpha - (\alpha + \varphi)]}. \quad (2.54)$$

Substituting equalities (2.54) and (2.42) into expression (2.53), we will obtain

$$f = \frac{\pi(R^2 - R_A^2)}{M \cos[\alpha - (\alpha + \varphi)]}. \quad (2.55)$$

Whence

$$R = R_A \sqrt{1 + \frac{fM}{\pi R_A^2} \cos[\alpha - (\alpha + \varphi)]}. \quad (2.56)$$

Substituting equality (2.56) into expression (2.54), we will obtain:

$$L = \frac{R_A}{\cos[\alpha - (\alpha + \varphi)]} \left\{ \sqrt{1 + \frac{fM}{\pi R_A^2} \cos[\alpha - (\alpha + \varphi)]} - 1 \right\}; \quad (2.57)$$

$$Z = \frac{L}{R_A} = \frac{1}{\cos[\alpha - (\alpha + \varphi)]} \left\{ \sqrt{1 + \frac{fM}{\pi R_A^2} \cos[\alpha - (\alpha + \varphi)]} - 1 \right\}. \quad (2.58)$$

Example of the Calculation of a Nozzle with a Central Body

Determine the basic dimensions and contour of the central body of a nozzle with external expansion.

The pressure in the combustion chamber $p_2^* = 60 \text{ kgf/cm}^2$ (5.92 MN/m^2); the design ambient pressure $p_1 = p_0 = 0.40 \text{ kgf/cm}^2$ (0.048 MN/m^2); the temperature in the combustion chamber $T_2 = 3650^\circ\text{K}$; the index of the isentrope $n_{22} = 1.2$; the gas constant of products of combustion $R = 37 \text{ kgf}\cdot\text{m/kg}\cdot\text{deg}$ ($363 \text{ J/kg}\cdot\text{deg}$). The theoretical thrust of the engine $P = 10 \text{ T}$ ($9.81 \cdot 10^4 \text{ N}$). Losses are not considered.

Solution 1. By formula (1.23) we find the M_3 number of the flow:

$$M_3 = \sqrt{\frac{2}{n_{22}-1} \left[\left(\frac{p_2^*}{p_1} \right)^{\frac{2n_{22}-1}{n_{22}}} - 1 \right]} = \sqrt{\frac{2}{1.2-1} \left[\left(\frac{60}{0.40} \right)^{\frac{1.2-1}{1.2}} - 1 \right]} = 3.5.$$

2. We find f_{sup} :

$$\frac{f_1}{f_{sup}} = \frac{1}{M_3} \left(\frac{1 + \frac{n_{22}-1}{2} M_3^2}{\frac{n_{22}+1}{2}} \right)^{\frac{n_{22}+1}{2(n_{22}-1)}} = \frac{1}{3.5} \left(\frac{1 + \frac{1.2-1}{2} 3.5^2}{\frac{1.2+1}{2}} \right)^{\frac{1.2+1}{2(1.2-1)}} = 14.67.$$

3. The specific thrust P_{7a} and fuel consumption G :

$$P_{7a} = \frac{P}{S} = \frac{1}{S} \sqrt{2g \frac{n_{22}}{n_{22}-1} RT_2 \left[1 - \left(\frac{p_1}{p_2^*} \right)^{\frac{2n_{22}-1}{n_{22}}} \right]} =$$

$$= \frac{1}{0.81} \sqrt{2 \cdot 9.81 \cdot \frac{1.2}{1.2-1} \cdot 37 \cdot 3650 \left[1 - \left(\frac{0.40}{60} \right)^{\frac{1.2-1}{1.2}} \right]} = 273 \text{ kg}\cdot\text{s/kg} \text{ (2660 N}\cdot\text{s/kg)}$$

$$G = \frac{P}{P_{7a}} = \frac{10000}{273} = 36.6 \text{ kg/s}.$$

4. The complex β and area of critical section f_{sp} :

$$\beta = \frac{\sqrt{RT_3}}{A_3} = \frac{\sqrt{37 \cdot 3650}}{2.02} = 182;$$

$$f_{sp} = \frac{p_3}{\rho_3} = \frac{182 \cdot 26.6}{80 \cdot 10^4} = 112 \text{ cm}^2.$$

5. The area of section f_3 and radius R_3 :

$$f_3 = 14.67 f_{sp} = 1643 \text{ cm}^2; R_3 = \sqrt{\frac{f_3}{\pi}} = \sqrt{\frac{1643}{3.14}} = 229 \text{ mm}.$$

6. The angle of inclination of the external edge to the axis of the nozzle ω_3 and angle ψ :

$$\omega_3 = \sqrt{\frac{n_{33}+1}{n_{33}-1}} \operatorname{arctg} \sqrt{\frac{n_{33}-1}{n_{33}+1} (M_3^2-1)} - \operatorname{arctg} \sqrt{M_3^2-1} =$$

$$= \sqrt{\frac{1.2+1}{1.2-1}} \operatorname{arctg} \sqrt{\frac{1.2-1}{1.2+1} (3.5^2-1)} - \operatorname{arctg} \sqrt{3.5^2-1} = 77^\circ 26';$$

$$\psi = 90^\circ - \omega_3 = 12^\circ 34'.$$

7. Let us determine the contour of central body. For this by formulas (2.42) and (2.47) we find θ and L , which correspond to various values of M . Data of the calculation are given in Table 2.3. Here values ω and ψ , are determined or according to the available tables or graphs or by formulas (2.37) and (2.38). A constructed contour of the central body of an ideal nozzle is shown on Fig. 2.31, from which it is clear that its length was obtained long.

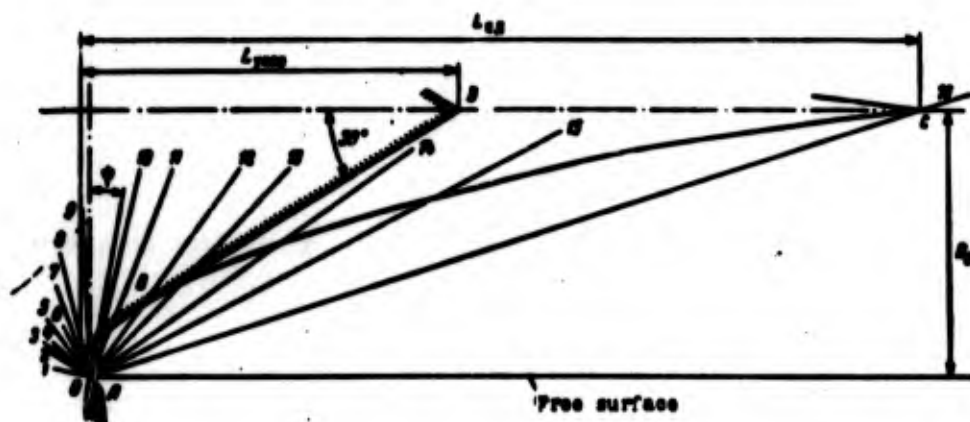


Fig. 2.31. Example of the construction of a contour of a central body.

For the shortening of the central body we replace part of the profiled contour by a cone with a half-angle of opening of the cone $\beta = 30^\circ$. Then the generatrix of the shortened central body will be line OBD, and the length of the shortened nozzle is 55% less than the length of the ideal nozzle of a central body.

Advantages and Deficiencies of Nozzles with a Central Body

Investigations of nozzles with a central body have begun relatively recently. Therefore, it is possible to conduct only a preliminary analysis of their basic possible advantages and deficiencies.

The basic merits of engines with a nozzle with a central body are the best characteristics of the change in thrust and smaller dimensions than for engines with a round nozzle. As was noted above, the reason for this is their ability of self-regulation in operating conditions corresponding to conditions of overexpansion in round nozzles.

The length of the engine with a shortened nozzle with a central body is considerably less than the length of the standard engine. Furthermore, the cavity of the central body can be used for the distribution in it of units of installation (for example, turbopump unit [TNA]) which also permits decreasing the dimensions. Figure 2.32 shows a model diagram of the distribution of units in the cavity of a central body, and a comparison of a ZhRD with a round nozzle and with a nozzle with a central body is given. The expected advantage of nozzles with a central body is the possibility of controlling the thrust vector by means of dividing the annular chamber into separate segments and changing the fuel consumption in each of the separate chambers. Incidentally, with this it is possible to expect that due to the dividing of annular chamber into chambers of smaller dimension, the probability of the appearance of vibration burning also will decrease.

Table 2.3.

1	M	1.05	1.07	1.1	1.12	1.2	1.3	1.4	1.5	1.7	2.0	2.2	2.5	2.7	3.0	3.2	3.5
2	$\sqrt{\frac{m_{sp}+1}{m_{sp}-1} \operatorname{arctg} \frac{m_{sp}-1}{m_{sp}+1} (M^2-1)} - \operatorname{arctg} \sqrt{M^2-1}$	0	0°22	1°22	4°6	6°08	10°12	13°27	20°44	31°28	37°28	48°34	54°51	63°43	68°19	77°25	
3	$\alpha = \arcsin \frac{1}{M}$	90°	72°15	68°22	58°23	50°17	43°26	41°48	38°2	30°	27°2	23°26	21°44	19°28	18°13	16°38	
4	$\alpha = (u+\psi)$	77°28	59°09	55°45	51°16	39°46	30°44	22°49	15°38	2°44	-14°2	-33°	-37°33	-45°41	-56°49	-63°40	-73°24
5	$\cos [a-(u+\psi)]$	0.2176	0.5127	0.5628	0.6257	0.7087	0.8085	0.9217	0.9830	0.9999	0.9702	0.9205	0.7946	0.6088	0.5473	0.4436	0.285
6	$\theta = 90^\circ + \alpha - (u+\psi)$	167°26	149°9	145°45	141°11	129°46	120°44	112°49	105°38	92°44	75°58	67°	52°27	41°19	33°11	26°20	16°36
7	f/f_{sp}	1.000	1.0021	1.0045	1.009	1.039	1.076	1.134	1.208	1.208	1.891	2.358	3.403	4.461	6.735	9.185	14.67
8	$\frac{f}{f_s} = \frac{f}{f_{sp}} \frac{f_{sp}}{f_s}$	0.0581	0.0683	0.0685	0.0688	0.0709	0.0734	0.0774	0.0825	0.086	0.1289	0.1605	0.2320	0.3040	0.4590	0.6260	1.000
9	$\frac{f}{f_s} M \cdot [5]$	0.0148	0.0349	0.0412	0.0473	0.0653	0.0820	0.1000	0.1190	0.1429	0.2503	0.3245	0.4610	0.5730	0.7550	0.8900	1.000
10	$1-[9]$	0.9852	0.9532	0.9589	0.9527	0.9347	0.9180	0.9000	0.8810	0.8371	0.7497	0.6755	0.5390	0.4270	0.2450	0.1100	0
11	$\sqrt{[10]}$	0.9925	0.9814	0.9792	0.9713	0.9740	0.958	0.949	0.9385	0.914	0.866	0.822	0.734	0.531	0.395	0.331	0
12	$1-[11]$	0.0075	0.0185	0.0208	0.024	0.033	0.042	0.051	0.0615	0.086	0.134	0.178	0.266	0.344	0.505	0.669	1
13	$Z = \frac{[12]}{[5]}$	0.0344	0.0362	0.0370	0.0383	0.043	0.0499	0.0630	0.0789	0.0961	0.138	0.1935	0.335	0.496	0.923	1.506	3.5
14	$L = LK_0 =$	7.08	8.3	8.47	8.79	9.85	11.4	12.9	14.6	19.7	31.6	44.4	76.7	111	212	315	803

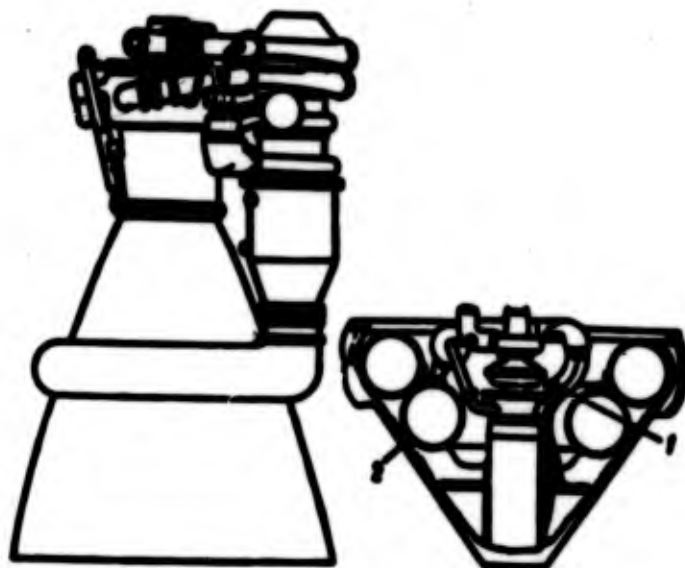


Fig. 2.32. Model diagram of the distribution of units in the cavity of a central body (shown on the left for comparison is a single-chamber engine of the same thrust): 1 - Turbopump unit; 2 - auxiliary tanks.

Of the deficiencies of nozzles with a central body, in the first place it is necessary to note the difficulty of organization of the cooling of engines with such a nozzle because of highly developed perimeter of the throat and complexity of feed of the coolant (see section 4.13). Difficulties of cooling somewhat decrease with the use of a plate nozzle.

In comparing plate nozzles with nozzles with external expansion, it is necessary to note as an advantage of plate nozzles the lesser effect of interferences from the side of the environment, which appear with movement of the rocket in the atmosphere. The weight of the engine with a plate nozzle on the whole somewhat decreases because of the considerable decrease in weight of the combustion chamber. However, as we noted above, because of the ejecting action of the flow in plate nozzle overexpansion up to $p_n' < p_n$ is possible, which leads to an impairment of thrust characteristics.

C H A P T E R III

CARBURETION AND CHAMBERS HEAD OF A ZhRD

The efficiency of the combustion chamber of a liquid fuel rocket engine [ZhRD] to a considerable degree depends on organizing the processes of carburetion and combustion, which in turn essentially depend on properties of the fuel and construction of the chamber head of the engine.

3.1. Basic Elements of Carburetion and Combustion Processes

Carburetion and Conversion of Fuel

Carburetion is defined as the complex of processes taking place from the moment of introduction of fuel components into the chamber to the formation of a uniform mixture. Thus, the process of carburetion is composed of the supplying of components to the chamber through injectors, breaking the streams into drops, evaporation, and mixing.

Process of carburetion should ensure:

1. Maximum combustion of components in the chamber.
2. The most homogeneous distribution of the proportion of components (i.e., α) and flow intensity r per chamber section (see section 5.1).
3. Minimum tendency to appearance of unstable burning.

4. Formation of a boundary layer necessary for shielding the walls of the chamber from high heat flow into the wall.

Conversion of fuel into products of combustion will be defined as the total process of the combined processes of carburetion and combustion of fuel.

Processes of conversion depending upon type of fuel (hypergolic or nonhypergolic) are schematically represented in Fig. 3.1.

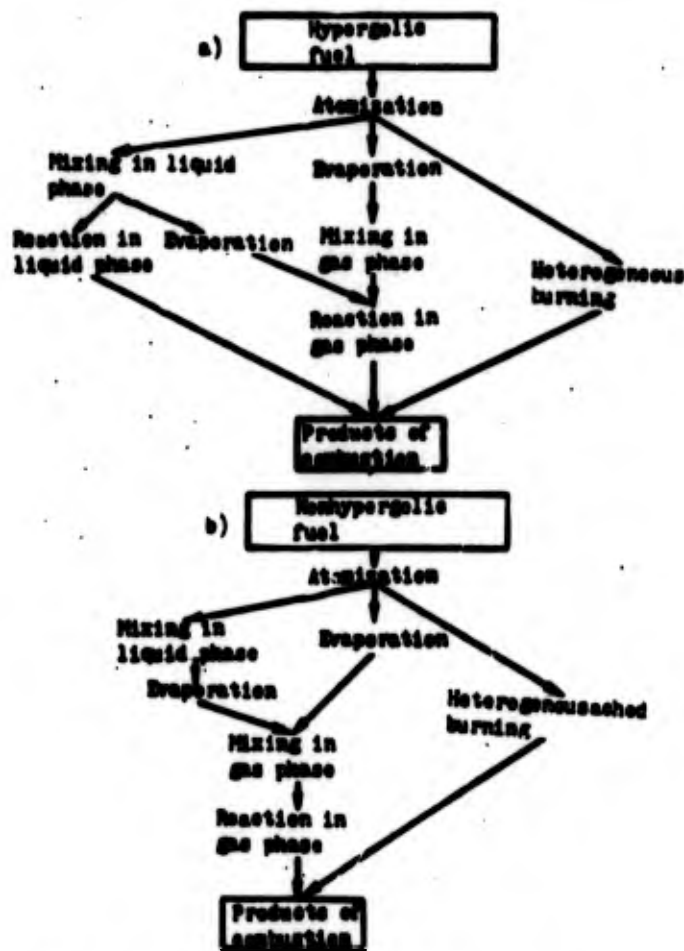


Fig. 3.1. Diagram of flow of conversion processes.

With hypergolic fuel, after atomization of the components, the process of combustion proceeds in three directions. Part of the fuel is evaporated prior to mixing in the liquid phase. After that mixing of components occurs in the gas phase and their combustion, which leads to formation of the products of combustion.

The second part of fuel is mixed in the liquid phase. In the contact between drops of fuel and the oxidizer the burning reaction starts directly in the liquid phase. In connection with the sharp increase of temperature during burning, part of the fuel, insufficiently mixed in the liquid phase, is evaporated without succeeding in entering into the reaction. Further mixing and combustion of this fuel occurs even in the gas phase.

Simultaneously with homogeneous, there can occur heterogeneous burning, i.e., burning of liquid drops of one of the components in gaseous vapors of the other. Such burning can take place in case of advance evaporation of one of the components or during formation of very large drops as a result of atomization which evaporate more slowly than small drops.

The burning reaction in the liquid phase is characteristic only for hypergolic components.

With nonhypergolic components, the reaction in the liquid phase does not appear, and the conversion process proceeds according to the diagram in Fig. 3.1b. After atomization of components their mixing occurs in the liquid phase. In so doing, preliminary mixing is possible (for example, in an air-boost system). Then there occurs evaporation of fuel components, their further mixing and reaction. Simultaneously there also takes place heterogeneous combustion of drops.

According to the flow of the processes determining the conversion process the combustion chamber of a liquid fuel rocket engine can be divided lengthwise into the following basic zones (Fig. 3.2):

I - atomization zone.

II - evaporation zone.

III - mixing and combustion zone.

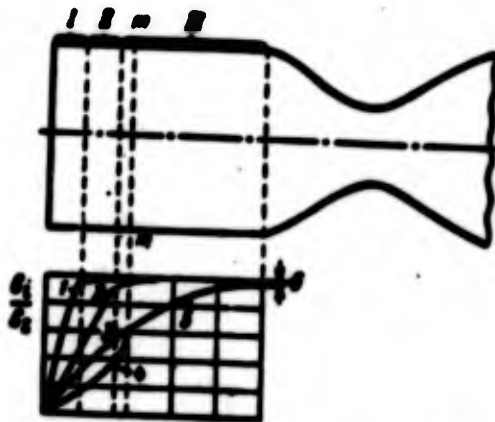


Fig. 3.2. Diagram of flow of processes in the combustion chamber: 1 - atomization; 2 - evaporation; 3 - mixing and burning; 4 - kinetic burning; 5 - diffusion burning; 6 - incompleteness of combustion.

It must be noted that division of the chamber into the zones mentioned is somewhat conventional since the processes of atomization, evaporation, mixing and combustion, do not go on in strict sequence, and it is impossible to say that evaporation starts only after full atomization, and after evaporation - mixing, etc. In each zone partially simultaneously two or three process take place. Thus, the name of the zone determines only the process most characteristic for it. Let us sort out the flow of processes in each of the zones.

Atomization

The basic indices characterizing the quality of atomization are fineness and homogeneity of atomization, and also the range of the stream and distribution of flow intensity along its section.

The quality of atomization of the fuel proceeding into the chamber determines the flow of further processes in the chamber - evaporation, mixing and combustion of fuel. The processes both in the fuelpassing system and injectors, and also in combustion chamber have an effect on the quality of atomization. The type of injectors (jet or centrifugal), the construction and their mutual location to a considerable degree predetermine the process of atomization of the fuel.

Disintegration of the stream into drops and splitting of drops occurs after exit of the stream from the injectors under the action of external and internal forces.

External forces (sometimes called aerodynamic) include forces of interaction of the component with the medium into which it is injected. The magnitude of these forces depends on environment, velocity of the stream, and dimensions of the drops of liquid. External forces also include the force of interaction during crossing of streams or during encounter of the stream with the hard wall. With an increase of velocity of the stream with respect to the medium in which injection occurs, the action of external forces grows, whereby disturbance of the surface of the stream grows, which leads to the most rapid splitting of the stream, and consequently also to improvement in the quality of atomization.

However, disintegration and splitting of the stream can occur in the absence of external forces. Thus, for example, during injection of a component in a vacuum, atomization occurs under the action of internal forces.

Internal forces include the action of turbulence and molecular forces. In a stream of a component emanating from the injector, turbulent pulsations of velocity appear; inside the stream, moles of liquid accomplish random motion. Intensity of the turbulence depends on pressure drop at the injector, density, viscosity, and also on the design of the injector. Increase of pressure drop (i.e., increase of exit velocity) promotes an increase in intensity of turbulence, in consequence of which splitting of the stream is accelerated, i.e., the quality of atomization is improved. Molecular forces — these are forces of viscosity and surface tension.

During exit of the stream from the injector, external forces and turbulent pulsations of velocity inside the stream strive to break up the stream (liquid sheet) on the other hand, the force of surface tension and force of viscosity prevent splitting. Thus, splitting of the stream and formation of drops occurs in the following manner.

During the injection of the component through the injector there will be formed a liquid stream (liquid sheet). Under the action of external forces and turbulent pulsations in the stream disturbance appears on the surface of the liquid. As a result of further action of external and internal forces on the component there will be formed a film of liquid and the stream (liquid sheet) breaks up into particles of different size and shape. Small particles under the action of surface tension take the shape of a sphere and will form drops; the large ones continue to disintegrate further (Fig. 3.3).

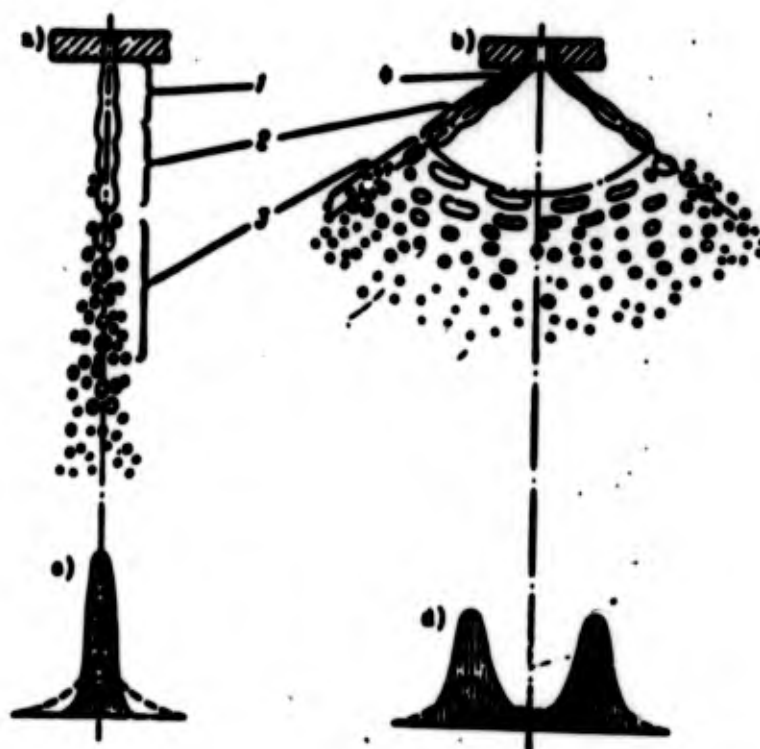


Fig. 3.3. Mechanism of disintegration of stream (liquid sheet): a) jet injector; b) swirler; c, d) distribution diagrams of flow intensity. 1 - stream; 2 - disturbance of surface and formation of connecting necks; 3 - splitting of streams (liquid sheets) into parts; 4 - liquid sheet.

Fineness of atomization is characterized by the size of the average diameter of the forming drops.

Homogeneity of atomization is characterized by the distribution curve of drops of a given diameter.

Fineness and homogeneity of atomization depend on properties of the component, design of the injector, and also on the parameters of operation of the combustion chamber in which injection is produced, and in the first place on the density of the products of combustion. With an increase in density of the medium, in which injection is produced and also with an increase of pressure drop at the injector, fineness of atomization is improved. For a liquid fuel rocket engine, the average diameter of a drop is within limits of 25-250 microns. It is interesting to note that for a diesel engine having considerably greater pressure drop at the injector, the average diameter of a drop is less and is within limits of 10-100 microns. Basic cause of this consists in the fact that in diesel engines injectors are set with considerably greater pressure drop Δp_{ϕ} than in a liquid fuel rocket engine.

The range of the stream (or depth of penetration) is determined by the exit velocity of the stream from the injector (i.e., pressure drop at the injector), direction and angle of atomization, and also density of medium in which atomization of components occurs. An increase of range is undesirable since it increases the dimensions of the atomization zone, and consequently also the dimensions of the combustion chamber.

Distribution of flow intensity of component over the cross section of stream is determined primarily by the type of injector.

Typical distribution diagrams of flow intensity for a jet and a swirler are shown in Fig. 3.3c, d. For a jet injector the peak of flow intensity at the axis of the injector is typical. For section of stream of a swirler the presence of two peaks a certain distance from axis is characteristic.

As the stream is removed from the nozzle of injector a certain smoothing of peaks occurs (dotted line on Fig. 3.3c). Usually it is assumed that flow intensity along the circumference of stream is constant, although in reality flow intensity is nonuniform.

Evaporation

The process of evaporation is an important stage in the preparation of fuel for ignition and combustion, since the basic quantity of fuel in the chamber of a ZhRD ignites and burns in the gas phase. On the reaction rate of the evaporation process strongly depends the total time elapsing to formation of the products of combustion. The complexity of the evaporation process in the chamber of a ZhRD is increased by the fact that here simultaneous evaporation of not one component occurs, but a complicated mixture of components with different physical chemistry properties. Thus the evaporation process should be completed after a very short interval of time on the order of 0.002-0.008 s [66]. The heat necessary for evaporation of drops in the chamber of ZhRD is supplied from the combustion zone primarily by means of convection heat radiation from reverse currents of hot gases. Reverse currents appear as a result of ejecting action of the stream of injected fuel. The stream of the component attracts to itself gases found in cavities between the streams. Into the zones of rarefaction thus formed new portions of hot products of combustion proceed (Fig. 3.4).



Fig. 3.4. Appearance of reverse currents.

Part of the heat is supplied to the drops by radiation from the core of the flame. Furthermore, the supply of heat occurs also by means of the combustion beginning in the evaporation zone.

The rate of heating and evaporation of drops, and consequently also the length of the evaporation zone depend on ambient temperature, dimension of the drops, relative velocity (to flow of gases) of movement of drops, and also on physical chemistry properties of the substance of the drop.

An increase in temperature of the medium accelerates the evaporation process; an increase of pressure, conversely, somewhat retards it. A decrease in dimension of a drop and increase in relative velocity of a drop leads to acceleration of evaporation.

For an illustration of the influence of the dimension of relative velocity and properties of a liquid let us examine the graph (Fig. 3.5, 3.6, 3.7). In Fig. 3.5 there are graphs of change along the length of the combustion chamber of temperature of drops of heptane of different dimension. We see that, with an increase in dimension of drops, the length of section of heating of a drop to boiling point grows. Thus, for a decrease of the evaporation zone it is desirable to have finer atomization.

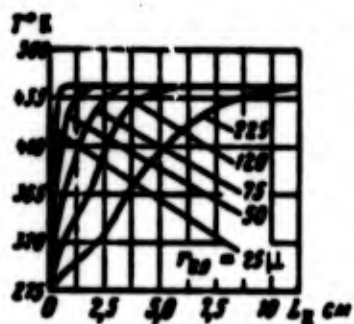


Fig. 3.5. Change in temperature of heptane drops of different dimension along the length of the combustion chamber.

In Fig. 3.6 there is shown the change in velocity of drop w_R and gas w_T along the length of the combustion chamber.

Velocity of drop w_R , in the beginning is delayed since there occurs deceleration of the drop in a gas medium having slower velocity w_T . As the rate of evaporation of the drop w_T grows, and with $L_R > 25$ mm exceeds the velocity of the drop. Now already the flow of gas

attracts the drop to itself, which leads to an increase in its velocity. Thus, the relative velocity of drop ($w_T - w_K$) initially grows. However, as the drop evaporates, in connection with the decrease in dimension of the drop and decrease due to this influence of forces of inertia on velocity w_K , relative velocity ($w_T - w_K$) again decreases. The quantity of evaporating liquid $G_{\text{исп}}$ at first grows slowly, but in a region of high relative velocities ($w_T - w_K$) there occurs strong growth of $G_{\text{исп}}$.

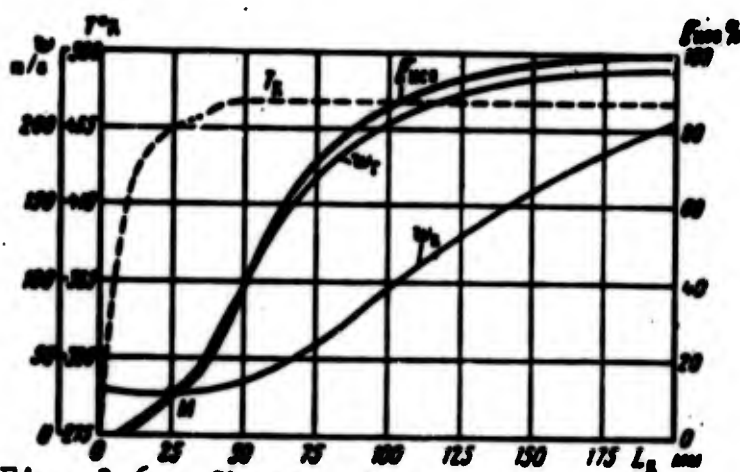


Fig. 3.6. Change of parameters of evaporated drop of heptane and velocity of gas along the length of the chamber.

The effect of physical properties on change of temperature of drop T_K is shown in Fig. 3.7a and on rate of evaporation - in Fig. 3.7b. We see that drops of low-boiling components O_2 and F_2 attain boiling point considerably quicker than drops of other components. In accordance with this, for evaporation of low-boiling components a smaller section of length of combustion chamber is necessary. Comparison of graphs 1 and 3, Fig. 3.7b shows also that rate of evaporation depends not only on boiling point, but also on heat of phase transition of liquid into vapor. At an assigned pressure of $p_2 = 21 \text{ kgf/cm}^2$ ($\sim 21 \text{ MN/m}^2$) the boiling point of heptane (curve 1) is higher than the boiling point of ammonia (curve 3). However, the heat of evaporation of heptane (52 kcal/kg) (217 kJ/kg) is considerably lower than the heat of evaporation of ammonia (269 kcal/kg) (1125 kJ/kg), and due to this, full evaporation of heptane occurs more rapidly, in spite of the higher boiling point.

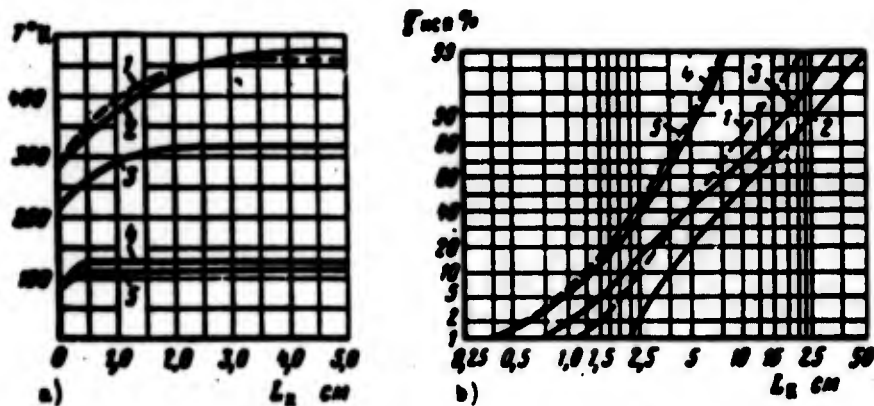


Fig. 3.7. Change of T_K and g_{MCH} of drops of different components: 1 -- heptane C_7H_{16} ; 2 -- hydrazine N_2H_4 ; 3 -- ammonia NH_3 ; 4 -- oxygen O_2 ; 5 -- fluorine F_2 .

We examined the effect of different factors on evaporation of a separate drop. In the process of evaporation in the combustion chamber of a ZhRD, as was indicated, there takes place simultaneous evaporation of a multicomponent mixture of drops of various dimensions. Thus the process of evaporation is essentially complicated as compared to the process of evaporation of individual drops. Irregularity of atomization leads at the beginning of evaporation to formation of a large quantity of vapors at the expense of rapid evaporation of fine drops. However, further evaporation of the remaining bigger drops is protracted and on the whole the period of evaporation of a mixture of drops of different dimension is greater than the period of evaporation of a drop of average dimension. The greater the irregularity of atomization, the more the period of evaporation of a mixture of drops is increased.

During evaporation of drops of multicomponent liquids which frequently takes place in a ZhRD, according to the evaporation in a drop concentration of the higher-boiling component is increased, which furthermore can lead to protraction of the process of evaporation.

Besides irregularity of atomization and the presence of multi-component drops of liquid, on rate of flow of the evaporation process of fuel during use of hypergolic fuels the presence of reactions in the liquid phase appearing in the zone of evaporation also has an effect. Heat thus released can significantly accelerate the evaporation process.

Mixing and combustion

As a result of atomization and evaporation a vapor of fuel and oxidizer will be formed, from which a fuel mixture is obtained. Mixing of fuel and oxidizer occurs both in the liquid and also in the vapor phase. The most desirable, but also very difficult to achieve in a ZhRD is a method of mixing - formation of a monopropellant or emulsion by means of complete preliminary mixing of components in the liquid phase just prior to introducing them into the combustion chamber. For a ZhRD, mixing of components in the actual combustion chamber is characteristic. Intensity of mixing of components is determined by turbulent diffusion.

The process of mixing the fuel components in the chamber of a ZhRD begins directly from the moment of their introduction into the combustion chamber and is finished only as the combustion of the fuel. In zones of atomization and evaporation there occurs mixing of part of the components both in the liquid and also in the gas phase. By means of flow of reactions of combustion directly in the liquid phase (with hypergolic components), and also by means of the intense supply of heat addition from the flame front (which also leads to the appearance of first sources of burning of the gas phase still in the zone of evaporation) process of mixing in these zones is considerably intensified. However, due to irregularity of atomization and different rate of evaporation of components, the process of mixing is not completed in these zones, but continues further in the zone of mixing and combustion. Consequently, part of the fuel enters this zone after evaporation and mixing, i.e., in a form completely prepared for combustion of a mixture in which the reaction of combustion already has partially begun. During combustion of this part of fuel, formation of the flame front begins.

The remaining fuel (a large part) enters the zone of mixing and combustion basically in an evaporated form, but still insufficiently mixed for combustion (even introduction of separate liquid drops of components is possible). Further mixing of this part of the fuel occurs. Owing to the great difference between the temperatures of the flame and the entering components, the intensity of mixing in this zone is very great. Simultaneously in zone of mixing and combustion there occurs combustion of the fuel already mixed. Due to such "parallel" flow of the processes of mixing and combustion, the flame front in the combustion chamber of a ZhRD is not any clearly outlined surface separating the prepared fuel mixture from products of combustion. Width of the flame front is determined by fineness and homogeneity of atomization, volatility of fuel components, and intensity of turbulent diffusion determining, in turn, the rate of flow of the mixing processes.

The process of combustion of the atomized fuel can be divided schematically in two: mixing of components and chemical reaction.

Rate of flow of the reaction is determined by temperature and activation energy. At low temperatures, chemical reaction rate is relatively low and less than the speed of mixing of components. Rate of flow of the burning process, on the whole is thus determined by rate of the chemical reactions. Such burning, whereby the speed of the process is limited by the chemical reaction rate, is called kinetic burning.

In the combustion chamber of a ZhRD kinetic burning can take place only in the very beginning of the zone of mixing and combustion, where the temperature is still comparatively low. Let us limit this region of the zone of mixing and combustion to the section m-m (see Fig. 3.2) and call it the region of kinetic burning. After section m-m high temperature is developed. Here already the chemical reactions flow practically instantly. Thus the rate of the burning process is determined by rate of mixing. Such burning, with which the rate of the process is limited by the rate of the mixing process, is called diffusion burning. Therefore, the region after section m-m we will call the region of diffusion burning. In the combustion chamber of a

ZhRD, the region of kinetic burning is very small and diffusion burning plays a decisive role. Therefore, it is frequently assumed that, on the whole, diffusion burning takes place in the chamber of a ZhRD.

In Fig. 3.2 the graph of change of quantity of burning fuel along the length of the combustion chamber does not reach a value of $G_1/G_\Sigma = 1$. It is obvious that the value G_1/G_Σ determines by itself the degree of physical combustion efficiency. Accordingly difference $1 - (G_1/G_\Sigma)$ characterizes incompleteness of combustion. For a ZhRD combustion efficiency $\varphi_{CR} = 0.95-0.99$.

Curve and conversion and time of stay

The degree of completeness of conversion of fuel into products of combustion is customarily estimated by the change of combustion efficiency along the length of the combustion chamber or in the time elapsing from the moment of introduction of components into the chamber. The curve characterizing change of combustion efficiency along the length of the chamber or in time is called the fuel conversion curve (burnout curve). Sometimes the conversion curve is constructed in the form of change of temperature or specific volume of the mixture of components (fuel or products of combustion) along the length of the chamber or in time.

An example of a conversion curve is shown in Fig. 3.8a, where there is given a typical qualitative dependence of change of specific volume along the length of the combustion chamber. Specific volume v_2 corresponds to calculated specific volume with full combustion. The conversion curve does not reach v_2 , which is a result of incompleteness of combustion. Within the limits of tolerated incompleteness of combustion point 2 corresponds to completion of process of conversion. In Fig. 3.8b there is given a conversion curve showing change of specific volume in time. Time τ_{np} elapsing from the moment of introduction of fuel into the combustion chamber to completion of the conversion process is called conversion time.

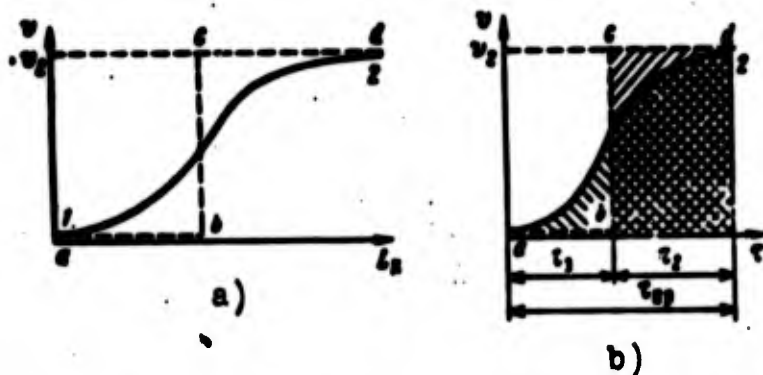


Fig. 3.8. Conversion curves: a) along the length of the chamber. b) in time.

It is obvious that the volume of the combustion chamber should be such that time of stay of the admitted components will equal the conversion time. With a smaller volume combustion efficiency will worsen, increase of volume is inexpedient, since it will lead to an increase in dimensions and weight of the chamber without essential improvement of combustion efficiency.

Time of stay of fuel and products of combustion in the chamber

$$\tau = \frac{V_K}{G v_{cp}}, \quad (3.1)$$

where V_K - volume of the combustion chamber; G - fuel consumption; v_{cp} - average specific volume of fuel and products of combustion.

If conversion time is equal to time of stay, the value of average specific volume can be determined as the average for time of stay, i.e.,

$$v_{cp} = \frac{\int_0^{\tau} x v dx}{\tau}. \quad (3.2)$$

Since the value v_{cp} is difficult to determine immediately then for appraisal of time of stay usually there is used certain conditional time of stay referred to specific volume of products of full combustion v_2 (with a given ratio of components):

$$\tau_{\text{cond}} = \frac{V_K}{G v_2}. \quad (3.3)$$

For simplification of analysis frequently the conversion curve conditionally is replaced by broken line abcd (Fig. 3.8b), i.e., it is assumed that the process of conversion occurs instantly at the time τ_3 . The location of the position of the vertical line of instantaneous conversion bc is determined from the condition of equality of area under the conversion curve 1-2 and the area under section cd. Thus, conversion time is split into two components:

$$\tau_{np} = \tau_1 + \tau_2 \quad (3.4)$$

where τ_3 delay time of conversion. Time τ_2 according to condition of construction of broken line abcd is determined from the equation

$$\int_0^{\tau_2} \tau d\tau = \tau_3 \tau_2 \quad (3.5)$$

whence by formula (3.2), considering that $\tau = \tau_{np}$,

$$\tau_2 = \frac{\tau_{np}^2}{\tau_3} \quad (3.6)$$

Comparing expressions (3.6), (3.1), and (3.3), we will obtain $\tau_2 = \tau_{yca}$. Putting $\tau = \tau_{np}$ and $\tau_2 = \tau_{yca}$ in expression (3.4), we obtain

$$\tau = \tau_1 + \tau_{yca} \quad (3.7)$$

i.e., time of stay in the combustion chamber can be presented as the sum of delay time of conversion and conditional time of stay.

Delay time of conversion τ_3 depends on the kind of fuel, design parameters of the mixing devices, and on parameters of operation of the combustion chamber.

During operation of the chamber of a ZhRD in a steady state, delay time of conversion is determined primarily by temperature in the combustion chamber, and also by conditions of atomization and heat supply to the injected fuel.

Value of conditional time of stay τ_{ycg} is one and a half times less than actual. For chambers of a ZhRD, value τ_{ycg} is within limits of 0.0015-0.005 s. Conditional time of stay (or simply time of stay) is an important parameter of the combustion chamber and is used for determination of its volume (see section 5.2).

The process of conversion in the combustion chamber of a ZhRD is characterized by intense heat emission. Heat release rate of the volume of the combustion chamber of a ZhRD is 100 times higher than the heat release rate of a boiler furnace and 10 times higher than the heat release rate of the chamber of a jet engine.

As a result, in the combustion chamber of a ZhRD there takes place an intense heat supply to the admitted fuel, which leads to considerable reduction in time of evaporation and the entire time of carburation and ensures rapid evaporation of even comparatively large drops of fuel.

In connection with this, fineness of atomization in a ZhRD has less effect on fullness of conversion than in ordinary thermal machines. This permits producing atomization of fuel with comparatively small pressure drops at the injectors 3-15 kgf/cm² (0.29-1.47 MN/m²) as opposed to 50-100 kgf/cm² (4.95-9.81 MN/m²) in jet engine and 200-1000 kgf/cm² (19.62-98.1 MN/m²) in diesel engines. Decrease in pressure drop at the injectors up to 3-15 kgf/cm² (0.29-1.47 MN/m²) permits decreasing power, and consequently also the weight of the supply system.

3.2 Spray Injectors

Fuel supply to the combustion chamber is carried out by injectors. The basic requirement for injectors is to ensure the finest possible and most uniform spray of fuel with sufficiently low pressure drop at the injector.

Usually in a ZhRD there are two separate basic forms of injectors: spray and centrifugal. There are also cases of application of slot injectors which can be considered as a variety of jet injectors

having not a round, but a slot-like form of outlet. Injectors are possible which combine both forms of injectors.

The spray injector consists of a hole in the head of the engine chamber connecting the fuel or oxidizer cavity with the combustion chamber. Different forms of spray injectors are shown schematically in Fig. 3.9.

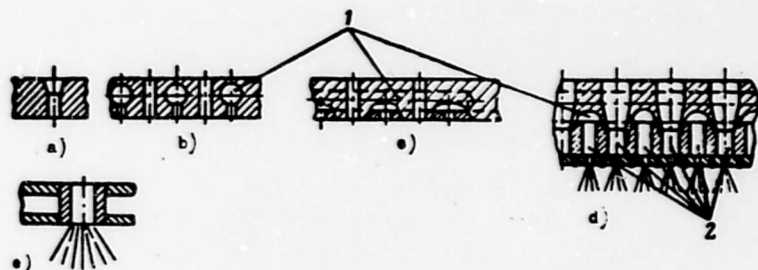


Fig. 3.9. Spray injectors: 1 - drillings for supply of components; 2 - concentric annular channels.

Basic advantages of spray injectors are first, simplicity of manufacture and secondly, the great carrying capacity of the head with the spray injectors.

Carrying capacity of the head we will call the quantity of fuel passed through a unit of surface of the bottom of the head under a specified pressure drop.

A spray injector occupies less space than a centrifugal. This permits placing a greater number of spray injectors on a unit of surface of head. Furthermore, discharge coefficient of spray injectors is 2.5-3 times greater than the discharge coefficient of swirlers.

As a result, with the same pressure drop, spray injectors permit ensuring a large flow rate through a unit of the surface of the bottom of the head, i.e., they have great carrying capacity.

However, a major deficiency of spray injectors is their relatively large range and small angle of atomization ($10-20^\circ$); fineness of

atomization of jet injectors is less than that of centrifugal. Furthermore, due to the channels for supply of the component to the spray injectors, the head frequently is made relatively heavy (Fig. 3.9b, c, d).

A larger angle of atomization and better splitting of drops can be obtained if the injectors are set in such a manner that their sprays cross (for injectors with crossing sprays, see Fig. 3.12). Thus, as a result of collision of components there occurs splitting of drops, and the angle of atomization is increased up to 60-100°, but the passing ability of such injectors decreases somewhat. A block of injectors with crossing sprays can consist of two, three, and even four spray injectors. In Fig. 3.24, 3.25, 3.27 there are diagrams and photographs of various heads with spray injectors.

Design of Spray Injectors

Spray injector are designed on the basis of the following considerations. As is known, theoretical exit velocity of an incompressible liquid from an opening

$$w = \sqrt{2g \frac{\Delta p_0}{\gamma}}, \quad (3.8)$$

where $\Delta p_0 = (p_0 - p)$ - pressure drop, γ - density of the liquid.

Flow rate of a liquid through an injector is determined by the equation of flow rate

$$G_0 = \mu f_c w / \gamma. \quad (3.9)$$

where f_c - area of cross section of hole in m^2 ; μ - discharge coefficient, considering narrowing of the spray and decrease of actual flow rate as compared to theoretical.

Substituting in equation (3.9) the value w from equality (3.8), we will obtain

$$G_0 = \mu f_c \sqrt{2g \Delta p_0} / \gamma. \quad (3.10)$$

from which

$$l_c = \frac{Q}{n \cdot v} \quad (3.11)$$

Flow rate of a component through one injector Q_p can be determined, knowing the full flow rate of the component and number of injectors n . If it is assumed that flow rate through all the injectors is identical, then

$$Q_p = \frac{Q}{n} \quad (3.12)$$

However, practically rarely does it occur that all the injectors of components have identical flow rate. Usually there are several groups of injectors of one component with various flow rate, and sometimes various construction.

Density of the component is known. Pressure drop at the injector Δp_p is usually given within limits of 3-15 kgf/cm² (0.29-4.7 MN/m²); to create a large pressure drop is unprofitable since this requires accordingly a large supply pressure. Decrease Δp_p below 3 kgf/cm² is irrational since besides it strongly worsens atomization and carburation, and also increases the possibility of appearance of low-frequency oscillations.

Discharge coefficient μ is assigned in accordance with the dimensions of the drilling of the spray injector.

When $l_c/d_c = 0.5-1$ flow rate decreases by means of narrowing of the spray. In this case (Fig. 3.10a) $\mu = 0.60-0.65$. When $l_c/d_c = 2-3$ narrowing of the spray also occurs, but pressure in the narrow section 1-1 (Fig. 3.10b) due to negative pressure is less than in the first case, therefore velocity along the narrow section is higher. Thus flow rate of the liquid increases in spite of the narrowing of the spray. Therefore when $l_c/d_c = 2-3$, value of the discharge coefficient is higher and amounts to $\mu = 0.75-0.85$. Using an injector with large l_c/d_c ratio is inexpedient since thereby there will be increased loss due to friction. Besides, the ratio l_c/d_c ,

although to a lesser degree, still a number of factors have an effect on discharge coefficient μ :

a) geometry of the injectors; beveling or rounding of the inlet edges increases the value of μ ;

b) pressure drop at the injector Δp_{ϕ} ; with growth of Δp_{ϕ} there can occur separation of flow from the walls of the nozzle of the injector, which with a given geometry will lead to worsening μ . In Fig. 3.11 there is an example of the dependence of μ on Δp_{ϕ} with various geometry of the injector, from which it is evident that with very slight beveling or absence of it in the region $\Delta p_{\phi} = 2-3 \text{ kgf/cm}^2$ ($0.19-0.29 \text{ MN/m}^2$) μ sharply drops as a result of separation of flow from the walls due to poor exit conditions. Increasing the depth of face e permits avoiding breakaway in a large range of Δp_{ϕ} ;

c) temperature of component. With temperature rise the value of drop Δp_{ϕ} with which separation of flow from walls can occur drops;

d) pressure in chamber p_2 (counterpressure). Decrease of counterpressure to $5-6 \text{ kgf/cm}^2$ ($0.49-0.58 \text{ MN/m}^2$) can lead to breakaway of the spray from the walls, and consequently also to a decrease of value of μ ;

e) quality of surface of the opening. Various burrs on the edges and much roughness of walls of the opening can lead to considerable reduction of μ .

Beforehand it is impossible to exactly consider the effect of all these factors, therefore during adjustment of construction there always are conducted hydraulic channels for more precise definition of parameters of the injectors. The diameter of the openings of injectors for liquid d_c is usually made within limits of 0.8-2.5 mm.

With a diameter of drilling less than 0.8 mm the openings are easily obstructed. When $d_c \geq 2.5 \text{ mm}$, atomization of the component worsens, since the stream of the component is made too powerful and breaks up into drops poorly.

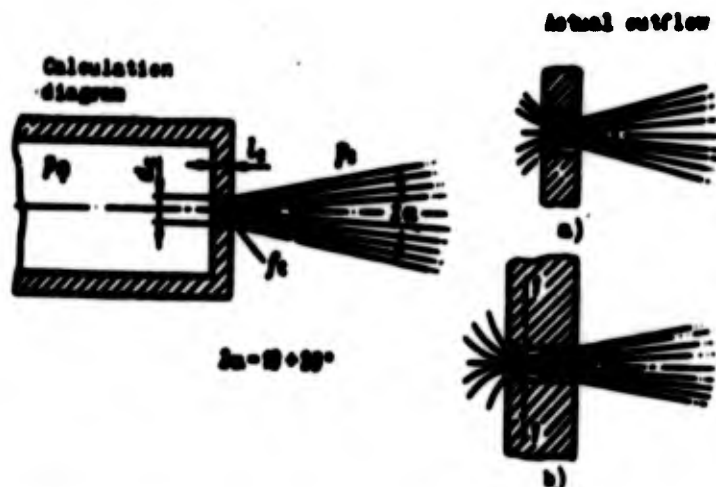


Fig. 3.10. Outflow of component from spray injector.

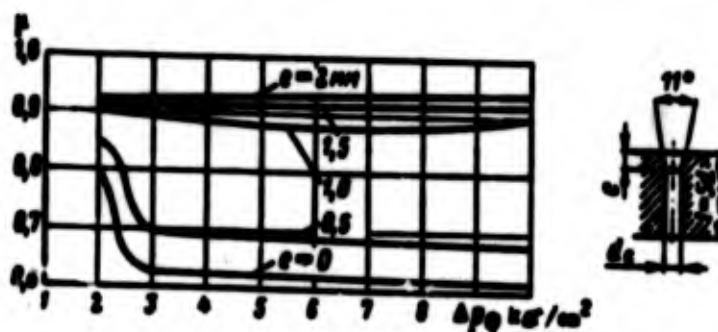


Fig. 3.11. Dependence of μ on Δp_ϕ and on shape of the injector.

Jet Injectors for Generating Gas

During operation of the propulsion system according to a closed diagram (see Chap. VIII) part of the fuel burns in a gas generator. The forming products of combustion are used to drive the turbine of a turbopump unit and then enter the combustion chamber at high temperature ($800-1000^\circ\text{C}$). For supplying these gases to the chamber it is expedient to use spray injectors (see Fig. 3.9e). Initially, for calculation of these injectors there will be the equation of flow rate

$$G_0 = \rho_0 f_0 \gamma_{\text{max}} \quad (3.13)$$

here $\mu = 0.7-0.85$; γ_{BHX} - density of products of combustion at outlet pressure from nozzle $p_{\text{BHX}} = p_2$;

$$\gamma_{\text{out}} = \gamma_{\text{in}} \left(\frac{p_{\text{out}}}{p_{\text{in}}} \right)^{1/\mu} \quad (3.14)$$

where p_{BX} and γ_{BX} are pressure and density of gas in front of the injector.

Since pressure drop at the injector $p_{\text{BX}} - p_{\text{BHX}}$ as compared to pressure in chamber p_2 , equal to several tens of atmospheres, there is little, outflow of gas through the injector will be subcritical with exit velocity

$$v = \sqrt{2g \frac{n}{n-1} RT_{\text{in}} \left[1 - \left(\frac{p_{\text{out}}}{p_{\text{in}}} \right)^{\frac{n-1}{n}} \right]} \quad (3.15)$$

where R and T_{BX} gas constant and temperature of gas in front of the injector.

Placing expression (3.14), (3.15) in equation (3.13), we will obtain calculation expression for determination of f_c :

$$f_c = \frac{a_0}{\gamma_{\text{in}} \left(\frac{p_{\text{out}}}{p_{\text{in}}} \right)^{1/\mu} \sqrt{2g \frac{n}{n-1} RT_{\text{in}} \left[1 - \left(\frac{p_{\text{out}}}{p_{\text{in}}} \right)^{\frac{n-1}{n}} \right]}} \quad (3.16)$$

Injectors with Intersecting Sprays

As we noted above, the use of injectors with intersecting sprays increases the angle of atomization and improves splitting of drops, which leads to an increase of chamber efficiency. In the United States such injectors first appeared and were successfully used in a ZHRD with nitric acid fuel. Diverse variants of the diagrams of injectors with intersecting sprays are represented in Fig. 3.12.

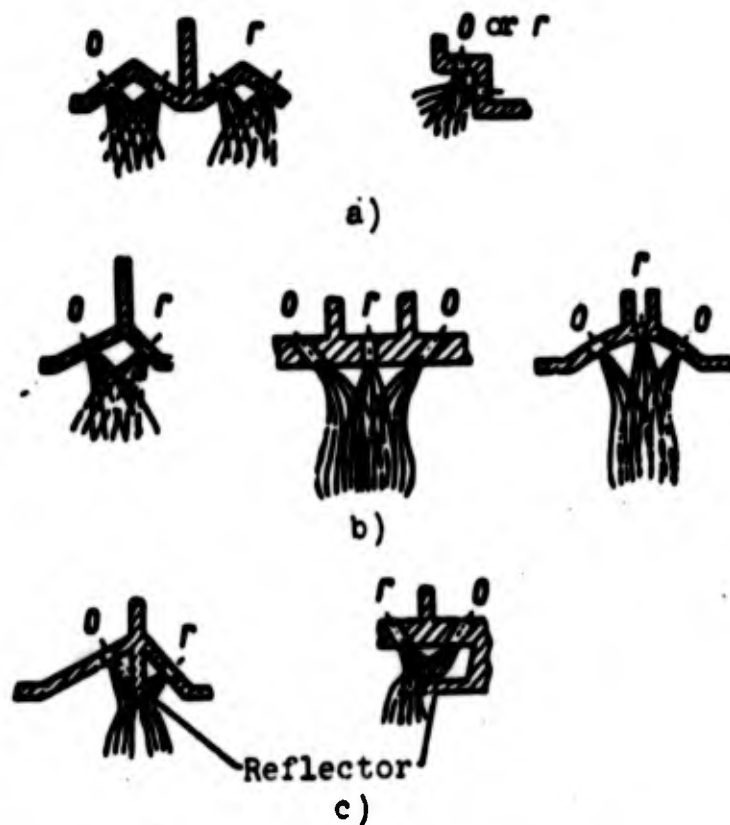


Fig. 3.12. Blocks of injectors with intersecting sprays: a) intersection of sprays of one component; b) intersection of several sprays of two components; c) injector with a "sprayer"; O - oxidizer; Γ - fuel.

It is possible to separate three basic forms of injectors with intersecting sprays:

a) injectors, ensuring paired intersection of sprays of one component (Fig. 3.12a).

b) injectors ensuring intersection of sprays of both components (Fig. 3.12b). Thus in dependence on the ratio of flow rates of fuel and oxidizer (ν) on one fuel injector there can be fixed one, two, three, and even four injectors for supply of oxidizer. With intersection of two and more streams of oxidizer with one of propellant, for best atomization it is recommended that exit velocity of combustible exceed exit velocity of oxidizer by 50-60%;

c) injectors with mixing screen (reflector) (Fig. 3.12c). In these injectors, best splitting is ensured by means of collision of stream and wall.

With intersection of two streams, angle of inclination of the resultant stream can be determined, proceeding from the following considerations (Fig. 3.13).

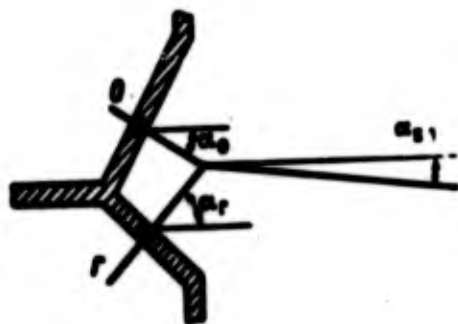


Fig. 3.13. To calculate angles of slop of walls (or openings) in blocks of injectors.

Let us designate α_0 , α_r , and α_z , respectively as angles of inclination of streams of oxidizer, combustibles, and that stream of fuel formed after collision; m_0 , m_r , and m_z and w_0 , w_r , and w_z , respectively mass flow rates and velocities of oxidizer, combustibles, and fuel. If one were to consider that the momentum of streams before and after their collision remains constant, then projections on a horizontal and vertical axis can be described by the following equations:

$$m_r w_r \cos \alpha_r + m_0 w_0 \cos \alpha_0 = m_z w_z \cos \alpha_z \quad (3.17)$$

$$m_0 w_0 \sin \alpha_0 - m_r w_r \sin \alpha_r = m_z w_z \sin \alpha_z \quad (3.18)$$

Dividing equation (3.18) by equation (3.17), we obtain an equation of angle of inclination of the resultant stream of fuel

$$\operatorname{tg} \alpha_z = \frac{m_0 w_0 \sin \alpha_0 - m_r w_r \sin \alpha_r}{m_r w_r \cos \alpha_r + m_0 w_0 \cos \alpha_0} \quad (3.19)$$

Since frequently intersection of streams is ensured by corresponding

location of surfaces of walls to which the axis of holes are perpendicular, then obviously, angles α_o and α_r determine slope of walls. In most cases it is desirable to select angles of inclination of walls, flow rates of components and velocities (i.e., Δp_{ϕ}) in such a manner that direction of the resultant stream will coincide with axial direction, i.e., $\alpha_{\Sigma} = 0$. Then

$$m_o w_o \sin \alpha_o = m_r w_r \sin \alpha_r \quad (3.20)$$

or

$$G_o r_o \sin \alpha_o = G_r r_r \sin \alpha_r \quad (3.21)$$

It must be noted that manufacture with the necessary degree of accuracy of a large number of injectors with intersecting streams is no less complicated a problem than manufacture and installation of separate swirlers.

Example of calculation of spray injectors

To determine the dimensions of spray injectors and angle of inclination of oxidizer injectors with $\alpha_r = 30^\circ$; $\alpha_{\Sigma} = 0$;

$$Q_{o_r} = 43.5 \text{ g/s}; \Delta p_{o_r} = 6 \text{ kg/cm}^2 (0.59 \text{ MPa}); \gamma_r = 0.8 \text{ g/cm}^3$$

$$Q_{o_o} = 73 \text{ g/s}; \Delta p_{o_o} = 7 \text{ kg/cm}^2 (0.68 \text{ MPa}); \gamma_o = 1.3 \text{ g/cm}^3$$

Solution. Considering $l/d = 3$, we take for both injectors, discharge coefficient $\mu = 0.8$.

We determine dimensions of injectors. By formula (3.11):

$$f_{o_r} = \frac{Q_{o_r}}{\mu \sqrt{2g \Delta p_{o_r} \gamma_r}} = \frac{43.5 \cdot 10^{-3}}{0.8 \sqrt{2 \cdot 981 \cdot 6 \cdot 0.8 \cdot 10^{-3}}} = 1.77 \cdot 10^{-3} \text{ cm}^2$$

$$f_{o_o} = \frac{73 \cdot 10^{-3}}{0.8 \sqrt{2 \cdot 981 \cdot 7 \cdot 1.3 \cdot 10^{-3}}} = 2.01 \cdot 10^{-3} \text{ cm}^2$$

Considering coefficient of velocity to equal discharge coefficient μ , we determine actual exit velocity:

$$w_r = 0.8 \sqrt{\frac{\Delta P_{02}}{\gamma_r}} = 0.8 \sqrt{\frac{2 \cdot 9.81 \cdot \frac{6 \cdot 10^4}{800}}{1}} = 30.6 \text{ m/s};$$

$$w_o = 0.8 \sqrt{\frac{7 \cdot 10^4}{1800}} = 24.2 \text{ m/s}.$$

Since $\alpha_2 = 0$, when α_0 we will define by equation (3.21):

$$\sin \alpha_0 = \frac{Q_r w_r}{Q_o w_o} \sin \alpha_r = \frac{43.5 \cdot 30.6}{73 \cdot 24.2} \sin 30^\circ = 0.377.$$

whence angle of inclination of oxidizer injector $\alpha_0 = 22^\circ 10'$.

3.3. Centrifugal Injectors

Centrifugal is the name applied to an injector in which there is artificially created a swirl of the stream of liquid passed through it. After exit of the liquid from the nozzle under action of centrifugal forces there will be formed a thin coneshaped liquid sheet of component which rapidly breaks up into drops (see Fig. 3.3b). Therefore, the diagram of flow intensity of a centrifugal injector has two peaks (see Fig. 3.3d).

Centrifugal injectors have a wide and comparatively short spray cone. The spray of centrifugal injectors is finer than for jet. This all leads to a decrease of zones of atomization and evaporation. However, a disadvantage of centrifugal injectors is their great structural complexity and smaller carrying capacity as compared to spray injectors.

According to the method of obtaining the flow swirl of component, centrifugal injectors are divided into tangential (Fig. 3.14a, b and 3.15a, b, c) and injectors with swirl vane (or screw (Fig. 3.14c and 3.15e)).

In a centrifugal tangential injector, the liquid enters the cavity of the injector through one or several inlets, the axes of which are perpendicular to the axis of the injector but do not intersect it. Sometimes the opening is made at an acute angle to the axis of the injector. As a result, the liquid obtains swirl with respect to the axis of the injector.

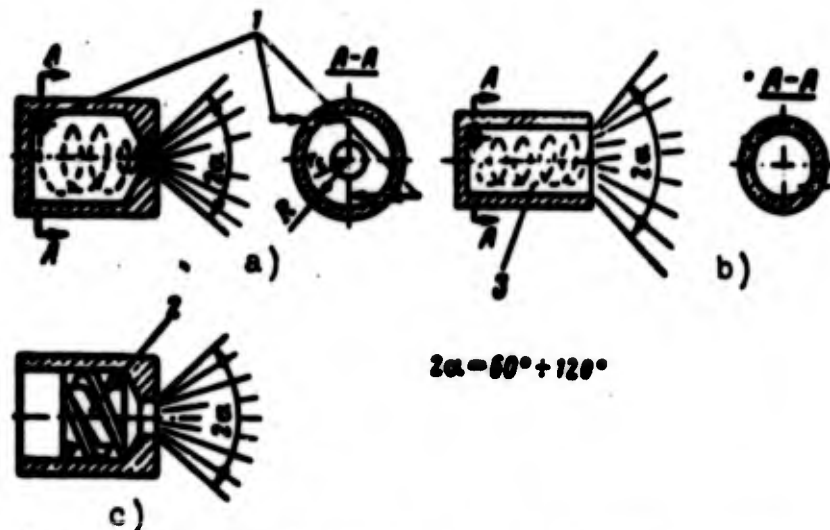


Fig. 3.14. Diagrams of centrifugal injectors: a) tangential closed; b) tangential open; 1 - liquid inlet; 2 - swirl vane (screw); 3 - swirl chamber.

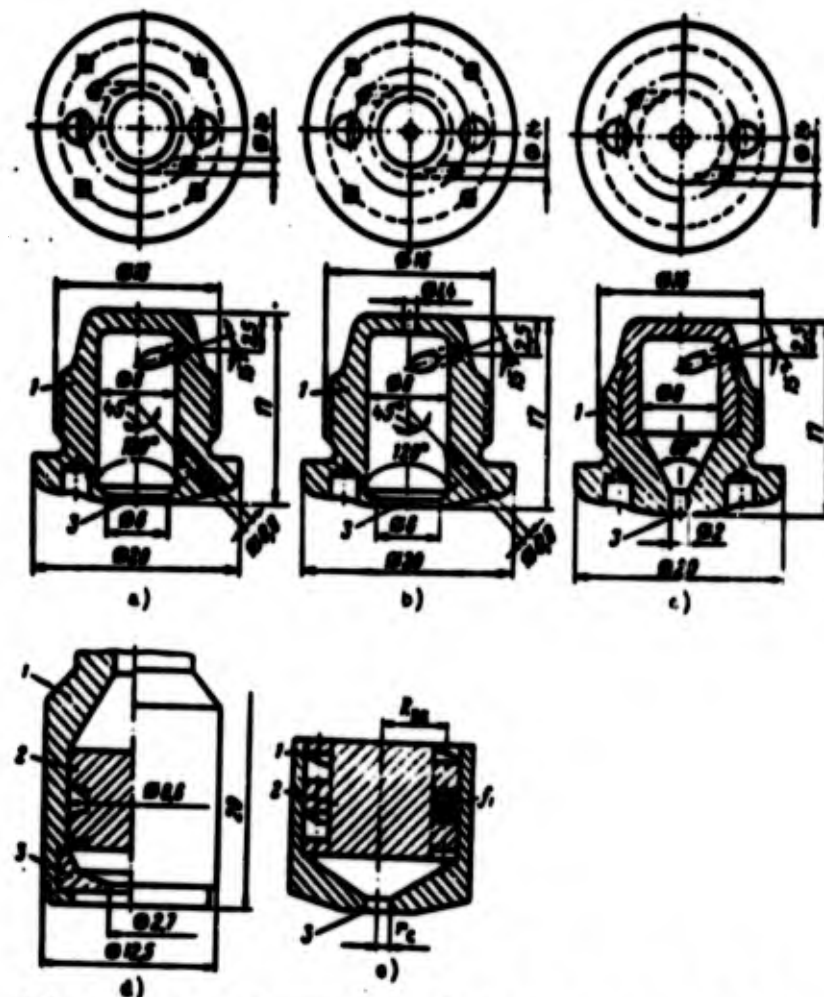


Fig. 3.15. Centrifugal injectors: a, b, c) tangential; d, e) screw; 1 - body; 2 - screw; 3 - nozzle.

There are open and closed tangential centrifugal injectors. For closed tangential injectors (see Fig. 3.14a), radius of nozzle r_c is less than radius of the swirl chamber R . For open injectors, radius of nozzle is equal to radius of swirl chamber (see Fig. 3.14b). In an injector with a swirl vane (see Fig. 3.14c) swirl is created by means of a special swirl vane (screw) which has a screw thread on the external surface. Moving by screw thread, the liquid obtains a swirl with respect to the axis of the injector. Let us consider the operation of a centrifugal injector [1].

Operation of an Injector

In a centrifugal tangential injector (Fig. 3.16), the liquid enters the cavity of the injector through an inlet having radius r_{BX} with velocity w_{BX} . This opening is located so that its axis is tangent to the circumference of radius R_{BX} with the center located on the axis of the injector nozzle. Thanks to this inlet, liquid passes through the cavity into the nozzle of the injector, revolving. Let us consider a stream of liquid which, moving along the injector, gets to the nozzle at distance r from its axis.

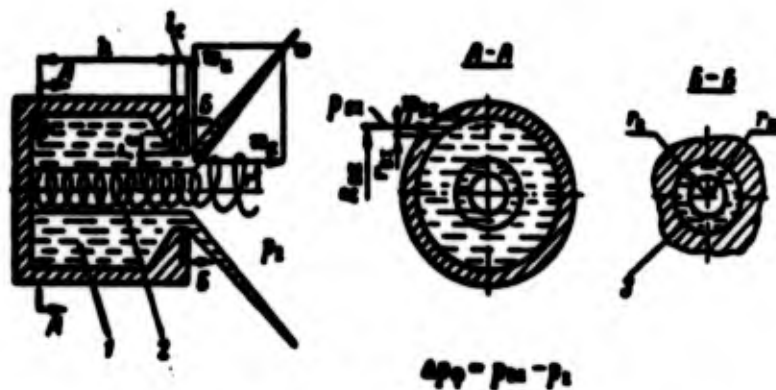


Fig. 3.16. Motion of liquid in a swirler:
1 - liquid; 2 - gas swirl; 3 - "active"
section.

If we disregard the action of forces of friction, then angular momentum of any liquid particle with respect to the axis of injector should maintain constant value all the way from entrance into the injector to exit from nozzle of it, i.e.,

$$w_u r_u = w_r r. \quad (3.22)$$

where w_u - peripheral velocity of motion of a particle of liquid in the nozzle at distance r from the nozzle axis.

Since one may assume that on the average for all streams (with slight error due to change of value r_{BX}) the momentum of the liquid, achieved by it in the inlet is the same, then velocity w_u depends on radius r , on which this stream gets into the nozzle:

$$w_u = \frac{w_{BX} r_{BX}}{r}. \quad (3.23)$$

Disregarding the insignificant difference of levels of location of inlet and nozzle openings, pressure in the stream of liquid can be determined by the Bernoulli equation:

$$\frac{P_{BX}}{\gamma} + \frac{w_{BX}^2}{2g} = \frac{P}{\gamma} + \frac{w_u^2}{2g} + \frac{w_a^2}{2g} = \text{const.} \quad (3.24)$$

where P_{BX} - pressure of liquid in the inlet; w_{BX} - entrance velocity of the liquid into the injector; w_u - tangential component of velocity of liquid at exit from the injector; w_a - axial component of velocity of liquid at exit from the injector.

Designating total pressure drop at the injector through Δp_{ϕ} and expressing it through pressure H , we will obtain

$$\frac{\Delta p_{\phi}}{\gamma} = H = \frac{P_{BX}}{\gamma} + \frac{w_{BX}^2}{2g} = \text{const.} \quad (3.25)$$

After that, from equation (3.24) we will obtain

$$\frac{P}{\gamma} = H - \left(\frac{w_u^2}{2g} + \frac{w_a^2}{2g} \right). \quad (3.26)$$

From equations (3.23) and (3.26) it is clear that with $r \rightarrow 0$ there will be $w_u \rightarrow \infty$, i.e., pressure of liquid on the axes of the injector should have infinitely large negative value. This is impossible for liquids since a liquid in general does not withstand negative stresses, i.e., does not work on extension.

In reality, in the injector the following occurs. As the liquid approaches, the axis of the injector, velocity w_u will be increased, and pressure p will drop, but only until it becomes equal to ambient pressure in which outflow occurs (with injection into the chamber - pressure in chamber). Further decrease of pressure in the central region of flow is impossible. Since by its only base this region emerges through the nozzle into the environment, the central part of the injector will not be filled with liquid. In it there will be a gas vortex with a pressure equal to ambient pressure (pressure in the chamber). Flow of liquid by the nozzle or the injector will be carried out not through the whole section but only through the annular, the internal radius of which is equal to radius of the gas vortex r_m , and external radius - radius of the nozzle r_c .

This section we will call the useful cross section of nozzle of the injector; its area

$$f_n = \pi (r_c^2 - r_m^2) \quad (3.27)$$

Flow rate through the nozzle of the injector

$$Q = f_n w_n = w_n \pi (r_c^2 - r_m^2) = w_n \pi \varphi r_c^2 \quad (3.28)$$

where φ - coefficient of useful cross section.

It is obvious that

$$\varphi = 1 - \frac{r_m^2}{r_c^2} \quad (3.29)$$

We will define change of w_a and w_u by cross section of stream. Let us consider section of stream at the nozzle exit section of the injector (Fig. 3.17). Let us separate in useful cross section at distance r from the axis, annular element dr . According to the d'Alembert principle, difference of pressures on the surface of the annular element Δp is balanced by centrifugal force. For an individual element, the equation of equilibrium will have the form

$$dp = -\frac{w_u^2}{r} dm, \quad (3.30)$$

where dm - mass of individual element

$$dm = -\frac{\gamma}{g} dr. \quad (3.31)$$

According to equation (3.22) it is possible to write

$$w_r = w_{um} r_m. \quad (3.32)$$

where w_{um} - tangential velocity of liquid with $r = r_m$. Hence

$$r = \frac{w_{um} r_m}{w_r}; \quad dr = -\frac{w_{um} r_m}{w_r^2} dw_r. \quad (3.33)$$

After substitution of expressions (3.31) and (3.33) in equation (3.30) we will obtain

$$dp = -\frac{\gamma}{g} w_r dw_r. \quad (3.34)$$

and after integration

$$\frac{p}{\gamma} = -\frac{w_r^2}{2g} + C. \quad (3.35)$$

Let us find constant C. With $w_u = w_{um}$ it will be $p = p_m$, where p_m - pressure, excess above pressure in vortex p_2 . Obviously, on border of swirl and liquid $p_m = 0$, whence

$$C = \frac{w_{um}^2}{2g}.$$

Then equation (3.35) will have the form

$$\frac{p}{\gamma} = \frac{w_{um}^2}{2g} - \frac{w_r^2}{2g}. \quad (3.36)$$

Comparing expression (3.36) and (3.26), we will obtain

$$\frac{w_a^2}{2g} = H - \frac{w_{um}^2}{2g}, \quad (3.37)$$

i.e., axial component of velocity of liquid in useful cross section of the nozzle of the injector w_a does not depend on r and is constant over the whole section, i.e.,

$$w_a = \text{const.} \quad (3.38)$$

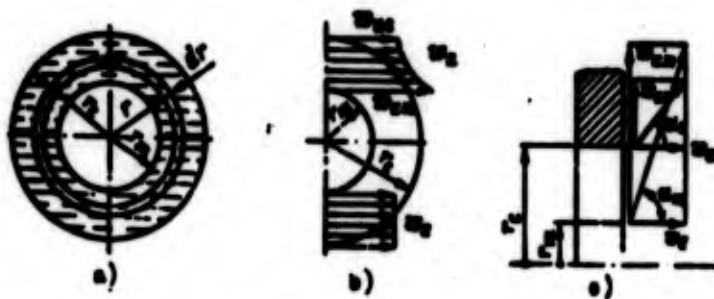


Fig. 3.17. For determination of forces having effect on the annular element: a) useful cross section; b, c) change of w_a , w_u , and 2α by useful cross section.

We will define change w_u by section. Equation of constancy of flow rate for inlet and for section on nozzle exit section of the injector

$$G_0 = w_a f_{in} \gamma = w_u \pi r_{ex}^2 \gamma = w_u \pi r_{in}^2 \gamma. \quad (3.39)$$

Placing from equation (3.22) the value w_{BX} in equation (3.39), we obtain

$$w_u = w_a \varphi \frac{R_{in} r_s}{r_{ex}} \frac{r_s}{r}. \quad (3.40)$$

Diagrams of change of w_a and w_u by useful cross section are represented in Fig. 3.17b.

Geometric Characteristics of an Injector

Into expression (3.40) there enters complex $R_{in} r_s / r_{ex}^2$, connecting the basic dimensions of an injector. This complex is usually designated as A and called the geometric characteristic of a centrifugal injector, i.e.,

$$A = \frac{R_{in} r_s}{r_{ex}^2}. \quad (3.41)$$

As we will see further on, the geometric characteristic is the most important parameter of centrifugal injector.

In the analysis made, we determined the geometric characteristic A for a tangential injector with a single inlet. Conducting analogous computations, it is easy to find the expression of geometric characteristic for other types of centrifugal injectors.

Thus, in general, for a tangential injector with several inlets inclined at an angle to the axis of the injector:

$$A = \frac{R_{BX} f_1}{i r_m} \sin \beta, \quad (3.42)$$

where i - number of inlets; β - angle between directions of axes of inlets and nozzle of injector.

For an open injector (see Fig. 3.14b), since $r_c \approx R_{BX}$,

$$A \approx \frac{r_c^2}{i r_m} \sin \beta. \quad (3.43)$$

For a screw injector (see Fig. 3.15e)

$$A = \frac{R_{BX} f_1}{i} \sin \beta, \quad (3.44)$$

where R_{BX} - average radius of screw channel of the swirl vane; β - angle of ascent of the spiral; f_1 - area of cross section of one channel; i - number of approaches of the screw thread of the swirl vane (number of channels).

With help of the geometric characteristic in the general expression (3.40) for determination of tangential speed, w_u can be present thus:

$$w_u = w_0 A \frac{r_c}{r}. \quad (3.45)$$

Where $r = r_m$, velocity $w_u = w_{um}$ and since $r_c/r_m = 1/\sqrt{1-\varphi}$ [see (3.29)] tangential velocity on border of whirl

$$w_{um} = w_0 \frac{1}{\sqrt{1-\varphi}} A \quad (3.46)$$

Where $r = r_c$

$$w_{a1} = w_{a2} A \quad (3.47)$$

Discharge Coefficient of an Injector

Using the obtained dependences, we will define flow rate through the injector G_{ϕ} .

Since $H = \Delta p_{\phi} / \gamma$ (3.25), then from equations (3.37) and (3.46) we will obtain

$$w_{a2} = \frac{\sqrt{\frac{2g \Delta p_{\phi}}{\gamma}}}{\sqrt{\frac{1}{\varphi^2} + \frac{A^2}{1-\varphi}}} \quad (3.48)$$

Then according to equation (3.39)

$$G_{\phi} = \frac{w_{a2}^2 \sqrt{2g \Delta p_{\phi} \gamma}}{\sqrt{\frac{1}{\varphi^2} + \frac{A^2}{1-\varphi}}} \quad (3.49)$$

If one were to designate

$$\mu = \frac{1}{\sqrt{\frac{1}{\varphi^2} + \frac{A^2}{1-\varphi}}} \quad (3.50)$$

and to substitute $f_c = \pi r_c^2$, then we will obtain an expression identical to the equation of flow rate through a spray injector (3.10):

$$G_{\phi} = \mu f_c \sqrt{2g \Delta p_{\phi} \gamma} \quad (3.51)$$

where μ — discharge coefficient of a centrifugal injector.

From expression (3.50) it is clear that the discharge coefficient μ depends on the coefficient of useful cross section φ , i.e., on area of useful cross section f_{κ} . It is obvious that with $f_{\kappa} \rightarrow 0$, discharge coefficient and flow rate will approach zero. However, even a strong increase of f_{κ} also will lead to a decrease of μ , inasmuch as with large f_{κ} (i.e., with very small radii of whirl r_m) axial velocity w_a decreases considerably since a large part of the

pressure will be expended on creation of high peripheral velocity w_u . Consequently, there is some optimum value of coefficient φ with which value μ will be the greatest. According to the principle of maximum flow rate known in hydraulics during flow of a component through the injector there should be established such value of useful cross section f_x , with which flow rate through the injector will be the greatest. Thus, for each given value of A with change of useful cross section, i.e., coefficient φ is its maximum value of discharge coefficient μ . For its determination the derivative $d\mu/d\varphi$ will equate to zero:

$$\frac{d\mu}{d\varphi} = -\frac{1}{2} \frac{-2\frac{1}{\varphi^2} + A^2 \frac{1}{(1-\varphi)^2}}{\left(\frac{1}{\varphi^2} + \frac{A^2}{1-\varphi}\right)^{3/2}} = 0, \quad (3.52)$$

whence

$$\frac{A^2}{1-\varphi^2} - \frac{2}{\varphi^2} = 0. \quad (3.53)$$

Consequently, the greatest discharge coefficient will be during condition

$$A = \frac{\sqrt{2(1-\varphi)}}{\varphi\sqrt{\varphi}}. \quad (3.54)$$

Dependence of φ on A with a condition of maximum flow rate is shown in Fig. 3.18. Substituting expression (3.54) in equation (3.50), we will obtain a connection between μ and φ :

$$\mu = \varphi \sqrt{\frac{\varphi}{2-\varphi}}. \quad (3.55)$$

after which it is possible to construct the dependence of μ on geometric characteristic A (Fig. 3.18).

Thus, the value of discharge coefficient μ is determined by the value of geometric characteristic of a centrifugal injector A . Limits of change of μ are easy to find from expressions (3.54) and (3.55): where $A \rightarrow 0$ there will be $\varphi \rightarrow 1$ and $\mu \rightarrow 1$; where $A \rightarrow \infty$ there will be $\varphi \rightarrow 0$ and $\mu \rightarrow 0$; with all remaining values of A $1 > \varphi > 0$, and the

values of μ according to the relationship (3.55) will always be smaller than φ .

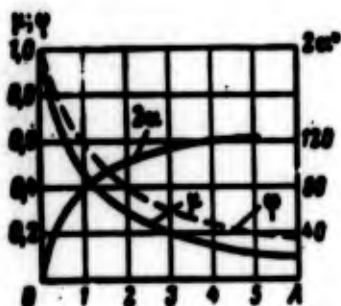


Fig. 3.18. Change of μ , φ , and 2α depending on geometric characteristic A .

Knowing μ , we can determine the necessary area of nozzle of an injector from equation (3.51):

$$f_0 = \frac{G_0}{\rho \sqrt{2g\Delta P_0 \gamma}} \quad (3.56)$$

Geometric characteristic A is connected also with angle of flame of atomization 2α .

As can be seen from Fig. 3.17c, the angle of atomization α is inconstant for useful cross section and for peripheral streams decreases in conformity with decrease of w_u . Therefore we will determine the average angle of flame of atomization for a mean value of radius of useful cross section

$$r_{cp} = \frac{r_s + r_n}{2} \quad (3.57)$$

It is obvious that

$$\operatorname{tg} \alpha = \frac{w_{ucp}}{w_0} \quad (3.58)$$

Since $w_{ucp} = w_{ux} r_c / r_{cp}$ (3.22) than taking into account expressions (3.29), (3.47) and (3.57) we will obtain

$$w_{ucp} = \frac{w_0 \sqrt{5(1-\varphi)}}{\sqrt{\varphi(1-\sqrt{1-\varphi})}} \quad (3.59)$$

and after substitution of equality (3.59) in formula (3.58)

$$\operatorname{tg} \alpha = \frac{2\sqrt{2}(1-\varphi)}{\sqrt{\varphi}(1-\sqrt{1-\varphi})}. \quad (3.60)$$

Substituting in the last expression instead of φ the value of A connected with φ equation (3.54), we will find the dependence of average angle of flame of atomization 2α on geometric characteristic A (see Fig. 3.18).

Effect of Viscosity on Operation of an Injector

Above we have given an analysis of the operation of a centrifugal injector with supply of an ideal liquid. With supply of an actual liquid possessing viscosity, the presence of forces of friction leads to a change of discharge coefficient μ and angle of atomization 2α . Friction leads to a decrease of angular momentum of fluid flow along the length of the injector. Due to this, swirl of flow, i.e., w_u decreases, which leads to a decrease in radius of gas whirl r_m , decrease of r_m signifies increase of useful cross section of injector nozzle, i.e., increase of discharge coefficient μ and although due to losses of pressure by friction, flow rate decreases, on the whole, the effect of decrease of intensity of swirl turns out to be stronger than the effect losses of pressure by friction. Therefore, discharge coefficient μ for an actual liquid is greater than for ideal.

Angle of atomization 2α thus decreases, since tangential component of speed w_u decreases. Thus, viscosity leads to a decrease of angle of atomization 2α , and paradoxically, at first glance, the result — increase of discharge coefficient of a centrifugal injector μ . As can be seen from the graph in Fig. 3.18, we would come to the same result with a decrease in value of geometric characteristic A .

Therefore, a centrifugal injector having geometric characteristic A , with supply of actual liquid can be calculated with the use of the so-called equivalent characteristic of injector A_φ , smaller than A :

$$A_\varphi = K_\varphi A, \quad (3.61)$$

where $K_\varphi < 1$.

According to L. A. Klyachko [27]

$$K_0 = \frac{1}{1 + \frac{\lambda}{2} \left(\frac{B^2}{i} \sin \beta - \lambda \right)} \quad (3.62)$$

and

$$A_0 = \frac{A}{1 + \frac{\lambda}{2} \left(\frac{B^2}{i} \sin \beta - \lambda \right)} \quad (3.63)$$

where i - number of inlet channels; B - dimensionless geometric parameter of injector; $B^2 = R_{BX}^2 / \tau_{BX}^2$ - for tangential injector; $B^2 = R_{BX} \pi / f_1$ - for screw injector; λ - coefficient of friction, determined during conditions of entrance into the injector by the formula:

$$\lg \lambda = \frac{25.8}{(\lg Re_m)^{1.5}} - 2 \quad (3.64)$$

Where

$$Re_m = \frac{w_m d_{np}}{\nu} \quad (3.65)$$

where d_{np} - given diameter of inlet channels. For an injector with i number entrance channels by overall area $f_{BX} i$

$$d_{np} = \sqrt{\frac{4 f_{BX} i}{\pi}} = d_m \sqrt{i}$$

Entrance velocity of component

$$w_m = \frac{Q_0}{f_m \gamma} = \frac{4 Q_0}{\pi d_{BX}^2 \gamma}$$

Substituting the expressions for d_{np} and w_{BX} in equation (3.65), and considering that $\nu = g \mu / \gamma$, we will obtain a calculation formula for determination of Re_{BX} :

$$Re_m = \frac{4 Q_0}{g \mu d_m \sqrt{i}} \quad (3.66)$$

Obviously, for an ideal liquid, the coefficient of friction $\lambda = 0$ and according to formula (3.63)

$$A_0 = A.$$

During calculation of injector formula (3.63) it is more convenient to reduce to the form (with $\sin \beta = 1$)

$$A_0 = \frac{R_{BX} r_c}{v_{BX}^2 + \frac{\lambda}{2} R_{BX} (R_{BX} - r_c)}. \quad (3.67)$$

Effect of Design Parameters of an Injector

We will examine the effect of different design parameters on the operation of a centrifugal injector.

Increase of height (length) of injector h (see Fig 3.16) increases the effect of forces of viscosity which along with increase of μ and decrease of angle 2α leads also to increase of losses of pressure in the injector, i.e., to certain impairment of atomization. Therefore it is fully sufficient with a screw injector to make the height of the screw not more than $1/4$ - $1/3$ pitch of turn, and with a tangential injector — equal R_{BX} , although in practice, due to purely structural considerations frequently it is necessary to accept considerably higher injectors.

Ratio R_{BX}/r_c is usually selected within limits from 1 (for an open injector) to 2.5.

As experimental data show, with values $R_{BX}/r_c < 2.5$, experimental values of discharge coefficient $\mu_{\text{ЭКП}}$ are obtained less than the theoretical obtained on the graph in Fig. 3.18. In Fig. 3.19 there is a graph of dependence of ration $\mu_{\text{ЭКП}}/\mu$ on ratio R_{BX}/r_c [27].

Change of ratio l_c/d_c (see Fig. 3.16) essentially does not effect discharge coefficient μ . However, with growth of l_c/d_c angle of atomization 2α decreases. Therefore usually $l_c/d_c = 0.25$ -1.

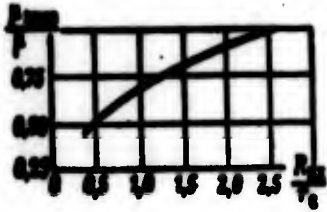


Fig. 3.19. Dependence of μ_{max}/μ on R_{BX}/r_c .

Thickness of wall of the injector is selected from condition $l_{BX}/d_{BX} = 1.5-3$. With values $l_{BX}/d_{BX} < 1.5$ the tangentialness of inlet is disturbed (Fig. 3.20) which leads to a decrease of angular momentum with respect to the axis of the injector. Increasing l_{BX}/d_{BX} is also inexpedient since it leads to unnecessary pressure losses by friction in the inlets.



Fig. 3.20. Change of direction of inlet of liquid with small values of l_{BX}/d_{BX} . 1 - direction with tangential inlet. 2 - actual direction.

The number of entrance channels 1 (or approaches of the screw) usually is taken as equal to 2-4. Increase in the number of entrance channels, obviously, improves distribution of flow intensity along the circumference of the flame.

Effect of Preheating the Component

Since the combustion chamber of a ZhRD is usually cooled by one of the components (and sometimes by two components), the cooling component proceeds to injector heated and thus, frequently up to a temperature close to the boiling point or even equal to it. Therefore the question about effect of temperature of preheating of component on operation of a centrifugal injector has practical value. If the temperature of liquid, entering the injector is such that the pressure of saturated vapors (vapor pressure) p_g does not exceed pressure in the gas vortex (equal to pressure in combustion chamber p_2), then there will not be essential changes in operation of the injector.

It is necessary only to consider change of density of component due to temperature. However if $p_s > p_2$, when boiling of component occurs in the injector and from the nozzle or the injector into the combustion chamber there proceeds not liquid but a vaporliquid mixture. Naturally this affects the operation of the injector and, primarily the discharge coefficient of injector μ .

A sufficiently detailed analysis of operation of an injector during flow of heated or boiling liquid is given in [58], [61]. In [58] it is proposed that the effect of preheating on discharge coefficient be considered by introduction of a discharge coefficient of heated liquid μ_t :

$$\mu_t = \mu \sqrt{\frac{p_0 - p_1}{p_0 - p_s}} \quad (3.68)$$

where μ - discharge coefficient during outflow of cold liquid; p_0 - pressure in front of injector. It must be considered that with p_s , close to p_0 , formula (3.68) gives a decreased value of μ_t , and with $p_s = p_0$ there is obtained $\mu_t = 0$ which does not correspond to experimental data. Therefore, with values of p_s close to p_0 one should take somewhat oversized values μ_t as compared to those obtained by formula (3.68). When more exact analytic determination of μ_t is necessary it is possible to use the results in [62], where there is a more precise but considerably more complicated dependence for determination of μ_t . In Fig. 3.21 there is a comparison of values of μ_t obtained from experiment by formula (3.68) and the formulas in [62].

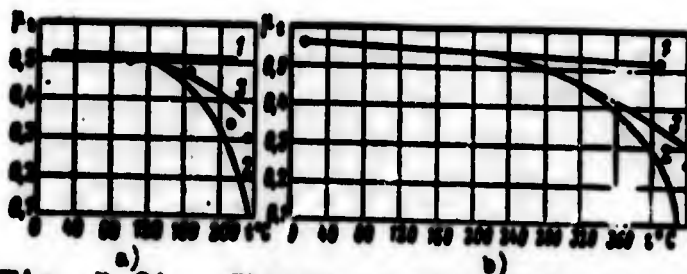


Fig. 3.21. Change of discharge coefficient μ_t depending upon temperature of liquid: a) water; $p_0 = 30 \text{ kgf/cm}^2$ ($\approx 3 \text{ MN/m}^2$); b) diesel fuel; $p_0 = 20 \text{ kgf/cm}^2$ ($\approx 2 \text{ MN/m}^2$); 1 - disregarding evaporation of liquid in the vortex; 2 - according to formula (3.68); 3 - according to formulas in [62].

Calculation of a Centrifugal Injector

In the calculation of a centrifugal injector we assume as known the flow rate of the component through the injector G_{ϕ} and its physical properties. Thus the following order of calculation of a centrifugal injector is used.

1. Depending upon operating conditions of the injector there is selected angle 2α and drop Δp_{ϕ} within limits of $2\alpha = 30-120^{\circ}$; $\Delta p_{\phi} = 3-15 \text{ kgf/cm}^2$ ($0.29-1.47 \text{ MN/m}^2$). The most widely used values of angle 2α lie within limits of $90-120^{\circ}$, however under certain specific conditions injectors with smaller angles can be required. Limits of pressure drop Δp_{ϕ} are determined under the same considerations as for a spray injector.

2. Knowing angle 2α , from the graph of Fig. 3.18 we determine geometric characteristic A and discharge coefficient μ .

3. We determine area of section of the nozzle of the injector and diameter of the nozzle. According to formula (3.56)

$$f_1 = \frac{G_{\phi}}{\mu \sqrt{2g \Delta p_{\phi}}}, \text{ whence } d_1 = \sqrt{\frac{4}{\pi}} f_1.$$

4. From constructive considerations, considering the effect of different parameters on operation of the injector, we select the number of inlets i and the "arm" swirl R_{BX}/r_c . Knowing i and R_{BX}/r_c we determine

$$r_m = \sqrt{\frac{r_m^2}{iA}}.$$

5. Knowing r_{BX} , from formulas (3.66) and (3.64) we determine coefficient of friction λ .

6. With r_c , R_{BX} , r_{BX} , and λ now known by formula (3.67) we determine

$$A_0 = \frac{R_{BX}^2}{r_m^2 + \frac{1}{2} R_{BX} (R_{BX} - r_c)}.$$

If the obtained value A_3 differs from geometric characteristic A by no more than 5%, then this calculation is finished; values r_c , R_{BX} , and r_{BX} of first approximation are taken for final and the remaining dimensions of the injector are determined. If the divergence of A and A_3 is large, then the calculation is conducted repeatedly. Taking for the base the obtained value A_3 according to the graphs of Fig. 3.18 we determine a new μ (already taking into account viscosity), and then new values r_c , R_{BX} , and r_{BX} .

According to the new values r_c , R_{BX} , and r_{BX} we determine the equivalent geometric characteristic of the second approximation A_3^{II} and compare it with A_3 of first approximation. If large divergence is again obtained than a third approximation is made. But usually by the second approximation A_3^{II} is sufficiently close to A_3 of first approximation.

7. According to values obtained during the last approximation for r_c , R_{BX} , and r_{BX} the remaining dimensions of the injector are determined (see Fig. 3.16):

$$l_m = (1.5 + 3)d_m; \quad l_s = (0.25 + 1)d_s; \quad k > R_m.$$

Radius of swirl chamber $R_3 = R_{BX} + r_{BX}$. If, during calculation of the injector it appears necessary to consider preheating of the component passed to the injector, then, according to formula (3.58) we correct the value of the discharge coefficient obtained in point 2, and conduct further calculation with a new value of discharge coefficient μ_t .

Example of calculation of a centrifugal injector

To calculate, taking into account viscosity, a tangential centrifugal injector for supplying nitric acid at its temperature of 288°K. Flow rate of acid through the injector $G_\phi = 68$ g/s; density $\gamma_{HNO_3} = 1.51$ g/cm³; viscosity $\mu = 0.981 \times 10^{-3}$ kgf/m × s (0.981×10^{-3} N × s/m²).

Solution. We are assigned angle of atomization $2\alpha = 100^\circ$ and pressure drop $\Delta p_\phi = 8$ kgf/cm² (0.78 MN/m²). In accordance with the

graph in Fig. 3.18 for angle 2α we determine geometric characteristic A and discharge coefficient μ :

$$A=4.2; \mu=0.16$$

We determine the dimensions of the nozzle of the injector:

$$f_c = \frac{Q_0}{\rho \sqrt{2g} \rho_0 \gamma} = \frac{0.008}{0.16 \sqrt{2 \cdot 9.81 \cdot 8 \cdot 1.51 \cdot 10^{-3}}} = 8.72 \cdot 10^{-3} \text{ cm}^2;$$

$$d_c = \sqrt{\frac{4}{\pi} f_c} = \sqrt{\frac{4}{3.14} \cdot 8.72} = 3.34 \text{ mm}; r_c = 1.67 \text{ mm}.$$

Since we are conducting calculation taking into account viscosity, then correction of dimensions obtained in first approximation (rounding to integers) for the time being will not be made.

We take $R_{BX}/r_c = 2.5$ and $i = 2$. Then

$$R_{ex} = 2.5 r_c = 2.5 \cdot 1.67 = 4.18 \text{ mm}; Q_{ex} = Q_0/2 = 34 \text{ s/cm}^2;$$

$$r_{ex} = \sqrt{\frac{R_{ex} r_c}{iA}} = \sqrt{\frac{4.18 \cdot 1.67}{2 \cdot 4.2}} = 0.912 \text{ mm}; d_{ex} = 1.824 \text{ mm}.$$

We determine coefficient of friction λ . By formula (3.66)

$$Re_{ex} = \frac{4Q_0}{(\rho \pi)^2 \sqrt{1} d_{ex}} = \frac{4 \cdot 0.008}{0.001 \cdot 10^{-3} \cdot 3.14 \cdot 1.41 \cdot 1.824 \cdot 10^{-3}} = 34130.$$

By formula (3.64) we determine $\lambda = 0.0331$. By formula (3.67) we determine

$$A_0 = \frac{R_{ex} r_c}{v_{ex}^2 + \frac{\lambda}{2} R_{ex} (R_{ex} - r_c)} = \frac{4.18 \cdot 1.67}{2 \cdot 0.912^2 + \frac{0.0331}{2} \cdot 4.18 (4.18 - 1.67)} = 3.83.$$

The obtained value A_0 differs from A by 9.5%, therefore we calculate the injector in second approximation according to geometric characteristic A_0 .

According to the graph in Fig. 3.18 when $A_0 = 3.83$ we find the discharge coefficient, $\mu = 0.17$ taking viscosity into account.

We determine the dimensions of the nozzle of the injector. By formula (3.56)

$$f_c = \frac{0.008}{0.17 \sqrt{2.551 \cdot 8 \cdot 1.51 \cdot 10^{-3}}} = 8.21 \cdot 10^{-2} \text{ cm};$$

$$d_c = \sqrt{\frac{4}{3.14} \cdot 8.21} = 3.22 \text{ mm};$$

we take $d_c = 3.2 \text{ mm}$; $r_c = 1.6 \text{ mm}$; $R_{BX}/r_c = 2.5$.
Then

$$R_{BX} = 2.5 \cdot r_c = 2.5 \cdot 1.6 = 4 \text{ mm};$$

$$r_{BX} = \sqrt{\frac{R_{BX}^2}{1.6}} = \sqrt{\frac{4 \cdot 1.6}{2 \cdot 3.14}} = 0.914 \text{ mm}.$$

We take $r_{BX} = 0.9 \text{ mm}$; $d_{BX} = 1.8 \text{ mm}$. By formulas (3.65) and (3.64) we determine Re_{BX} and coefficient of friction λ with definitized dimensions of the injector: $Re_{BX} = 34,400$. Since Re_{BX} changed insignificantly, the coefficient of friction, calculated by formula (3.64), remains equal to $\lambda = 0.0331$.

We determine value A_9 according to second approximation:

$$A_9^{II} = \frac{4 \cdot 1.6}{2 \cdot 0.9^2 + \frac{0.0081}{2} \cdot 4(4 - 1.6)} = 3.61.$$

Value A_9^{II} differs from A_9 by 5% which is within permissible limits. Therefore we consider the values r_c , R_{BX} , and r_{BX} defined in second approximation as final.

Let us define the remaining dimensions of the injector:

$$l_{23} = 1.5d_{23} = 1.5 \cdot 1.8 = 2.7 \text{ mm};$$

$$l_4 = 0.5d_4 = 0.5 \cdot 3.2 = 1.6 \text{ mm};$$

height of injector $h = R_{BX} = 4 \text{ mm}$; radius of swirl chamber $R_3 = R_{BX} + r_{BX} = 4 + 0.9 = 4.9 \text{ mm}$.

3.4. Two-Component Injectors

Diagrams of Two-Component Injectors. Advantages and Disadvantages

Along with single-component injectors, use is also made of two-component centrifugal injectors, basic diagrams of which are presented in Fig. 3.22. Two forms of two-component injectors are distinguished:

A - with internal mixing (emulsion).

B - with external mixing.

In two-component injectors with internal mixing, the mixing of components occurs in the injector just prior to their entry into the combustion chamber. Inside the injector both components will form an emulsion mixture which enters the combustion chamber, therefore these injectors are frequently called emulsion. Such injectors frequently are used expediently with supply of nonhypergolic components, since with hypergolic components, the combustion reaction can begin before the emulsion of component emerge from the injector, which will lead to destruction of the injector and the combustion chamber.

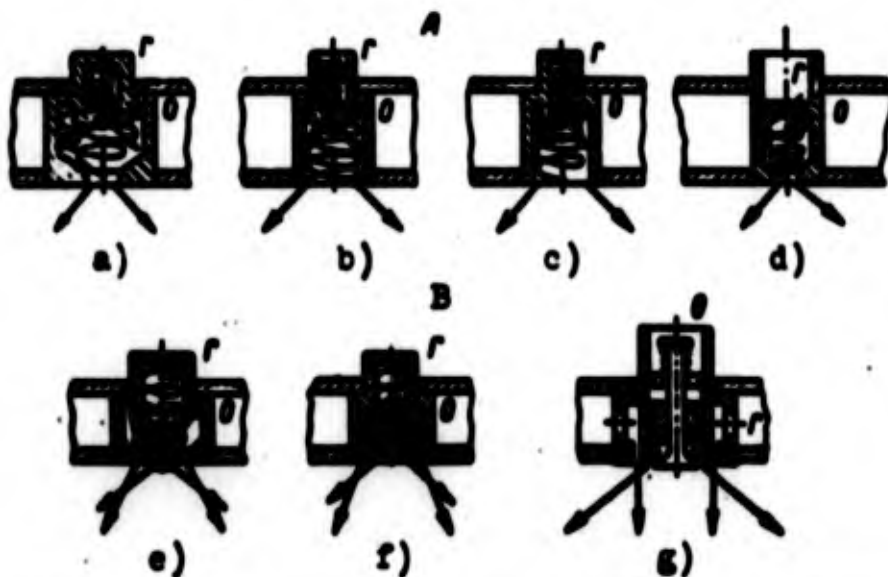


Fig. 3.22. Diagrams of two-component injectors: A) - with internal mixing (emulsion); B) - with external mixing; a, d, e) closed injectors; c, f) open injectors; b) semi-open injector; g) slot injector.

In two-component injectors with external mixing, the mixing of components occurs after they leave the injector. Thus, one may assume that a two-component injector with external mixing essentially consists of a structural block of two single-component injectors ensuring mixing of components in a prescribed ratio directly at the engine head.

Two-component injectors are not necessarily a combination of two centrifugal injectors. Different structural combinations of centrifugal, jet, and slot, injectors are possible. In Fig. 3.22g there is a diagram of a two-component injector with external mixing in which a centrifugal and a slot injector are combined.

Use of two-component injectors permits improving carburetion since basic mixing is ensured of components still in liquid phase, which leads to a more rapid flow of the entire process of combustion, and means that it permits decreasing the volume of combustion chamber required. The carrying capacity of a head with two-component injectors is greater than with single-component centrifugal injectors.

The disadvantages of two-component injectors are first, their great structural complexity and secondly, more rigid thermal conditions of head operation. Since in using two-component injectors the zones of atomization and evaporation are shortened, the flame front approaches the head and the intensity of heat flow from flame front to head increases.

Let us consider procedures for calculating two-component injectors.

Calculation of Emulsion Injectors

The calculation diagram is shown in Fig. 3.23a. Let us designate i_o ; i_f ; w_o ; w_f ; γ_o ; γ_f ; $G_{\phi.o}$; $G_{\phi.f}$ respectively as number of inlets, inlet velocity, density and flow rates of oxidizer and fuel through the injector. For convenience we consider that the openings for supply of fuel are inclined at angle β .

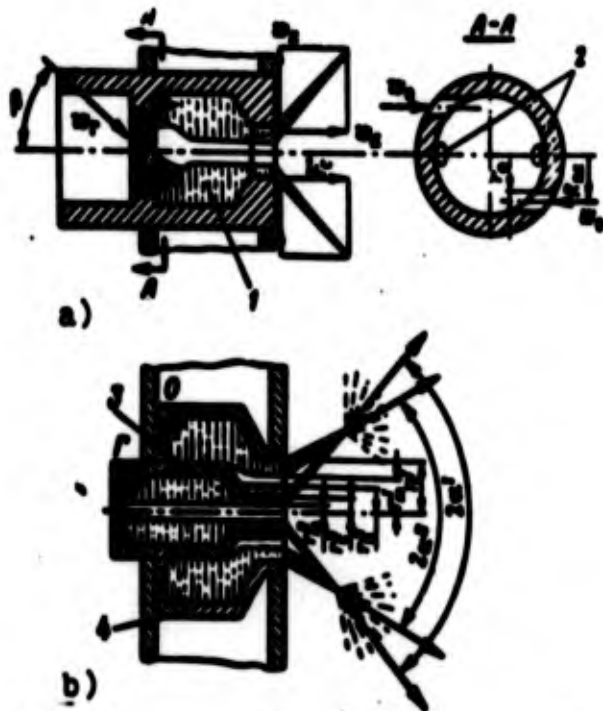


Fig. 3.23. For calculation of two-component injectors: a) with internal mixing; b) with external mixing; 1 - emulsion; 2 - opening for introduction of fuel; 3 - internal injector; 4 - external injector.

Let us assume that $R_{BX} \approx R_{BX,r} = R_{BX,o}$ and that operating pressure drops during supply of fuel and oxidizer are equal; action of forces of friction will be disregarded. Then it is possible to write down

$$P_0 = P_{B,o} + \frac{\gamma_0 v_0^2}{2\gamma} = P_{B,r} + \frac{\gamma_r v_r^2}{2\gamma}. \quad (3.69)$$

where $p_{B,o} = p_{B,r}$ - pressure of oxidizer and combustible in the mixing cavity of the injector.

From equation (3.69) it follows that with $p_{B,o} = p_{B,r}$

$$v_0 = \sqrt{\gamma v_r}. \quad (3.70)$$

where

$$\gamma = \frac{h}{v}. \quad (3.71)$$

Fuel consumption through the injector

$$G_{\phi, \Sigma} = G_{\phi, o} + G_{\phi, r} = G_{\phi, o} \left(\frac{1+v}{v} \right) = \pi d_o r_o^2 \gamma_o w_o \frac{1+v}{v}. \quad (3.72)$$

Based on the law of conservation of moment of momentum we can write down:

$$G_{\phi, r} w_{\Sigma} R_{\Sigma} = G_{\phi, r} w_o R_o \cos \beta + G_{\phi, o} w_o R_o. \quad (3.73)$$

where w_{Σ} - tangential component of velocity of mixed flow in the mixing cavity.

$$w_{\Sigma} R_{\Sigma} = w_o r_o. \quad (3.74)$$

where w_u - tangential component of velocity of emulsion at nozzle outlet.

From equation (3.73), taking into account expressions (3.70) and (3.72) we obtain

$$w_{\Sigma} = w_o \frac{v + \sqrt{m} \cos \beta}{1+v} \quad (3.75)$$

and from formulas (3.74) and (3.75) we determine

$$w_o = w_{\Sigma} \frac{1+v}{v + \sqrt{m} \cos \beta} \frac{r_o}{R_{\Sigma}}. \quad (3.76)$$

Let us define density of fuel γ_{Σ} formed during mixing of fuel and oxidizer in the injector. Since

$$\frac{G_{\phi, \Sigma}}{V_{\Sigma}} = \frac{G_{\phi, o}}{V_o} + \frac{G_{\phi, r}}{V_r}, \quad (3.77)$$

then taking into account expressions (3.71) and (3.72)

$$\gamma_{\Sigma} = \frac{v(1+v)}{v+m}. \quad (3.78)$$

We will define peripheral velocity of emulsion in nozzle of injector w_u .

Analogously to equation (3.39), taking into account dependence (3.72), the equation of flow rate through the injector

$$G_{02} = w_a \pi r_0^2 \gamma_2 = l_0 \pi r_0^2 \gamma_0 w_0 \frac{1+\nu}{\nu} \quad (3.79)$$

where w_a - axial component of velocity of emulsion in the nozzle.

Then, comparing expressions (3.76), (3.78), and (3.79), we obtain

$$w_a = w_0 \nu \frac{(\nu + \sqrt{m \cos \theta}) \nu}{(1 + \nu)(\nu + m)} \frac{R_m r_0}{l_0} \frac{r_0}{r} \quad (3.80)$$

Designating

$$A_{em} = \frac{(\nu + \sqrt{m \cos \theta}) \nu}{(1 + \nu)(\nu + m)} \frac{R_m r_0}{l_0} \quad (3.81)$$

we obtain

$$w_a = w_0 A_{em} \frac{r_0}{r} \quad (3.82)$$

where A_{em} - geometric characteristic of an emulsion injector.

Equations (3.82) and (3.45) are analogous.

Performing conversions analogous to the conversions for a single-component injector we can be convinced that dependence of μ and 2α on A_{em} is the same as for a single-component injector (see Fig. 3.18). Consequently, knowing the fuel (i.e., ν and m) and having the radius of oxidizer inlets r_0 and their number l_0 we can conduct further calculation of a two-component emulsion injector in that same order as the calculation of single-component injectors, using for this the geometric characteristic of an emulsion injector A_{em} instead of geometric characteristic A .

Calculation of Two-Component Injectors with External Mixing

Calculation of two-component injectors with external mixing (Fig. 3.23b) basically is reduced to the calculation of internal

and external injectors examined as independent single-component injectors. Thus the radius of swirl of the external injector r_m^I should be greater than the external radius of the body of the nozzle of the internal injector r_H^{II} , i.e., $r_m^I > r_H^{II}$. In the case when $r_m^I \leq r_H^{II}$ for the external injector part of the useful cross section will be blocked by the body of the internal injector.

Radius of swirl of the external injector r_m^I is easy to determine, knowing the geometric characteristic of the injector, since formulas (3.29) and (3.54) give us a connection between A , coefficient of useful cross section φ , and the ratio r_m/r_c .

Solving jointly equations (3.29) and (3.54), we find for an ideal liquid the connection between r_m/r_c and A .

Angle of atomization of an external injector $2\alpha^I$ can be less than the angle of atomization of an internal injector $2\alpha^{II}$ (as shown in Fig. 3.23b) and greater. In the first case intersection of the flames of atomization ensures the best mixing. With $2\alpha^I > 2\alpha^{II}$ there is ensured the best protection of the head against burnout (in so doing frequently fuel is fed into the external injector). Concluding the consideration of different types of injectors (spray, centrifugal, mono, and two-component, etc.), it must be noted that an important stage in the development of injectors is their hydraulic testing, which usually are conducted with water. These tests permit correcting the calculation discharge coefficients and angles of atomization, and also obtaining the necessary data on mixing and distribution of the component according to chamber section.

3.5. Chamber Heads for the ZhRD

The chamber head of an engine is the main subassembly providing correct carburetion in the combustion chamber. The head should be so designed as to ensure stable burning in the chamber, promote smooth run-up of the engine, and decrease the impulse of the aftereffect (see section 5.5). The design of the head should provide for

necessary placement and reliable attachment of injectors, most convenient feed of components to injectors, and simplest technologically possible attachment of the head to the combustion chamber.

Types of Heads for the ZhRD

The basic types of heads are flat, tent, and spherical.

Flat heads (Fig. 3.24a, b, c) are the most widespread type. The advantage of flat heads is simplicity of construction. Furthermore, flat heads make it possible to ensure homogeneity of velocity field and of concentrations of fuel over the cross section of the combustion chamber. The deficiency of flat heads is their relatively low strength and rigidity. Therefore in the flat heads of large engines it is necessary to provide reinforcing elements, ensuring required strength and rigidity of head.

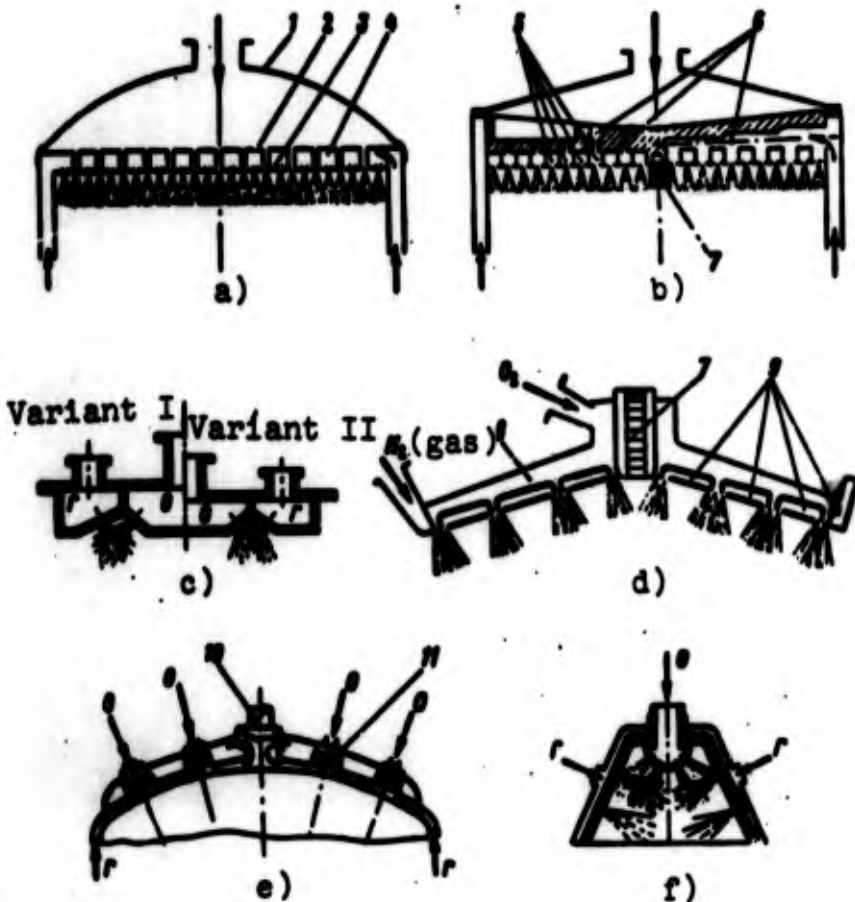


Fig. 3.24. Diagrams of heads for ZhRD:
 a) flat with double bottom; b) flat with drilled holes; c) flat with crossing streams of oxidizer and fuel; d) spherical; e) spherical with precombustion chambers; f) tent with central feed of oxidizer; 1 - upper bottom; 2 - middle bottom; 3 - lower bottom; 4 - coolant cavity; 5 - collector rings; 6 - drilled holes; 7 - igniter; 8 - O_2 cavity; 9 - H_2 annular passages; 10 - valve; 11 - precombustion chambers.

In Fig. 3.25 is shown a flat head, working as illustrated in Fig. 3.24a. Coolant 0 flows from the coolant passage to the cavity between middle 2 and lower 3 bottoms of the head, whence through screw injectors 6 it enters the combustion chamber. Component Γ passes through inlet tube 10 into the cavity between upper 1 and middle 2 bottoms and from there through screw injectors 5 to the combustion chamber. The injectors are attached by means of beading. The head is connected to the combustion chamber by connecting ring 4 and also directly by welding to the inner shell of the chamber 7.

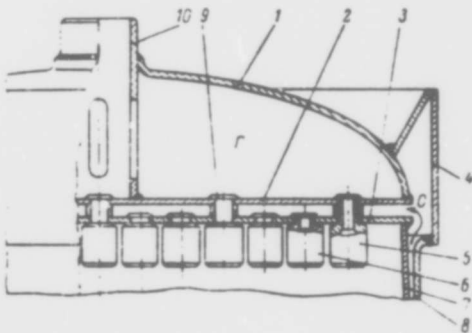


Fig. 3.25. Flat head: 1 - upper bottom; 2 - middle bottom; 3 - lower bottom; 4 - connecting ring; 5 - fuel injector; 6 - oxidizer injector; 7 - inner shell of combustion chamber; 8 - chamber housing; 9 - inlet tube; 10 - tube.

In Figs. 3.26 and 5.3 are shown the extremal appearance and cutaway view of a head with drilled holes, made in accordance with the diagram of Fig. 3.24b.

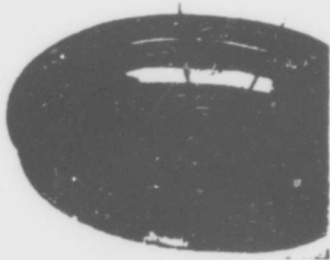


Fig. 3.26. Flat head with spray injectors.

Spherical heads have found application chiefly in high-thrust engines. The merit of such heads is structural rigidity.

In Figs. 3.24d and 3.27 are shown a diagram and external appearance of the spherical head of the RL-10 oxygen-hydrogen engine.

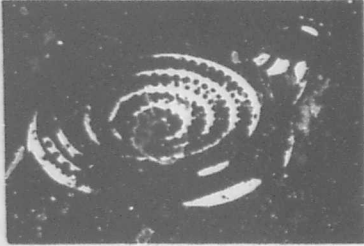


Fig. 3.27. Spherical head with spray injectors.

In Figs. 3.24d and 5.4 are shown a diagram and cutaway view of the spherical head of oxygen-alcohol engine of the A-4 missile.

Tent heads, shaped like tents (see Fig. 3.24e), find application in low- and medium-thrust engines and also as precombustion chambers. The advantages of the tent head are larger surface for placement of injectors than for flat head and good strength properties. The deficiencies of the head are complexity of manufacture and irregularity of fuel distribution over their cross section. With the tent head formation a "bunch" of atomized fuel is possible. In Fig. 3.28 is shown the precombustion chamber of the head.

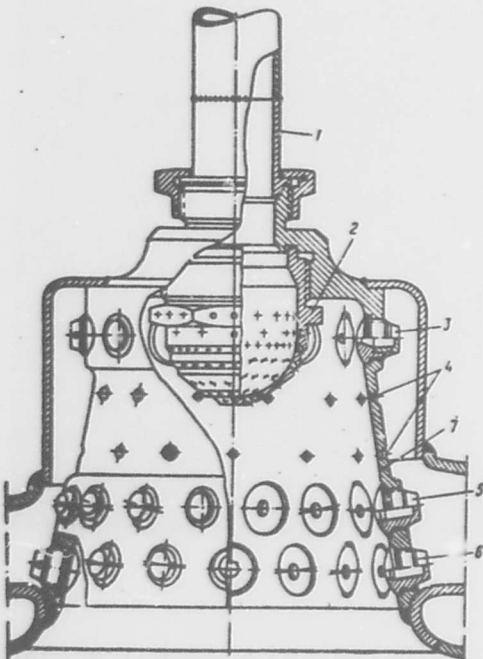


Fig. 3.28. Precombustion chamber of the head of the engine: 1 - oxidizer feed tube; 2 - central spray injector; 3 - upper row of swirlers; 4 - lateral spray injectors; 5, 6 - combined spray injectors and swirlers; 7 - inner shell of precombustion chamber.

Placement and Mounting of Injectors on Head

Placement of injectors on the head should promote fulfillment of the basic requirements imposed on carburetion while ensuring reliability and technological effectiveness of design, which basically is reduced to the following.

1. Most equal possible distribution over the cross section of the combustion chamber of the ratio of components α and flow intensity r .
2. Least possible inclination toward appearance of unstable burning.
3. Protection of combustion chamber walls from burnout.
4. Protection of combustion-chamber head from the influence of high heat flows from the flame front.
5. Convenience of feed of components.

Investigations have shown that the distribution of ratio and flow intensity of components obtained directly at the head for practical purposes is preserved along the entire combustion chamber and nozzle of the engine. In turn, irregularity of distribution of α and r over the cross section of a chamber affects specific thrust of an engine $P_{y\Delta}$ (see section 3.6).

Let us consider the basic schemes of injector placement. In engines operating on single-component injectors in order to ensure good carburetion uniform alternation of fuel and oxidizer is necessary injectors. Therefore it is possible to distinguish the following basic patterns for fuel and oxidizer injector placement.

Checkerboard placement. For which fuel and oxidizer injectors are arranged in checkerboard fashion in alternating order (Fig. 3.29a). The deficiency of this method consists in the fact that the number of fuel injectors is approximately equal to the number of oxidizer

injectors. Since the mass flow rate of the oxidizer is usually 2-4 times greater than that of fuel, with such placement the flow rate of each oxidizer injector is considerably greater than that of the fuel injector, which can worsen carburation, since the powerful stream of oxidizer mixes poorly with the relatively weak fuel spray, knocking it aside.

Honeycomb placement (Fig. 3.29b). Here each fuel injector is surrounded by a group of oxidizer injectors, making it possible to have a greater oxidizer than fuel injectors. The difference in flow rates of the oxidizer and fuel injectors is less here than with the checkerboard arrangements, which provided better atomization and mixing of fuel components.

Concentric placement. Here belts of fuel and oxidizer injectors are alternated (Fig. 3.29c). In certain designs such arrangement simplifies the feed of components to the injectors. An example of concentric location of injectors is the head of the oxygen-hydrogen engine (see Figs. 3.24d and 3.27). Here in concentric belts are groups of injectors, consisting of two fuel (H_2) and one oxidizer (O_2) injectors each.

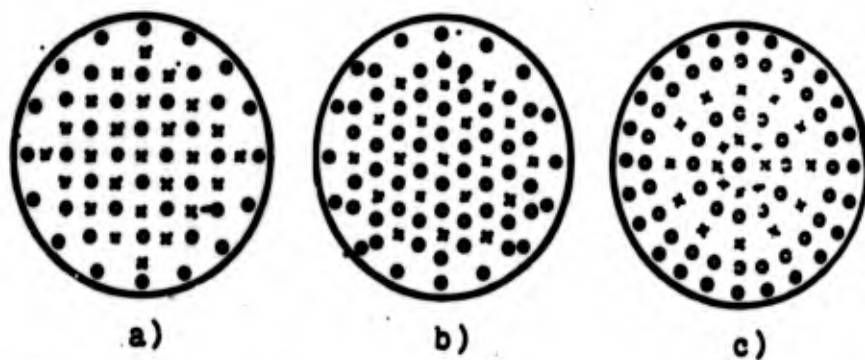


Fig. 3.29. Diagram of injector placement: a) checkerboard; b) honeycomb; c) concentric; x - fuel injector; o - oxidizer injector; ● - fuel injector for creation of near-wall layer.

Two-component injectors can be placed in any arrangement. It is necessary only to consider the possibility of appearance of unstable burning and the necessity of protecting the head from burnout.

To ensure conditions least promoting the appearance of unstable burning, both single- and two-component injectors are sometimes placed in orders, constituting different combinations of the above-mentioned arrangements, and attempts are also made to extend the process of burning somewhat over the length of the combustion chamber. At the end of chamber it is desirable that there be a heterogeneous zone, which damps as far as possible longitudinal high-frequency combustion instability [4]. This is attained by a certain alternation of injectors with different flow rates and spray angles (i.e., range).

For protection of combustion-chamber walls from burnout a protective near-wall layer, overly rich in fuel, and consequently of lower temperature than the flow core, is created. It is necessary to note that a near-wall layer with a great surplus of oxidizer also would have a temperature lower than that of the flow core and would apparently be a fully satisfactory protective layer, but the danger of appearance of local seats of burning at the wall in the oxidizing medium and burnout of walls due to oxidation of metal is the reason the fuel-enriched near-wall layer is usually created. For this purpose on the head there either is placed a special peripheral belt of fuel injectors, as in Fig. 3.29 or the outer oxidizer injectors are replaced by fuel injectors.

The peripheral fuel injectors usually have longer range and lower flow rate than the main injectors. The spacing between peripheral ("protective") injectors and their positions are selected in such a way as to ensure uniform thickness of the near-wall layer about the perimeter of the chamber. Local increase in thickness of the near-wall layer leads only to increased losses of thrust without improving protection of the walls. At the same time excessive thinning of the protective wall layer or its puncture by streams of oxidizer should not be allowed.

In laying out the injectors it is necessary also to provide protection for the head itself from burnout, which might be a result of high thermal conduction from the flame kernel. From this standpoint zones of atomization and evaporation are zones protecting the head

from large heat flows, but with great distance between injectors there can be sections of the surface of the head not sufficiently protected from the influence of reverse currents of hot products of combustion, which can lead to burnout of the head. Such danger arises with the application of two-component injectors, for which the flame front is nearer the head. When swirlers are used the least distance between injectors is usually determined by the size of the injector itself and also by considerations of strength of the head, weakened by the holes drilled for the injectors, varying from 12 to 30 mm [27]. Spray injectors are given the same spacing.

Flow rates through the single-component injector vary from 30 to 300 g/s and for peripheral injectors can be less. The flow rates through the two-component injector can reach 2.5-3 kg/s. With cooled heads it is possible to considerably increase the flow rate through one injector. Tests of heads cooled by fuel, with flow rate through one injector of the order of 20 kg/s, gave satisfactory results [67].

For protection of the head from burnout it is possible to use different heat-resistant coatings [69].

Fuel is fed to injectors either through special channels (see Fig. 3.24b) or by way of formation in the head of different cavities for fuel and oxidizer (see Fig. 3.24a, c, d), ensuring approximately identical pressure drop in all injectors.

Heads with supply of components through channels are structurally more complicated and usually are heavier than those with separate cavities. The lower cavity, usually for structural considerations, is fed the component that cools the combustion chamber.

Mounting of injectors. When injectors are made in the form of separate structural subassemblies, the most widespread method of mounting is soldering. Threaded connection and beading are also used.

Placement on a head of various auxiliary devices (igniter, scavenging devices, etc.) is undesirable since they reduce the useful area for placement of injectors and upset the uniformity of fuel distribution. In addition the points at which these devices are mounted are less well protected from heat fluxes, thus creating the danger of head burnout.

3.6. Influence of the Head on Carburetion and Specific Thrust

Investigation of the operation of ZhRD showed that the quality of the carburetion process and specific thrust depend on the design of the head, its shape, and the location and type of injectors. The placement of the injectors likewise influences conditions of burning and heat exchange in the chamber of the ZhRD.

Let us consider certain analytical schemes making it possible to conduct quantitative appraisal of the influence of injector placement on development of processes of mixing of components and on parameters of the ZhRD [8].

Qualitative Picture of the Process of Carburetion in the Chamber of the ZhRD

After entering the combustion chamber the oxidizer and fuel are mixed in both liquid and gaseous states.

One of the basic factors determining the mixing of components is the mutual location of oxidizer and fuel injectors. After the oxidizer and fuel leave the injectors there is collision drops of components and merging of them in addition to partial interpenetration of atomized streams, promoting mixing of components near the head. Most complete mixing takes place when injectors with crossing streams are used. However, even with parallel axes of injectors, as a result of the meeting of spray cones at a certain distance from the head, mixing and merging of drops also takes place.

Let us examine, for example, how the mixing of drops of components fed by swirlers occurs.

is limited primarily by the spacing between injectors, and at great distances from the axis of the injector the influence of the given injector on mixing is small. Consequently, if the placement of injectors in the head from the very beginning does not ensure uniform relationship of components over the cross section of the chamber the mixing of drops will smooth out this irregularity basically only within limits of the spacing between injectors.

The second factor promoting mixing of components is turbulence, appearing during evaporation of drops.

The intensity of turbulence here is influenced by:

- a) the difference in speeds of drops and gas;
- b) outflow of gases forming during evaporation of a drop normal to its surface;
- c) irregularity of intensity flow over the cross section of the chamber;
- d) difference in rates of evaporation of drops of components.

Let us consider the influence of each of these causes on mixing. As was noted above, directly at the head evaporation of drops starts as a result of reverse currents and radiation (see Fig. 3.4). While the amount of gas forming as a result of evaporation is still small drop speed w_K is greater than gas speed w_P . With evaporation of drops the speed of the gas increases and in some section of the chamber the speeds are levelled, i.e., $w_P = w_K$ (point M in Fig. 3.6). The quantity of evaporated components here attains 10-35% of the total quantity. With further motion of drops and gas the drop speed lags behind the gas speed, and accordingly the speed of the gas directly near a drop (or of the gas near formed bundles of drops) also lags behind the speed of the basic flow of gas w_P . The difference in speeds promotes turbulent mixing of the gas surrounding the drop (or bundle) with the basic flow of gas.

Presence of the stream of gas normal to a drop and forming as a result of evaporation of the drop also promotes turbulent mixing of gas with the basic flow.

Mixing of gas as a result of the shown causes occurs basically at distances of the order of the spacing between injectors H . The influence of this mixing we can consider on the basis of the corresponding law of distribution of components around the injector axis.

During mixing of gas nonuniformity of distribution of flow intensity r results in the flow of gases for distances of the order of the chamber radius, since even after the leveling of r at distances from the axis of a bundle equal to the spacing between injectors nonuniformity of r over the cross section of the chamber remains. Here gas flows to sections, in which flow intensity r is less. However, this process does not render decisive influence on change of distribution of components over the cross section of the chamber.

The distinction in speeds of evaporation of drops of component is also evident in turbulent mixing of gases. During the outflow of gases from drops the gases do not entrain liquid drops, and therefore when there is considerable difference in the rates of evaporation of drops of components (for example, of liquid oxygen and kerosene), there is a change in distribution of v and r , since the gases of the component evaporated earlier try to distribute themselves more evenly over the cross section. However, due to very high intensity of heat supply to drops in the chamber of ZhRD the rates of evaporation of drops are so high that the difference in time of evaporation of different components is very insignificant and does not succeed in significantly influencing the distribution of v and r over the cross section of the chamber as a whole.

Thus one may assume that the mixing of components as a result of evaporation, just as during the mixing drops, occurs basically within the limits of dimensions of the order of the spacing between injectors. Insignificant propagation of mixing of gases during evaporation over

larger distances can be allowed for through proper selection of the law of distribution of the component around the injector axis.

After termination of evaporation further mixing and combustion of components occur. However, up to defined chamber lengths full mixing in a chamber, i.e., complete levelling off of the composition of the gas over the cross section of the chamber is not realized.

During further motion of the products of combustion through the nozzle distribution of the relationship of components remains practically unchanged, first, due to the fact that the time of their presence in the nozzle is small, and secondly, because the intensity of turbulence in the flow core in the nozzle is considerably less than in the combustion chamber.

Thus if uniform composition of components over the cross section of the chamber were not ensured at the head by the injectors, the turbulent mixing of gases in the combustion chamber and in the nozzle would only smooth the "peaks" of distribution of v and r between injectors (Fig. 3.31), but does not eliminate as a whole irregularity. It is obvious that the greater the length of combustion chamber and nozzle, the less valid this conclusion, since the flow of gases through the chamber and nozzle certain mixing nevertheless continues, but up to a defined length of combustion chamber and nozzle for approximation one may assume that the composition of separate streams of the products of combustion leaving the nozzle is different, where this irregularity is determined in the first place by the location of injectors on the head.

For appraisal of the distribution of v over the cross section of a chamber it is sufficient to consider the distribution of v obtained as a result of mixing of drops at the head upon exit of components from the injectors. Here the influence of turbulent mixing of gases can be considered by means of the corresponding law of distribution of a component around the injector axis.



Fig. 3.31. Typical distribution of v over the cross section of a chamber: 1 - neglecting smoothing of peaks; 2 - average values of v .

Distribution of Components Around the Injector Axis

Let us examine the head with swirlers. For simplicity of analysis we will take checkerboard placement of oxidizer O and fuel F injectors (Fig. 3.32b).

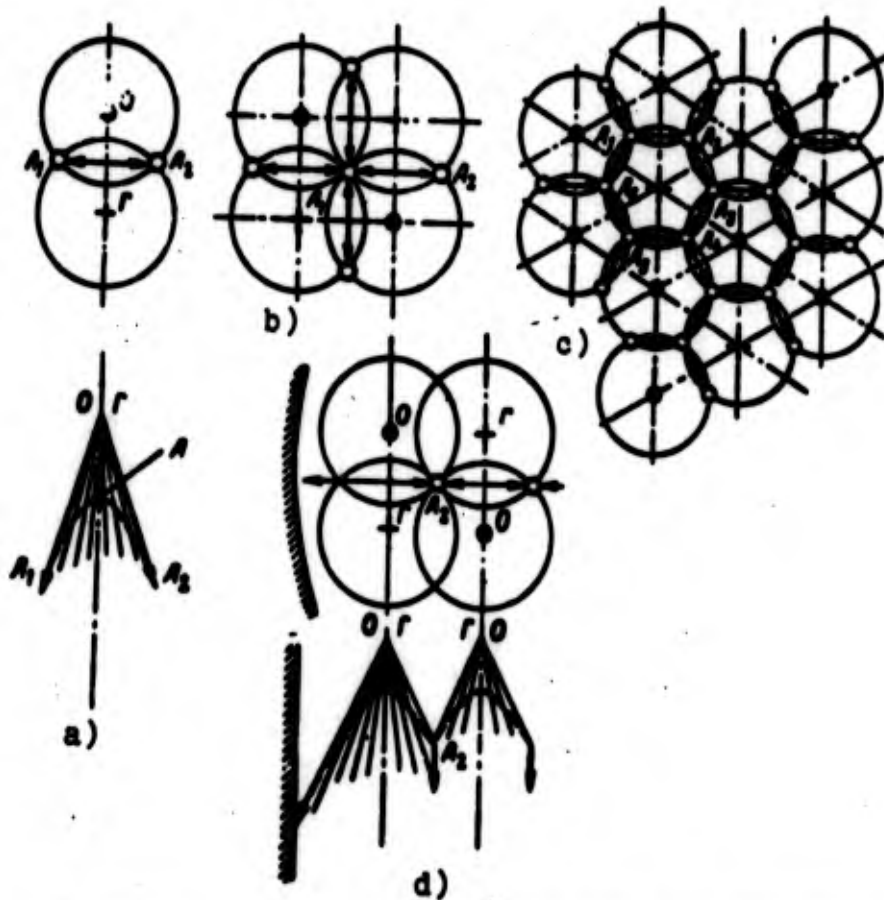


Fig. 3.32. Formation of bundles of mixture of components: a) two injectors; b) checkerboard layout; c) honeycomb layout; d) injectors \bullet - oxidizer injectors; $+$ - fuel injectors; o - points of formation of bundles.

We will also consider that momenta of oxidizer and fuel are equal. Consequently, after the crossing of torches at point A the bundle will be axially directed (see Fig. 3.30b). The crossing of torches of two adjacent injectors O and Γ follows hyperbola A_1AA_2 (Fig. 3.32a). The projection of the line of crossing of torches on the plane parallel to the head will be straight line A_1A_2 .

After merging of oxidizer and fuel on the line of crossing A_1AA_2 drops have component velocities directed vertically (along the axis) and horizontally. The horizontal component of velocity will obviously be directed from the line connecting the axis of injectors to points A_1 and A_2 . As a result at points A_1 and A_2 bundles of the mixture of components are formed.

During the interaction of injectors arranged in checkerboard fashion merging of the mixture of drops into a bundle occurs at points A_1, A_2, A_3, A_4 , where in each of these bundles there will be merging of components from the crossing of spray cones of the four injectors surrounding the bundle (Figs. 3.32b and 3.33).

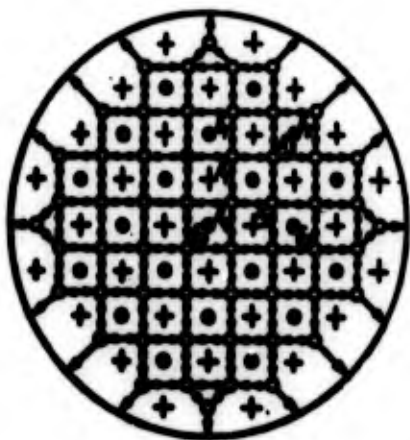


Fig. 3.33. Formation of bundles at head with checkerboard placement of injectors: ● - oxidizer injectors; + - fuel injectors; ○ - points of formation of bundles.

With honeycomb placement of injectors (see Fig. 3.32c) bundles will be formed at points A_1, A_2, A_3, A_4, A_5 , and A_6 .

In all cases of drops nearer the wall than the axis of the injectors nearest to it strike the wall (see Fig. 3.32d).

Bundles of drops formed in our case at points A_1 , A_2 , A_3 , and A_4 move parallel to the chamber axis. Here the bundles expand both as a result of entrainment of drops by gas and as a result of certain very slight penetration of drops, and also as a result of the evaporation of drops of components.

For approximation we will assume that at sufficient distance from the head the distribution of components around the axis of a bundle follows a certain law of distribution, close to Gaussian law (Fig. 3.34), where the value of root-mean-square deviation of oxidizer or fuel from the axis of the bundle is proportional to the spacing between injectors H , i.e.,

$$\frac{dG}{dF} = k e^{-\frac{r^2}{H^2}}, \quad (3.83)$$

where G — flow rate of component in bundle; r — distance from axis of bundle; dG — quantity of component in area dF at distance r from axis of bundle.

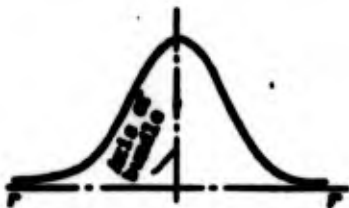


Fig. 3.34. Accepted distribution of component around the axis of a bundle.

Let us examine the distribution of a quantity of oxidizer around the axis of a selected injector. The oxidizer fed through the injector was distributed equally between bundles A_1 , A_2 , A_3 , and A_4 . Each of these bundles, furthermore, received oxidizer from injectors B_1 , B_2 , B_3 , and B_4 (see Fig. 3.33). The quantity of oxidizer at the axis of the injector examined by us is determined as the sum of the quantities coming from bundles A_1 , A_2 , A_3 , and A_4 (Fig. 3.35, curve 1).

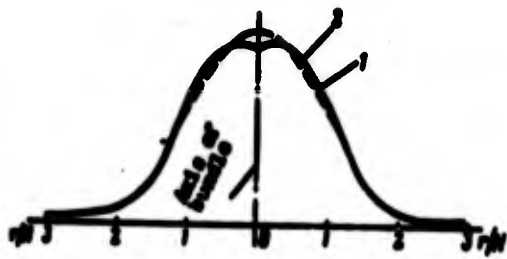


Fig. 3.35. Distribution of component around injector axis.

Distribution of component around the axis (curve 1) also follows a law close to Gaussian (curve 2). Therefore with sufficient degree of accuracy it is possible to consider that the distribution of oxidizer around the injector axis follows curve 2, i.e., obeys Gaussian law, where the root-mean-square deviation of the component is proportional to the spacing between injectors H :

$$\frac{dG_0}{dF} = k e^{-\frac{r^2}{2H^2}}, \quad (3.84)$$

where G_0 - flow rate of component through injector; dG_0 - flow rate of component through area dF , normal to the injector axis and at distance r from the axis; k - proportionality factor, determined through integration of equation (3.84):

$$G_0 = k \iint e^{-\frac{r^2}{2H^2}} r dr d\varphi = k \int_0^{2\pi} d\varphi \int_0^{\infty} r e^{-\frac{r^2}{2H^2}} dr = 2\pi k H^2,$$

whence

$$k = \frac{G_0}{2\pi H^2}. \quad (3.85)$$

Taking into account equation (3.85), we express the law of distribution of the component around the injector axis by equation

$$\frac{dG_0}{dF} = \frac{G_0}{2\pi H^2} e^{-\frac{r^2}{2H^2}}. \quad (3.86)$$

If the momentum of drops of one of the components is greater than that of the other, then, as was shown above, at point B bundles of components cross a second time (see Fig. 3.30).

Analysis shows that the secondary crossing does not introduce essential change, and expression (3.86) remains valid for appraisal of distribution of the component around the injector axis for both checkerboard and other injector arrangements.

Quantity of Component Reaching an Area of Cross Section from a Single Injector

Let us isolate in the cross section of the chamber an arbitrarily located area and determine the quantity of component $G_{\Pi\Pi}$, reaching it from injector B, located at distance r from the area (Fig. 3.36). From equation (3.86)

$$G_{\Pi\Pi} = \frac{G_{0B}}{2\pi H^2} \iint e^{-\frac{r^2}{H^2}} dx dy. \quad (3.87)$$

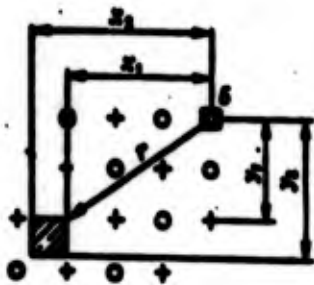


Fig. 3.36. Determination of quantity of component reaching an arbitrarily selected area of the chamber cross section.

Since $r^2 = x^2 + y^2$,

$$G_{\Pi\Pi} = \frac{G_{0B}}{2\pi H^2} \iint e^{-\frac{x^2}{H^2}} e^{-\frac{y^2}{H^2}} dx dy =$$

$$= \frac{G_{0B}}{2\pi H^2} H\sqrt{2} \int_0^{\frac{x_1}{H\sqrt{2}}} e^{-\left(\frac{x}{H\sqrt{2}}\right)^2} d\left(\frac{x}{H\sqrt{2}}\right) H\sqrt{2} \int_0^{\frac{y_1}{H\sqrt{2}}} e^{-\left(\frac{y}{H\sqrt{2}}\right)^2} d\left(\frac{y}{H\sqrt{2}}\right). \quad (3.88)$$

Expression (3.88) after reduction twice by $H\sqrt{2}$ can be written in the form

$$G_{\Pi\Pi} = \frac{G_{0B}}{2\pi} \left[\int_0^{\frac{x_1}{H\sqrt{2}}} e^{-\left(\frac{x}{H\sqrt{2}}\right)^2} d\left(\frac{x}{H\sqrt{2}}\right) - \int_0^{\frac{x_1}{H\sqrt{2}}} e^{-\left(\frac{x}{H\sqrt{2}}\right)^2} d\left(\frac{x}{H\sqrt{2}}\right) \right] \times$$

$$\times \left[\int_0^{\frac{y_1}{H\sqrt{2}}} e^{-\left(\frac{y}{H\sqrt{2}}\right)^2} d\left(\frac{y}{H\sqrt{2}}\right) - \int_0^{\frac{y_1}{H\sqrt{2}}} e^{-\left(\frac{y}{H\sqrt{2}}\right)^2} d\left(\frac{y}{H\sqrt{2}}\right) \right]. \quad (3.89)$$

If we introduce a function of form

$$\bullet(\varphi) = \frac{2}{\sqrt{\pi}} \int_0^{\varphi} e^{-z^2} dz, \quad (3.90)$$

then, considering that

$$\int_0^{\varphi} e^{-\left(\frac{z}{H\sqrt{2}}\right)^2} d\left(\frac{z}{H\sqrt{2}}\right) = \int_0^{\frac{\varphi}{H\sqrt{2}}} e^{-z^2} dz, \quad (3.91)$$

where $z = x/H\sqrt{2}$, and designating

$$\left. \begin{aligned} \varphi_{x,1} &= \frac{x_1}{H\sqrt{2}}; & \varphi_{x,2} &= \frac{x_2}{H\sqrt{2}}; \\ \varphi_{y,1} &= \frac{y_1}{H\sqrt{2}}; & \varphi_{y,2} &= \frac{y_2}{H\sqrt{2}}. \end{aligned} \right\} \quad (3.92)$$

we obtain:

$$\left. \begin{aligned} \bullet(\varphi_{x,1}) &= \frac{2}{\sqrt{\pi}} \int_0^{\frac{\varphi_{x,1}}{H\sqrt{2}}} e^{-\left(\frac{z}{H\sqrt{2}}\right)^2} d\left(\frac{z}{H\sqrt{2}}\right); \\ \bullet(\varphi_{x,2}) &= \frac{2}{\sqrt{\pi}} \int_0^{\frac{\varphi_{x,2}}{H\sqrt{2}}} e^{-\left(\frac{z}{H\sqrt{2}}\right)^2} d\left(\frac{z}{H\sqrt{2}}\right); \\ \bullet(\varphi_{y,1}) &= \frac{2}{\sqrt{\pi}} \int_0^{\frac{\varphi_{y,1}}{H\sqrt{2}}} e^{-\left(\frac{z}{H\sqrt{2}}\right)^2} d\left(\frac{z}{H\sqrt{2}}\right); \\ \bullet(\varphi_{y,2}) &= \frac{2}{\sqrt{\pi}} \int_0^{\frac{\varphi_{y,2}}{H\sqrt{2}}} e^{-\left(\frac{z}{H\sqrt{2}}\right)^2} d\left(\frac{z}{H\sqrt{2}}\right). \end{aligned} \right\} \quad (3.93)$$

Then expression (3.89) can be rewritten:

$$G_{\pi\pi} = \frac{G_{00}}{4} [\bullet(\varphi_{x,2}) - \bullet(\varphi_{x,1})][\bullet(\varphi_{y,2}) - \bullet(\varphi_{y,1})] \quad (3.94)$$

Numerical determination of $G_{\pi\pi}$ requires the ability to calculate integral (3.90) for any values of φ . Since integral (3.90) in finite form is not expressed through elementary functions, for calculations we use Table 3.1 of values of $\Phi(\varphi)$ for different values of φ .

Table 3.1. Values of function $\Phi(z) \cdot 10^4$

z	0	1	2	3	4	5	6	7	8	9
0.0	0	113	226	336	451	564	675	789	901	1013
0.1	1125	1236	1348	1459	1569	1680	1790	1900	2009	2118
0.2	2227	2336	2443	2550	2657	2763	2869	2974	3079	3183
0.3	3286	3390	3491	3593	3694	3794	3893	3992	4090	4187
0.4	4304	4399	4475	4569	4662	4755	4847	4937	5027	5117
0.5	5305	5392	5479	5565	5649	5733	5816	5898	5979	6059
0.6	6309	6317	6394	6470	6546	6620	6694	6766	6838	6908
0.7	6778	6847	6914	6981	7047	7112	7175	7238	7300	7361
0.8	7421	7489	7556	7623	7689	7754	7818	7881	7943	8004
0.9	7969	8019	8068	8116	8163	8209	8254	8299	8342	8385
1.0	8427	8468	8508	8548	8586	8624	8661	8698	8733	8768
1.1	8802	8835	8868	8900	8931	8961	8991	9020	9048	9076
1.2	9103	9130	9155	9181	9205	9229	9252	9275	9297	9319
1.3	9338	9359	9379	9399	9418	9437	9455	9473	9490	9507
1.4	9523	9539	9554	9569	9583	9597	9611	9624	9637	9649
1.5	9661	9673	9684	9695	9705	9716	9726	9736	9745	9755
1.6	9763	9772	9780	9788	9796	9804	9811	9818	9825	9832
1.7	9838	9844	9850	9856	9861	9867	9872	9877	9882	9886
1.8	9891	9895	9899	9903	9907	9911	9915	9918	9922	9925
1.9	9929	9931	9934	9937	9939	9942	9944	9947	9949	9951
2.0	9953	9957	9957	9959	9960	9962	9964	9965	9967	9968
2.1	9970	9971	9972	9974	9975	9976	9977	9978	9979	9980
2.2	9981	9982	9983	9984	9984	9985	9986	9986	9987	9988
2.3	9989	9989	9990	9990	9990	9991	9991	9992	9992	9992
2.4	9993	9993	9993	9994	9994	9994	9995	9995	9995	9995
2.5	9995	9995	9995	9995	9995	9995	9997	9997	9997	9997
2.6	9997	9997	9997	9998	9998	9998	9998	9998	9998	9998
2.7	9998	9998	9998	9998	9998	9998	9999	9999	9999	9999
2.8	9999	9999	9999	9999	9999	9999	9999	9999	9999	9999
2.9	9999	9999	9999	9999	9999	9999	9999	9999	9999	9999

With change of ϕ from 0 to π function $\Phi(\phi)$ changes from 0 to 1. Substituting in equation (3.93) values of $\phi_{x,2}$; $\phi_{x,1}$; $\phi_{y,1}$; $\phi_{y,2}$ and determining from Table 3.1 corresponding values of function $\Phi(\phi)$, we can, using formula (3.94), determine the quantity of component reaching the area from injector B.

In calculating distances x_1 , x_2 , y_1 , y_2 it is necessary to take them with their sign, and the condition (taking sign into account) $x_2 > x_1$; $y_2 > y_1$.

Relationship of Components in Flow Core

In accordance with formula (3.94) quantities of oxidizer $G_{O.пл}$ and fuel $G_{F.пл}$, reaching an arbitrarily selected area in the cross section area of the chamber section from i_0 and i_r of the injectors will be equal

$$\left. \begin{aligned} G_{O.пл} &= \frac{1}{4} \sum_{i_0} G_{O_i} [\phi(r_{x,2}) - \phi(r_{x,1})] [\phi(r_{y,2}) - \phi(r_{y,1})]; \\ G_{F.пл} &= \frac{1}{4} \sum_{i_r} G_{F_r} [\phi(r_{x,2}) - \phi(r_{x,1})] [\phi(r_{y,2}) - \phi(r_{y,1})]. \end{aligned} \right\} \quad (3.95)$$

The mean value of the relationship of components passing through the area

$$v_{пл} = \frac{G_{O.пл}}{G_{F.пл}} = \frac{\sum_{i_0} G_{O_i} [\phi(r_{x,2}) - \phi(r_{x,1})] [\phi(r_{y,2}) - \phi(r_{y,1})]}{\sum_{i_r} G_{F_r} [\phi(r_{x,2}) - \phi(r_{x,1})] [\phi(r_{y,2}) - \phi(r_{y,1})]}. \quad (3.96)$$

If flow rates through all injectors O and F are identical,

$$G_{O_i} = \frac{G_O}{i_0}; \quad G_{F_r} = \frac{G_F}{i_r} \quad (3.97)$$

and expression (3.96) will take form

$$v_{пл} = v_{OF} \frac{i_r}{i_0} \cdot \frac{\sum_{i_0} [\phi(r_{x,2}) - \phi(r_{x,1})] [\phi(r_{y,2}) - \phi(r_{y,1})]}{\sum_{i_r} [\phi(r_{x,2}) - \phi(r_{x,1})] [\phi(r_{y,2}) - \phi(r_{y,1})]}. \quad (3.98)$$

Formula (3.98) gives us the average value of the relationship of components passing through the arbitrarily selected area of the chamber. Here the dimensions of the area were not limited.

For practical calculations it is fully sufficient to take linear dimensions of the area equal to the spacing between injectors. The shape of the area can be different for every selected injector layout.

Relationship of Components v_{CT} in the Near-Wall Layer

As noted above, all drops of components exceeding the limits of the line connecting the axes of the extreme injectors strike the

wall. Since in striking the wall all drops remain within the limits of the area, one may assume that the quantity of component reaching a near-wall area of width $x_2 - x_1$ (Fig. 3.37) will be equal to the quantity of component in a strip of infinite length (i.e., $y_2 = \infty$).



Fig. 3.37. Determination of v_{CT} .

When $y_2 = \infty$ function $\Phi(\phi_{y,2}) = 1$ and the expression of (3.95) for the area located at the wall will be recorded in the form:

$$\left. \begin{aligned} G_{o,cr} &= \frac{1}{4} \sum_i G_{\phi_o} [\Phi(\varphi_{x,2}) - \Phi(\varphi_{x,1})] [1 - \Phi(\varphi_{y,1})]; \\ G_{r,cr} &= \frac{1}{4} \sum_i G_{\phi_r} [\Phi(\varphi_{x,2}) - \Phi(\varphi_{x,1})] [1 - \Phi(\varphi_{y,1})]. \end{aligned} \right\} \quad (3.99)$$

Hence the ratio of components in the near-wall layer

$$v_{cr} = \frac{G_{o,cr}}{G_{r,cr}} = \frac{\sum_i G_{\phi_o} [\Phi(\varphi_{x,2}) - \Phi(\varphi_{x,1})] [1 - \Phi(\varphi_{y,1})]}{\sum_i G_{\phi_r} [\Phi(\varphi_{x,2}) - \Phi(\varphi_{x,1})] [1 - \Phi(\varphi_{y,1})]}. \quad (3.100)$$

Just as during determination of v for average sections of the chamber, during determination of v_{CT} the size of the area ($x_2 - x_1$) is expediently taken equal to the spacing between injectors. Formulas (3.95), (3.96), and (3.99) and (3.100) permit determining flow rates and the relationship of components with account be taken of all injectors, in a head. However, as one may see from Fig. 3.35 the influence of injectors apart from the area by a distance greater than three spacings is very insignificant. Therefore during calculation of the shown parameters it is fully permissible to consider only

injectors distant from a given area (in middle of the cross section or at the wall) by no further than three spacings.

Usually arrangements of injectors on a head have axial symmetry. Therefore there is no need to calculate flow rate and the relationship of components for all sections of a chamber, but it is sufficient to calculate only for one sector of the head (for example, with checkerboard layout for 1/8 of the cross section). Since the influence of a large number of injectors located at various distances is considered here, for practical purposes it is convenient to perform calculations by using a scale diagram of the injector layout and measuring distances x_2 , x_1 , y_2 , y_1 directly on the diagram.

Example of calculation of relationship of components v_{CT}

Find the relationship of components at the wall in section No. 1 of the combustion chamber head of an engine. A plan view of injector placement and the location of the selected section are shown in Fig. 3.38.

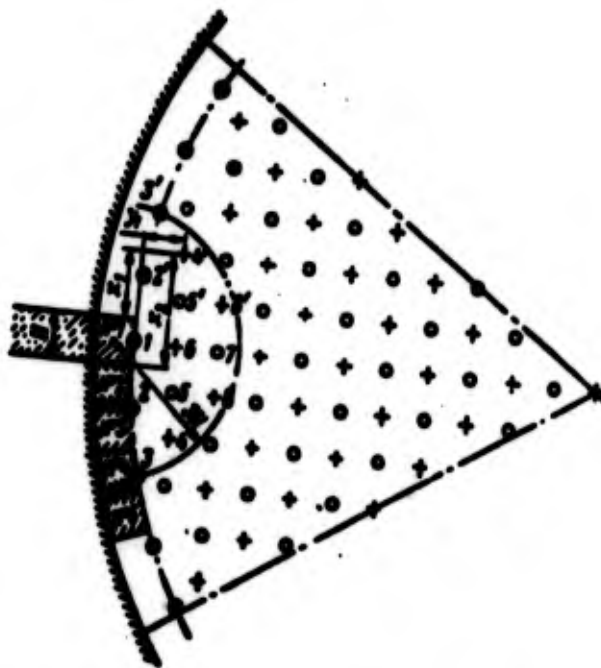


Fig. 3.38. Solution of example: o - screen injectors Γ_3 ; + - fuel injectors Γ ; o - oxidizer injectors O.

Flow rates through the injectors: screen fuel $G_{T.3} = 10$ g/s; fuel $G_T = 33$ g/s; oxidizer $G_O = 90$ g/s.

Solution: We consider that the section is reached only by components from injectors located at distance $\leq 3H$. Drawing an arc with radius equal to $3H$, we define the region containing injectors influencing the relationship of components passing through area No. 1. We see that this region contains 13 injectors.

For convenience of further calculation of data on flow rate, distances, and values of auxiliary functions for these injectors is given in Table 3.2.

Having determined all necessary data, we calculate the relationship of components in section No. 1 (3.100):

$$v_{cr} = \frac{\sum G_{O,i} [\phi(\varphi_{x,2}) - \phi(\varphi_{x,1})] [1 - \phi(\varphi_{y,1})]}{\sum G_{T,i} [\phi(\varphi_{x,2}) - \phi(\varphi_{x,1})] [1 - \phi(\varphi_{y,1})]} = \frac{2 \cdot 13,8 + 3,16}{7,88 + 2 \cdot 2,80 + 2 \cdot 0,116 + 3 \cdot 1,26 + 8,03 + 2 \cdot 0,733} = 1,22.$$

It is possible to determine the relationship of components in any other section analogously.

Geometric Method of Calculation of Relationship of Components Over the Cross Section of a Chamber

Calculation of the distribution of the relationship of components over the cross section of a chamber is quite labor-consuming. Therefore for tentative calculation of the distribution of v and r over this section it is possible to use simplified geometric method, the essence of which consists in the following. The entire area of the head is split into sections. As limits of the sections are usually taken lines connecting the centers of oxidizer injectors (Fig. 3.39). For each of the sections we determine the number of included oxidizer i_O and fuel i_T injectors. If part of the injectors are on the boundary of sections, the i_O or i_T can be and fractional, since in this case the separated section receives only part of a component from a given injector.

Table 3.2.

No. of layers	Compo- nent	Dimensionless distances to section				Values of γ				Values of ϕ (γ)				$\left[\frac{\phi(\gamma_{n,2}) - \phi(\gamma_{n,1})}{\phi(\gamma_{n,2})} \right] \times 100$	$\left[\frac{\phi(\gamma_{n,2}) - \phi(\gamma_{n,1})}{\phi(\gamma_{n,1})} \right]$	$\left[\frac{\phi(\gamma_{n,2}) - \phi(\gamma_{n,1})}{\phi(\gamma_{n,1})} \right] \times 100$
		$\frac{z_1}{H}$	$\frac{z_2}{H}$	$\frac{z_3}{H}$	$\frac{z_4}{H}$	$\frac{H\sqrt{z_1}}{H}$	$\frac{H\sqrt{z_2}}{H}$	$\frac{H\sqrt{z_3}}{H}$	$\frac{H\sqrt{z_4}}{H}$	$\phi(\gamma_{n,1})$	$\phi(\gamma_{n,2})$	$\phi(\gamma_{n,3})$	$\phi(\gamma_{n,4})$			
1	Γ	0.5	0.5			0.353	0.353			-0.353	0.353			0.706	1	7.06
2 and 2'	Γ	0.9	1.9	0.1		0.026	1.31	0.071		0.031	0.920	0.000		0.200	0.920	2.6
3 and 3'	Γ	2.4	3.4	0.26		1.00	2.1	0.208		0.003	0.999	0.274		0.006	0.726	0.116
4 and 4'	Γ	1.5	2.5	1		1.00	1.76	0.705		0.006	0.997	0.001		0.121	0.319	1.26
5 and 5'	Γ	0.5	1.5	1		0.353	1.06	0.705		0.353	0.646	0.001		0.403	0.319	13.8
6	Γ	0.5	0.5	1		0.353	0.353	0.705		-0.353	0.353	0.001		0.706	0.319	8.03
7	Γ	0.5	0.5	2		0.353	0.353	1.41		-0.353	0.353	0.554		0.706	0.046	3.16
8 and 8'	Γ	0.5	1.5	2		0.353	1.06	1.41		0.353	0.646	0.554		0.403	0.046	0.733

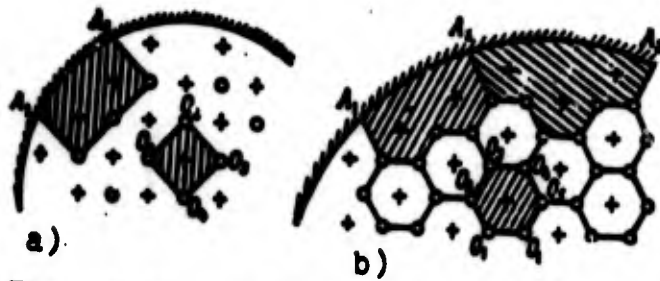


Fig. 3.39. Determination of local values of v by geometric method.

Relationship of components v and flow intensity r are determined by formulas:

$$v = \frac{\sum i_o a_o}{\sum i_r a_r}; \quad (3.101)$$

$$r = \frac{\sum i_o a_o + \sum i_r a_r}{F_{yu}}; \quad (3.102)$$

where G_o and G_r - flow rates through one injector of oxidizer of fuel respectively; F_{yu} - area of section. For an example let us examine sections $O_1 O_2 O_3 O_4$ (Fig. 3.39a) and $O_1 O_2 O_3 O_4 O_5 O_6$ (Fig. 3.39b).

Section $O_1 O_2 O_3 O_4$ from each of the oxidizer injectors is fed only $1/4$ of the flow, while section $O_1 O_2 O_3 O_4 O_5 O_6$ receives $1/3$. For the shown sections the number of oxidizer injectors i_o will be $1/4 \times 4 = 1$ and $1/3 \times 6 = 2$ respectively. The number of fuel injectors $i_r = 1$ for both sections.

The relationship of components the near-wall layer is calculated analogously (see Fig. 3.39b). For section $A_1 A_2$

$$i_o = \frac{1}{3} + \frac{1}{3} + \frac{2}{3} + \frac{1}{3} + \frac{1}{3} = 2; \quad i_r = 2; \quad v_{cr} = \frac{2G_o}{2G_r}.$$

For section $A_2 A_3$

$$i_o = \frac{1}{3} + \frac{2}{3} + \frac{1}{3} + \frac{1}{3} + \frac{2}{3} + \frac{1}{3} = \frac{8}{3}; \quad i_r = 3; \quad v_{cr} = \frac{8G_o}{2G_r}.$$

In this method no allowance is made for the influence of injectors located beyond the limits of the section, although, as was noted above (see Fig. 3.35), such influence prevails and most significantly affects the relationship of components in the near-wall layer.

Therefore the geometric method of calculation of distribution of components gives less reliable results and for calculation of the relationship of components at the wall is entirely unsuitable.

Influence of Irregularity of v and r Over the Cross Section of a Chamber on Specific Thrust and Complex β

Thus it has been established that in any of the sections of the chamber relationships of components v and flow intensity r are distributed nonuniformly. In other words, in certain sections the values of v and r differ from calculated average values. Deviation in some section of values of v from the average (most frequently optimum) means that in these sections true combustion temperatures and the composition of combustion products also differ from those calculated.

If we assume that the selected mean value of the relationship of components over the entire chamber is optimum, i.e., corresponding to the biggest value of $P_{y\Gamma}$, specific thrust in sections where values of v differ from optimum in either direction will be lower, and the specific thrust of the combustion chamber on the whole, obviously, will also decrease.

Having split the cross section of the chamber into sections and determined by some or other method the values of flow rates, relationships of components, and flow intensity for each of the sections, we find the specific thrust of the engine and the computed value of complex β_p as the average value of specific thrust and complex β_1 of separate streams of different composition:

$$P_{y\Gamma} = \frac{\sum P_{y\Gamma i} G_i}{G}; \quad (3.103)$$

$$\beta_p = \frac{\sum \beta_1 G_i}{G}. \quad (3.104)$$

where $P_{y\Gamma i}$ - specific thrust for the true relationship of components in the i -th section; G_i - flow rate of fuel through the i -th section;

G - total fuel flow rate; β_1 - value of complex β , corresponding to composition of components passing through i -th section.

C H A P T E R IV

COOLING OF ZhRD

4.1. Heat Exchange in ZhRD

Organization of chamber cooling is one of the most important problems in designing the ZhRD, and as compared to other types of heat engines is complicated considerably by peculiarities of the process of heat exchange in such engines.

The first peculiarity consists in that the process in the chamber of the liquid fuel rocket engine takes place at high temperatures (3000-4000°K and pressures (to 100 [atm(abs.)] and more). Since combustion products move through the engine chamber at very high speed, the coefficient of convective heat transfer from hot combustion products to chamber walls and convective heat fluxes q_K , reaching in the critical section of the nozzle $20-60 \cdot 10^6$ kcal/m²h ($23.3-69.7 \cdot 10^6$ W/m²), increase sharply.

The second peculiarity of heat exchange in the ZhRD is the high level of radiation in the combustion chamber, which leads to large radiant heat fluxes q_R .

As it is known, the emittance of gases is proportional to the absolute temperature in degree of 3-3.5, and therefore at the shown temperatures in combustion chamber and nozzle of the ZhRD large heat fluxes are caused by radiation q_R , which for conventional propellants reach 20-40% of the total heat flux to combustion chamber walls. With reduction of the temperature of gas in the

nozzle the relative part of radiant heat flux decreases.

The third peculiarity of heat exchange consists in that powerful total convective and radiant heat fluxes to the chamber wall cause its temperature to reach impermissibly high values. Therefore in the ZhRD materials possessing heat resistance and greatest possible thermal conductivity should be used - but this, however, is very difficult since heat-resistant materials, as a rule, have comparatively low thermal conductivity.

The fourth peculiarity of heat exchange is due to the conditions of application of the ZhRD as a propulsion system for flight vehicles (rocket, satellite, and aircraft). Therefore it is not rational to use special liquid for cooling such engines. Usually the ZhRD is cooled by one of the components of fuel by passing it prior to its entry into the combustion chamber through the cooling cavity. Such principle of cooling complicates chamber design and imposes additional requirements on fuel components, since the quantity of the component passed through the coolant passage is limited by its flow rate.

In addition to the indicated chief characteristics of the ZhRD on the whole the process of cooling is also influenced by the kind of fuel, type and assignment of engine, and its design.

Thus the application of a low-boiling pair of components (for example, oxygen + hydrogen) means that the chamber is cooled basically not by liquid, but gas, resulting in additional requirements being imposed on the engine design. The application of nozzles with central body sharply complicates the problem of cooling the ZhRD in connection with increase of the surface of the combustion chamber, and especially the perimeter of the critical section, in which heat flux is greatest.

A number of specific problems in the organization of cooling of ZhRD arise during the use of different types of fuels, application of different chamber designs and coolant passages, and during the use of different forms of cooling.

These problems will be discussed below in greater detail in corresponding sections.

The temperature of the chamber walls of the ZhRD can be held within permissible limits by one of the following methods:

1. External (or regenerative) cooling.
2. Internal cooling.
3. Mixed cooling.
4. Radiation cooling.
5. Ablation cooling.
6. Shielding internal walls with heat-resistant coverings.
7. Protecting walls from burnout by accumulation of heat.

Heat Exchange in the ZhRD with External Cooling

In order to understand processes of heat exchange in the ZhRD we will examine the basic factors affecting the effectiveness of cooling in reference to the most widespread method - external cooling.

A typical diagram of development of the process of heat exchange in the ZhRD with external cooling is presented in Fig. 4.1. Here T_2 - temperature of combustion products, $T_{r.ct}$ - temperature of chamber wall on the hot-gas side ("gas" wall), $T_{ж.ct}$ - temperature of chamber wall on the coolant side ("liquid" wall), $T_{ж}$ - temperature of coolant.

Heat is transferred by convection and radiation from hot combustion products 1 to combustion-chamber wall 3. Thus it is possible to say that the total specific heat flux from hot gases to chamber walls q_r is composed of two specific heat fluxes:

convective q_K and radiant q_R , i.e.,

$$q_s = q_K + q_R \quad (4.1)$$

where

$$q_K = \alpha_r (T_s - T_{r,cr}). \quad (4.2)$$

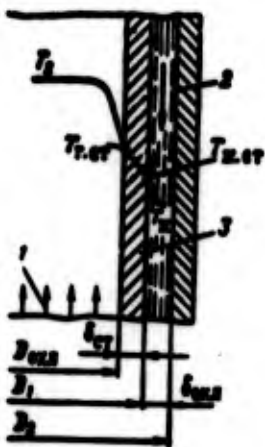


Fig. 4.1. Diagram of the process of heat exchange in the chamber of ZhRD.

Thanks to thermal conduction heat is transmitted through the chamber wall and then by convection to coolant 2, passing through the cooling cavity.

At the initial moment of operation of an engine, when chamber and nozzle walls are still cold, part of the heat flux goes to heating the chamber walls. Such are the cooling conditions of the ZhRD for which wall temperature and heat flux into the liquid coolant change with time are called nonstationary cooling conditions.

As time passes equilibrium is established. Here the entire heat flux from hot combustion products to chamber walls is removed. From this moment (under given engine operating conditions) the temperature of the gas and liquid walls of the chamber and heat flux through the walls remain constant. Such conditions are called steady-state cooling conditions.

We will subsequently examine only steady-state cooling conditions.

Dependence of $T_{r.ct}$ on Coolant Speed

The speed of liquid coolant w affects the value of the coefficient of heat transfer from wall to it $\alpha_{ж}$, where with increase of this speed $\alpha_{ж}$ also increases.

With the same specific heat flux q_{Σ} and temperature of liquid $T_{ж}$ the temperature of the wall on the liquid side $T_{ж.ct}$ is determined by expression

$$q_{\Sigma} = \alpha_{ж} (T_{ж.ct} - T_{ж}), \quad (4.3)$$

which after conversion takes the form

$$T_{ж.ct} = T_{ж} + \frac{q_{\Sigma}}{\alpha_{ж}}, \quad (4.4)$$

i.e., with increase of $\alpha_{ж}$ temperature $T_{ж.ct}$ decreases. In turn heat flux is transmitted through the chamber wall by thermal conduction, i.e.,

$$q_{\Sigma} = \frac{\lambda}{\delta_{ct}} (T_{r.ct} - T_{ж.ct}), \quad (4.5)$$

where γ - coefficient of thermal conductivity of the chamber wall material, whence

$$T_{r.ct} = q_{\Sigma} \frac{\delta_{ct}}{\lambda} + T_{ж.ct}. \quad (4.6)$$

Thus for the same metal wall thickness δ_{ct} and specific heat flux q_{Σ} the temperature of the gas wall $T_{r.ct}$ will be lower, the lower the temperature of the wall on the liquid side $T_{ж.ct}$.

However, with decrease of $T_{ж.ct}$ total heat flux from gases to chamber wall will increase somewhat as a result of the decrease of $T_{r.ct}$ (4.2), which leads again to growth $T_{r.ct}$, $T_{ж.ct}$, etc.

Finally, steady-state cooling conditions after increase of speed of the liquid coolant are established at smaller $T_{r.ct}$ and

$T_{\text{ж.сг}}$ than prior to the increase of speed (Fig. 4.2a). Thus the temperature of the gas wall $T_{\text{г.сг}}$ in great degree depends on the speed of the liquid coolant: the greater the speed, the less is $T_{\text{г.сг}}$. Consequently, necessary $T_{\text{г.сг}}$ can be maintained by increasing the speed of the liquid coolant w , for example, by decreasing the cross section of the coolant passage.

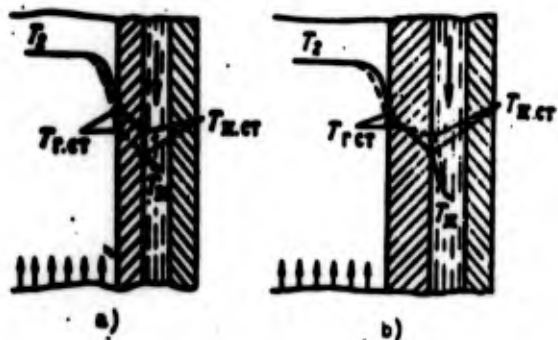


Fig. 4.2. Dependences of $T_{\text{г.сг}}$:
 a) on speed of liquid coolant; b) on coefficient of thermal conductivity of metal λ ; ---- at high values of w or λ .

Influence of Surface Boiling of Liquid Coolant on the Value of $T_{\text{г.сг}}$

In the process of heat transfer from the wall of the combustion chamber to the liquid coolant two cases of the relationship between $T_{\text{ж.сг}}$ and the boiling point of the liquid T_s at a given pressure in the cooling cavity are possible:

$$T_{\text{ж.сг}} < T_s; T_{\text{ж.сг}} > T_s. \quad (4.7)$$

In the first case ebullition of the liquid in the coolant passage is impossible. In the second case the liquid coolant can boil on the surface of the liquid wall of the chamber. If the mass of liquid here has temperature below T_s , bubbles of vapor formed on the surface of the liquid wall bubbles of vapor will be washed off by the stream of fluid and condensed in the colder flow core. Thus these bubbles, agitating the stream, will increase the heat transfer from wall to liquid, i.e., $\alpha_{\text{ж}}$ will increase for the same speed of the cooling liquid.

The increase of $\alpha_{\text{ж}}$ due to surface boiling will lead to the same results as an increase of $\alpha_{\text{ж}}$ due to an increase of speed, i.e., to a decrease of $T_{\Gamma.\text{CT}}$ with a certain increase of total flux q_{Σ} .

Conditions of cooling of the wall in this case can be improved without an increase of the feed pressure of the liquid coolant for increasing the speed of its motion. However, intense boiling on the surface can lead to such vigorous vaporization that the bubbles of vapor, not being washed off by the fluid, will form a solid film of vapor on the surface of the wall. Since vapor conducts and transmits heat poorly, in this case the coefficient of heat transfer $\alpha_{\text{ж}}$ decreases sharply, leading to the reverse result - to increase of $T_{\Gamma.\text{CT}}$ and, possibly, to burnout of the wall.

Dependence of $T_{\Gamma.\text{CT}}$ on the Thermal Conductivity λ of the Material of the Chamber

As can be seen from relationship (4.6)

$$T_{\Gamma.\text{CT}} = q_{\Sigma} \frac{\delta_{\text{CT}}}{\lambda} + T_{\text{ж.CT}}$$

for the same values of $T_{\text{ж.CT}}$, δ_{CT} and q_{Σ} the temperature of the gas wall $T_{\Gamma.\text{CT}}$ will be lower, the greater the coefficient of thermal conductivity of the wall material λ . However, even here with decrease of $T_{\Gamma.\text{CT}}$ in accordance with expression (4.2) total heat flux q_{Σ} will increase, as a result of which $T_{\Gamma.\text{CT}}$ is again raised somewhat. In this case (just as in the case of lowering of $T_{\text{ж.CT}}$ with increase of $\alpha_{\text{ж}}$) steady-state cooling is established at a smaller value of $T_{\Gamma.\text{CT}}$, than would be the case for the wall with smaller value of λ .

As follows from expression (4.5), the curve of temperature drop through the wall of an engine with growth of λ will be more sloping. Since q_{Σ} increases somewhat, $T_{\text{ж.CT}}$ will also increase (4.4).

Thus the line of change of temperature through the wall for metal with greater λ intersects the line of change of temperature through the wall corresponding to smaller λ (see Fig. 4.2b). Consequently, for the manufacture of chambers of the ZhRD it is expedient to use materials with greatest possible coefficient of thermal conductivity λ . However, as a rule, such metals rapidly lose their strength with temperature increase.

Dependence of $T_{r.ct}$ from Thickness of Wall of Engine Chamber δ_{ct}

From expression (4.6) it also is clear that with constant $T_{ж.ct}$ and q_{Σ} the temperature of the gas wall $T_{r.ct}$ will be lower the less the thickness of the wall δ_{ct} .

Although with decrease of $T_{r.ct}$ heat flux q_{Σ} , according to expression (4.2), increases somewhat, steady-state cooling conditions are established with smaller $T_{r.ct}$. Consequently, the chambers of ZhRD should be made with smallest possible wall thickness δ_{ct} .

The Influence of Pressure and Temperature in the Combustion Chamber on Values of $T_{r.ct}$ and q_{Σ}

With increase of pressure in the chamber the density of the gas moving in it is increased. In connection with this the coefficient of heat transfer from gas to wall α_r and the value of convective flux q_K (see section 4.6) increase.

As increase of pressure in an engine chamber will also lead to growth of partial pressures of components p_{H_2O} and p_{CO_2} the radiation of which makes up the radiant heat flux to the wall q_R (see section 4.8).

Thus an increase of pressure leads to an increase in total specific thermal flux to the chamber wall q and, in accordance with formulas (4.4) and (4.6), to an increase of $T_{ж.ct}$ and $T_{r.ct}$.

It is true that with growth of $T_{r.ct}$ heat flux q_r somewhat decreases, but a new steady state is established at new, greater values of $T_{r.ct}$ and q_r .

Thus increasing the pressure in the chamber of an engine, other things being equal, leads to an increase of $T_{r.ct}$ and q_r .

With an increase of T_2 convective and radiant heat fluxes increase, which, as does an increase of pressure in the chamber, leads to growth of $T_{r.ct}$ and q_r .

Therefore frequently for ZhRD working on fuels with greater calorific power H_u more intense chamber cooling is also required.

Influence of Dimensions and Shape of Coolant Passage on $T_{r.ct}$

With decrease in the cross section of the coolant passage coolant speed is increased.

The influence of the shape of the coolant passage is due to the ribbing effect. The presence of longitudinal or helical ribs, corrugations, tubes, etc., increases the surface of heat removed from the coolant side. The latter leads to increase of the effective coefficient of heat transfer from the liquid wall to the coolant, and consequently to a decrease of $T_{r.ct}$. The degree of influence of the ribbing effect on $T_{r.ct}$ in great measure depends on the thermal conductivity of the material of the inner shell of the engine chamber (see section 4.11).

Influence of Engine Operating Conditions on $T_{r.ct}$

During operation of ZhRD under different conditions of chambers cooled by one of the components rated conditions are usually those of greatest thrust.

During transition of an engine to operation at lower thrust the pressure in the combustion chamber p_2 drops and T_2 decreases

somewhat, as a result of which heat flux q_z decreases. However, with decrease of thrust there is a simultaneous decrease in the flow rate of the coolant component, and consequently of the speed of the coolant through the passage w and of the coefficient of heat transfer from wall to liquid α_{κ} . Since the cooling surface of the chamber remains constant, the decrease in flow rate of the coolant can lead to such growth of T_{κ} that the coolant can boil.

Thus with reduction of thrust, in spite of the decrease of heat flux q_z , the temperature of the gas wall $T_{r,CT}$ can increase. Therefore, if an engine must operate with variable thrust, it is necessary to check out cooling under conditions of low thrust.

Having examined the basic factors influencing the effectiveness of external chamber cooling, one can make the following conclusion.

For decrease of $T_{r,CT}$ with external cooling one should increase the speed of the liquid coolant. It is desirable that the chamber be made of metals with greatest possible thermal conductivity and with least wall thickness and maximum cooling surface. Cooling must be effective under engine operating conditions.

If it is impossible to ensure permissible value of $T_{r,CT}$ by external cooling alone, it is necessary to decrease heat fluxes to the wall, or to employ additional other forms of cooling (internal) or to protect the wall with heat-resistant coverings.

4.2. Methods of Cooling the ZhRD

External Cooling

The simplest arrangement for external cooling by one of the components of fuel is shown in Fig. 4.3a. The liquid coolant enters collector 1 and passes from it into the coolant passage. In flowing through the passage the liquid cools the walls and is itself heated. The heated liquid leaves the cooling jacket and enters head 4. As was already pointed out, with external cooling the chamber of the

engine is usually cooled by the components themselves. The liquid coolant can be fuel or oxidizer.

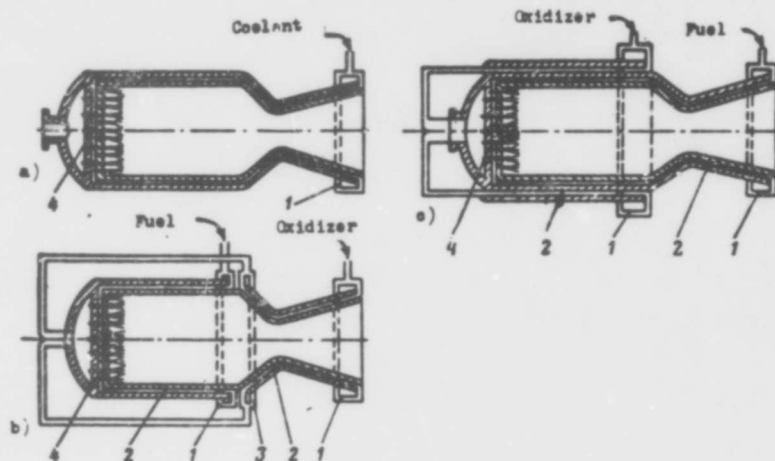


Fig. 4.3. External cooling arrangements: a) by one component; b, c) by two components; 1 - inlet collector; 2 - coolant passage; 3 - outlet collector; 4 - head.

It is necessary to note that for every fuel and chamber pressure p_2 there corresponds a minimum thrust, below which external cooling alone becomes insufficient. The cause of this is the fact that with decrease of nominal thrust (with constant p_2) the necessary volume of the combustion chamber decreases in proportion to the total consumption of fuel, while the cooled surface of the chamber decreases only in proportion to the $2/3$ power. Thus the lower the nominal thrust of an engine, the greater the ratio of the cooled surface of the chamber to its volume. Furthermore, with decrease of critical throat diameter D_{kp} , other things being equal, normal to the wall convective heat flux q_K , according to formula (4.181) increases in proportion to $D_{kp}^{-0.13}$. All of this leads to the fact that in chambers of low thrust the coolant receives a greater part of the heat developed during combustion of fuel than in high-thrust chambers. Thus for a combustion chamber with a thrust of the order of 500 kg (≈ 5000 N) and working on hydrocarbon fuels paired with oxygen or nitric acid for $p_2 = 20$ kg/cm² (≈ 1.98 MN/m²) the quantity of heat going into the coolant is approximately 2% of the

total quantity of heat generated. For the engine of the A-4 missile, having a thrust of 25 T (≈ 0.25 MN), this heat amounts of only 0.7%, i.e., the greater the thrust of an engine, the more easily external chamber cooling is accomplished.

For comparable thrust and pressures the higher the rate of full conversion of fuel into products of combustion, the smaller the volume necessary for combustion of the same quantity of fuel, and consequently the smaller the surface that must be cooled. Hence the lower limit of minimum thrust, for which external cooling is effective is lower, the shorter the conversion time.

For normally used fuels this limit is considerably below 500 kg (≈ 5000 N), while for slow-heating fuels, requiring more time, external cooling can be insufficient even with high thrust.

For very limited quantities of fuel and oxidizer both components are sometimes used for cooling. Here one of them cools the nozzle of the engine while the second cools the combustion chamber (Fig. 4.3b). Sometimes the second component is used for lowering the temperature of the component directly cooling the chamber of the engine and is itself heated (Fig. 4.3c). External cooling by components also can be applied during the use as fuel of vapors of low-boiling components (for example, oxygen + hydrogen). The specific character of such external cooling consists in that the coolant is in liquid state only in the initial section of the coolant passage, and the main part of the chamber surface is cooled by gaseous coolant.

In Fig. 8.7 is given an example of a simplified arrangement for cooling a chamber with a low-boiling component - hydrogen. Liquid hydrogen enters pump 6 and passes from there into the coolant passage, where it is evaporated, so that the greater part of the chamber surface is cooled by gaseous hydrogen, which is heated in the process to 200-250°K (see section 4.13).

Furthermore, there have been projects proposing the cooling of ZhRD of high thrusts by water in such a way that the water in the

coolant passage is heated to the boiling point [25]. The steam formed here enters turbine and is used to drive fuel pumps.

Internal Cooling

With internal cooling wall temperature $T_{r,ct}$ is reduced thanks to its protection by liquid film or gas layer of temperature lowered as compared to the core and created on the internal side of the wall.

Such layer usually is called the near-wall layer.

If for external cooling the problem is reduced to finding how it is possible to more effectively remove the heat entering the wall, not protected from the influence of gases heated to high temperature, then for internal cooling by way of creation of near-wall layer of reduced temperature heat flux into chamber walls is reduced.

The temperature of the gas in the near-wall layer is reduced because of the artificial enriching of this layer by one of the components, which in this case is also the coolant. Usually such component is fuel (although the protective layer could also be a near-wall layer with a surplus of oxidizer). For internal cooling it is possible to use water or gas also.

The surplus of fuel for creation of the near-wall layer is fed either through injectors, located about the periphery of the head, or through special belts, which can be located both directly at the head of the chamber and in the cylindrical and nozzle parts of the chambers.

With supply of surplus fuel through peripheral injectors (Fig. 4.4a) mixing and combustion of components take place at the wall when $\alpha \ll 1$, with formation of a near-wall layer of combustion products which protects the wall from high heat flux. The advantage of such arrangement of internal cooling is implicitness of creation

of the protective near-wall layer without complication chamber design.

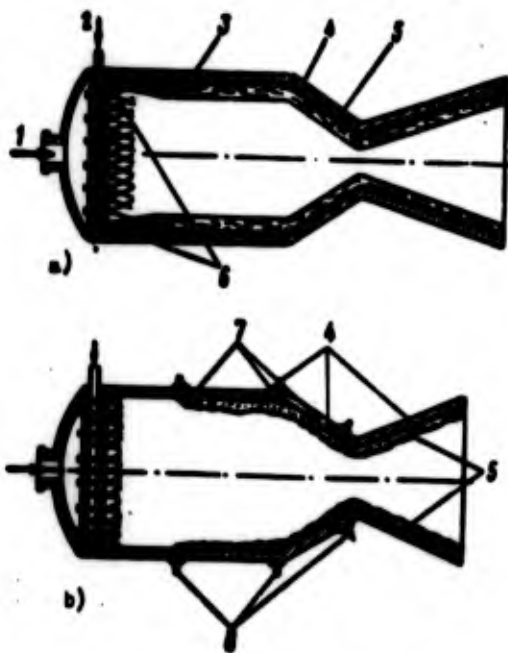


Fig. 4.4. Creation of the near-wall layer for internal cooling: a) with the help of peripheral injectors; b) with help of cooling belts; 1 - oxidizer; 2 - fuel; 3 - chamber wall; 4 - boundary layer; 5 - near-wall layer; 6 - peripheral injectors; 7 - liquid coolant; 8 - bents of coolant supply.

However, with increase of chamber length the economy of this method of cooling worsens, since the farther the section of the wall is from the head, the greater the erosion of the near-wall layer.

For certain engines it is more economical, but structurally more difficult to apply internal cooling by passing coolant through special belts (Fig. 4.4b).

When the coolant is fed through the belt, the mechanism of protection of the wall from burnout can be represented as follows (Fig. 4.5). Under the influence of high heat flux the liquid is evaporated, and above the layer of liquid is created a protective layer of vapors of liquid and combustion products (if combustion takes place in the layer).

Thus, in essence, are obtained two protective layers: liquid and vapor. The entering liquid, entrained at high speed by the stream of combustion products, spreads over the chamber wall in a very thin layer.

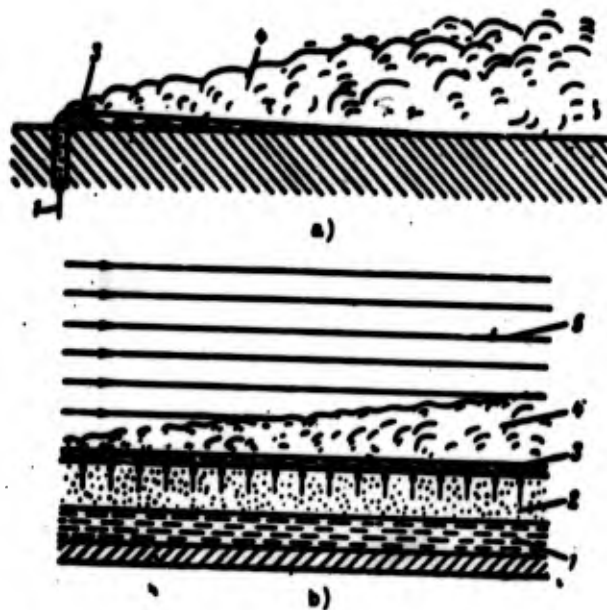


Fig. 4.5. Diagram of the protective action of internal cooling: a) supply through cooling belt; b) sweat cooling; 1 - coolant; 2 - porous wall; 3 - liquid layer; 4 - vaporous protective layer; 5 - stream of combustion products.

Owing to evaporation, the thickness of the vapor layer above the liquid grows in the direction of motion of the stream of combustion products up to the section where the liquid is completely evaporated. Following this section there is a gradual decrease in the thickness of the vapor layer as a result of its mixing with the basic flow, i.e., erosion of the screen, but the intensity of erosion of the vapor layer is relatively low, and therefore the protective action of the layer is preserved over relatively greater distances.

Since the density of the coolant vapor is many times less than that of the liquid, the thickness of the vapor layer also is greater than that of the layer of liquid. Furthermore, inasmuch as the thermal conductivity of the vapor is many times less than that of the liquid, the thermal resistance of the vapor layer is several times higher than that of the liquid layer.

As a result of the joint influence of these two factors the protective layer can be considered the vapor layer (or the mixture of vapor and products of combustion).

In Fig. 4.6 are given data from experiments on change of heat flux in different sections along the length of the chamber of a ZhRD as a function of the per-second flow rate of the water used on internal cooling.

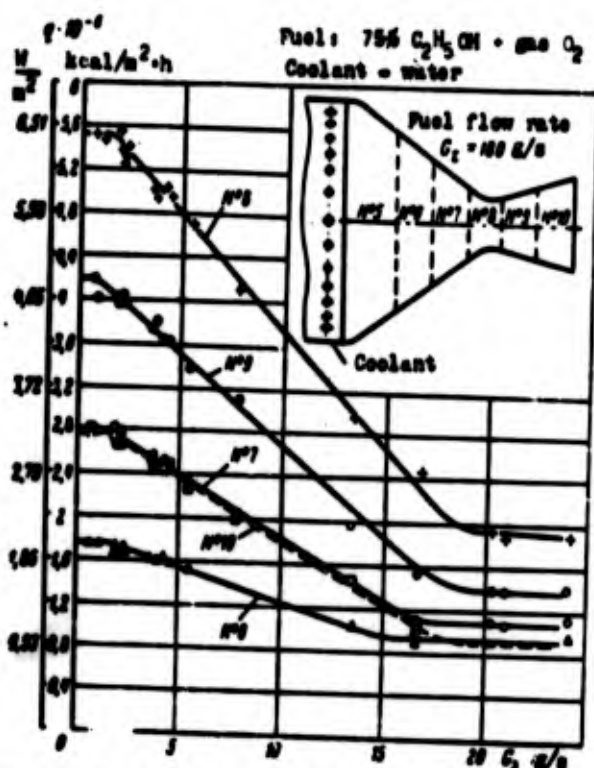


Fig. 4.6. Influence of internal cooling on the value of heat flux.

Thus, for example, in section No. 8 (critical) with a flow rate of water of up to 1 g/s heat transfer to the chamber wall remains practically unchanged, since all steam formed here is washed off by the gas stream. With further increase in the flow rate of cooling water a steam screen is formed and heat fluxes to the chamber wall decrease noticeably in direct proportion to the coolant expended on the screen. However, for coolant flow rates higher than 18 g/s there is no further noticeable decrease of heat fluxes. The cause of this phenomenon is that as soon as the liquid film reaches the examined section and, thus, the entire surface of the nozzle from the coolant supply to belt section 8 is covered by the liquid film, further increase of coolant flow rate does not change the surface of the liquid from which the formation of the vapor protecting the given section of the wall occurs or the thickness of the protective

vapor layer above the examined section. This leads only to increase in the thickness of the liquid layer, which, as was mentioned, has no significant influence on heat exchange. Thus the basic problem during creation of internal cooling is creation of a stable screen of steam at the wall.

A variety of internal cooling is so-called sweat cooling. In this case the chamber wall is made of porous material and the coolant passes through the pores evenly over the entire surface of the chamber (see Fig. 4.5b). Both liquid and gas can be used as coolant with the porous wall.

With porous internal cooling for creation of a reliable screen an insignificant quantity of coolant is required. There is no need to make the entire chamber of porous material since a stable screen of steam can be created by using a porous cooling belt.

The deficiency of available porous materials is that during engine operation the pores can be rapidly obstructed. Therefore it is very difficult to create porous material with time-constant flow friction over its entire surface.

In certain designs of ZhRD internal cooling is carried out either by means of peripheral injectors in the engine head or by means of special cooling belts made in the form of a annular slot or row of holes in the combustion chamber (Fig. 4.7).

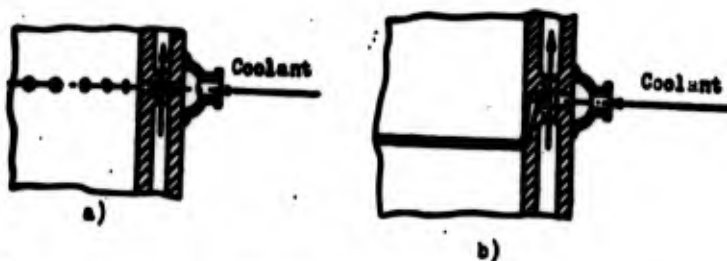


Fig. 4.7. Diagrams of belts for internal cooling: a) belt of holes; b) slot belt.

Apparently, it is possible to so organize internal cooling that it will ensure operation of the engine chamber for the necessary time without burnout. However, with internal cooling alone it is

necessary to use such a quantity of coolant that part of it remains unburned, and losses of thrust are comparatively high (see section 3.6). Therefore the combination of internal and external cooling, mixed cooling, utilized in the overwhelming majority of ZhRD is the most expedient.

Mixed cooling makes it possible with a use for internal cooling 1-3% of the total fuel consumption to realize reliable protection of chamber walls from burnout with comparatively small losses of thrust. Here internal cooling is accomplished by means of both peripheral injectors and by installation of cooling belts.

In Fig. 4.8a is a diagram showing the arrangement used to cool the RZ-2 engine, while Fig. 4,8b shows that used in the engine of the A-4 missile. In the first case the near-wall layer is formed by way of corresponding placement of injectors, and in the second four cooling belts are employed.

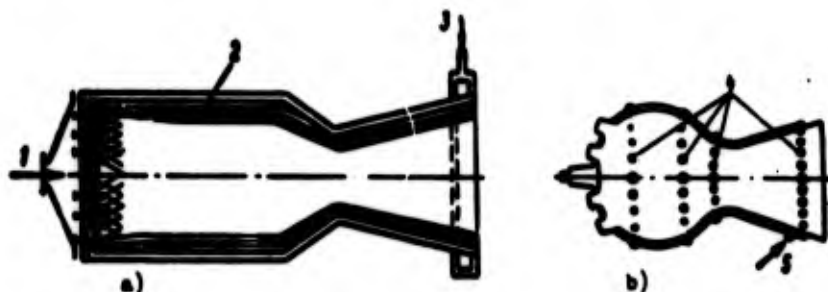


Fig. 4.8. Examples of mixed cooling arrangements:
a) internal cooling by means of cooling belts;
1 - coolant; 2 - near-wall layer; 3 - fuel; 4 - cooling belt.

Other combinations of all the above-described methods of external and internal cooling are also possible.

Radiation Cooling

In engines having large values of p_2/p_3 the nozzle there is a sharp decrease in density and temperature of the products of combustion, which in turn leads to considerable decrease of

convective and radiant heat fluxes. Here wall cooling can be provided by means of heat removal from the wall by radiation into the surrounding medium (or vacuum).

Such cooling is called radiation cooling. With radiation cooling wall temperature T_{CT} can be much higher than the thermodynamic temperature of the stream of combustion products. With growth of T_{CT} radiant heat fluxes from the wall increase as a result both of growth of T_{CT} of increase in the degree of blackness of the wall ϵ_{CT} . As a result of strongly increasing radiation of the wall into the surrounding medium (or vacuum) intense cooling of the wall will also take place. Furthermore radiation from the wall into the products of combustion can be higher than radiation of these products and the direction of q_{π} will be from the wall to the gases which also leads to certain cooling of the wall.

During radiation cooling owing to equilibrium between supply and removal of heat from the wall certain equilibrium wall temperature $T_{CT,p}$ is estimated. If values of $T_{CT,p}$ do not exceed those permissible for the given material, pure radiation cooling of the wall is possible. With values of $T_{CT,p}$ larger than permissible additional protection of the wall by means of internal cooling or heat resistant coverings is necessary (for details about radiation cooling see section 4.13).

Ablation Cooling

Ablation consists of the processes of evaporation (or sublimation), fusion, combustion, and destruction of the surface layer of a body, accompanied removal of material by a high-speed gas stream.

In ZhRD wide use has been made of ablation cooling, by which protection of walls from burnout is provided by putting ablating coverings on the internal surface.

Since during ablation cooling there is ablation of the protective covering, such cooling is sometimes called cooling by removal of mass. Ablation cooling is used very effectively and widely for burnout protection of the chambers of upper-stage engines, and nozzle caps.

However, for prolonged operation of a ZhRD the weight of the heat shielding material is rather considerable, which is a serious drawback to this method. The second deficiency of ablation cooling is change of shape of chamber and nozzle due to ablation, and sometimes due to exfoliation and breaking off of material.

Other Methods of Protecting Chamber Walls from Burnout

A very effective method of protecting the chamber walls of ZhRD from burnout is to heat-resistant coverings on the fire side.

K. E. Tsiolkovskiy suggested that the inner walls of these chambers be covered with graphite, tungsten, or other heat-resistant materials.

In Fig. 4.9 is a diagram of the ORM-9 combustion chamber, developed in 1930, in which was used ceramic thermal insulation based on zirconium and magnesium oxides. In the nozzle part of the chamber was a copper insert for accumulation of heat.

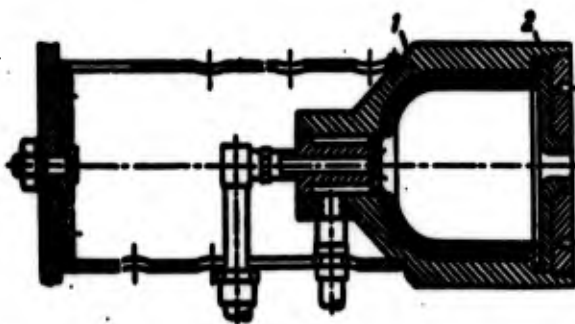


Fig. 4.9. Combustion chamber of the ORM-9 engine. 1 - ceramic covering; 2 - copper insert for accumulation of heat.

The basic deficiency of ceramic coatings consists in the fact that ceramics crack under the influence of high-temperature flux.

For the chambers of the ZhRD of the long-duration (of the order of several minutes) it is very possible to use a combination of close-grained heat-resistant coverings (0.1-0.4 mm) and flow-through external cooling - combined cooling. With combined cooling it is possible to manage without internal cooling and its related losses of thrust, but it is difficult to satisfy the stringent requirements on the covering imposed by conditions of operation of ZhRD. The covering must have a high melting point, resistance to thermal shocks, low thermal conductivity, a coefficient of linear expansion close to that of the base material, good adhesion to the chamber material, and satisfactory anticorrosive properties.

In Table 4.1 are given the thermophysical properties of certain refractory materials.

Combined cooling frequently is created naturally in existing ZhRD as a result of deposition of soot on the inner walls of the chambers. It has been found that chamber cooling is improved here.

Protection of chamber walls from burnout for a certain time can also be provided by applying materials with high thermal conductivity. In this case the heat entering the chamber walls, thanks to their good thermal conductivity, spreads rapidly through the entire mass of material, is absorbed as a result of heat capacity, and thus is essentially accumulated in the walls. Such method is therefore called protection by accumulation of heat.

The use of accumulation of heat is expedient under such engine operating conditions when short-term operation is followed by a prolonged period of cooling.

To ensure efficiency of an uncooled chamber for a prolonged time (60-100 s) a combination of heat-resistant coverings and heat-accumulating materials is frequently used. In Fig. 4.10 is given an example of the construction of the wall of the nozzle part of an uncooled engine chamber.

Table 4.1. Thermophysical properties of refractory materials (under normal conditions).

Material	Symbol	Density g/cm ³	Melting point, °C	Coefficient of thermal conductivity		Coeffi- cient of linear expansion $10^6 \frac{1}{\text{deg}}$	Heat capacity		Elastic modulus	
				$\frac{\text{kcal}}{\text{m}^2 \cdot \text{deg}}$	$\frac{\text{W}}{\text{m} \cdot \text{deg}}$		$\frac{\text{kcal}}{\text{kg} \cdot \text{deg}}$	$10^{-3} \frac{\text{J}}{\text{kg} \cdot \text{deg}}$	$10^{-9} \frac{\text{kg}}{\text{cm}^2}$	$10^{-10} \frac{\text{N}}{\text{m}^2}$
Tungsten	W	19.36	3380 ± 50	145	109	4.44	0.082	0.124	49	39.3
Graphite (pressed)	C	1.4-1.9	3500	65-250	75-220	7-10	-	-	-	-
Graphite (pure)	C	2.26	3600	20-300	20-350	-	0.17	0.712	0.6-0.8	0.80-0.705
Zirconium dioxide	ZrO ₂	5.25	2700	1.4-1.7	1.63-1.98	10	-	-	-	-
Tantalum carbide	TaC	14.5	3000 ± 100	19	22.1	-	-	-	-	-
Titanium carbide	TiC	4.9	3140	14.35	16.7	4.1	0.047	0.197	34.5	33.8
Zirconium carbide	ZrC	6.6	3175-3572	17.64	20.5	6.3	-	-	35.5	34.8
Polycrystalline	Mo	10.2	2622 ± 50	116	137	5.1	0.053	0.264	28.6	33
Aluminum oxide	Al ₂ O ₃	3.7	2200	24-36	27.9-39.2	8.8	-	-	-	-
Magnesium oxide	MgO	3.4	2800	20	31.9	13.5	-	-	-	-
Tantalum	Ta	16.6	2990 ± 50	47	54.6	6.57	0.053	0.128	19	19.65

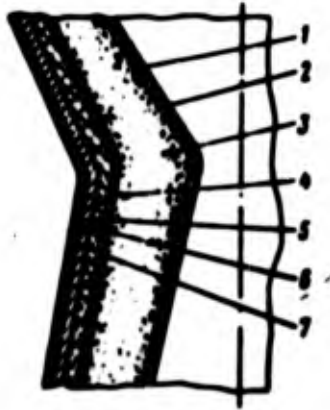


Fig. 4.10. Wall of uncooled nozzle: 1 - tungsten; 2 - carbide layer; 3 - graphite; 4 - ceramic; 5 - plastic; 6 - metal frame; 7 - sheath of plastic filaments.

The internal (fire) wall 1 is made of a thin layer of tungsten, withstanding high temperatures (to 2700-3300°K), and fulfilling only the function of heat resistant protective covering. The graphite layer 3 is the basic accumulating layer. Intermediate carbide layer 2 serves for prevention of diffusion of carbon into the tungsten shell and accumulation of gas between the heat-resistant wall and the heat-absorbing layer. Ceramic layer 4 and plastic layer 5 are heat-insulating layers for protection of the metal load-bearing frame 6. On the outside of the wall is an additional sheath of plastic filaments 7. For the uncooled sections of chamber or nozzle the possibility is also being investigated of using porous materials with a filler of fusible materials. Under the influence of high heat flux the filler is evaporated and sweats from the pores, result in formation at the wall of a protective cooling screen.

4.3. Process of Convection Heat Transfer from the Gas to the Wall

Dynamic and Thermal Boundary Layers

With the motion of a compressible liquid with high speed along the wall of a combustion chamber and nozzle of a ZhRD, on the surface of the wall dynamic and thermal boundary layers will be formed (Fig. 4.11).

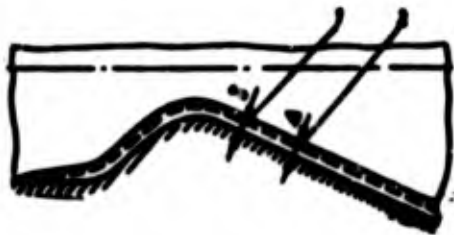


Fig. 4.11. Boundary layers: 1 - dynamic; 2 - thermal.

In the dynamic boundary layer under the action of forces of viscosity the speed of motion of the flow decreases from the speed in the nucleus of flow down to zero at the wall, where it is as though the gas "adheres" to it. In the thermal boundary layer the temperature of the gas is changed from values in the nucleus of the flow to values at the wall $T_{p,CT}$. Depending upon whether there is heat removal from the surface of the wall or not (heat-insulated wall), the nature of the change in temperature is distinguished. With a completely heat-insulated wall (sometimes it is called impenetrable) quantity $T_{p,CT}$ in an ideal case will be equal to the stagnation temperature of the nucleus of the flow T_{00} (Fig. 4.12). With heat removal from the wall $T_{p,CT}$ will be lower than T_{00} , which is determined by the intensity of heat transfer from the surface inside the wall.

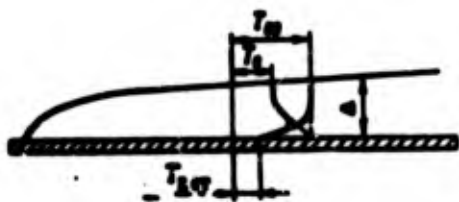


Fig. 4.12. Change in thermodynamic temperature T_0 and stagnation temperature T_{00} over the thickness of the thermal boundary layer: ----- for a heat-insulated wall; ——— with heat removal from the wall.

In general the thickness of the thermal boundary layer Δ can be greater than, smaller than or equal to the thickness of the dynamic layer δ .

In the boundary layer both laminar and turbulent flow can take place. Accordingly, we will have a laminar or turbulent boundary layer. At flow rates common for a ZhrD, on walls of the chamber and nozzle a turbulent boundary layer will be formed. With this on

the main motion it is as if there is superimposed disordered pulsational motion, so that at every given point the flow parameters (speed, pressure, etc.), do not remain time-independent, and frequently and nonuniformly are changed along and across the flow. As a result there occurs a shift and mixing of particles of liquid (or gas). These travelling particles are usually called turbulent moles or moles of liquid. Although the magnitude of pulsations of flow parameters is insignificant and in all is several percent of their mean values, the pulsations, have a decisive influence on processes of friction and heat exchange.

Averaged and Pulsational Motion

Due to the complexity of the pulsational motion a strict theoretical calculation of parameters of turbulent flow is impossible, and therefore regularities of it are investigated for time averaged values characterizing this flow. Here the turbulent flow is examined as consisting of two forms of motion: averaged and pulsational. Thus, if, for example, at the given point the time averaged value of the speed is equal to \bar{w} , and the value of the pulsational speed is equal to w' , then the speed at the given point during the time τ

$$w = \bar{w} + w' \quad (4.8)$$

where

$$\bar{w} = \frac{1}{\tau} \int_0^{\tau} w dt \quad (4.9)$$

Analogously, all the remaining flow parameters can also be represented in terms of averaged and pulsational values.¹

Additional (apparent) turbulent frictional stresses and heat transfer

The presence of pulsational speeds affects the averaged motion in such a way that in it is as if the deformation drag is increased, i.e., there appears a certain additional, apparent, viscosity. Actually, when one examines in the boundary layer a line parallel

to the axis (Fig. 4.13), then the component along the y-axis of the momentum flow through a unit area per unit time

$$J_y = \rho \overline{uv}. \quad (4.10)$$

In conducting the averaging of speeds, we will obtain

$$J_y = \rho (\overline{u+v})(\overline{v+v'}) = \rho (\overline{uv} + \overline{vv'} + \overline{uv'} + \overline{v'v'}).$$

The mean value of the momentum flow will be equal to

$$J_y = \rho (\overline{uv} + \overline{vv'} + \overline{uv'} + \overline{v'v'}). \quad (4.11)$$

Since according to rules of averaging

$$\overline{v'v'} = \overline{v'v'} = 0, \quad \overline{v'v} = \overline{vv'}, \quad (4.12)$$

then

$$J_y = \rho \overline{uv} + \rho \overline{v'v'}. \quad (4.13)$$

That is, owing to pulsations the momentum flow is changed by the quantity $\rho \overline{v'v'}$. The transfer of the impulse component through the area parallel to the x-axis is equivalent to tangential stress; consequently, the magnitude of additional turbulent (or apparent) stress owing to pulsations

$$\tau_{app} = -\rho \overline{v'v'}. \quad (4.14)$$

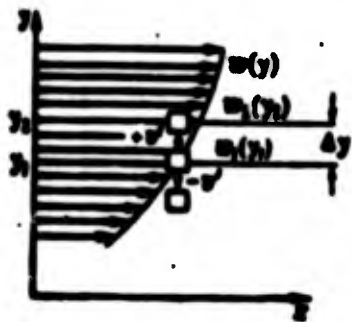


Fig. 4.13. Momentum transfer with turbulent pulsations.

This stress has a positive direction along the x-axis, in which one can be certain of the following reasoning. Particles of liquid, which due to transverse pulsations enter into the element from below ($v' > 0$), move from a region with averaged speed \bar{w} and therefore cause a negative pulsation w' . Conversely, particles, arriving into the element from above ($v' < 0$), i.e., having larger \bar{w} , cause a positive pulsation w' ; consequently, product $w'v'$ always has a negative sign, and the additional turbulent stress $\tau_{\text{turb}} = -\rho \overline{w'v'}$ is always positive, i.e., it has the same sign as does the laminar stress

$$\tau_{\text{lam}} = \mu \frac{dv}{dy}. \quad (4.15)$$

The full tangential stress of friction τ can be expressed in the form of a sum of two components expressing laminar and turbulent friction:

$$\tau = \mu \frac{dv}{dy} - \rho \overline{w'v'}. \quad (4.16)$$

Together with the secondary stress of friction with turbulent motion owing to pulsations, an additional heat transfer also appears.

Since mechanisms of heat transfer and momentum are similar, then, not repeating aforementioned reasonings, the expression for the additional convection heat flow will immediately be written in the form

$$q_{\text{turb}} = -\rho c_p \overline{v'T'}. \quad (4.17)$$

where T'_{00} - pulsation of stagnation temperature.

As is known, convection heat flow with laminar flow is equal to (when $Pr = 1$).

$$q_{\text{lam}} = \rho c_p \frac{dv}{dy} = \lambda \frac{dT}{dy}. \quad (4.18)$$

The total heat flow, caused by laminar processes and turbulent mixing, can be expressed in the form of the sum of two components (4.17) and (4.18):

$$q_x = q_{x, \text{lam}} + q_{x, \text{turb}} = g p c_p \frac{dT_0}{dy} - g \rho c_p \overline{v' T_0'} = \lambda \frac{dT_0}{dy} - g \rho c_p \overline{v' T_0'}. \quad (4.19)$$

Expression of secondary stress of friction and heat transfer through the length of the path of mixing

By analogy with molecular friction the secondary stress of friction

$$\tau_{xy} = -\rho \overline{v' u'} = \rho \epsilon \frac{d\bar{u}}{dy} = \rho \epsilon \frac{d\bar{u}}{dy}, \quad (4.20)$$

where $\epsilon = \mu_{\text{turb}}/\rho$ - apparent kinematic viscosity.

To calculate ϵ Prandtl proposed the following simplified scheme of flow. If one were to return to Fig. 4.13 and examine the two layers of liquid at distance Δy , then the turbulent mole, travelling due to pulsation from one layer into the other, maintains at a certain distance the component of momentum in the direction of the x-axis.

This distance, at which the mole of liquid preserves its properties in the direction of the x-axis, is called the length of path of mixing and is designated usually l . Thus, if $\Delta y = l$, then particles proceeding from the lower layer into the upper preserve the horizontal component of speed \bar{w}_1 . The difference between the average speed at point y_2 and average speed of particles proceeding here from the lower layer will give in this place pulsation of the speed

$$v' = \Delta w_1 = \bar{w}_1(y_2) - \bar{w}_1(y_1). \quad (4.21)$$

If l is small, then $\Delta w_1 = l \partial \bar{w} / \partial y$, and then

$$v' = l \frac{d\bar{w}}{dy}. \quad (4.22)$$

Considering pulsation $v' \approx w'$, we can express $\tau_{\text{typ}6}$ in the form

$$\tau_{\text{typ}6} = -\overline{v'w'} = -\rho \left(\frac{\delta \bar{v}}{\delta y} \right)^2. \quad (4.23)$$

Similarly, the length of the path of mixing can be expressed as

$l_{\text{typ}6}$. Assuming in equation (4.17) $v' = l_1 \partial \bar{v} / \partial y$; $T'_m = l_1 \partial T_m / \partial y$, where l_1 is the length of the path of mixing for energy, and considering $l \sim l_1$, we obtain

$$l_{\text{typ}6} = -\overline{v'T'_m} = \overline{v'w'} \frac{\delta \bar{v}}{\delta y} \frac{\partial T_m}{\partial y}; \quad (4.24)$$

Structural Diagram of the Turbulent Boundary Layer

A structural diagram of the turbulent boundary layer is shown in Fig. 4.14. The initial section of it is laminar. With an increase in thickness of the layer, the laminar layer is turned into a turbulent layer. The limiting thickness of the layer δ_{lam} and length of the laminar section l_{LAM} depend on parameters of the boundary layer, M number, state of the surface of the wall and critical value of the Re number

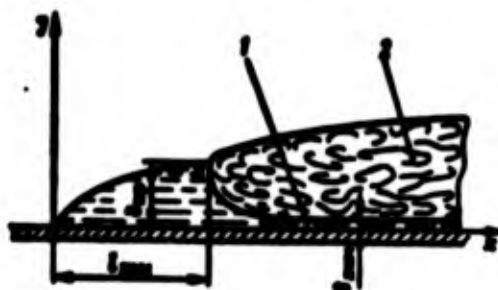


Fig. 4.14. Structural diagram of the turbulent boundary layer: 1 - laminar sublayer; 2 - turbulent layer.

Under appearing turbulent boundary layer near the wall there remains a thin layer in which the laminar flow is preserved. This layer is called a laminar sublayer.

The thickness of the laminar sublayer δ_{LAM} is determined by the critical value of the complex

$$\sigma = \frac{\mu \frac{du}{dy}}{\rho \nu},$$

(4.25)

where u_{max} , ρ_{max} and μ_{max} - speed, density and viscosity, respectively, on the border of laminar sublayer.

For an incompressible liquid the experimental value $\alpha = 11.5$.

In examining equations characterizing the magnitude of fractional stress (4.16) and convection heat flow (4.19) in reference to the given diagram of the boundary layer, let us note that in the turbulent part of the layer the value of the first terms in the equations shown is small as compared to values of the second components. And, conversely, in the laminar sublayer the magnitude of the frictional stress and convection heat flow is determined only by first components, since here because of the absence of turbulent mixing second components lose their meaning.

Calculation of the Effect of Dissociation

As is noted above, in the turbulent boundary layer heat is transmitted due to the shift in moles from sections with high temperature into colder layers. The process of heat exchange in conditions of the chamber of a ZhRD is complicated by the fact that heat radiation toward the wall occurs from the high-temperature flow of dissociated combustion products. Therefore, with movement of moles not only physical heat is transferred, but also the reserve of energy contained in these dissociated combustion products. With the cooling of the mole in them reactions of recombinations occur, which are accompanied by an additional liberation of heat. This even more intensifies the process of heat exchange. If it is considered that in the boundary layer the composition of combustion products remains balanced then the total amount of energy transferable by the mole can be estimated by the magnitude of the change in full heat content of this mole in extreme points of its path. Thus, in the presence of chemical reactions the role of the temperature will be played by the total heat content I_{H00} .

The expression determining the total convection heat flow, caused by laminar processes and turbulent mixing in the presence of chemical reactions, will be written in the form similar to expression (4.19):

$$q_c = \frac{\lambda}{\epsilon_p} \frac{dI_{00}}{dy} - \overline{g_{00}'} I_{00}. \quad (4.26)$$

where I_{00} - pulsation of full heat content of stagnated flow.

The presence of reactions of dissociation or recombinations, which follow after a change in temperatures and pressures in the boundary layer, greatly hampers the problem of averaging of the equation of state and quantity $I_0 = I_0(T, p)$, since the value of the gas constant R depends on the composition of products of combustion, which is itself a function of temperature and pressure. Therefore, with the averaging of the equation of state it is necessary to examine additionally the question of whether the composition of the gas, calculated with average temperature, coincides with the average composition of the gas at a given point of the boundary layer.

In order to simplify the problem V. M. Iyevlev produce introducing the concept of effective temperature $T_{\text{эф}}$, which is determined from condition

$$T_{\text{эф}} = \frac{RT}{R_H}. \quad (4.27)$$

where T and R - temperature and gas constant of the dissociated gas; R_H - gas constant of undissociated combustion products of the fuel of the same initial composition.

Since, obviously, $R_H \leq R$, then $T_{\text{эф}} \geq T$.

Thus, by using in the carrying out of all calculations a higher effective temperature $T_{\text{эф}}$, we consider this to be the intensification of heat exchange in the boundary layer of the flow of dissociated products of combustion, which takes place owing to the flow of reactions of recombinations. Here the heat capacity

$$\rho_{\text{eff}} = \frac{\rho_0}{1 - \frac{u^2}{a^2}} \quad (4.28)$$

The effective stagnation temperature of the gas having temperature T_{eff} ,

$$T_{\text{eff}} = T_{\infty} + A \frac{u^2}{2c_p}, \quad (4.29)$$

where c_p - average heat capacity in the range of temperatures $T_{\text{eff}} - T_{\infty}$.

4.4. Integral Relations of Energy and Impulses for the Boundary Layer.

Initial Equations

Equations of the turbulent boundary layer with an axisymmetrical gas flow have the following form:²

1. The continuity equation

$$\frac{\partial(\rho r v)}{\partial x} + \frac{\partial(\rho r w)}{\partial y} = 0. \quad (4.30)$$

2. The equation of motion

$$\rho v \frac{\partial v}{\partial x} + \rho w \frac{\partial v}{\partial y} = -\frac{dp}{dx} + \frac{1}{r} \frac{\partial(\tau r)}{\partial y}, \quad (4.31)$$

where

$$\tau = \mu \frac{\partial v}{\partial y} - \rho \overline{v'w'}. \quad (4.32)$$

3. The equation of energy

$$\rho v \frac{\partial H}{\partial x} + \rho w \frac{\partial H}{\partial y} = \frac{1}{r} \frac{\partial(q_r r)}{\partial y}, \quad (4.33)$$

where

$$q_r = \frac{\lambda}{c_p} \frac{\partial H}{\partial y} - \rho \overline{v'w'H'}$$

4. The equation of state taking into account equation (4.27)

$$p = \rho R_0 T_{00} \quad (4.34)$$

5. Equations expressing the dependence of viscosity and thermal conduction on temperature

$$\mu = c_\mu (T_{00})^\nu; \quad \lambda = c_\lambda (T_{00})^\nu \quad (4.35)$$

where c_μ and c_λ - constants.

Here r - the shortest distance from the axis of the combustion chamber to a given point inside the boundary layer; w and v - projections of averaged speed on the x - and y -axes; τ - stresses from frictional force on an area perpendicular to the axis; q_x - convection heat flow normal to the wall; I_{n00} and I_{n00}^i - total stagnation heat content and its pulsational value; x - distance along the generatrix of the chamber and nozzle; y - distance along the normal to the surface.

The boundary conditions are the following:

1. When $y = 0$ (at the wall)

$$r = R; \quad w = v = 0; \quad T_{00} = T_{00n} = T_{00i}; \quad q_x = q_{0i}; \quad \tau = \tau_{0i}$$

2. When $y = \delta$

$$w = \bar{w}; \quad v = 0 \quad (\bar{w} - \text{speed in nucleus of the flow}).$$

3. When $y = \Delta$

$$q_x = 0; \quad I_{n00} = I_{n00c}$$

where I_{n00c} - total stagnation heat content of the core of the flow. We consider I_{n00c} to be constant along the chamber and nozzle; values of $\bar{w}(x)$ and $T_{r,0T}(x)$ are known, since $\bar{w}(x)$ is known from the calculation, and $T_{r,0T}(x)$ is usually assigned.

4. Conditions when $x = 0$ will be examined below.

Integral Relations of Energy and Impulses for the Boundary Layer

On the basis of initial equations (4.30)-(4.35), let us derive the integral relation of energy for the boundary layer.³

Multiplying equations (4.30) by $I_{\Pi 00}$ and (4.33) by r and adding, we obtain

$$\frac{\partial(r g v \bar{l}_{\infty})}{\partial x} + \frac{\partial(r g v \bar{l}_{\infty})}{\partial y} = -\frac{\partial(r q_{\infty})}{\partial y}. \quad (4.36)$$

Let us multiply equation (4.30) by the total stagnation heat content of the core of the flow $I_{\Pi 00}$. Since $I_{\Pi 00}$ does not depend on x and y , then

$$\frac{\partial(r g v \bar{l}_{\infty})}{\partial x} + \frac{\partial(r g v \bar{l}_{\infty})}{\partial y} = 0. \quad (4.37)$$

Subtracting from expression (4.37) equality (4.36), and introducing designations $i_{00} = I_{\Pi 00} - I_{CT}$; $\bar{I}_{00} = \bar{I}_{\Pi 00} - I_{CT}$ (where I_{CT} - total heat content of gas at $T_{\Gamma, CT}$ and pressure p in the given section), we will obtain

$$\frac{\partial}{\partial x} [r g v (\bar{l}_{\infty} - l_{\infty})] + \frac{\partial}{\partial y} [r g v (\bar{l}_{\infty} - l_{\infty})] = -\frac{\partial(r q_{\infty})}{\partial y}. \quad (4.38)$$

Let us integrate equation (4.38) within limits of the thickness of the thermal boundary layer Δ :

$$\int_0^{\Delta} \frac{\partial}{\partial x} [r g v (\bar{l}_{\infty} - l_{\infty})] dy + \int_0^{\Delta} \frac{\partial}{\partial y} [r g v (\bar{l}_{\infty} - l_{\infty})] dy = -\int_0^{\Delta} \frac{\partial(r q_{\infty})}{\partial y} dy. \quad (4.39)$$

With the boundary conditions accepted by us, the second term of the left-hand side of equation (4.39) is equal to zero, and the right side is equal to Rq_{CT} , whence

$$\int_0^{\Delta} \frac{\partial}{\partial x} [r g v (\bar{l}_{\infty} - l_{\infty})] dy = Rq_{CT}$$

or

$$\frac{d}{dx} \int_0^{\delta} r g c w (\bar{i}_m - i_m) dy = R q_{cr}. \quad (4.40)$$

Let us reduce equation (4.40) to a dimensionless form, for which we will divide and multiply the left-hand side by corresponding characteristic values not dependent on y : the distance from the axis to the wall is R , the density on the boundary of the laminar sublayer is ρ_{220} and the speed in the nucleus is \bar{w} . Furthermore, both sides of equation (4.40) will be divided by $\bar{\mu}_{3\phi 00}$ - coefficient of viscosity of gas at a temperature of the nucleus $T_{3\phi 00}$; we obtain

$$\frac{d}{dx} \left[\frac{R \rho_{220} \bar{w} \bar{i}_m}{T_{3\phi 00}} \int_0^{\delta} \frac{r}{R} \frac{\rho}{\rho_{220}} \frac{w}{\bar{w}} \left(1 - \frac{i_m}{\bar{i}_m}\right) dy \right] = \frac{R q_{cr}}{T_{3\phi 00}}. \quad (4.41)$$

The quantity

$$\theta = \int_0^{\delta} \frac{r}{R} \frac{\rho}{\rho_{220}} \frac{w}{\bar{w}} \left(1 - \frac{i_m}{\bar{i}_m}\right) dy \quad (4.42)$$

is customarily called the thickness of the loss of energy [79].

Let us give the Re_{θ} number in the form

$$Re_{\theta} = \frac{\rho_{220} \bar{w} \theta}{T_{3\phi 00}}. \quad (4.43)$$

Substituting expressions (4.42) and (4.43) into equation (4.41), we obtain

$$\frac{d}{dx} (Re_{\theta} \bar{i}_m) = \frac{R q_{cr}}{T_{3\phi 00}}. \quad (4.44)$$

Differentiating and multiplying both sides by $L/R\bar{i}_m$ (where L - the arbitrarily selected characteristic dimension), we obtain

$$\frac{d Re_{\theta}}{dx} + Re_{\theta} \frac{d(\ln \bar{R})}{dx} + Re_{\theta} \frac{d(\ln \bar{i}_m)}{dx} = \frac{q_{cr} L}{T_{3\phi 00} \bar{i}_m}, \quad (4.45)$$

where $\bar{x} = x/L$; $\bar{R} = R/L$.

Since we are free in the selection of a characteristic dimension, then we will subsequently take for it the critical throat diameter D_{kp} .

Then in equation (4.45)

$$\bar{x} = \frac{x}{D_{kp}}; \quad \bar{R} = \frac{R}{D_{kp}}.$$

In order to reduce equation (4.45) to a more convenient form for integration, let us produce the dimensionless complexes:

$$Re_{00} = \frac{D_{kp} \bar{\rho}_{00} \bar{w}_{max}}{\mu_{00}}; \quad (4.46)$$

$$A_T^2 = \frac{\bar{\rho}_{00} \bar{w}_{max}^2 \frac{p}{p_{00}} i_{00}}{g_{cr}}; \quad (4.47)$$

$$\beta = \frac{\bar{w}}{\bar{w}_{max}}; \quad (4.48)$$

where \bar{p}_{00} and $\bar{\rho}_{00}$ - pressure and density of the stagnated core of the flow; \bar{w}_{max} - highest possible speed of the core of the flow with expansion down to zero;

$$\bar{w}_{max} = \sqrt{\frac{2g}{\lambda} \bar{c}_{p, \phi, cp} \bar{T}_{\phi 00}}; \quad (4.49)$$

where $\bar{c}_{p, \phi, cp}$ - average heat capacity in the interval of temperatures $\bar{T}_{\phi 00} - \bar{T}_{\phi 0}$.

Considering the characteristic dimension D_{kp} and substituting expressions (4.46) and (4.47) into equation (4.45), we will obtain the integral relation of energy

$$\frac{d Re_0}{dx} + Re_0 \frac{d(\ln \bar{R})}{dx} + Re_0 \frac{d(\ln i_{00})}{dx} = \frac{Re_{00}}{A_T^2} \beta \frac{p}{p_{00}}. \quad (4.50)$$

Conducting analogous transformations of equations (4.30) and (4.31), we will obtain the integral relation of impulses

$$\frac{d Re_0}{dx} + Re_0 \frac{d(\ln \bar{R})}{dx} + \frac{e Re_0}{1 - \beta^2} \frac{d(\ln \beta)}{dx} = \frac{Re_{00}}{A_w^2} \beta \frac{p}{p_{00}}. \quad (4.51)$$

Here Re_δ - Reynolds number obtained on the thickness of the loss of impulse δ ; Re_δ and δ are determined from expressions

$$\delta = \int_0^{\delta} \frac{r}{R} \frac{\rho}{\rho_{\infty}} \frac{v}{v_{\infty}} \left(1 - \frac{v}{v_{\infty}}\right) dy; \quad (4.52)$$

$$Re_\delta = \frac{\rho_{\infty} v_{\infty} \delta}{\mu_{\infty}}; \quad (4.53)$$

complex

$$A_w = \bar{w} \sqrt{\frac{\rho_{\infty} \rho}{\tau_{cr} \rho_{\infty}}}; \quad (4.54)$$

the dimensionless quantity

$$c = H_w + 1 - (1 - T_{cr}) H_T, \quad (4.55)$$

where

$$H_w = \frac{1}{\delta} \int_0^{\delta} \frac{r}{R} \frac{\rho}{\rho_{\infty}} \left(1 - \frac{v}{v_{\infty}}\right) dy; \quad (4.56)$$

$$H_T = \frac{1}{\delta} \int_0^{\delta} \frac{r}{R} \frac{\rho}{\rho_{\infty}} \left(1 - \frac{t_{00}}{t_{\infty}}\right) dy; \quad (4.57)$$

$$T_{cr} = \frac{t_{cr}}{t_{\infty}}. \quad (4.58)$$

As we will subsequently see, the solution to the system of equations (4.50) and (4.51) under certain conditions can be reduced to the solution of one of them.

For this we must set the connection between quantities entering into these equations (A_T ; A_w ; Re_θ ; Re_δ).

The Connection Between Re_θ , A_T , A_w , and Re_δ

In order to find the connection between the indicated values, let us find the expressions for them in terms of quantities known to us. For this it is necessary, in the first place, to determine velocity and temperature (or heat content) profiles in the boundary layer.

In accordance with the structural diagram of turbulent boundary layer, let us examine separately the motion and heat exchange in turbulent and laminar parts of the layer.

Turbulent part of the layer. In examining this part of the layer, it is possible to disregard the first components in expressions (4.16) and (4.26). Then from these equations, by introducing the length of the path of mixing l according equations (4.23) and (4.24) and considering expressions (4.28) and (4.29), we will obtain:

$$\tau = \tau_{\text{тurb}} = \rho^2 \left(\frac{dw}{dy} \right)^2; \quad (4.59)$$

$$q_x = q_{x, \text{тurb}} = c_{\text{тurb}} \rho^2 \frac{dw}{dy} \frac{dT_{\text{тurb}}}{dy} = c_{\text{тurb}} \rho^2 \frac{dw}{dy} \frac{dT_{\text{ст}}}{dy}, \quad (4.60)$$

where

$$l_{\text{ст}} = T_{\text{ст}} - T_{\text{ст,ст}}. \quad (4.61)$$

To obtain velocity and temperature velocity it is thus necessary for us to assign this distribution l , τ and q_x across the boundary layer, so that it is possible to integrate equations (4.59) and (4.60). Calculations show that, although depending upon the assigned distribution τ , different dependences $l(y)$ and $w(y)$ on the section of boundary layer are respectively obtained, and the numerical difference of the final results with different profiles of τ is small, since the change in l as though compensates the change in τ .

Furthermore, profiles τ and q_x in the turbulent part of the layer should be assigned in such a manner than on the boundary with the laminar sublayer they take the corresponding values $\tau_{\text{лам}}$ and $q_{x, \text{лам}}$. (Let us note that in the laminar sublayer it is possible to assume $\tau_{\text{лам}}(y) = \text{const} = \tau_{\text{ст}}$; $q_{x, \text{лам}}(y) = \text{const} = q_{\text{ст}}$).

The law of the change in length of the path of mixing will be defined by the Karman function.

$$l = \tau \frac{dw/dy}{d\tau/dy^2}. \quad (4.62)$$

where κ - empirical constant ($\kappa = 0.38-0.4$).

Modifying the substitution of Dorodnitsyn, let us introduce the new variable

$$d\eta = \frac{r}{R} \frac{e}{e_{\text{max}}} dy. \quad (4.63)$$

Then the quantity of the path of mixing from equality (4.62) will be expressed as

$$l = -\kappa \frac{\frac{\partial w}{\partial \eta}}{\frac{r}{R} \frac{e}{e_{\text{max}}} \frac{\partial^2 w}{\partial \eta^2}}. \quad (4.64)$$

where

$$\kappa = \frac{1}{1 + \frac{\frac{\partial w}{\partial \eta}}{\frac{r}{R} \frac{e}{e_{\text{max}}} \frac{\partial^2 w}{\partial \eta^2}} \frac{\partial}{\partial \eta} \left(\frac{r}{R} \frac{e}{e_{\text{max}}} \right)}. \quad (4.65)$$

Substituting expressions (4.63) and (4.64) into formula (4.59), we will obtain

$$\tau = \rho e^2 x^2 \frac{(\partial w / \partial \eta)^4}{(\partial^2 w / \partial \eta^2)^2}. \quad (4.66)$$

Considering considerations mentioned above on the selection of the profile τ and proceeding from conditions of the convenience of integration of equations (4.66), the profile τ will be assigned in such a manner that the following equality will be satisfied

$$\frac{\tau}{\rho e^2} = \frac{\tau \tau}{e_{\text{max}}^2 e_{\text{max}}} = \text{const} = W_0^2. \quad (4.67)$$

Then equation (4.66) can be reduced to the form

$$W_0 = -\kappa \frac{(\partial w / \partial \eta)^2}{\partial^2 w / \partial \eta^2}. \quad (4.68)$$

(We place the minus sign from considerations of physical meaning).

The integration of equation (4.68) gives

$$\frac{\partial w}{\partial \eta} = \frac{W_0}{x(\eta + \delta)}, \quad (4.69)$$

where b – constant of integration.

Integrating expression (4.69) and determining the constant of integration from the condition that when $w = \bar{w}$; $\eta = \delta_\eta$, we obtain the equation of the velocity profile in the turbulent part of the layer:

$$\frac{w}{\bar{w}} = 1 + \frac{1}{\xi} \ln \frac{\eta + \delta}{\delta_\eta + \delta}, \quad (4.70)$$

where

$$\xi = x\bar{w}/W_0; \quad (4.71)$$

δ_η – thickness of the boundary layer in plane $x-\eta$.

Using expressions (4.63), (4.64), (4.68), and (4.69), from equation (4.60) we will obtain

$$\frac{q_x}{c_p \rho c_p x^2} = x W_0 (\eta + \delta) \frac{d t_{20}}{d \eta}. \quad (4.72)$$

Let us assign now the profile q_x in such a way that there will be satisfied the equality

$$\frac{q_x}{c_p \rho c_p x^2} = \frac{q_{x, \text{lam}}}{c_p \rho c_p x^2 \text{lam}^2}$$

where $c_p \rho c_p \text{lam}^2$ – value of $c_p \rho c_p$ on the boundary of the laminar sublayer.

Integrating equation (4.72), we will obtain the equation of the profile of temperatures in the turbulent part of the boundary layer.

$$\frac{t_{20}}{t_{20}} = 1 + \frac{1}{\xi_r} \ln \frac{\eta + \delta}{\delta_\eta + \delta}, \quad (4.73)$$

where Δ_η – thickness of the boundary layer in coordinates $x-\eta$;

$$\xi_r = \frac{c_p \rho c_p \text{lam}^2 \text{lam}^2 W_0}{q_{x, \text{lam}}}. \quad (4.74)$$

Let us turn to the consideration of the motion in the second (laminar) part of the boundary layer.

Laminar sublayer. Let us determine the thickness of the laminar sublayer $\delta_{\text{лам}}$. For the case of an incompressible liquid it is determined by the condition of Karman:

$$\frac{\delta_{\text{лам}} \partial_x \rho_{\text{лам}}}{\rho_{\text{лам}}} = \alpha, \quad (4.75)$$

where

$$\begin{aligned} \delta_x &= \sqrt{\tau / \rho_{\text{лам}}}, \\ \alpha &= 11,5. \end{aligned} \quad (4.76)$$

Substituting instead of τ quantity $\mu_{\text{лам}} \partial_x w_{\text{лам}} / \delta_{\text{лам}}$ from conditions (4.75) and (4.76), we obtain

$$\alpha^2 = \frac{\delta_{\text{лам}} w_{\text{лам}} \rho_{\text{лам}}}{\rho_{\text{лам}}} = \text{Re}_{\text{лам}}, \quad (4.77)$$

where $\text{Re}_{\text{лам}}$ — Reynolds number of the laminar sublayer; $\rho_{\text{лам}}$ — coefficient of viscosity on the boundary of the laminar sublayer.

For the case of the flow of the incompressible liquid the mass flow rate \mathfrak{M} can be expressed by unit width of the laminar sublayer in the form

$$\mathfrak{M} = \frac{\delta_{\text{лам}} w_{\text{лам}} \rho_{\text{лам}}}{2}. \quad (4.78)$$

From a comparison of expressions (4.77) and (4.78)

$$\text{Re}_{\text{лам}} = \frac{2\mathfrak{M}}{\rho_{\text{лам}}}. \quad (4.79)$$

Expanding equality (4.79), obtained for an incompressible liquid, in case of the flow of gas, we obtain

$$\frac{2\mathfrak{M}}{\rho_{\text{лам}}} = \frac{2 \int_0^{\delta_{\text{лам}}} \rho w dy}{\rho_{\text{лам}}} = \alpha^2. \quad (4.80)$$

Let us introduce a new independent variable

$$d\eta = \frac{\rho_{\text{лам}}}{\rho} dy. \quad (4.81)$$

Considering that in the laminar sublayer $\tau_{\text{лам}} = \tau_{\text{СТ}} = \text{const}$ and $q_{\text{к.лам}} = q_{\text{СТ}} = \text{const}$, on the basis of equality (4.15) and (4.18) we can write:

$$\tau_{\text{СТ}} = \rho \frac{\partial w}{\partial y} = \rho_{\text{лам}} \frac{\partial w}{\partial \eta}; \quad (4.82)$$

$$q_{\text{СТ}} = c_p \rho \delta T = c_p \rho_{\text{лам}} \delta T_{\text{лам}}. \quad (4.83)$$

Integrating equations (4.82) and (4.83), we obtain

$$w = \frac{\tau_{\text{СТ}}}{\rho_{\text{лам}}} \eta; \quad w_{\text{лам}} = \frac{\tau_{\text{СТ}}}{\rho_{\text{лам}}} \delta_{\eta \text{ лам}}; \quad (4.84)$$

$$t_{\text{СТ}} = \frac{q_{\text{СТ}}}{c_p \rho_{\text{лам}} \delta T_{\text{лам}}} \eta; \quad t_{\text{СТ лам}} = \frac{q_{\text{СТ}}}{c_p \rho_{\text{лам}} \delta T_{\text{лам}}} \delta_{\eta \text{ лам}}. \quad (4.85)$$

where $\delta_{\eta \text{ лам}}$ — thickness of the laminar sublayer in coordinates $x-\eta$; $w_{\text{лам}}$ and $t_{\text{СТ лам}}$ — on the boundary of the laminar sublayer.

Using expressions (4.81) and (4.84) and considering the initial equations (4.34) and (4.35), let us define

$$\text{NR} = \int_0^{\delta_{\eta \text{ лам}}} q w dy = \int_0^{\delta_{\eta \text{ лам}}} q \frac{\rho_{\text{лам}}}{\rho} w \frac{\rho}{\rho_{\text{лам}}} d\eta = \rho_{\text{лам}} \int_0^{\delta_{\eta \text{ лам}}} \frac{T_{\text{эф лам}}}{T_{\text{эф}}} \frac{\tau_{\text{СТ}}}{\rho_{\text{лам}}} \eta \left(\frac{T_{\text{эф}}}{T_{\text{эф лам}}} \right)^n d\eta = \frac{\rho_{\text{лам}} \tau_{\text{СТ}}}{\rho_{\text{лам}}} \int_0^{\delta_{\eta \text{ лам}}} \left(\frac{T_{\text{эф}}}{T_{\text{эф лам}}} \right)^{1-n} \eta d\eta. \quad (4.86)$$

When $n = 0.7$ we assume $(T_{\text{эф}}/T_{\text{эф лам}})^{1-n} \approx 1$, and then from equation (4.86) we obtain

$$\text{NR} = \frac{\rho_{\text{лам}} \tau_{\text{СТ}} \delta_{\eta \text{ лам}}^2}{2 \rho_{\text{лам}}}. \quad (4.87)$$

Substituting the obtained expression into equality (4.80) and considering condition (4.57), we will obtain

$$\delta_{\eta \text{ лам}} = \frac{2 \rho_{\text{лам}}}{c_{\text{СТ}} w_{\text{эф лам}}}. \quad (4.88)$$

In plane x-y the thickness of the laminar sublayer

$$\delta_{lam} = \int_0^{t_{lam}} \frac{\rho}{\rho_{lam}} d\eta = \int_0^{t_{lam}} \left(\frac{T_{\infty}}{T_{\infty, lam}} \right)^2 d\eta. \quad (4.89)$$

Let us convert quantity $T_{\infty}/T_{\infty, lam}$ entering into equality (4.80).

In accordance with expressions (4.29) and (4.61)

$$\frac{T_{\infty}}{T_{\infty, lam}} = \frac{T_{r, \infty} + t_{\infty} - A \frac{w^2}{2g^2 \rho_{\infty} c_p}}{T_{r, \infty} + t_{\infty, lam} - A \frac{w_{lam}^2}{2g^2 \rho_{\infty} c_p}}, \quad (4.90)$$

where c_p - mean value of c_p in the interval of temperature $T_{\infty} - T_{\infty, 00}$.

Dividing the numerator and denominator of the right side of equation (4.90) by $T_{\infty, 00}$ and introducing the designation

$$\bar{c}_p = \frac{c_p}{c_{p, 00}}, \quad (4.91)$$

where \bar{c}_p - value of c_p in the range of temperature $T_{\infty} - T_{\infty, 00}$, and considering

$$\bar{c}_p / c_{p, 00} \approx 1, \quad (4.92)$$

after transformations we will obtain

$$\frac{T_{\infty}}{T_{\infty, lam}} = \frac{T_{r, \infty} + (1 - T_{r, \infty}) \frac{t_{\infty}}{t_{\infty, lam}} - \mu \left(\frac{w}{g} \right)^2}{T_{r, \infty} + (1 - T_{r, \infty}) \frac{t_{\infty, lam}}{t_{\infty, 00}} - \mu \left(\frac{w_{lam}}{g} \right)^2}, \quad (4.93)$$

where $T_{r, \infty} = T_{r, \infty} / T_{\infty, 00}$; $t_{\infty} = T_{\infty, 00} - T_{r, \infty}$. Let us define now quantities w_{lam} / w ; $t_{\infty, lam} / t_{\infty, 00}$; $t_{\infty, 00} / t_{\infty, 00}$ entering into equation (4.93). From expression (4.84), replacing τ_{∞} according to equation (4.67), and using equalities (4.71) and (4.88), we will obtain

$$\frac{w_{lam}}{w} = \frac{t_{\infty, lam}}{t_{\infty, 00}} \delta_{lam} \quad (4.94)$$

Similarly, from equality (4.85), replacing q_{CT} according to formula (4.74) and $\delta_{\eta_{LAM}}$ according to formula (4.88), we obtain

$$\frac{l_{\eta_{LAM}}}{l_{\eta_0}} = \frac{q_{\eta_0}}{q_{\eta_{LAM}}} \delta_{\eta_{LAM}} \quad (4.95)$$

From equations (4.74) and (4.85) we obtain

$$\frac{l_{\eta_0}}{l_{\eta_{LAM}}} = \frac{q_{\eta_0} \sqrt{v_{\eta_0}}}{q_{\eta_{LAM}}} \eta \quad (4.96)$$

Substituting now expressions (4.94), (4.95) and (4.96) into equality (4.93) and the obtained expression for $T_{\eta_0}/T_{\eta_{LAM}}$ - into formula (4.89), using expression (4.88), after transformations we will obtain the final formul for $\delta_{\eta_{LAM}}$ [quantity $\beta^2(w/\bar{w})^2$ will be disregarded]:

$$\delta_{\eta_{LAM}} = \Phi \delta_{\eta_{LAM}} \quad (4.97)$$

where

$$\Phi = \frac{l_{\eta_0} \left\{ \left[T_{r,CT} + (1 - T_{r,CT}) \frac{v_{\eta_0}}{l_{\eta_0}} \right]^{n+1} - T_{r,CT}^{n+1} \right\}}{v_{\eta_{LAM}} (n+1) (1 - T_{r,CT}) \left[T_{r,CT} + (1 - T_{r,CT}) \frac{v_{\eta_0}}{l_{\eta_0}} - \left(\frac{v_{\eta_{LAM}}}{l_{\eta_0}} \right)^n \right]} \quad (4.98)$$

Knowing now $\delta_{\eta_{LAM}}$, we can determine the constant of integration b in equations (4.70) and (4.73). The length of the path of mixing on the boundary of the laminar sublayer

$$l_{\eta_{LAM}} = \alpha \delta_{\eta_{LAM}} \quad (4.99)$$

On the other hand, we find $l_{\eta_{LAM}}$ from expressions (4.64), (4.68), and (4.69) when $\eta = \delta_{\eta_{LAM}}$; $l = l_{\eta_{LAM}}$; $q = q_{\eta_{LAM}}$, and considering $r/R \approx 1$:

$$l_{\eta_{LAM}} = \alpha_{\eta_{LAM}} (\delta_{\eta_{LAM}} + \delta) \quad (4.100)$$

Solving equations (4.99) and (4.100) jointly with respect to b , taking into account equality (4.97) we obtain

$$\delta = \delta_{\eta_{LAM}} \left(\frac{\alpha}{\alpha_{\eta_{LAM}}} - 1 \right) \quad (4.101)$$

or

$$\delta_{q, \text{лам}} + b = \delta_{q, \text{лам}} \frac{\phi}{\delta_{\text{лам}}} \quad (4.102)$$

Quantity $b < \delta_{\eta \text{ лам}}$, and consequently, $b \ll \delta$ and Δ . Therefore, in sums $(\delta + b)$ and $(\Delta + b)$, which enter into expression (4.70) and (4.73), quantity b can be disregarded. Then, considering equalities (4.102) and (4.88), we obtain

$$\frac{\delta_{q, \text{лам}} + b}{\delta + b} \approx \frac{\delta_{q, \text{лам}} \phi}{\delta_{\text{лам}}} = \frac{\phi \alpha \mu_{\text{лам}}}{\sigma_{\text{лам}}^2 \delta_{\text{лам}} W_{\phi}} \quad (4.103)$$

Substituting value W_{ϕ} from expression (4.71) and considering that according to equality (4.35) $\mu_{\text{лам}} = \bar{\mu}_{\text{лам}} (T_{\text{эф. лам}})^n$, we obtain

$$\frac{\delta_{q, \text{лам}} + b}{\delta + b} = \frac{\alpha \phi (T_{\text{эф. лам}})^n}{\sigma_{\text{лам}}^2 \text{Re}_{\phi}} \quad (4.104)$$

where

$$\text{Re}_{\phi} = \frac{\bar{\mu}_{\text{лам}}}{P_{\text{эф. лам}}} \quad (4.105)$$

By similar transformations we will also obtain

$$\frac{\delta_{q, \text{лам}} + b}{\Delta + b} \approx \frac{\delta_{q, \text{лам}} \phi}{\Delta \sigma_{\text{лам}}} = \frac{\phi \alpha \mu_{\text{лам}}}{\sigma_{\text{лам}}^2 \Delta \sigma_{\text{лам}} W_{\phi}} = \frac{\alpha \phi (T_{\text{эф. лам}})^n}{\sigma_{\text{лам}}^2 \text{Re}_{\Delta}} \quad (4.106)$$

where

$$\text{Re}_{\Delta} = \frac{\bar{\mu}_{\text{лам}}}{P_{\text{эф. лам}}} \quad (4.107)$$

Comparing formulas (4.105) and (4.107) with equations (4.53) and (4.43), which determine Re_{ϕ} and Re_{δ} , we obtain

$$\text{Re}_{\phi} = \text{Re}_{\delta} \frac{\phi}{\delta}; \quad (4.108)$$

$$\text{Re}_{\phi} = \text{Re}_{\Delta} \frac{\phi}{\Delta}. \quad (4.109)$$

Having velocity and temperature profiles in the turbulent part of the layer and laminar sublayer, let us produce conjugation of the corresponding profiles by substitution of w_{LAM}/\sqrt{w} from equation (4.94) and $(\delta_{\eta\text{LAM}} + b)/(\delta + b)$ from equation (4.104) into equation (4.70). After transformations

$$Re_{\Delta} = \frac{c\theta(T_{\text{ср.лам}})^{1/2}t^2}{\nu_{\text{лам}}^2} \quad (4.110)$$

Similarly [see equations (4.95), (4.106), and (4.73)].

$$Re_{\delta} = \frac{c\theta(T_{\text{ср.лам}})^{1/2}t^2}{\nu_{\text{лам}}^2} \quad (4.111)$$

Values $\bar{T}_{\text{ср.лам}}$ and $\alpha_{\text{лам}}$ entering in equations (4.110) and (4.111) can be determined in the following way. According to equalities (4.29), (4.61), and (4.91), using equation (4.92), (4.94), and (4.95), the expression for $\bar{T}_{\text{ср.лам}}$ can be reduced to the following form:

$$\bar{T}_{\text{ср.лам}} = \bar{T}_{\text{r.сr}} + (1 - \bar{T}_{\text{r.сr}}) \frac{\nu_{\text{лам}}}{\xi_T} - \left(\frac{\nu_{\text{лам}}}{\xi_T} \right)^2 \quad (4.112)$$

Expression for $\alpha_{\text{лам}}$ can be obtained from equation (4.65). Omitting the transformation, we will obtain the final dependence in the form

$$\alpha_{\text{лам}} = \frac{\bar{T}_{\text{ср.лам}}}{\bar{T}_{\text{ср.лам}} + \frac{1 - \bar{T}_{\text{r.сr}}}{\xi_T} - 2 \frac{\nu_{\text{лам}}}{\xi_T}} \quad (4.113)$$

With known or given quantities $\bar{T}_{\text{r.сr}}$ and β , ξ , ξ_T , solving jointly equations (4.112) and (4.113), $\bar{T}_{\text{ср.лам}}$ and $\alpha_{\text{лам}}$ can be found by knowing them one can also determine Re_{Δ} and Re_{δ} .

Using all dependences obtained above, we can turn now to the determination of quantities A_T , A_W , Re_{θ} , Re_{δ} , and c interesting to us in terms of quantities known to us and in terms of ξ and ξ_T . According to the equation of state (4.34)

$$\frac{p}{p_0} = \frac{p_{\text{лам}}}{p_0} = \frac{c_{\text{лам}}}{c_0} \frac{T_{\text{ср.лам}}}{T_{\text{ср.0}}} = \frac{c_{\text{лам}}}{c_0} \bar{T}_{\text{ср.лам}} \quad (4.114)$$

Transforming now equation (4.47), taking into account expressions (4.114), (4.74), and (4.71), we obtain

$$A_T = \frac{\sqrt{F_{\text{exp. max}}}}{u_{\text{max}}}. \quad (4.115)$$

Similarly, from equation (4.54), taking into account expressions (4.114), (4.71), and (4.57), we obtain

$$A_{\theta} = \frac{\epsilon \sqrt{F_{\text{exp. max}}}}{u_{\text{max}}}. \quad (4.116)$$

To determine Re_{θ} and Re_{δ} , we will find preliminarily the expressions for determining the thicknesses of the loss of energy θ and impulse δ .

Replacing in equation (4.42) the variable according to expression (4.53), we obtain

$$\theta = \int_0^{\Delta} \frac{\epsilon}{u} \left(1 - \frac{\eta}{\Delta}\right) d\eta = \int_0^{\Delta} \frac{\epsilon}{u} \left(1 - \frac{\eta}{\Delta}\right) d\eta. \quad (4.117)$$

where Δ_{η} - thickness of the thermal boundary layer in coordinates $x-\eta$.

Substituting into expression (4.117) values w/\bar{w} according to formula (4.70) and t_{00}/\bar{t}_{00} according to formula (4.73), considering in view of the smallness of b that $(\delta + b) \approx \delta$ and $(\Delta + b) \approx \Delta$, and also assuming $\delta = \Delta$, we obtain

$$\theta = \frac{1}{u_T} \int_0^{\Delta} \ln \left(\frac{\Delta}{\Delta - \eta}\right) d\eta = \frac{1}{u_T} \int_0^{\Delta} \ln^2 \left(\frac{\Delta}{\Delta - \eta}\right) d\eta. \quad (4.118)$$

Integrating by parts, we define

$$\frac{\theta}{\Delta} = \frac{1}{u_T} \left(1 - \frac{2}{3}\right). \quad (4.119)$$

Similarly, from equation (4.52) after transformations we obtain

$$\frac{\delta}{\Delta} = \frac{1}{u_T} \left(1 - \frac{2}{3}\right). \quad (4.120)$$

To determine Re_ξ and Re_θ , we substitute into equality (4.108) expressions (4.110) and (4.120) and obtain

$$Re_\theta = \frac{c_0 \sigma_{\text{max}}^2 \epsilon^{\frac{1}{2}} \left(1 - \frac{2}{\xi}\right)}{c_0^2 \sigma_{\text{max}}^2 \epsilon^{\frac{1}{2}}}, \quad (4.121)$$

and into equality (4.109) - expressions (4.111) and (4.119), then

$$Re_\xi = \frac{c_0 \sigma_{\text{max}}^2 \epsilon^{\frac{1}{2}} \left(1 - \frac{2}{\xi}\right) \epsilon^{\frac{1}{2}}}{c_0^2 \sigma_{\text{max}}^2 \epsilon^{\frac{1}{2}}}. \quad (4.122)$$

Similarly, determining preliminarily H_T and H_w from equation (4.55), we will obtain the expression for the dimensionless value

$$c = \frac{2\left(1 - \frac{1}{\xi}\right) - \left(1 - \sigma_{\text{max}}\right) \frac{1}{\xi} \epsilon^{(n-1)}}{1 - \frac{2}{\xi}}. \quad (4.123)$$

Thus, we obtained dependences (4.115), (4.116), (4.121), and (4.122), which express variables entering into the integral relations of energy (4.50) and impulses (4.51) in terms of quantities known to us and in terms of ξ and ξ_T . Substitution of these expressions in equations (4.50) and (4.51) will lead to a system of two differential equations with two unknowns ξ and ξ_T .

The approximate solution of this system for the general case of motion in a boundary layer can be found; however, for practical calculations of heat exchange in a ZhRD it is more convenient to use the approximate but very simple dependence

$$\xi_T = \xi = 0.5. \quad (4.124)$$

The use of dependence (4.124) permits reducing the solution of the system of equations (4.50) and (4.51) to the solution of one equation.

4.5. Solution of the Integral Relation of Energy

Earlier we obtained the following integral relation of energy (4.50):

$$\frac{d Re_{\theta}}{dx} + Re_{\theta} \frac{d(\ln \bar{R})}{dx} + Re_{\theta} \frac{d(\ln \bar{t}_{00})}{dx} = \frac{Re_{\theta}}{A_T} \beta \frac{L}{\rho_{00}}$$

Examining expressions (4.115) and (4.122), which determine Re and A_T , let us note that quantities $\bar{T}_{\text{эф.лам}}$, $a_{\text{лам}}$ and Φ entering into these formulas are functions $\bar{T}_{\text{r.ct}}$, β , ξ and ξ_T . Consequently, considering dependence (4.124) connecting ξ and ξ_T , we can say that Re_{θ} and A_T are functions of only three quantities: $\bar{T}_{\text{r.ct}}$, β , and ξ_T , i.e.,

$$Re_{\theta} = f_1(\bar{T}_{\text{r.ct}}, \beta, \xi_T); \quad A_T = f_2(\bar{T}_{\text{r.ct}}, \beta, \xi_T), \quad (4.125)$$

The joint solution of equations (4.115) and (4.122) with the assigned different values of $\bar{T}_{\text{r.ct}}$ permits excluding ξ_T and finding the connection between Re_{θ} and A_T at different values of β . Expressing this dependence graphically it is possible to select the approximate formula of the connection between Re_{θ} and A_T .

In the range of the change in $\bar{T}_{\text{r.ct}} = 0-1$; $\beta = 0-0.8$, and $\lg Re_{\theta} = 2.5-6$

$$A_T = (1 + 1.5 \bar{T}_{\text{r.ct}}^{0.728}) \ln \left[\frac{4.14 Re_{\theta}}{\left(1 + \frac{\beta^2}{1 + 1.5 \bar{T}_{\text{r.ct}}^{0.728}}\right)^{4.4} (\bar{T}_{\text{r.ct}} + 0.04)^{2.616}} \right] \quad (4.126)$$

Let us introduce the following designations:

$$b_T = 1 + 1.5 \bar{T}_{\text{r.ct}}^{0.728}; \quad (4.127)$$

$$\xi_T = \ln \left[\frac{4.14 Re_{\theta}}{\left(1 + \frac{\beta^2}{1 + 1.5 \bar{T}_{\text{r.ct}}^{0.728}}\right)^{4.4} (\bar{T}_{\text{r.ct}} + 0.04)^{2.616}} \right] = \frac{A_T}{b_T}, \quad (4.128)$$

$$a_T = \frac{1}{4.14} \left(1 + \frac{\beta^2}{b_T}\right)^{4.4} (\bar{T}_{\text{r.ct}} + 0.04)^{2.616}. \quad (4.129)$$

Then formula (4.128) acquires the form

$$Re_{\theta} = a_T e^{b_T \xi_T}. \quad (4.130)$$

Let us substitute expressions (4.128) and (4.130) into the integral relation of energy (4.50) and reduce it to the form

$$\psi d(a_T e^{a_T}) + \psi_T e^{a_T} d \ln(R T_{00}) = \frac{2\alpha_T}{a_T} \psi \frac{p}{\rho_0} dx. \quad (4.131)$$

Let us introduce into equality (4.131) instead of \bar{R} and T_{00} quantities $D/2 = \bar{R}$ and

$$c_{p, \text{eff}} T_{00} (1 - T_{r, \text{eff}}) = c_{p, \text{eff}} (T_{00} - T_{r, \text{eff}}) = T_{00} - T_{r, \text{eff}} = T_{00}. \quad (4.132)$$

where $c_{p, \text{eff}}$ — effective heat capacity in the interval of temperatures $(T_{00} - T_{r, \text{eff}})$. We consider it to be constant along the length of the chamber, i.e., not dependent on x .

Substituting equality (4.132) into equation (4.131), differentiating and dividing everything by a_T , we will obtain

$$\psi d e^{a_T} + \psi_T e^{a_T} d \ln(a_T D (1 - T_{r, \text{eff}})) = \frac{2\alpha_T}{a_T} \psi \frac{p}{\rho_0} dx. \quad (4.133)$$

For the convenience of the solution of equation (4.133), we denote

$$z_T = (\psi_T - 2\psi_T + 2) e^{a_T}. \quad (4.134)$$

It is easy to be convinced that

$$dz_T = \psi_T d e^{a_T}, \quad (4.135)$$

and

$$\psi_T e^{a_T} = k_T z_T, \quad (4.136)$$

where

$$k_T = \frac{1}{1 - \frac{2}{\psi_T} + \frac{2}{\psi_T}}. \quad (4.137)$$

With the practical range of the change in ψ_T within 7-15, the change in k_T corresponding to dependence (4.137) is small and amounts

to 1.32-1.15. Therefore, it is quite permissible to consider $k_T = \text{const} = 1.2$. Substituting equality (4.135) and (4.136) into equation (4.133), we obtain

$$dz_T + z_T \delta_T d \ln [a_T \bar{D} (1 - \bar{T}_{r,ct})] = \frac{Re_{00}}{a_T \delta_T^2} \beta \frac{p}{p_{00}} d\bar{x},$$

or

$$dz_T + z_T \frac{d [a_T \bar{D} (1 - \bar{T}_{r,ct})]^{\delta_T}}{[a_T \bar{D} (1 - \bar{T}_{r,ct})]^{\delta_T}} = \frac{Re_{00}}{a_T \delta_T^2} \beta \frac{p}{p_{00}} d\bar{x},$$

whence

$$d [z_T [a_T \bar{D} (1 - \bar{T}_{r,ct})]^{\delta_T}] = \frac{Re_{00}}{\delta_T^2} a^{\delta_T - 1} [\bar{D} (1 - \bar{T}_{r,ct})]^{\delta_T} \beta \frac{p}{p_{00}} d\bar{x}. \quad (4.138)$$

Integrating equation (4.138), we find

$$z_T = \frac{1}{[a_T \bar{D} (1 - \bar{T}_{r,ct})]^{\delta_T}} \left\{ B_T + \int_0^{\bar{x}} \frac{Re_{00}}{\delta_T^2} a^{\delta_T - 1} [\bar{D} (1 - \bar{T}_{r,ct})]^{\delta_T} \beta \frac{p}{p_{00}} d\bar{x} \right\}, \quad (4.139)$$

where B_T - constant of integration

When $\bar{x} = 0$

$$B_T = [z_T [a_T \bar{D} (1 - \bar{T}_{r,ct})]^{\delta_T}]_{\bar{x}=0}. \quad (4.140)$$

Determination of z_T in Conditions of a ZhRD

In reference to conditions taking place in a ZhRD, it is possible to make the following simplifications of equation (4.139).

1. The constant of integration B_T characterizes by itself the boundary layer on sections lying up to the beginning of the reading (i.e., up to the point where $\bar{x} = 0$). The whole preceding analysis of heat exchange in the boundary layer in no way considered the influence of the mixing and burning on the development of the boundary layer. Therefore, strictly speaking, we should consider the beginning of the reading to be the section in which combustion was completely completed. However, in this case we will have

remaining constant B_T , which we cannot determine, since we do not know the influence of processes of mixing and combustion on the development of the boundary layer.

In order to exclude the problem of determining B_T , let us assume conditionally that combustion occurs only in a certain narrow, "effective" flame front, lying immediately behind the zone of evaporation and mixing. With this, disregarding the initial section of the laminar boundary layer ($l_{lam} = 0$), we consider that in the indicated section of the effective flame front there immediately starts the formation of a turbulent boundary layer, on the further development of which along the length of the chamber processes of mixing and combustion have no effect.

Taking now for the reading point the section where there starts to be formed a boundary layer, we thereby exclude from consideration constant B_T , since at this point $B_T = 0$. In carrying out practical calculations, the position of the effective flame front, i.e., the reading point $\bar{x} = 0$, can be determined, considering that the length of zones I and II (see Fig. 3.2) consists of 25% of the length of the combustion chamber. The possible error in the determination of the reading point does not have considerable effect on the value of maximum convection flows in the nozzle and is therefore not dangerous.

2. Let us take the assumption about the constancy of temperature of the gas wall according to the length of the chamber and nozzle, i.e., we will consider $T_{r,0T} \approx T_{r,0T}/T_{g,00} = \text{const}$. Such an assumption does not correspond to the real distribution of $T_{r,0T}$ along the length of the chamber of the ZhRD; however, as we will see later (section 4.7), the error appearing with this in the determination of q_R can be easily corrected, and the assumption of constancy $T_{r,0T}$ permits greatly simplifying the problem of the determination of z_T (and, consequently, heat flows).

3. In accordance with equation (4.127) when $T_{r,0T} = \text{const}$ and $b_T = \text{const}$.

4. From equation (4.129) we see that when $T_{r.ct} = \text{const}$ quantity a_T still depends on β . However, since in expression (4.139) quantity a_T is contained in power $(k_T - 1) \approx 0.2$, then the effect of the change in a_T^{-1} on the change in β is small and with integration of the right side of expression (4.139) it is possible to take also

$$a_T^{-1} = \text{const.}$$

5. In the preceding analysis we assumed $Pr = 1$. For products of combustion of a ZhRD $Pr = 0.75-0.8$. Since this distinction of the Pr number from unity appear in the final determination of convection heat flow, we will examine the influence of the Pr number on q_K below.

Taking the assumptions noted above and considering that Re_{00} does not depend on \bar{x} , formula (4.139) after transformations takes the form

$$s_T = \frac{Re_{00}}{a_T D^{1.5}} \int_0^{\bar{x}} \beta \frac{p}{p_0} D^{1.5} d\bar{x}. \quad (4.141)$$

Let us examine the obtained expression. As we noted above, $\bar{x} = x/D_{kp}$, where x is the coordinate counted off along the generatrix of the contour of the chamber and nozzle. In the calculations it is more convenient to calculate with respect to the coordinate counted off along the axis of the engine x_1 (Fig. 4.15).

From consideration of Fig. 4.15 it is obvious that

$$d\bar{x} = \frac{dx_1}{\cos \gamma}. \quad (4.142)$$

According to well-known formulas of gas dynamics (see, for example [1]) entering into equality (4.141), quantities β , p/p_{00} and D are defined as

$$\beta = \lambda \sqrt{\frac{k-1}{k+1}}$$

where $\lambda = \frac{v}{a_{00}}$ - velocity coefficient;

$$\frac{p}{p_0} = (1 - \gamma)^{\frac{1}{\gamma-1}}; \quad (4.143)$$

$$D^2 = \frac{f}{f_{kp}} = \frac{\left(\frac{2}{k+1}\right)^{\frac{1}{k-1}}}{\lambda \left(1 - \frac{k-1}{k+1} \lambda^2\right)^{\frac{1}{k-1}}} = \frac{\left(\frac{2}{k+1}\right)^{\frac{1}{k-1}}}{\sqrt{\frac{k+1}{k-1} \beta (1-\beta)^{\frac{1}{k-1}}}} \quad (4.144)$$

Replacing in reference to conditions of a ZhRD the adiabatic index k by the index of the isentrope $n_{\text{из}}$ and substituting equalities (4.142) and (4.143) into formula (4.141), we will obtain

$$z_T = \frac{Re_{00}}{a_T^2 D^{1.5}} \int_0^{\bar{x}_1} \beta (1-\beta)^{\frac{n_{\text{из}}}{n_{\text{из}}-1}} D^{1.5} \frac{d\bar{x}_1}{\cos \gamma}$$

Calculations show that a change in $n_{\text{из}}$ does not have a considerable effect on quantity z_T , since the effect of the change in $n_{\text{из}}$ on the integrand expression and on quantity Re_{00} , determined by expression (4.46), is the opposite. Therefore, with a sufficient degree of accuracy it is possible to assume $n_{\text{из}} = 1.2$.

From expression (4.144) we see that with constant $n_{\text{из}}$ with one-dimensional motion in the nozzle quantity β depends only on the ratio $f/f_{kp} = (D/D_{kp})$, i.e., it is the function $\bar{D} = D/D_{kp}$. Accordingly, the complex

$$\beta (1-\beta)^{\frac{n_{\text{из}}}{n_{\text{из}}-1}} D^{1.5} = f(\bar{D}). \quad (4.145)$$

Taking into account relation (4.145) it is convenient to present the formula for the determination of z_T in the form

$$z_T = \frac{Re_{00}}{a_T^2 D^{1.5}} \int_0^{\bar{x}_1} \frac{f(\bar{D})}{\cos \gamma} d\bar{x}_1. \quad (4.146)$$

For the convenience of determining $f(\bar{D})$ in Appendix I on Fig. I.1 there is given an auxiliary graph of the dependence of $f(\bar{D})$ on values \bar{D} .

As can be seen from expressions (4.127) and (4.129), the complex

$$\frac{1}{a_T^2 D^{1.5}} = f(\bar{T}_{\text{из}}, \bar{D}).$$

and therefore for easing the calculations z_T it is convenient to represent this dependence graphically (see appendix, Fig. I.3, I.4).

Determination of z_T for an Engine with a Cylindrical Combustion Chamber

In the determination of z_T for an engine with a cylindrical combustion chamber, it is expedient to divide the integral in the right side of (4.146) into two integrals, i.e.,

$$z_T = \frac{R_{00} D_{00}}{c_T + D_{00}} \left(\int_0^{\bar{x}_K} \beta \frac{D}{D_{00}} D^{1.2} d\bar{x}_1 + \int_{\bar{x}_K}^{\bar{x}_2} \beta \frac{D}{D_{00}} D^{1.2} d\bar{x}_1 \right), \quad (4.147)$$

where \bar{x}_K - distance from the reading point ("effective flame front") to the end of the cylindrical section of the combustion chamber (see Fig. 4.15).



Fig. 4.15. Determination of coordinate x_1 .

If the chamber is not high-speed, then for its cylindrical part it is possible to assume $p/\bar{p}_{00} = 1$, $\beta = \text{const}$. Then the first integral of equation (4.147) is easily solved:

$$\int_0^{\bar{x}_K} \beta \frac{D}{D_{00}} D^{1.2} d\bar{x}_1 = \beta_K \bar{D}_K^{1.2} \bar{x}_K, \quad (4.148)$$

where β_K and D_K - values of β and \bar{D} in the combustion chamber.

Considering that zones of evaporation and mixing occupy 25% of the length of the cylindrical part of the combustion chamber, we assume

$$\bar{x}_z = 0.75L_{zs} \quad (4.149)$$

where

$$L_{zs} = \frac{L_z}{D_{zs}}$$

Since in the combustion chamber β is small and $\beta^2 \ll 1$, then, disregarding in expression (4.144) value β^2 , when $n_{H_2O} = 1.2$, we will obtain

$$\beta = \sqrt{\frac{n_{H_2O} - 1}{n_{H_2O} + 1}} \left(\frac{2}{n_{H_2O} + 1}\right)^{\frac{1}{n_{H_2O} - 1}} \frac{f_{sp}}{f_z} = \frac{0.189}{D_{zs}} \quad (4.150)$$

Substituting equality (4.148) into expression (4.147) and using dependences (4.142), (4.145), (4.149), and (4.150), we will obtain in final form the formula for determining z_T for a cylindrical non-high-speed combustion chamber:

$$z_T = \frac{Re_{00}}{0.75 D_{zs}^2} \left[\frac{0.142 L_{zs}}{D_{zs}^2} + \int_{z_{min}}^{\bar{x}_z} \frac{f(D)}{\cos \gamma} dx_1 \right] \quad (4.151)$$

4.6. Calculation of Convection Heat Exchange in a ZhRD

Using expressions obtained above for Re_{00} , z_T , ψ_T , and A_T , one can determine the magnitude of convection heat flows q . However, for carrying out the calculations the basic formulas in the dependence are expediently obtained in a more convenient form.

Determination of Effective Stagnation Temperature $T_{\phi 00}$

Although the determination of effective temperature in general is sufficiently clear from its formal expression (4.27), let us give

the order of calculation of the effective stagnation temperature T_{eff} in reference to conditions in the chamber of a ZhRD. According to the indicated formula

$$\bar{T}_{\text{eff}} = \frac{R_2 T_2}{R_H} \quad (4.152)$$

where T_2 and R_2 - real temperatures and the gas constant of products of fuel combustion in the chamber, which are determined by conventional methods (see for example, [2], [25]); R_H - gas constant of undissociated products of fuel combustion of the same composition.

In the determination of the composition of undissociated products of the combustion, the system of design equations is considerably simplified, since equations of reactions of dissociation dropout. Thus, with the application of a four-element fuel with H, O, N, and C as a base, it is possible to cite the prepared formulas of determining the composition of products of combustion for a particular case when at $\alpha < 1$ oxygen suffices for the full oxidation of carbon but is insufficient for the full oxidation of hydrogen. In this case the products of combustion will consist of CO_2 , H_2O , H_2 , and N_2 . Calculation formulas for the determination of partial pressures of undissociated products of combustion will take the form

$$\begin{aligned} p_{\text{CO}_2} &= \frac{P_2}{1 + 6 \frac{H_r + vH_o}{C_r + vC_o} + \frac{3}{7} \frac{N_r + vN_o}{C_r + vC_o}}; \\ p_{\text{H}_2\text{O}} &= \frac{P_2 \left(\frac{3}{4} \frac{O_r + vO_o}{C_r + vC_o} - 2 \right)}{1 + 6 \frac{H_r + vH_o}{C_r + vC_o} + \frac{3}{7} \frac{N_r + vN_o}{C_r + vC_o}}; \\ p_{\text{H}_2} &= \frac{P_2 \left(2 + 6 \frac{H_r + vH_o}{C_r + vC_o} - \frac{3}{4} \frac{O_r + vO_o}{C_r + vC_o} \right)}{1 + 6 \frac{H_r + vH_o}{C_r + vC_o} + \frac{3}{7} \frac{N_r + vN_o}{C_r + vC_o}}; \\ p_{\text{N}_2} &= \frac{P_2 \frac{3}{7} \frac{N_r + vN_o}{C_r + vC_o}}{1 + 6 \frac{H_r + vH_o}{C_r + vC_o} + \frac{3}{7} \frac{N_r + vN_o}{C_r + vC_o}}. \end{aligned} \quad (4.153)$$

Having determined the composition of undissociated products of combustion, let us find for them R_H , and with respect to expression (4.152) - $T_{\text{эф00}}$ (Fig. 4.16).

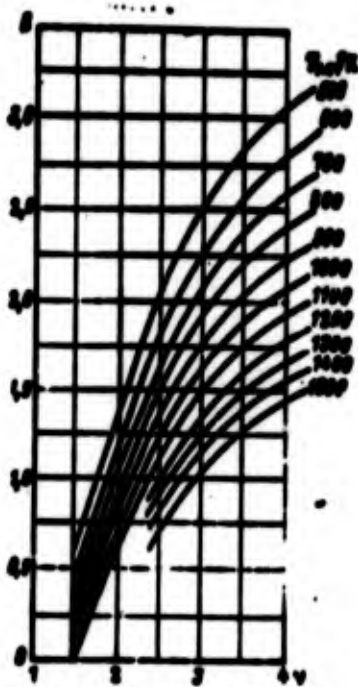
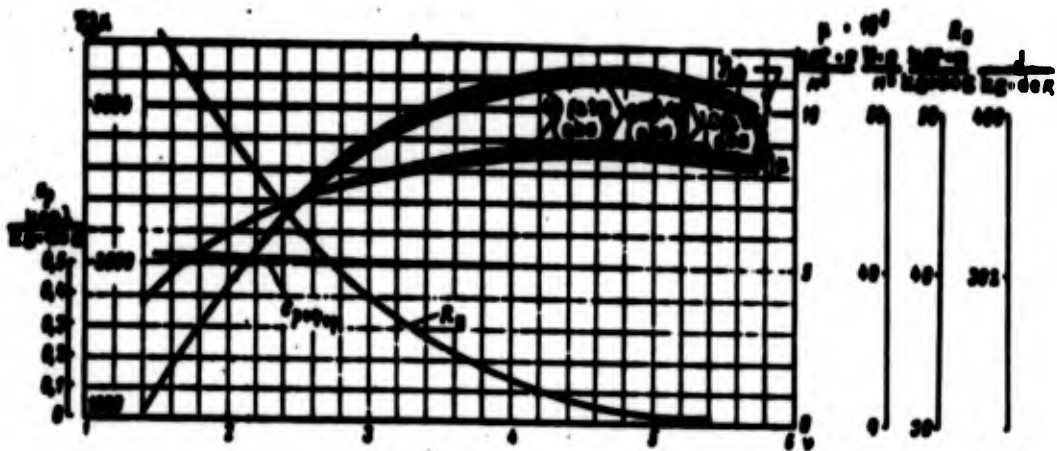


Fig. 4.15. Dependences $c_p \text{ эф.ср}$, $\bar{u}_{\text{эф}}$, $T_{\text{эф}}$, R_H and S on the relationship of components for fuel (80% HNO_3 + 20% N_2O_4) + Tonka 250.

Determination of the Value of Effective Heat Capacity $c_{p, \text{эф}}$

An examination of the afore mentioned formulas shows that contained in them are different values of $c_{p, \text{эф}}$: in formula (4.49) in determining \bar{w}_{max} it is the average in the interval of temperatures ($T_{\text{эф}} - T_{\text{эф00}}$), and in expression (4.90) and dependences $c_{p, \text{эф}}$ resulting from it is the heat capacity on the boundary of the laminar sublayer. Since the difference in $c_{p, \text{эф}}$ is small, it is convenient in carrying out calculations to use one mean value of effective heat capacity, and therefore in further calculations we will use $c_{p, \text{эф}}$, taken at the mean temperature $T_{cp} = (T_{\text{эф00}} + T_{\text{r.ct}})/2$.

Quantity $c_{p, \text{эф}}$ can be determined directly by formula (4.28). To calculate the dependence $c_{p, \text{эф}}$ on effective temperature, it is necessary to produce a thermodynamic calculation of the composition of dissociated products of combustion of the assigned fuel at different temperatures and calculate the appropriate values of effective temperature, after which, by using formula (4.28), it is possible to construct the unknown dependence (see Fig. 4.16).

Determination of the Coefficient of Dynamic Viscosity of Products of Combustion $\bar{\mu}_{\text{эф00}}$

Entering into calculation formulas is the coefficient of dynamic viscosity $\bar{\mu}_{\text{эф00}}$ of products of combustion corresponding to temperature $T_{\text{эф00}}$. It can be determined in the following way. By knowing the composition of products of combustion, we determine the coefficient of dynamic viscosity μ at an arbitrarily selected temperature T according to the well-known formula

$$\frac{1}{\mu} = \sum \frac{1}{\mu_i}$$

where μ_1 - viscosity of components of the mixture at the selected temperature [7], [25]; $g_1 = \frac{p_1 m_1}{\sum p_1 m_1}$ - weight part of the component, where m_1 - molecular weight of the component.

Usually value T is assigned within 1000-1400°K, since for higher temperatures there is no data on the viscosity of components of the mixture.

The found value μ at the assigned temperature T is calculated on the coefficient of dynamic viscosity at temperature $T_{\text{эф00}}$ according to the initial formula (4.35) when $n = 0.7$:

$$\bar{\mu}_{\text{эф00}} = \mu \left(\frac{T_{\text{эф00}}}{T} \right)^{0.7}. \quad (4.154)$$

Fig. 4.16 gives values of $\mu_{\text{эф00}}$ for fuel (80% HNO_3 + 20% N_2O_4) + + Tonka 250.

Conversion of Formula for the Calculation of Re_{00}

According to equation (4.46)

$$\text{Re}_{00} = \frac{D_{\text{эф}} \bar{\rho}_{00} \bar{u}_{\text{эф}}}{\bar{\mu}_{\text{эф00}}}.$$

The density of the stagnated flow $\bar{\rho}_{00}$ according to the equation of state (4.34)

$$\bar{\rho}_{00} = \frac{p_{00}}{R_{\text{эф}} T_{\text{эф00}}}. \quad (4.155)$$

The maximum exit velocity by formula (4.49):

$$\bar{u}_{\text{эф}} = \sqrt{\frac{2 p_{00}}{\bar{\rho}_{00}}}. \quad (4.156)$$

where $\bar{c}_{p \text{ эф.ср}}$ - mean effective heat capacity.
According to the well-known thermodynamic relationship.

$$\bar{c}_{p \text{ эф.ср}} = \frac{2 \mu R_H}{n_{H_2} - 1} \quad (4.157)$$

Substituting expressions (4.155), (4.156), and (4.157) into equation (4.46) and considering $n_{H_2} = 1.2$, we will obtain

$$Re_{00} = \frac{D_{np} \bar{p}_{00} \sqrt{\frac{2 \mu R_H}{n_{H_2} - 1} T_{000}}}{\bar{\mu}_{\text{эф.ср}} T_{000}} = \frac{1.107 D_{np} \bar{p}_{00}}{\bar{\mu}_{\text{эф.ср}} \sqrt{R_H T_{000}}} \quad (4.158)$$

Inasmuch as in the graphs and information tables the coefficient of viscosity is usually given in the form of $\mu \cdot 10^6 \text{ kgf} \cdot \text{s/m}^2$ and pressure \bar{p}_{00} - in [atm (abs.)], the calculation formula (4.157) can be thus converted:

$$Re_{00} = \frac{1.107 \cdot 10^{10} D_{np} \bar{p}_{00}}{(\bar{\mu}_{\text{эф.ср}} \cdot 10^6) \sqrt{R_H T_{000}}} \quad (4.159)$$

or in the International Unit System

$$Re_{00} = 3.46 \frac{D_{np} \bar{p}_{00}}{\bar{\mu}_{\text{эф.ср}} \sqrt{R_H T_{000}}}$$

where D_{np} in m, \bar{p}_{00} in N/m^2 , $\bar{\mu}_{\text{эф.ср}}$ in $\text{N} \cdot \text{s/m}^2$, R_H in $\text{J/kg} \cdot \text{deg}$ and T_{000} in $^{\circ}\text{K}$.

Determination of Convection Heat Flow q_K

By knowing Re_{00} , we can determine by formula (4.146) or (4.151) the change in z_T along the length of the chamber and nozzle of a ZhRD, and then by formula (4.134) - ψ_T . Since in formula (4.134) ψ_T is not expressed in evident form, then for determining ψ_T it is convenient to use the auxiliary graph $\psi_T = f(z_T)$ (Fig. 4.17).

Substituting into equation (4.47) value A_T , expressed by ψ_T and b_T from equation (4.128), and having replaced \bar{I}_{00} according to equality (4.132), we will obtain for the determination of convection heat flow:

$$q_s = q_{s0} = \frac{\bar{p}_{00} \beta (1 - \beta^2)^{\frac{n_{H_2}}{n_{H_2} - 1}} \bar{p}_{00} p_{00} F_{000} (1 - F_{r,00})}{4 \sqrt{\beta}} \quad (4.160)$$

Let us replace \bar{p}_{00} in equation (4.160) according to formula (4.155) p/\bar{p}_{00} according to formula (4.143), and instead of speed \bar{w} we will substitute its expression

$$\bar{w} = \beta \bar{w}_{00} = \beta \sqrt{2g \frac{n_{H_2}}{n_{H_2} - 1} R_0 T_{000}} \quad (4.161)$$

and then we will obtain

$$q_s = \sqrt{2g} \sqrt{\frac{n_{H_2}}{n_{H_2} - 1}} \frac{\beta (1 - \beta^2)^{\frac{n_{H_2}}{n_{H_2} - 1}} \bar{p}_{00} p_{00} F_{000} (1 - F_{r,00})}{4 \sqrt{\beta} \sqrt{R_0 T_{000}}} \quad (4.162)$$

Here q_s is expressed in kcal/m²s and \bar{p}_{00} - in kgf/m². Changing the dimension of q_s and p_{00} and considering $n_{H_2} = 1.2$, after calculation of the constant coefficient, we will obtain

$$q_s = 391 \cdot 10^3 \frac{\beta (1 - \beta^2)^{\frac{1.2}{1.2 - 1}} \bar{p}_{00} p_{00} F_{000} (1 - F_{r,00})}{4 \sqrt{\beta} \sqrt{R_0 T_{000}}} \text{ kcal/m}^2 \text{ h} \quad (4.163)$$

where \bar{p}_{00} - in [atm (abs.)]

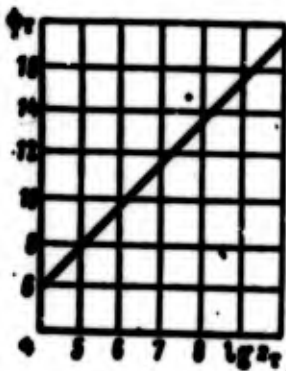


Fig. 4.17. Dependence $q_s = f(p_{00})$.

Quantity $\beta(1 - \beta^2)^6$, as was mentioned above, is the function $\bar{D} = D/D_{kp}$. For the convenience of calculations in Appendix I on Fig. I.2 an auxiliary graph of the dependence $\beta(1 - \beta^2)^6 = f(\bar{D})$ and auxiliary graphs of the dependence β and $(1 - \beta^2)^6$ on \bar{D} are given.

Calculation of the Effect of the Pr Number
and Final Calculation Formula for
Determining q

Formula (4.163) is obtained by us in the assumption $Pr = 1$. In reality for products of combustion of a ZhRD the Pr number is $Pr = 0.75-0.8$, and therefore to obtain the final calculation formula we must introduce into formula (4.163) the appropriate correction.

In accordance with formulas (4.2) and (4.47) and taking into account equality (4.132), the coefficient of heat radiation from gas to the wall α_r is equal to

$$\alpha_r = \frac{q_r}{T_{cgs} - T_{cst}} = \frac{\bar{c}_{p,gs} \bar{v} \frac{t}{A_f} \epsilon_{p,gs}}{\lambda} \quad (4.164)$$

Considering $\delta \approx \Delta$, the number Nusselt of the boundary layer will determine in the form

$$Nu = \frac{\alpha_r \delta}{\lambda} = \frac{\alpha_r \delta}{\epsilon_{p,gs} \delta^2} \frac{\epsilon_{p,gs} \delta^2}{\lambda} = \frac{\alpha_r \delta^2}{\epsilon_{p,gs} \delta^2} Pr, \quad (4.165)$$

where λ and μ - coefficients of thermal conduction and viscosity of gas at a certain average temperature along the boundary layer. Substituting value α_r (4.164) into equality (4.165) and replacing p/\bar{p}_{00} by $\bar{c}_{p,gs} T_{cgs} / \bar{c}_{p,gs} T_{cgs}$, we will obtain

$$Nu = \frac{\bar{c}_{p,gs} \bar{v} \frac{t}{A_f} Pr}{\lambda} \quad (4.166)$$

where

$$\bar{T}_{cgs} = \frac{T_{cgs}}{T_{cgs}}$$

Introducing $Re = \frac{\bar{c}_{p,gs} \bar{v} \delta}{\mu}$, we get

$$Nu = \frac{Re \cdot Pr \bar{T}_{cgs}}{A_f} \quad (4.167)$$

As is known, with motion in a pipe at low speeds (i.e., β) heat exchange is determined by a dependence of the form

$$Nu = Pr^{0.4} f(Re, T_{r,cr}).$$

In general, taking into account the effect of β on heat exchange, it is possible to write

$$Nu = Pr^{0.4} f(Re, T_{r,cr}, \beta). \quad (4.168)$$

Examining approximately the motion in the boundary layer as the motion in a pipe whose diameter of which is proportional to δ , and substituting the value Nu from the dependence (4.168) into expression (4.167), we obtain

$$\frac{A_f^2}{Pr^{0.8}} = \frac{Re T_{cp}}{f(Re, T_{r,cr}, \beta)}, \quad (4.169)$$

whence, considering that T_{cp} is proportional to $T_{r,cr}$, and Re is proportional to Re_θ , we will obtain

$$A_f^2 \approx Pr^{0.8} f_1(Re_\theta, T_{r,cr}, \beta) = (A_f^2)_{Pr=1} Pr^{0.8}. \quad (4.170)$$

Comparing expressions (4.170), (4.160), and (4.128), we obtain that, taking into account the influence of the Pr number

$$q_z \approx \frac{(q_z)_{Pr=1}}{Pr^{0.8}}. \quad (4.171)$$

Thus, a decrease in the Pr number of products of combustion leads to a certain increase in heat flow. In conditions of the operation of a ZhRD ($Pr = 0.75-0.8$) the correction for the influence of the Pr number is equal to 1.15, i.e.,

$$q_z = 1.15 (q_z)_{Pr=1}. \quad (4.172)$$

Introducing this correction into the numerical coefficient of formula (4.163), we will obtain the final calculation formula for determining the convection heat flow:

$$q_z = 480 \cdot 10^3 \frac{(1 - \beta) \bar{v}_{cp} \bar{v}_{cr} T_{cr} (1 - T_{r,cr})}{4 \sqrt{Re_\theta} Pr^{0.8}} \text{ kcal/m}^2 \text{ h} \quad (4.173)$$

or in the International Unit System:

$$q_w = 2,98 \frac{\bar{p}_{00} (1 - \epsilon) \sqrt{c_p} T_{00} (1 - T_{r,cr})}{\sqrt{R_H} T_{00}} \text{ W/m}^2,$$

where

\bar{p}_{00} in N/m^2 , c_p in $\text{J/kg}\cdot\text{deg}$ and R_H in $\text{J/kg}\cdot\text{deg}$, T_{00} in $^{\circ}\text{K}$.

If in the calculation of heat exchange in a ZhRD it is necessary to determine the coefficient of convection heat radiation from gases to the wall α_r , then with the known q_w it, in accordance with equation (4.2), will be determined by the expression

$$\alpha_r = \frac{q_w}{T_{00} - T_{r,cr}}.$$

Effect of the Boundary Layer on Heat Exchange and Calculation q_w with Internal Cooling

The aforementioned method of the calculation of convection heat transfer assumes that between the core of the flow and the wall there are no intermediate layers of gas with parameters different from parameters of the core of the flow. Such a case is fully possible when walls of the chamber of a ZhRD are protected by thermoresistant coverings applied to the internal surface of the walls so that the necessity in internal cooling drops. However, with the protection of the walls by internal cooling, between the core of the flow and the wall a protective boundary layer of gases of lower temperature will be formed.

As was shown, this boundary layer can be formed by both installing on the head special peripheral injectors and with help of feeding internal cooling through cooling belts. An analysis of the effect of the distribution of injectors on ν_{CT} and the method of calculation of the distribution of ν_{CT} along the perimeter of the chamber are given above in section 3.6.

With the supply of internal cooling through the belts, very approximately one can assume that below them along the flow there will be formed a boundary layer with the relationship of components

$$\nu_{CT} = \frac{G_{F.OXII} + G_{O.OXII}}{G_{F.OXII} + G_{O.OXII}}$$

where $G_{F.OXII}$ and $G_{O.OXII}$ - flow rate of fuel and oxidizer for internal cooling; $G_{F.CT}$ and $G_{O.CT}$ - flow rate and oxidizer through the annular the wall whose thickness is equal to the spacing between the injectors.

With a boundary layer near the wall there will be formed a boundary layer whose parameter are determined already by parameters of the given boundary layer.

If the thickness of the boundary layer δ_{np} is quite great as compared to the thickness of the boundary layer Δ , then one can assume that convection heat transfer in the wall occurs no longer from the core of the flow but from the boundary layer.

In this case the aforementioned method of calculation of convection heat flow remains acceptable under the condition that by effective stagnation temperature of the core of the flow $T_{\text{эф}00}$ is implied effective stagnation temperature of products of combustion $T_{\text{эф}00}$, which is obtained with the relationship of components in the boundary layer ν_{CT} . In conformity with these values $T_{\text{эф}00}$ and ν_{CT} , it is also necessary to take quantities R_H , c_p эф.ср and μ_{00} .

Calculations show (Fig. 4.18) that in the boundary layer temperature $T_{\text{эф}}$ is very close to the temperature of the undissociated gas T_H , determined also under the condition of constancy of full heat content; in the range of temperatures usually taking place in the boundary layer (1700-2200°K), in practice temperatures $T_{\text{эф}}$, T_H and T coincide.

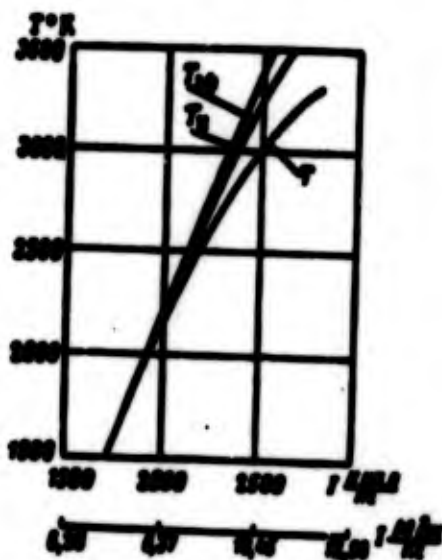


Fig. 4.18. Dependence of of T , T_H , and $T_{0\phi}$ on heat content for a fuel of oxygen +95% ethyl alcohol.

Proceeding from this, in calculations by definition of convection heat flows, with internal cooling the effective stagnation temperature of the boundary layer can be taken as equal to the temperature of products of combustion with given ν_{CT} of the boundary layer.

Depending upon the distribution of ν_{CT} along the perimeter of the chamber, distribution of temperature of the boundary layer and convection heat flow along the perimeter of the chamber will be changed accordingly.

Figure 4.19 gives graphs showing the effect of the change in ν_{CT} along the perimeter of the cross section of the chamber on the magnitude of convection heat flow q_K .

The calculation of the cooling of a ZhRD, obviously, should be conducted under the most difficult conditions for the wall. This means that in the case of a screen of cooling with a surplus of fuel ($\alpha_{CT} < \alpha_{\text{дгрв}}$) the computed value ν_{CT} should be the largest of its values along the perimeter of the chamber of the engine. With this, obviously, in places with smaller values of ν_{CT} convection heat flows and total heat removal from the surface of the chamber and nozzle of ZhRD will be less than their computed values determined

with the greatest (i.e., the worst) value of ν_{CT} . But this inaccuracy will proceed as if it is in the safety margin of cooling of the chamber.

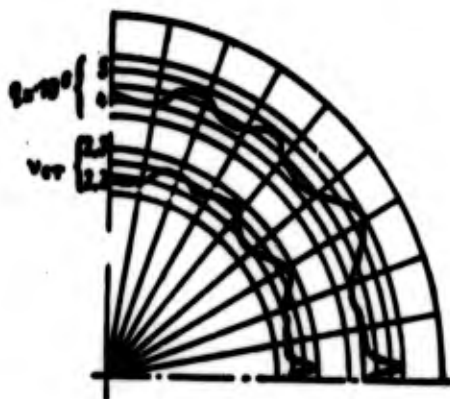


Fig. 4.19. Effect of the change in ν_{CT} along the chamber on quantity q_R .

Order of Calculation of Convection Heat Flows

Let us assume that geometric contours of the combustion chamber and nozzle are known. The fuel and relationship of components in the core of the flow or in the boundary layer are also known (in case if there is a boundary layer). Then the calculation of convection heat flow can be conducted in the following order:

1. Let us divide the chamber and nozzle lengthwise into separate sections. The nozzle part, depending upon the expansion ratio, is usually divided into 12-20 sections. The combustion chamber is divided into 3-4 sections lengthwise. If, however, the combustion chamber is of cylindrical form, then sometimes the entire part of the chamber from the effective flame front up to the beginning of the narrowing part is considered as one section. For every section we determine the average dimensionless diameter \bar{D} and average angle of inclination of the generatrix γ , which for the given section are considered constant.

2. Let us assign the distribution of temperature of the gas wall $T_{r.ct}$ along the length of the chamber and nozzle of a ZhRD. For the simplification of calculations, usually in the first approximation we consider $T_{r.ct}$ constant along the length of the chamber and nozzle.

Here it is convenient to take the value $T_{r.ct}$ as the average between the maximum allowed material of the wall by value $T_{r.ct}$ and expected value $T_{r.ct}$ in the chamber or on the section. For steel walls the mean value $T_{r.ct} = 600-800^{\circ}\text{K}$; for walls of copper or alloys with copper as a base the average $T_{r.ct} = 400-700^{\circ}\text{K}$.

By determining the values of heat flows with $T_{r.ct}$ constant along the length, we determine the final values of q_k at the assigned distribution $T_{r.ct}$ along the length of the wall with the help of the conversion formula (see section 4.7).

If in calculating q_k it appears necessary immediately to assign the distribution $T_{r.ct}$ along the length of the chamber, then values and the character of distribution $T_{r.ct}$ in the first approximation are selected according to recommendations discussed later (see section 4.12).

3. Let us determine $T_{\text{эф00}}$, $\bar{\mu}_{\text{эф00}}$, $c_p \text{ эф.ср}$, and R_H . The order of determination of the values shown is stated above. In the presence of a boundary layer values $T_{\text{эф00}}$, $\bar{\mu}_{\text{эф00}}$, $c_p \text{ эф.ср}$ and R_H are taken not for the core of the flow but for parameters of products of combustion with the relationship in the boundary layer v_{ct} . Determining $T_{\text{эф00}}$, we find the distribution along the length $T_{r.ct} = T_{r.ct} / T_{\text{эф00}}$ and necessary for further calculation auxiliary quantities b_T , b_T^2 , and $1/(c_p \text{ эф.ср}) D_{r,00}^2$.

4. According to formula (4.159)

$$Re_{00} = \frac{1.187 \cdot 10^5 D_{r,00} \bar{p}_{00}}{6.400 \cdot 10^7 \sqrt{R_H \bar{p}_{00}}}$$

For the isobaric chamber $\bar{p}_{00} = p_2$; for the high-speed combustion chamber $\bar{p}_{00} = p_{200}$.

5. Let us calculate the quantity z_T along the length of the chamber and nozzle. According to formula (4.146)

$$z_T = \frac{R_{\text{exp}}}{a_T b_T^2 D^2} \int_{z_{\text{noz}}}^{\bar{z}_1} \frac{f(\bar{D})}{\cos \gamma} d\bar{x}_1.$$

In the calculation of z_T with a cylindrical combustion chamber let us use formula (4.151):

$$z_T = \frac{R_{\text{exp}}}{a_T b_T^2 D^2} \left[\frac{0.142 T_{\text{ex}}}{D^2} + \int_{z_{\text{noz}}}^{\bar{z}_1} \frac{f(\bar{D})}{\cos \gamma} d\bar{x}_1 \right].$$

In the given formulas quantities $1/a_T b_T^2 D^2$ and $f(\bar{D})$ are found by auxiliary graphs (see Appendix I, Fig. I.1-I.4).

6. On the auxiliary graph (Fig. 4.17) let us find the change in $\psi_T = f(z_T)$ along the length of the chamber and nozzle.

7. By knowing ψ_T , according to formula (4.173) let us determine for every section

$$q_c = 450 \cdot 10^3 \frac{\beta(1-\beta^2) \bar{P}_{\text{noz}} \rho_{\text{noz}} \bar{F}_{\text{noz}} (1-\bar{F}_{\text{noz}})}{b_T^2 \sqrt{R_{\text{exp}}}}.$$

We find value $\beta(1 - \beta^2)$ by the auxiliary graph (see the appendix, Fig. 1.2).

Determination of Convection Heat Flows by Critical Equations

As we see, the calculation of convection heat flows on the basis of the solution of a system of equations of a turbulent boundary layer is a very laborious problem. Therefore, sometimes for obtaining the distribution of specific convection heat flows along the length of the chamber of the engine critical formulas are used.

To determine q_K the application of the criterial formula of Gukhman-Ilyukhin [73] is the most widespread:

$$Nu = 0,0162 Pe^{0,4} \left(\frac{T_{00}}{T_{r,CT}} \right)^{0,25}$$

After the substitution into this formula of values of criteria, we will obtain the following formula for determining the coefficient of heat transfer from gas to the wall [25]:

$$\alpha_r = 74,3 c_{p,CT} (Gr_{CT})^{0,4} \frac{G^{0,25}}{D^{0,75}} \left(\frac{T_{00}}{T_{r,CT}} \right)^{0,25} \text{ kcal/m}^2 \text{ h} \cdot \text{deg} \quad (4.174)$$

or in the International Unit System: $\alpha_r = 0,0206 c_{p,CT} (Gr_{CT})^{0,4} \frac{G^{0,25}}{D^{0,75}} \left(\frac{T_{00}}{T_{r,CT}} \right)^{0,25} \text{ W/m}^2 \text{ deg}$, where c_p c_T kcal/kg·deg (or J/kg·deg) and G μ_{CT} kgf/m·s (or μ_{CT} N·s/m²) - heat capacity and viscosity of products of combustion at the temperature of the gas wall; G - fuel consumption in kg/s; D - diameter of section in m; T_{00} and $T_{r,CT}$ - stagnation temperature of the flow of products of combustion and temperature of the gas wall in °K.

By knowing α_r , we determine the specific heat flows by formula

$$q_K = \alpha_r (T_{00} - T_{r,CT})$$

The order of calculation q_K by criterial equations and an example of the calculation are discussed in detail in work [25].

4.7. Conversion of Convection Thermal Flows

As can be seen from the preceding, the calculation of convection heat flows is a laborious problem. Therefore, considerably more convenient is the method of the conversion of data according to convection heat flows for the "base" engine well-known to us into a projected one.

To obtain formulas of the conversion, let us find the approximate connection between q_K for two geometrically similar chambers of a ZhRD, which are different in dimensions, pressure in the chamber,

form of fuel, and relationship of components and temperature of the wall. Let us examine the expression (4.146). For geometrically similar engines in similar sections (i.e., in sections where \bar{D} are identical) the complex

$$D = \frac{1}{D^{0.13}} \int_0^{\bar{z}} \frac{f(\bar{D})}{\cos \gamma} d\bar{x}_1 = \frac{\sigma_T \sigma_T^2}{Re_{00}} \quad (4.175)$$

will have an identical value.

In formula (4.175) quantity z_T is connected with ψ_T by the dependence (4.134). Approximately

$$\psi_T^2 = 15.8 z_T^{0.13}.$$

Substituting here value z_T from formula (4.175), we will obtain

$$\psi_T^2 = 15.8 \frac{D^{0.13} Re_{00}^{0.13}}{(\sigma_T^2)^{0.13}}. \quad (4.176)$$

Substituting expression (4.176) into equality (4.173) and replacing Re_{00} by formula (4.159), we will obtain the following dependence for the determination of q_K :

$$q_K = 450 \cdot 10^3 \frac{(1-\beta)^2 \bar{P}_{00}^{0.13} \sigma_{p,00} (T_{000} - T_{r,07}) (\sigma_T^2)^{0.13} (\bar{P}_{000} \cdot 10^3)^{0.13} (\sqrt{R_n \bar{T}_{000}})^{0.13}}{15.85^{0.13} \sqrt{R_n \bar{T}_{000}} (1.107 \cdot 10^3)^{0.13} D_{sp}^{0.13} \bar{P}_{00}^{0.13}}. \quad (4.177)$$

The quantity $\sigma_T^2 / \psi_T^{0.13}$ entering in formula (4.177) can be approximately represented in the form

$$\sigma_T^2 / \psi_T^{0.13} \approx T_{r,07}^{-0.13}$$

Substituting this expression into formula (4.177) and uniting the constant factors into constant k_1 , we will obtain

$$q_K = k_1 \frac{(1-\beta)^2 \bar{P}_{00}^{0.13} \sigma_{p,00} (T_{000} - T_{r,07}) (\bar{P}_{000} \cdot 10^3)^{0.13}}{D_{sp}^{0.13} \bar{P}_{00}^{0.13} (\sqrt{R_n \bar{T}_{000}})^{0.13} T_{r,07}^{-0.13}}. \quad (4.178)$$

Comparing the convection heat flows of the "base" (index I) engine and the engine geometrically similar to it, we will obtain for similar points, in which \bar{D} and, consequently, complex B are identical, the following relation:

$$\frac{q_K}{q_K^I} = \left(\frac{\bar{p}_{00}}{\bar{p}_{00}^I}\right)^{0.87} \left(\frac{D_{sp}^I}{D_{sp}}\right)^{0.13} \left(\frac{R_n^I}{R_n}\right)^{0.005} \frac{c_{p,sp} (T_{sp00} - T_{r,ct}) (\bar{p}_{00})^{0.13}}{c_{p,sp}^I (T_{sp00}^I - T_{r,ct}^I) (\bar{p}_{00}^I)^{0.13}} \times \left(\frac{T_{sp00}^I}{T_{sp00}}\right)^{0.075} \left(\frac{T_{r,ct}^I}{T_{r,ct}}\right)^{0.25} \quad (4.179)$$

Introducing in it the designation

$$S = \frac{c_{p,sp} (T_{sp00} - T_{r,ct}) \bar{p}_{00}^{0.13}}{R_n^{0.005} T_{sp00}^{0.075} T_{r,ct}^{0.25}} \quad (4.180)$$

We will obtain the formula for the conversion of heat flow:

$$\frac{q_K}{q_K^I} = \left(\frac{\bar{p}_{00}}{\bar{p}_{00}^I}\right)^{0.87} \left(\frac{D_{sp}^I}{D_{sp}}\right)^{0.13} \frac{S}{S^I} \quad (4.181)$$

Quantity S depends on the kind of fuel, the relationship of components and the temperature of the gas wall. For each fuel it is possible to calculate auxiliary graphs of the change in S depending upon $T_{r,ct}$ and the relationship of components ν . For certain fuels such graphs are shown in Fig. 4.16 and in Appendix II (Fig. II.1-II.5)

Formula (4.181) is obtained for geometrically similar engines. However, it can be used also for approximate calculations of engines geometrically not similar but similar in form. With these values of q_K and S for both engines must be taken in sections where \bar{D} are identical. It is convenient to use formula (4.181) also with the necessity of the conversion of heat flows in the same engine but at different values of $T_{r,ct}$. In this case, since \bar{p}_{00} and D_{sp} remain constant, the formula of conversion has the form

$$q_K/q_K^I = S/S^I,$$

where q_K^I and S^I - values at some rated temperature.

4.8. Determination of Radiant Heat Flows

Radiant Heat Exchange in a ZHRD

In the chamber of the engine radiation of products of combustion occurs. As is known, the radiative and absorbing ability of gases entering into the composition of products of combustion is different; the greatest radiative and absorbing ability is possessed by polyatomic gases, in the first place, water vapor H_2O and carbon dioxide CO_2 .

The radiation and absorption of gases has the following basic distinctions from the radiation and absorption of solids.

Solids radiate and absorb energy of all wavelengths from $\lambda = 0$ to $\lambda = \infty$ and gases - only in definite intervals of wavelengths (so-called bands) which are different for different gases. Such radiation or absorption is called selective.

Solids in their majority are opaque for thermal rays, and one may assume that their radiation and absorption occur in the surface layer. In gases radiation and absorption occurs in a volume. Here the radiative and absorbing ability of the gas are determined by the quantity of molecules of gas occurring in the volume. At a given temperature the quantity of molecules of gas is proportional to the partial pressure of gas p and volume of gas characterized by the length of the path of the ray l . The average length of the path of the ray l depends on the form of the volume occupied by the radiating gas. Table 4.2 gives values of l for gas bodies of different form.

According to experimental data for gases, the radiation and absorption of water vapor are proportional to T^3 and of carbon dioxide - proportional to $T^{3.5}$. Thus, for case of radiation of the volume of products of combustion in industrial furnaces the following empirical formulas for determining the radiant heat flow are obtained [5]:

$$\left. \begin{aligned} q_{H_2O} &= 3.5 p_{H_2O}^{0.75} l \left[\left(\frac{T_f}{100} \right)^4 - \left(\frac{T_{amb}}{100} \right)^4 \right]; \\ q_{CO_2} &= 3.5 \sqrt{p_{CO_2}} l \left[\left(\frac{T_f}{100} \right)^4 - \left(\frac{T_{amb}}{100} \right)^4 \right]. \end{aligned} \right\} \quad (4.182)$$

where partial pressures p_{H_2O} and p_{CO_2} are taken in kgf/cm^2 and the length of the path of the ray l in m. Here the total radiant heat flow

$$q_r = q_{H_2O} + q_{CO_2}. \quad (4.183)$$

These formulas can be used for a tentative estimate of quantity q_r in the combustion chamber and nozzle of the engine. However, at high pressures taking place in the combustion chamber of a ZhRD, the use of empirical formulas (4.182) insufficiently admissible, since they are obtained at atmospheric pressure and temperatures up to 2500°K . Therefore, a more strict method of the calculation of q_r in a combustion chamber will be given below.

Table 4.2. Length of the path of the ray for gas bodies of different form.

Form of the gas body	l/D_K
Sphere with diameter D_K ; spheric combustion chamber with diameter D_K .	0.6
Cylinder with diameter D_K , infinitely long; radiation on the lateral surface.	0.9
Cylinder with length $h = D_K$; radiation on the lateral surface.	0.6
Cylindrical combustion chamber L_K/D_K	
1	0.6
1.5	0.75
2-3	0.85
>4	0.9

For convenience the basis of calculation of the radiation of gases is the Stefan-Boltzmann law. Here the radiation and absorption of gas, referred to a unit surface of volume occupied by, are taken proportional to the fourth power of absolute temperature.

In general the radiant heat flow in the chamber of the engine from gases to the wall is determined by expression

$$q_r = \epsilon_{\text{CT.ЭФ}} \epsilon_r c_0 \left(\frac{T_r}{100} \right)^4 - \epsilon_{\text{CT.ЭФ}} A_r c_0 \left(\frac{T_{\text{CT}}}{100} \right)^4, \quad (4.184)$$

where T_r and T_{CT} - temperature of products of combustion and gas wall, respectively, in $^{\circ}\text{K}$; $\epsilon_{\text{CT.ЭФ}}$ - effective degree of blackness of the wall; ϵ_r - degree of blackness of products of combustion; $c_0 = 4.9 \text{ kcal/m}^2\text{h}\cdot\text{deg}^4$ ($5.67 \text{ W/m}^2\cdot\text{deg}^4$) - radiation factor of an ideal blackbody; A_r - absorbing ability of gas at a temperature equal to T_{CT} .

The first term of equation (4.184) determines the radiation from the gases to the wall and the second - radiation from the wall to the gases. The order of the determination of $\epsilon_{\text{CT.ЭФ}}$, ϵ_r , and A_r will be examined below.

Formula (4.184) should be used in the calculation of q_{H} in engines having high values of T_{CT} , for example, in the application of various kinds of ceramic or other heat-resistant coverings. In engines with copper or steel cooled walls not having any special heat-resistant coverings, T_{CT} is comparatively small, and therefore the role of the second term of (4.184) is also small; and, consequently, the radiation of the wall can be disregarded. In this case formula (4.184) will have the form

$$q_r = \epsilon_{\text{CT.ЭФ}} \epsilon_r c_0 \left(\frac{T_r}{100} \right)^4. \quad (4.185)$$

Since the magnitude of radiant heat flow is determined in the first place by thermodynamic temperature, along the length of the nozzle a sharp lowering of values of q_{H} always takes place. Figure 4.20 shows a typical diagram of the distribution of q_{H} along the length of the chamber of the engine. Into the entrance part of the nozzle there occurs a sharp drop in values of q_{H} , and in the supercritical part they are negligible as compared to values of $q_{\text{H.X}}$ in the combustion chamber. Therefore, in calculations of radiant heat flow it makes no sense to determine q_{H} for every section of the combustion chamber and nozzle, and by finding values of $q_{\text{H.X}}$ in the

combustion chamber, it is possible with a sufficient degree of accuracy to take the following distribution of $q_{\text{л}}$ along the length of the chamber and nozzle; near the head $q_{\text{л}} \approx 80\%$ of the value of $q_{\text{л.к}}$, on the initial section of the combustion chamber with a length of 50-100 mm $q_{\text{л}}$ increases up to the value of $q_{\text{л.к}}$ and further remains constant up to the section of the subcritical part of the nozzle, where $D = 1.2D_{\text{кр}}$. In the critical section $q_{\text{л}} = 0.5q_{\text{л.к}}$; in the supercritical part of the nozzle in the section where $D = 1.5D_{\text{кр}}$, $q_{\text{л}} = 0.1q_{\text{л.к}}$ and in the section where $D = 2.5D_{\text{кр}}$ $q_{\text{л}} = 0.02q_{\text{л.к}}$.

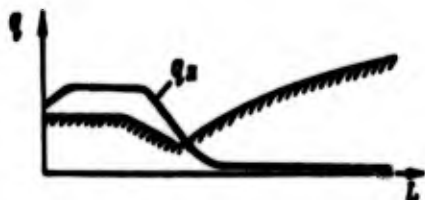


Fig. 4.20. Distribution of $q_{\text{л}}$ along the length of the engine.

Determination of $\epsilon_{\text{CT.эФ}}$, $\epsilon_{\text{Г}}$, and $A_{\text{Г}}$

Values of $\epsilon_{\text{CT.эФ}}$, $\epsilon_{\text{Г}}$, and $A_{\text{Г}}$ depend on the degree of blackness of the gases, components of products of combustion, and also on the degree of blackness of the wall of the chamber. Let us examine the method of the determination of these values given below.

Determining the degree of blackness of products of combustion $\epsilon_{\text{Г}}$. As was shown, from the number of gases comprising the products of combustion of a ZhRD, only the radiation of H_2O and CO_2 is of practical importance for the calculation of $q_{\text{л}}$. Therefore, it is assumed that the degree of blackness of products of combustion $\epsilon_{\text{Г}}$ depends on the degree of blackness of water vapors $\epsilon_{\text{H}_2\text{O}}$ and carbon dioxide ϵ_{CO_2} and is determined by expression

$$\epsilon_{\text{Г}} = \epsilon_{\text{H}_2\text{O}} + \epsilon_{\text{CO}_2} - \epsilon_{\text{H}_2\text{O}} \epsilon_{\text{CO}_2}. \quad (4.186)$$

The last term in expression (4.186) means that the radiation of the mixture of H_2O and CO_2 is somewhat less than the sum of the radiations

of these gases, since the bands of radiation and absorption for H_2O and CO_2 partially coincide. Therefore, the energy of the radiation, for example, of H_2O is partially absorbed by the carbon dioxide, and conversely.

The degree of blackness of water vapors ϵ_{H_2O} is a function of temperature, parameter (p) and pressure in the chamber. Taking into account all these factors ϵ_{H_2O} is determined by formula

$$\epsilon_{H_2O} = 1 - (1 - \epsilon_{H_2O}^0)^{1 + k_{H_2O} p_{H_2O}} \quad (4.187)$$

where $\epsilon_{H_2O}^0 = f(T, (p_{H_2O}))$ - degree of blackness of H_2O when $p_{H_2O} \rightarrow 0$ and $p_2 = 1$ [atm(abs.)]; $k_{H_2O} = f(p_{H_2O}, (p_{H_2O}))$ - coefficient taking into account the effect of pressure on ϵ_{H_2O} .

The value of $\epsilon_{H_2O}^0 = f(T, (p_{H_2O}))$ is determined from graphs of Fig. 4.21, obtained by means of extrapolation of data of Hottel and Egbert [84]. The dependency $1 + k_{H_2O} = f(p_{H_2O}, (p_{H_2O}))$ is represented on Fig. 4.22 (the effect of temperature on k_{H_2O} is insignificant and is therefore not considered).

To calculate ϵ_{H_2O} by formula (4.187), it is possible to use an auxiliary graph of the dependence $\epsilon_{H_2O} = f(\epsilon_{H_2O}^0, k_{H_2O}, p_{H_2O})$ (Fig. 4.23).

The degree of blackness of carbon dioxide $\epsilon_{CO_2} = f(T, (p_{CO_2}))$ is determined from graphs represented on Fig. 4.24 (ϵ_{CO_2} depends insignificantly on pressure).

Determining ϵ_{H_2O} and ϵ_{CO_2} , by formula (4.186) let us find the degree of blackness of products of combustions ϵ_r .

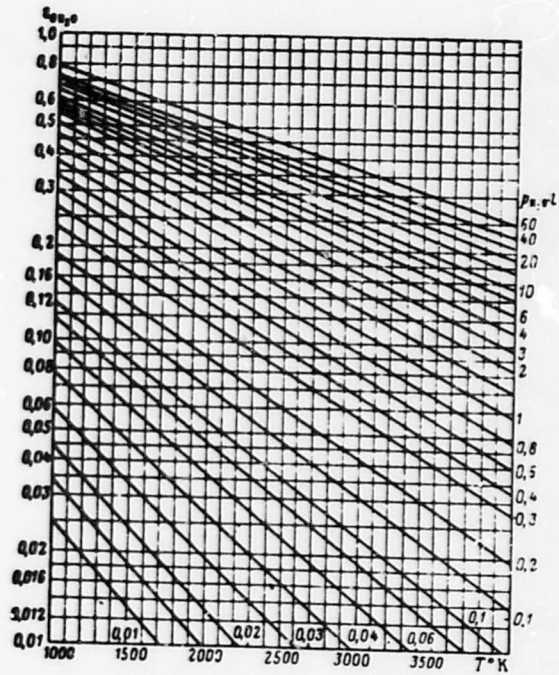


Fig. 4.21. Dependence $\epsilon_{H_2O} = f(T, (p_{H_2O}))$.

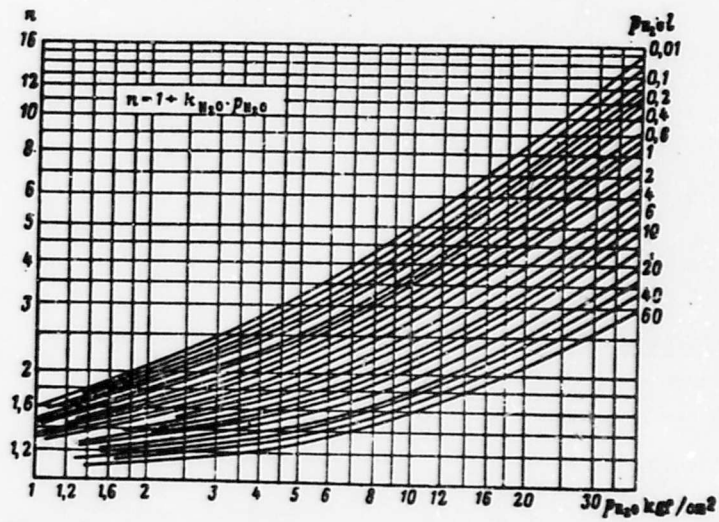


Fig. 4.22. Dependence $1 + k_{H_2O} p_{H_2O} = f(p_{H_2O}, (T))$.

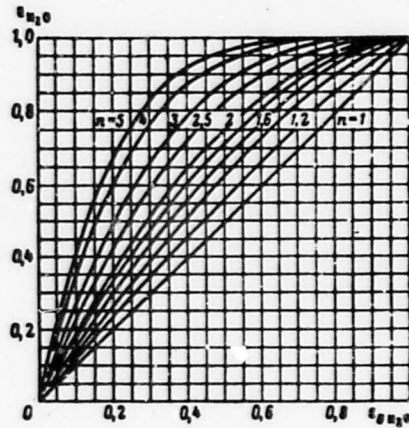


Fig. 4.23. Auxiliary graph for the calculation of $\epsilon_{H_2O} = f(\epsilon_{OH_2O}, k_{H_2O}, p_{H_2O})$.

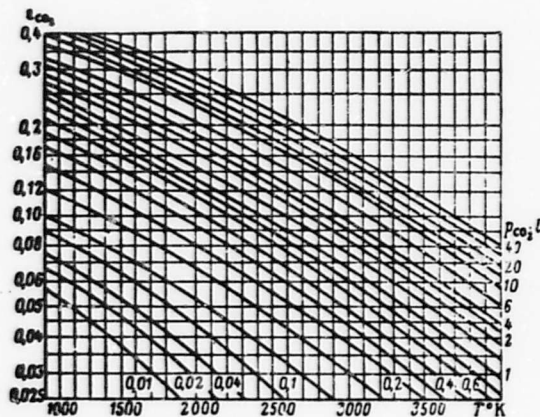


Fig. 4.24. Dependence $\epsilon_{CO_2} = f(T, (p_{CO_2}))$
 $\epsilon_{CO_2} = f(T, (p_{CO_2}))$.

Determination of effective degree of blackness of the wall

$\epsilon_{CT, \text{эф}}$. In the presence of a radiating gas the effective degree of blackness of the wall $\epsilon_{CT, \text{эф}}$ is greater than the usual value of the degree of blackness of the wall ϵ_{CT} and still depends on the degree of blackness of the gas ϵ_T :

$$\epsilon_{CT, \text{эф}} = \epsilon_{CT} [1 + (1 - \epsilon_{CT})(1 - \epsilon_T)], \quad (4.188)$$

where ϵ_T - degree of blackness of products of combustion (4.186);
 ϵ_{CT} - degree of blackness of the wall with respect to the radiation

of gases and depends on the material of the wall and state of its surface. Since frequently the walls are covered by carbon black, then in this case independently of the material of the wall, it is possible to assume $\epsilon_{CT} = 0.8$. If, however, the carbon black on the walls is absent, tentative values of ϵ_{CT} for different materials can be taken from Table 4.3.

Table 4.3. Degree of blackness ϵ_{CT} for different metals.

Materials	t_w °C	ϵ_w
Aluminum oxidised at 600°C	200-600	0.11-0.19
Polished bronze	20	0.1
Rough bronze	20-100	0.25
Tungsten	600-1000	0.1-0.16
	1000-2000	0.24-0.31
Brass oxidised at 600°C	200-600	0.01-0.20
Copper oxidised at 600°C	200-600	0.27-0.27
Molybdenum	600-1000	0.20-0.13
Oxidised nickel	200-600	0.27-0.28
Niobium	200-600	0.17
	1000-1000	0.20
Alloyed steel	200	0.25
Oxidised steel	200-600	0.3
Steel greatly oxidised	200	0.20
Ground steel	200-1110	0.25-0.61
Titanium	200-1400	0.2-0.64
Chromium nickel	120-1004	0.04-0.70
Cast iron oxidised at 600°C	200-600	0.04-0.70

Determination of the absorbing ability of gas A_g . Since the temperature of the gas is not equal to the temperature of the wall, and since the gas absorbs selectively, then in general $\epsilon_g \neq A_g$. However, with technical calculations it is possible to take $A_g = \epsilon_g'$, where ϵ_g' - degree of blackness of the gas taken at a temperature of the gas wall $T_{r,CT}$. With this ϵ_g' is determined by formula (4.186).

Determination of q_R in the Absence of a Boundary Layer

In the calculation let us consider known the dimensions and form of the chamber, the composition and temperature of products of combustion, the pressure in the chamber and the temperature of the

gas wall. Having these data, it is possible to establish the following order of calculation q_R .

1. According to Table 4.2, let us determine the length of the path of the ray l .
2. Let us determine by formula (4.186) the degree of blackness of gas in the combustion chamber ϵ_T .
3. Considering $\epsilon_{CT} = 0.8$ in the presence of carbon black on the walls or determining ϵ_{CT} according to Table 4.3 in the absence of carbon black, let us find the effective degree of blackness of the wall $\epsilon_{CT,eff}$ from formula (4.188)
4. In the case of a high value of $T_{r,CT}$ let us determine A .
5. Let us determine radiant heat flows in the combustion chamber $q_{g,x}$. With ceramic or heat-resistant coverings, which cause high $T_{r,CT}$, let us calculate $q_{g,x}$ from formula (4.184). In the absence of coverings the radiation of the wall will be disregarded, and we calculate $q_{g,x}$ from the formula (4.185).
6. Knowing $q_{g,x}$, let us determine the distribution of radiant heat flows along the length of the combustion chamber and nozzle of a ZhRD.

Determination of q_R in the Presence of a Boundary Layer

The boundary layer of products of combustion with internal cooling of walls of the chamber of a ZhRD has a lower temperature than does the core of the flow. This layer plays the role of a semitransparent screen between the core of the flow and the wall.

The energy amount radiated by the boundary layer itself is comparatively low due to its low temperature. At the same time this layer can absorb a considerable part of the radiant energy proceeding from the core of the flow to the wall since in the

composition of components of the layer, just as in the composition of products of combustion of the core, the basic radiating and absorbing gases H_2O and CO_2 predominate.

Thus, the boundary layer lowers the radiant heat flows in the wall of the chamber of the engine by 30-60%.

Let us examine the simplified method of the calculation of the influence of the boundary layer.

In usual limits of the relationship $\nu_{CT}/\nu = 0.3-0.6$, the decrease in intensity of radiation into the wall can be taken as constant, and then the expression for the approximate calculation of q_R will be

$$q_{R,CT} = 0.65 \epsilon_{CT} \epsilon \phi q_R \quad (4.189)$$

where q_R - specific radiant heat flow in the absence of internal cooling (4.185); $\epsilon_{CT} \epsilon \phi$ - effective degree of blackness of the wall; 0.65 - coefficient considering the decrease in intensity of radiation with internal cooling; ϕ - coefficient considering the decrease in intensity of radiation of the core of the flow because of a decrease in the surface of the radiating volume of products of combustion as compared to the surface of the combustion chamber absorbing the radiation:

$$\phi = \frac{D_K - 2H}{D_K} \frac{L'_K - 2H}{L'_K} \quad (4.190)$$

where D_K - diameter of the combustion chamber; H - spacing between the injectors; L'_K - length of the combustion chamber to the critical section.

Thus, having determined the magnitude of the radiant heat flow in the absence of internal cooling in the order mentioned above, we find the final value of the radiant heat flow taking into account the boundary layer $q_{R,CT}$ by formula (4.189).

4.9. Determination of Heat Transfer from the Wall to the Cooling Liquid

Heat is transmitted from the wall to the liquid coolant by means of convection. The magnitude of heat flow from the wall to the coolant is determined by expression

$$q = \alpha_{\text{ж}}(T_{\text{ж.ст}} - T_{\text{ж}}) \quad (4.191)$$

where $\alpha_{\text{ж}}$ - coefficient of heat transfer from the wall to the liquid; $T_{\text{ж.ст}}$ - temperature of the liquid wall; $T_{\text{ж}}$ - temperature of the liquid.

The coefficient of heat transfer from the wall to the liquid $\alpha_{\text{ж}}$ is most expediently determined by using the criterial equations obtained as a result of the analysis of experimental data on heat exchange in channels of a different section. In reference to heat transfer in the coolant passage of a ZhRD with high heat flows the application of the formula of M. A. Mikheyev [84] is expedient and quite reliable:

$$Nu = 0.021 Re^{0.8} Pr^{0.43} \quad (4.192)$$

In the given formula the determining temperature is the temperature of the liquid coolant $T_{\text{ж}}$, and the characteristic dimension - equivalent (hydraulic) diameter of the coolant passage $d_{\text{э}}$.

Substituting into formula (4.192) the expression of Nu, Re, and Pr, we get

$$\frac{q}{\lambda_{\text{ж}}} = 0.021 \left(\frac{\lambda_{\text{ж}} d_{\text{э}}}{\mu_{\text{ж}}} \right)^{0.8} \left(\frac{c_{\text{ж}} \rho_{\text{ж}}}{\lambda_{\text{ж}}} \right)^{0.43} \quad (4.193)$$

where $\alpha_{\text{ж}}$ - coefficient of heat transfer from the wall to the liquid in kcal/m²·s·deg (W/m²·deg); $\lambda_{\text{ж}}$ - in kcal/m·s·deg (W/m·deg); $\rho_{\text{ж}}$ - in kg/m³ (or $\mu_{\text{ж}}$ in N·s/m²); $c_{\text{ж}}$ - in kcal/kg·deg (J/kg·deg) and $\gamma_{\text{ж}}$ - in kg/m³, respectively, are thermal conduction, viscosity, heat capacity and density of the liquid coolant taken at the average temperature of it on the given section; $d_{\text{э}}$ - equivalent diameter of

the cross section of the channel in m calculated from expression

$$\alpha_x = \frac{q_x}{\Pi} \quad (4.194)$$

where f_x - area of cross section of the channel in m^2 ; Π - total (moistened) perimeter of the section independently of what part of this perimeter participates in the heat exchange; β - coefficient considering the direction of heat flow and the temperature difference ($\Delta T = T_{\text{ж.ст}} - T_{\text{ж}}$).

Experience shows that with the heating of the liquid, i.e., in the direction of the heat flow from the wall to the liquid, the intensity of the heat exchange is higher than with the reverse direction of the heat flow, i.e., with the cooling of the liquid. Furthermore, the intensity of the heat exchange also depends on the temperature difference, i.e., on the value $T_{\text{ж.ст}} - T_{\text{ж}}$. With an increase in the temperature difference the coefficient of heat transfer α_x with the heating of the liquid increases and with cooling decreases.

The dependence of heat transfer on the direction of the heat flow and the temperature difference is conditioned by the fact that the field of temperatures and viscosity in the boundary layer and thicknesses of the actual boundary layer with the heating and cooling of the liquid are different. This dependence is considered by the coefficient

$$\beta = \left(\frac{\nu_{\text{ж.ст}}}{\nu_{\text{ж}}} \right)^{0.25} = \left(\frac{\rho_{\text{ж.ст}} c_{\text{ж.ст}} \lambda_{\text{ж.ст}}}{\rho_{\text{ж}} c_{\text{ж}} \lambda_{\text{ж}}} \right)^{0.25} \quad (4.195)$$

where $\nu_{\text{ж.ст}}$, $c_{\text{ж.ст}}$, $\lambda_{\text{ж.ст}}$ - viscosity, heat capacity and thermal conduction of the liquid coolant, respectively, at the temperature of the liquid wall.

For conditions of cooling of a Zhrd quantity β is changed within limits of 1-2.5.

Let us reduce the expression (4.193) to a more convenient form for calculations

$$\alpha_x = 0.0211 \lambda_x^{0.8} \frac{\rho_x^{0.4} (\nu_x)^{0.2}}{(\mu_x)^{0.4} \rho_x} \beta. \quad (4.196)$$

According to the equation of continuity

$$\nu_x = \frac{G_{Ox}}{f_x}, \quad (4.197)$$

where G_{Ox} - coolant flow rate per second through the cooling jacket in kg/s; f_x - area of cross section of the coolant passage in m^2 .

Substituting expression (4.197) into equality (4.196) and designating

$$\lambda_x \frac{\rho_x^{0.4}}{(\mu_x)^{0.4} \rho_x} = Z, \quad (4.198)$$

we obtain

$$\alpha_x = \frac{0.0211}{\rho_x} Z \left(\frac{G_{Ox}}{f_x} \right)^{0.2} \beta \text{ kcal/m}^2 \cdot \text{s} \cdot \text{deg}.$$

Depending upon the accepted system of units α_x will be obtained in $\text{kcal/m}^2 \cdot \text{s} \cdot \text{deg}$ or $\text{W/m}^2 \cdot \text{deg}$. To determine α_x in $\text{kcal/m}^2 \cdot \text{h} \cdot \text{deg}$ frequently this formula is used in the form

$$\alpha_x = 75.6 Z \frac{1}{\rho_x} \left(\frac{G_{Ox}}{f_x} \right)^{0.2} \beta \text{ kcal/m}^2 \cdot \text{h} \cdot \text{deg}. \quad (4.199)$$

Complex Z , as we see from formula (4.198), characterizes the physical properties of the coolant and is a function of the temperature. Values of complex Z for different components are shown in graphs of Fig. 4.25, where also values of the product of complexes $Z\beta$ are given for different components obtained when $T_{x,OT} = 200^\circ\text{C}$.

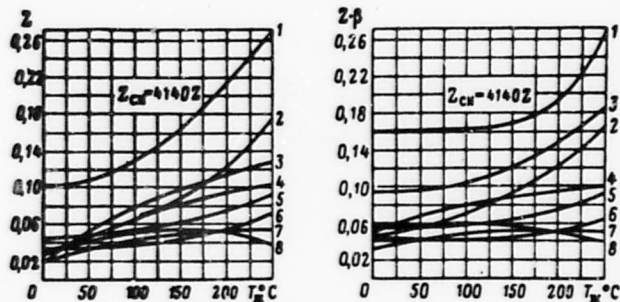


Fig. 4.25. Value of complex Z : 1 - H_2O ; 2 - 80% HNO_3 + 20% N_2O_4 ; 3 - 75% C_2H_5OH ; 4 - 96% C_2H_5OH ; 5 - 96% HNO_3 ; 6 - Tonka 250; 7 - kerosene; 8 - HDMG.

4.10. Forms of Coolant Passages of Chambers of a ZhRD

Figures 4.26 and 4.29 give different forms of coolant passages of the combustion chamber and nozzle of a ZhRD.

Slot Channel

The simplest coolant passage is in the form of a smooth slot channel (Fig. 4.26a); however, its main deficiency is in the small rigidity of the inner shell of the chamber. This can easily lead to the distortion of dimensions of the coolant passage and, as a result, to a change in the coefficient of heat transfer $\alpha_{\text{Ж}}$ and burnout of chamber.

Furthermore, with small quantities of coolant and the necessary speed along the coolant passage, the width of the slot δ_{OXJ} is obtained very small (0.8-1.5 mm) and technologically almost not feasible.

To increase the rigidity of the internal wall with slot channels and also for facilitating the manufacture of the coolant passage, between the wall and the jacket of the chamber of the engine inserts of plates or from wires are placed (Fig. 4.26b). The inserts as if calibrate the dimensions of the channel and, as a rule, serve also for the fastening of the internal and outer shells. With this a

so-called braced shell of the chamber of the engine possessing high strength properties is obtained. However, the installation of inserts is a very laborious operation, and therefore they are usually used for calibration of the duct or the fastening of shells only in separate places of the chamber of the engine.

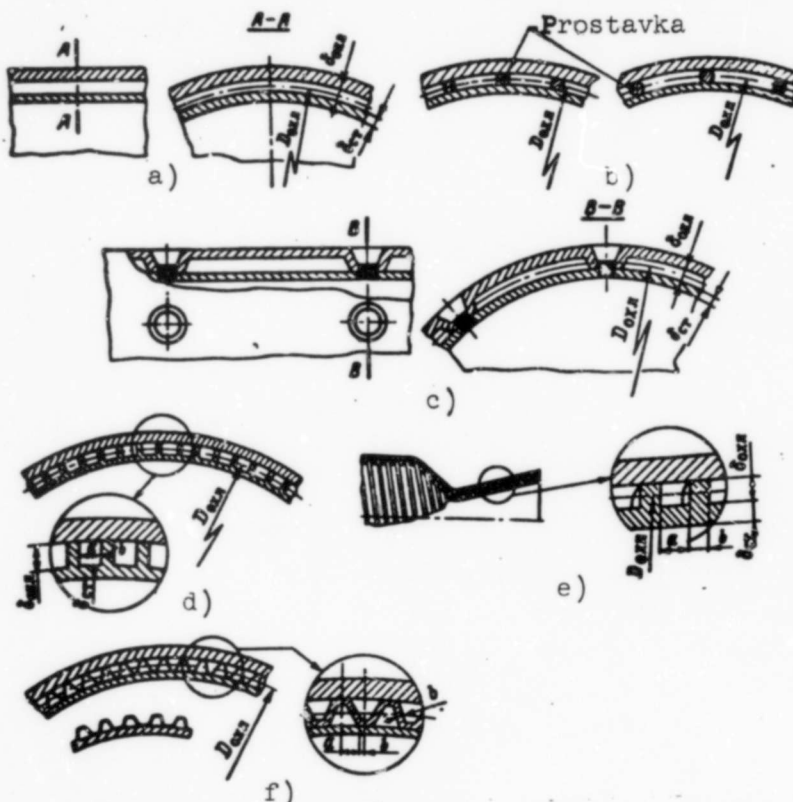


Fig. 4.26. Forms of coolant passages: a) smooth slot channel, b) slot channel with inserts, c) slot channel with forgings, d) coolant passage with ribs, e) coolant passage with screw channels, f) coolant passage with corrugations.

A variety of the slot coolant passage is a slot channel with forgings (Fig. 4.26c). Here in the external shell of the chamber of the engine there are forged (usually in checkerboard order) round or oval deepenings – forgings on which by spot welding the internal and outer shell are fastened. With such a method of fastening there is obtained a sufficiently durable and rigid shell, and the assigned dimensions of the coolant passage are ensured.

The equivalent diameter for the slot channel according to formula (4.194)

$$d_e = \frac{4F}{\pi} = \frac{4bD_{\text{int}}}{\pi D_{\text{ext}}} = 2b_{\text{ext}}$$

Here a decrease in the volume of the channels owing to forgings or separate inserts will be disregarded.

A common deficiency of chambers having a slot coolant passage is, first of all, the insufficient ability for heat removal of high heat flow appearing at high pressures in the chamber when using high-calorie fuels, etc. The reason for such a relatively low (under conditions of operation of a contemporary ZhRD) effectiveness of heat removal in slot ducts is the insufficiently developed surface of heat exchange on the part of the coolant and the difficulty in the fulfillment of the internal wall with widely spaced fastenings thinner than 1.5-2 mm, which also limits the heat removal. Furthermore, the rigidity of the chamber with slot coolant passage even with separate fastenings is insufficient.

Coolant Passages with Ribbing

The best heat removal and also the possibility of decreasing the thickness of the inner shell of the chamber is provided by ribbing of the inner shell. Furthermore, ribs usually serve also for the fastening of inner and outer shells. The obtained braced shell with frequent connections possesses great rigidity and strength.

Examples of such a construction are coolant passages with longitudinal or screw ribs and with corrugations shown on Fig. 4.26d, e, and f. In the case of providing the full contact of the insert with the shell, the effect of ribbing can take place and with the installation of inserts (see Fig. 4.26b), although the effect of it is negligible. An increase in heat transfer from the wall to the coolant owing to the effect of ribbing also takes place and in tubular chambers.

Figure 4.26d gives a diagram of a coolant passage with longitudinal ribs. The longitudinal or screw ribs with a thickness of 1-1.5 mm are usually obtained by means of milling of the channels along the generatrix of the chamber of the engine or along the screw curve. In the ribbed coolant passage the heat exchange is improved not only because of the increase in cooling surface, but also owing to the possibility of the fulfillment of a thinner inner shell with δ_{CT} of the order of 1 mm.

The equivalent diameter for a channel with longitudinal ribs is equal to

$$d_e = \frac{4F_n}{\Pi} = \frac{4st_{rib}}{2(s + t_{rib})} = \frac{2st_{rib}}{s + t_{rib}}$$

On Fig. 4.26e a coolant passage with screw channels is shown. The screw channel can be both single-filar and multifilar.

The main advantage of the screw coolant passage consists in the increase in motion rate of the coolant along the passage, which permits increasing heat removal. Thus on the ZhRD "Walter"⁴ the motion of the coolant along the helix (twist) was provided by a screw channel on the external shell. Obviously, in this case an increase in heat removal occurred only because of the increase in speed of the coolant and not owing to the effect of ribbing.

Figure 4.27 shows a cross section of a nozzle of a chamber of the engine ORM-45 where a twist of the fluid was created by a screw thread carried out along the inner shell on the part of the depth of the coolant passage.

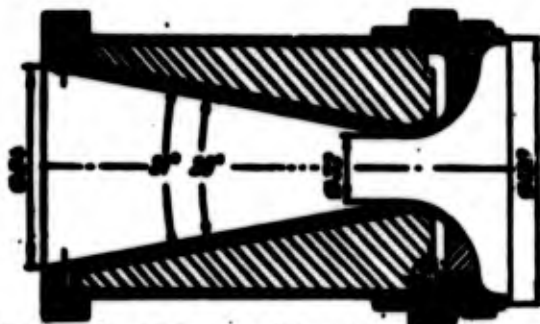


Fig. 4.27. Coolant passage of the nozzle part of the engine ORM-45.

With the noted merits of screw channels, the deficiencies of such ducts are the great laboriousness of their making and the considerable increase in flow friction of the duct.

Therefore, usually screw channels are made not along the entire length of the combustion chamber and nozzle but only on those sections where it is necessary to provide the greatest heat removal, most frequently in the throat. With this to decrease the laboriousness, the screw channel is frequently made simply by means of installing of spiraling various kinds of inserts or wire.

The equivalent diameter for the coolant passage with screw channels will obviously be determined just as for the straight channel:

$$d_e = \frac{4F}{\pi} = \frac{2s^2 \sin \alpha}{s + t_{\text{max}}}$$

Figure 4.26f shows a coolant passage in which the channels are formed by an insert of thin band [12]. For simplicity we will call such a duct a coolant passage with corrugations. In the obtained shell corrugations simultaneously play the role of ribs, which increase heat removal, and fastenings, which increase the rigidity and strength of walls of the chamber. With a quite high frequency of corrugations, it is possible to use a thin inner shell, which also improves the heat exchange.

The equivalent diameter d_e for a duct with corrugations is calculated by formula (4.194) in reference to the geometry of the obtained channel.

Approximately d_e for the coolant passage with corrugations (Fig. 4.28) can be determined by expression

$$d_e = \frac{2a_{cp}^2 \sin \alpha}{a_{cp} + t_{\text{max}}} \quad (4.200)$$

where a_{cp} — distance between the ribs along the center line of the "useful cross section" where

$$a_{cp} = a'_{cp} + 2\Delta a_{cp} = \frac{\pi D_{out} - b z_p}{z_p} + 2 \frac{b}{z_p} \tan \gamma = \frac{\pi D_{out} - b z_p}{z_p} + b \frac{\pi D_{out}}{z_p^2 \cos \gamma} \quad (4.201)$$

where z_p - number of ribs of corrugations.

In practice, with a sufficient degree of accuracy, it is possible to consider $a_{cp} \sim a'_{cp}$.

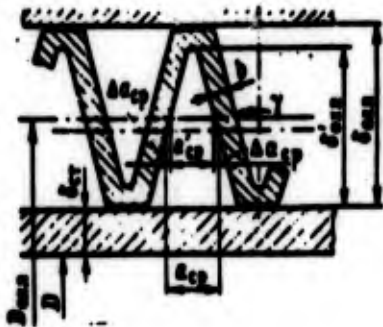


Fig. 4.28. Determination of d_3 for a coolant passage with corrugations.

Tubular Chambers

In recent years there has been widespread use of the so-called tubular chambers made of a set of tubes soldered to each other (Fig. 4.29). The tubes can be of round, oval or rectangular section and are located both along the generatrix of the chamber of the engine and also along the spiral. Tubular chambers with spiral winding (Fig. 4.30) have not received widespread use, since along with complexity of their manufacture the flow friction of the coolant passage of such a chamber is very high. Furthermore, with the spiral winding of pipes it is difficult to provide a smooth contour of the inner surface along the longitudinal generatrix of the chamber and nozzle. Therefore, for tubular chambers the longitudinal location of tubes is characteristic.

The most widespread form of the section of tubes is the rectangular or trapezoidal form with rounded angles. There are used both copper or aluminum tubes and tubes made from heat-resistant alloys. The thickness of the tubes, depending upon parameters of operation of a ZhrD and the material, lies within 0.3-1.0 mm. Usually 250-350 tubes are placed along the perimeter of the combustion chamber. To increase the strength of the tubular chamber along its length are

placed several force rings - bands, and on the most stressed sections of the chamber over the tubes frequently there is put a solid lip.

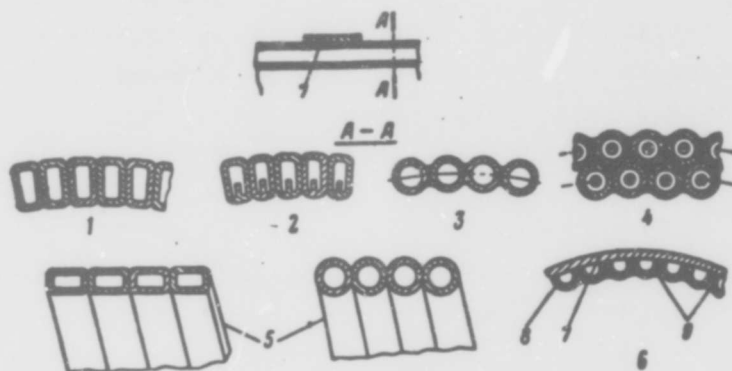


Fig. 4.29. Diagram of tubular chambers; 1 - rectangular tubes; 2 - tubes with ribbing; 3 - round tubes; 4 - two-row distribution of tubes; 5 - spiral tubes; 6 - duct of U-chaped profiles; 7 - force lips or winding; 8 - U-shaped profiles; 9 - places of soldering.

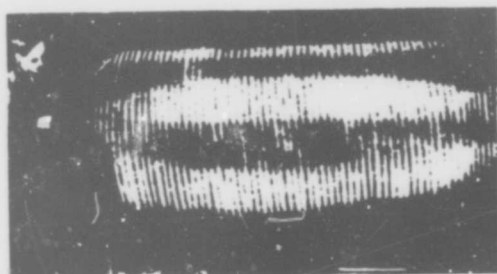


Fig. 4.30. Chamber of an engine from spirally wound tubes;

To increase the strength of the shell of the chamber and nozzle, also the distribution of tubes in two rows, one above the other is possible (see Fig. 4.29a).

The basic advantage of tubular chambers, as compared to other designs of the coolant passage, is the gain in weight. Furthermore, tubes maintain high pressures in the duct and provide good heat removal by the coolant both owing to the small thickness of the walls

and due to the effect of ribbing.

The difficulty of the making of chambers with the longitudinal distribution of tubes consists in the fact that along the length of the generatrix the tube should have a variable section (Fig. 4.31). The profile of tubes for chambers having a nozzle with a high expansion ratio is changed especially considerably.

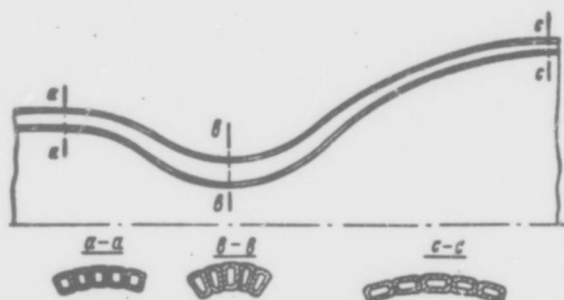


Fig. 4.31. Change in section of tubes along the length of the generatrix.

The installation of a different quantity of tubes along the length of the chamber of the engine, instead of a change in the profile (Fig. 4.32), is very difficult constructively and is used comparatively rarely.



Fig. 4.32. Tubular chamber with a variable number of tubes.

A variety of tubular chambers is chambers comprised of U-shaped profiles (see Fig. 4.29b) over which passes a cooling medium. The profiles are gathered in the form of a chamber, are soldered along the generatrix and are covered on the outside by a force winding.

Feed of the Coolant to the Coolant Passage

The uniformity of feed of the coolant along the perimeter of the coolant passage is very important, since otherwise there can appear the danger of burnout on sections where the flow rate of the coolant will be less nominal.

To ensure the uniformity of the coolant feed, at the entrance into the coolant passage combined collectors are installed (Fig. 4.33).

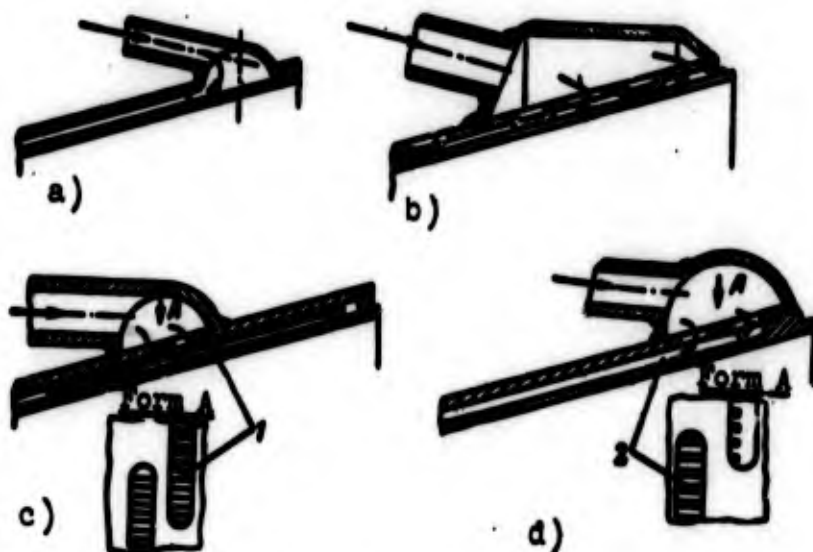


Fig. 4.33. Diagrams of coolant feed:
a, b) slot coolant passage; c, d) ribbed
coolant passage; 1 - corrugations; 2 - ribs.

In the engine of the A-4 rocket (see Fig. 5.4) the uniformity of the coolant feed is ensured by feeding it to a collector on six equally located tubes, which complicated and rendered heavier the construction of the whole installation. Subsequent experience showed that one to two feeder tubes is sufficient.

The selection of the place of location and form of the section of the collector is determined by design-technological considerations.

The entrance collector is usually set in the nozzle part of the engine. Thus, on Fig. 4.33a, b, and c the collector is set directly near the section of the nozzle. If cooling conditions are allowed, then for a decrease in the overall dimensions of the cross section of the engine and weight of the construction the collector is displaced in the direction of the throat.

The coolant proceeds from the collector into the passage either through slot (Fig. 4.33a) or through holes made in the external shell (Fig. 4.33b). In passages with longitudinal ribs or corrugations the location and dimensions of the holes should provide the entering of the coolant into all channels of the passage (Fig. 4.33c and d).

In tubular chambers it is frequently expedient to locate the entrance collector directly near the head of the chamber (see Fig. 5.3). Here the coolant from the collector enters into every second tube, passes through it up to the end of the cooled part of the nozzle and, returning back through a tube located in series, proceeds directly into the head. Such a method of separation of the coolant is frequently called "two-way" or "in two movements." With such separation of the coolant hydraulic losses in the coolant passage are somewhat increased, but then there is no need in a well-developed section of the collector in the nozzle part and the length the main supply lines of the cooling component decreases, which leads to a lowering of the weight.

With the location of the tubes shown on Fig. 4.32, the motion of the coolant through every other one of the tubes is used only at the entrance part of the nozzle. In the most thermally stressed, critical section the coolant moves through all tubes in a direction toward the head of the chamber. Such a separation is sometimes called "sesquipass." With the distribution of the tubes in two rows (see Fig. 4.29, 4), obviously, it is convenient to use the second row of tubes for a reverse motion of the coolant so that the

component moves into the inner row of tubes through all the tubes in one direction.

4.11. Calculation of Heat Transfer in a Ribbed Coolant Passage

Coefficient of Ribbing

In the presence of longitudinal ribs, corrugations or soldered inserts the heat transfer from the wall of the chamber of the engine to the liquid coolant increases because of the effect of ribbing of the surface. It is convenient to consider such a change in heat transfer as the introduction of concepts of the coefficient of the effectiveness of ribbing η_p and effective coefficient of heat transfer taking into account ribbing $\alpha_{\kappa.p}$, which are connected by the dependence

$$\alpha_{\kappa.p} = \eta_p \alpha_{\kappa} \quad (4.202)$$

By knowing η_p and $\alpha_{\kappa.p}$ for the assigned ribbed coolant passage, further calculations of cooling will be made as for the usual smooth surface, using the coefficient $\alpha_{\kappa.p}$ instead of α_{κ} .

Let us find the expressions for determining the coefficient of effective ribbing η_p [75]. The calculation diagram will be presented in the form of a flat wall with ribs (Fig. 4.34). Let us assume also the following: the coefficient of heat transfer α_{κ} is constant all along the perimeter of the coolant passage; the temperature of the coolant $T_{\kappa.0T}$ along the section of the passage is identical; the temperature of the rib at the base; thermal conduction of the ribbed wall λ does not depend on the temperature and is equal to some mean value.

Every rib will be examined as a rod of finite length $L = \delta_{0\kappa\lambda}$; heat transfer from the ends will be disregarded. Then, inasmuch as the temperature at the base of the rod is equal to $T_{\kappa.0T}$, the temperature distribution over the pitch of the rib and heat flow through the base of the rib Q will be determined by these expressions [84]:

$$t = t_0 \frac{\text{ch}[m \cdot (t_{\text{max}} - x)]}{\text{ch} m \cdot t_{\text{max}}};$$

$$Q_0 = -\lambda f m t_0 \text{th} m \cdot t_{\text{max}}.$$

Here $t_0 = T_{\text{max}} - T_m$; $t = T_p - T_m$; T_p - temperature of the surface of the rib, which is variable along its length; x - distance from the base of the rib; λ - thermal conduction of the material of the ribbed wall;

$$m = \sqrt{\frac{\alpha_{\text{ж.п}} \Pi}{\lambda}};$$

f and Π - area and perimeter of the cross section of the rib.

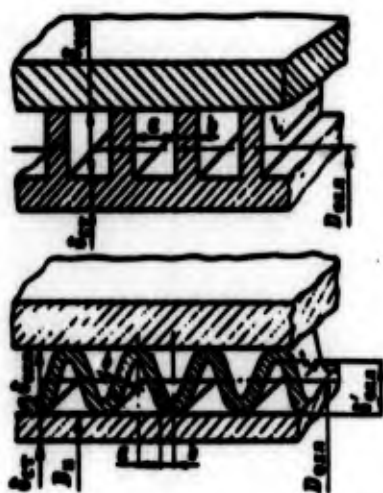


Fig. 4.34. Calculation diagram for determining η_p and $\alpha_{\text{ж.п}}$.

In coolant passages of a ZhRD the thickness of rib b is considerably less than its length l . Therefore,

$$\frac{\Pi}{f} = \frac{2l + 2b}{l \cdot b} \approx \frac{2}{b},$$

whence

$$m = \sqrt{\frac{2\alpha_{\text{ж.п}}}{\lambda}}.$$

The quantity of heat Q returned to the liquid from the ribbed wall on the section equal to the spacing of the ribbing ($a + b$) is determined by expression

$$Q = \alpha_{\text{ж.п}} a (T_{\text{max}} - T_m) + \lambda M m (T_{\text{max}} - T_m) \text{th} m \cdot t_{\text{max}} = \alpha_{\text{ж.п}} (T_{\text{max}} - T_m) \left(a + \sqrt{\frac{2\lambda}{\alpha_{\text{ж.п}}}} \text{th} \sqrt{\frac{2\alpha_{\text{ж.п}}}{\lambda}} \cdot t_{\text{max}} \right),$$

where a - transit between the ribs.

Since the surface area of the gas wall

$$F_{r,cr} = (a+b)l,$$

the specific heat flow q_{Σ} , referred to this area will be

$$q_{\Sigma} = \frac{Q}{F_{r,cr}} = \alpha_m (T_{m,cr} - T_m) \left(\frac{a}{a+b} + \frac{2r_{out}}{a+b} \frac{\operatorname{th} \sqrt{\frac{2\alpha_m b}{\lambda} \frac{r_{out}}{b}}}{\sqrt{\frac{2\alpha_m b}{\lambda} \frac{r_{out}}{b}}} \right). \quad (4.203)$$

Designating

$$\sqrt{\frac{2\alpha_m b}{\lambda} \frac{r_{out}}{b}} = \xi \quad (4.204)$$

and

$$\frac{\operatorname{th} \xi}{\xi} = f(\xi), \quad (4.205)$$

expression (4.203) can be copied in the form

$$q_{\Sigma} = \alpha_m \eta_p (T_{m,cr} - T_m), \quad (4.206)$$

where

$$\eta_p = \frac{a}{a+b} + \frac{2r_{out}}{a+b} f(\xi). \quad (4.207)$$

Expression (4.207) is the formula for determining the coefficient of effectiveness of ribbing. For the convenience of calculation Fig. 4.35 gives the dependence of $f(\xi)$ on ξ .⁵

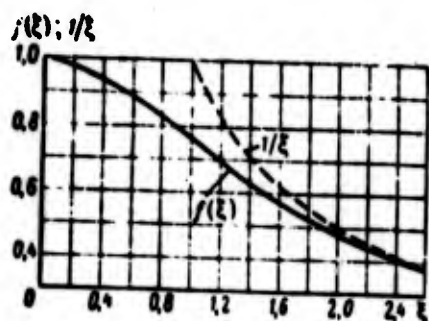


Fig. 4.35. Graph of the dependence of $f(\xi)$ on ξ .

Since according to expression (4.202) $\alpha_{\kappa}\eta_p = \alpha_{\kappa.p}$, formula (4.206) can be rewritten in the form

$$q_2 = \alpha_{\kappa} (T_{\text{max}} - T_2) \quad (4.208)$$

i.e., we obtain formula for the determination of q_2 , which is similar to formula (4.191) with the difference being that instead of α_{κ} enters effective coefficient of heat transfer taking into account the ribbing $\alpha_{\kappa.p}$.

Effectiveness and Optimum Geometry of Ribbing

By analyzing expression (4.207), taking into account equality (4.204), we see that the effectiveness of ribbing at the fixed value α_{κ} depends on the thermal conduction of the material λ and geometry of the ribbing.

With an increase in λ ξ decreases, and $f(\xi)$ and η_p increase. The reason for the growth in η_p is the fact that with an increase in λ thermal resistance of the rib becomes small as compared to the thermal resistance of the heat transfer to the coolant, and the temperature of lateral surfaces of the rib is compared with the temperature of the base, owing to which the heat exchange is improved. In the limit when $\xi \rightarrow 0$, $f(\xi) \rightarrow 1$ and according to equation (4.207) η_p will be equal to the ratio of the area of the ribbed surface to the smooth surface, i.e., the geometric coefficient of ribbing η_F instead of η_p always gives oversized values of $\alpha_{\kappa.p}$, and only in the case of very high thermal conduction of the material will the values of η_F and η_p be close.

For clarity Fig. 4.36 gives calculation graphs of the change in temperature of ribbed steel and bronze walls taking into account η_p , taking into account only η_F and neglecting the ribbing. Since for a steel wall the thermal conduction λ is comparatively low, then the value of ξ is great (usually more than two) and η_p noticeably differs from η_F . Therefore, the calculation taking into account only η_F leads to decreased values of the temperature of the wall. For a bronze wall for which ξ is small and values η_p and η_F are

similar, results of calculations with η_p or with η_F are also similar. From the graphs it also is clear that the calculation of cooling without taking into account ribbing gives in both cases sharply different results; thus, with ribbing calculation must always be conducted by taking ribbing into account.

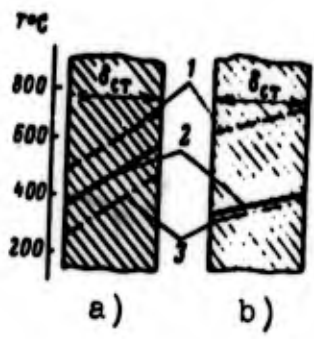


Fig. 4.36. Calculation changes in the temperature of the wall with calculation taking into account and neglecting ribbing: 1 - neglecting ribbing; 2 - taking into account η_p ; 3 - taking into account only η_F .

The geometry of ribbing (i.e., the relationship between a , b , and δ_{OXH}) also affects its effectiveness.⁶ With an unsuccessfully selected geometry of ribbing, instead of the intensification of heat transfer its impairment can be obtained. Actually, at value $b > 2\delta_{OXH}f(\xi)$ in equation (4.207) $\eta_p < 1$, i.e., heat transfer from the ribbed surface will be worse than that from a smooth surface.

The boundary of the rational application of ribbing is determined by the relation

$$2\delta_{OXH}f(\xi) = b,$$

or, taking into account equation (4.205),

$$\frac{\text{arc th } m'}{m'} = \frac{2\delta_{OXH}}{b}, \tag{4.209}$$

where

$$m' = \sqrt{\frac{a_m b}{2\lambda}}. \tag{4.210}$$

On Fig. 4.37 by formula (4.209) there is plotted the region of the rational application of ribbing (shaded) depending upon m' and δ_{OXH}/b , from which it is clear that for quite high ribs ($\delta_{OXH}/b > 2$)

there will be $\eta_p > 1$ under the condition

$$(\eta')^2 = \frac{a+b}{2a} < 1. \quad (4.211)$$

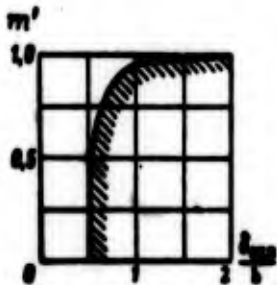


Fig. 4.37. Region of the rational application of ribbing.

Let us find the dependence between the width of channel a , thickness of rib b and coefficient of ribbing η_p at a fixed depth of the rib δ_{OXH} . To simplify the analysis, at first let us examine the particular case $\xi \geq 2$. Such values of ξ are characteristic with steel corrugations of ribs ($\lambda = 20-50$ kcal/m h·deg) (23.3-58 W/m·deg). Here, as one can see from the graphs of Fig. 4.35, with a sufficient degree of accuracy it is possible to consider $f(\xi) = 1/\xi$. Then, substituting $f(\xi) = 1/\xi$ into equation (4.207) and introducing m' according to expression (4.210), we will obtain

$$\eta_p = \frac{a + \frac{b}{m'}}{a + b}. \quad (4.212)$$

Let us introduce designation $z = \frac{b}{a}$; $x = \sqrt{\frac{2a\delta}{\lambda}}$. Then expression (4.212) can be written in the form

$$\eta_p = \frac{1 + z \frac{\sqrt{z}}{x}}{1 + z}. \quad (4.213)$$

From equality (4.213) it is clear that when $z = 4/x^2$ there will be $\eta_p = 1$. With an increase in z , i.e., with an increase in the relative thickness of the rib b/a , we obtain $\eta_p < 1$, i.e., the ribbing becomes irrational. With a decrease in z value $\eta_p > 1$, but when $z = 0$ again we obtain $\eta_p = 1$ (which corresponds to a smooth wall without ribbing). Consequently, in the interval

$$0 < z < \frac{4}{x^2}$$

there is a maximum η_p (Fig. 4.38). Let us find its optimum value from the condition $\frac{d\eta_p}{dz} = 0$.

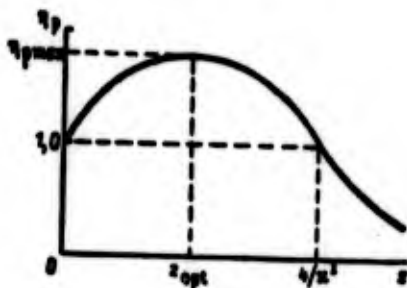


Fig. 4.38. Character of the dependence η_p on z .

Taking the derivative, we will obtain

$$z + z\sqrt{z} - 1 = 0,$$

whence

$$z_{opt} = 1 - 0.5z(\sqrt{z^2 + 4} - z). \quad (4.214)$$

From formula (4.214) it is clear that always $z_{opt} \leq 1$, i.e., always $b \leq a$.

The width of channel a is usually determined by technological considerations and the magnitude of permissible flow friction. According to equation (4.212), with the observance of condition (4.211) the effectiveness of ribbing will be higher the less a is.

Substituting the value z_{opt} from formula (4.214) into expression (4.213), we will obtain the maximum value of the coefficient of the effectiveness ribbing for the particular case ($\xi \geq 2$):

$$\eta_{p,max} = \frac{\frac{2}{z}}{\sqrt{4+z^2}-z} = \frac{1}{1-z_{opt}}. \quad (4.215)$$

In general the effectiveness of ribbing is also affected by the depth of the rib δ_{0xH} . Let us introduce designation $\bar{\delta} = \delta_{0xH}/a$. Then, considering that $z = b/a$, formula (4.207) can be thus convert:

$$\eta_p = \frac{1 + 2 \frac{\sqrt{x}}{x} \operatorname{th} \frac{\bar{b}_x}{\sqrt{x}}}{1 + x} \quad (4.216)$$

Equating derivative $d\eta_p/dz$ to zero we will obtain the following equation for the determination of z_{opt} :

$$\operatorname{th}^2 \frac{\bar{b}_x}{\sqrt{x}} + \frac{1-x}{1+x} \frac{\sqrt{x}}{\bar{b}_x} \operatorname{th} \frac{\bar{b}_x}{\sqrt{x}} = 1 + \frac{x/\bar{\delta}}{1+x} \quad (4.217)$$

Equation (4.217) was solved on a computer; the obtained values of z_{opt} were then put into equality (4.216), and the value $\eta_{p \max}$ was determined. Final results of the calculations are given on Fig. 4.39 [75]. For convenience the reverse quantity $\eta_{p \max}$ is plotted along the axis of the ordinates.

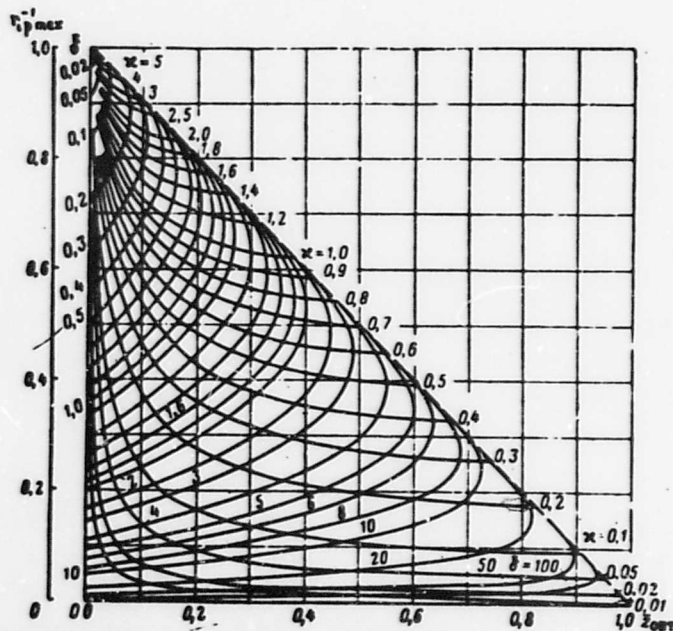


Fig. 4.39. Determination of $\eta_{p \text{ opt}}$.

The order of determining the geometry of ribbing will be examined with an example.

Example of the calculation of ribbing

Determine the number of ribs n , thickness of the rib b and effective coefficient of heat transfer $\alpha_{x,p}$ for the cylindrical part of the combustion chamber.

Given: diameter of the combustion chamber, including the thickness of the internal wall $D_x = 250$ mm; width of the channel $a = 2$ mm; depth of the rib $\delta_{0x1} = 2.8$ mm; thermal conduction of the ribbed wall $\lambda = 250$ kcal/m h·deg (291 W/m·deg); the coefficient of heat transfer from the wall to the liquid for a smooth slot channel $\alpha_x^1 = 1.2 \cdot 10^4$ kcal/m²h·deg ($1.395 \cdot 10^4$ W/m²·deg).

Solution. As yet the number of ribs is still not determined, and in the first approximation for calculation we take α_x equal to the value obtained for a smooth slot (α_x^1).

We determine:

$$\bar{\tau} = \frac{2.8}{2} = 1.4$$

$$\delta^1 = \sqrt{\frac{2.8 \cdot 2}{1.395 \cdot 10^4}} = \sqrt{\frac{2.19 \cdot 10^{-4}}{1.395}} = 0.039$$

From Fig. 4.39 when $\bar{\tau} = 1.4$ and $\delta^1 = 0.438$, we find

$$\delta_p = \left(\frac{\delta^1}{0.438}\right)^2 = 0.82$$

whence $\delta_p = 0.82 \cdot 2 = 1.64$ mm

Such thickness of rib corresponds to the number of ribs

$$n = \frac{250}{1.64} = 152$$

The coefficient of heat transfer α_x for a ribbed channel, obviously, will differ from α_x^0 of a smooth channel, since in connection with the obstruction of the passage by ribs the speed of the coolant w_{0xx} will increase.

In accordance with equation (4.196) it is approximately possible to assume

$$\alpha_x = \alpha_x^0 \cdot \eta$$

Let us determine the speed of the coolant through the passage blocked by the ribs $w_{0xx,p}$:

$$w_{0xx,p} = \frac{F_{0xx}}{F_{0xx,0}} w_{0xx,0} = \frac{\pi D_0^2 L_{0xx}}{\pi D_0^2 L_{0xx} - \pi b^2 L_{0xx}} w_{0xx,0} = \frac{2,14 \cdot 10^{-3} \cdot 2,0}{2,14 \cdot 10^{-3} \cdot 2,0 - 2,17 \cdot 10^{-6} \cdot 2,0} w_{0xx,0} = 1,24 w_{0xx,0}$$

whence

$$\alpha_x = \alpha_x^0 \left(\frac{w_{0xx,p}}{w_{0xx,0}} \right)^{0,8} = 1,2 \cdot 10^4 \cdot 1,24^{0,8} = 1,4 \cdot 10^4 \text{ kcal/m}^2 \text{ h} \cdot \text{deg}$$

$$\eta = \sqrt{\frac{2\alpha_x \cdot b}{\alpha_x^0}} = \sqrt{\frac{2 \cdot 1,4 \cdot 10^4 \cdot 2 \cdot 10^{-3}}{2 \cdot 10^4}} = 0,477$$

From Fig. 4.39 when $\bar{b} = 1,4$ and $\eta^{II} = 0,477$

$$\alpha_{xx}^0 = \left(\frac{\alpha_x}{\eta} \right)^{1,1} = 0,22$$

whence

$$\alpha_{xx}^0 = 0,22 = 0,21 \text{ kcal/m}^2 \text{ h} \cdot \text{deg}$$

$$\frac{1}{\alpha_{xx}^0} = 4,76 \cdot \alpha_{xx}^0 = 2,43$$

The number of ribs

$$n = \frac{2L_0}{b + \delta} = \frac{2 \cdot 14 \cdot 10^{-3}}{2 + 0,21} = 22$$

The number of ribs differs little from the number of ribs obtained in the first approximation. Therefore, we finally take $b = 0,5 \text{ mm}$ and $\eta_{p, \max} = 2,43$. The effective coefficient of heat radiation

from the wall to the coolant taking into account the ribbing is equal to

$$\alpha_{n, p} = \alpha_{n, r, \text{max}} = 1.42 \cdot 10^4 \cdot 2.43 = 3.55 \cdot 10^4 \text{ kcal/m}^2 \cdot \text{h} \cdot \text{deg}$$

$$\left(4.12 \cdot 10^4 \frac{\text{W}}{\text{m}^2 \cdot \text{deg}} \right)$$

Heat Transfer in Tubular Chambers

The expressions obtained above for the calculation of heat transfer from the ribbed surface can be used with approximate calculations of heat exchange in tubular chambers. Here the calculation diagram of the heat exchange in the tubular chamber can be represented in the form shown on Fig. 4.40

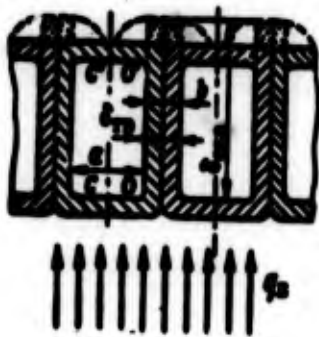


Fig. 4.40. Calculation diagram for the determination of $\alpha_{n, r, p}$.

Let us consider that the heat supply occurs only along the internal surface.

The quantity of heat tapped by the external frame or covering will be disregarded, and we will consider it equal to zero. Thus, all the proceeding heat is removed to the coolant through the surface $COO'C$. Having developed the upper wall of the tube (section $O'C$), we will obtain a conditional diagram for the calculation of heat exchange in the tubular chamber. With this the depth of the rib δ_{ox} is equal to the length of the section $OO'C$. The thickness of the rib is equal to doubled thickness of the tube $b = 2\delta_{\text{rp}}$.

The width of the channel a is considered equal to the internal width of the tube on the given section.

If one were to take with respect to $\alpha_{ж}$, $T_{ж}$, $T_{ж.от}$ and λ the same assumptions as in the calculation of heat exchange in the ribbed coolant passage, then it is obvious that with the designations accepted in our conditional diagram all the formulas (4.202-4.208) obtained above will remain correct. Consequently, for the tubular chamber

$$\alpha_{ж.тп} = \alpha_{ж} \eta_p; \quad (4.218)$$

$$q_3 = \alpha_{ж.тп} (T_{ж.от} - T_{ж}), \quad (4.219)$$

where $\alpha_{ж.тп}$ - coefficient of heat transfer from the wall to the coolant for the tubular chamber; $\alpha_{ж}$ - coefficient of heat transfer for a tubular channel obtained by formula (4.192); η_p - coefficient of ribbing determined in designations accepted on Fig. 4.40 according to formula (4.207).

Just as in case of the ribbed coolant passage, there can be formulated the problem on the determination of optimum dimensions of the tube. However, its solution is greatly hampered by a large number of factors affecting the relationships between dimensions of the tubes. The particular question of the determination of optimum thickness of the tube, depending upon conditions of heat exchange and strength properties of the material is examined in work [13]. The problem of the distribution of temperatures in the wall of the tubular chamber is examined in work [87].

4.12. Calculation of Cooling of a ZhRD

Order of the Calculation of Cooling

In the designing of a cooling system of a ZhRD, at first there is determined the construction of the coolant passage, method of cooling and basic dimensions of the passage, and then by calculation means it is checked whether there is provided cooling of the walls of the engine. The checking calculation of the cooling of the chamber of a ZhRD is conducted in the following order.

1. We divide the combustion chamber and nozzle lengthwise into separate sections. Usually in the nozzle part we take 12-20 and in the combustion chamber 1-4 sections, depending upon their form. In certain cases for obtaining specified data, we divide into separate sections places of the joint of fastenings (corrugations, ribs, etc.), and also sections having a specific form different from the form of the whole coolant passage. After the division with respect to each section, its geometric parameters necessary for further calculations are determined.

2. We assign the temperature of the gas wall $T_{r.ct}$ constant in length and determined the values of convection heat flows q_K for every section. The order of the determination of q_K is given in section 4.6. If there are data on the distribution of q_K for the base engine, then it is not possible to conduct a special calculation of q_K .

3. We assign the distribution of $T_{r.ct}$ along the length of the chamber of the engine, and by formulas of conversion (see section 4.7) we determine the distribution q_K . With this as the initial values it is possible to take following values of $T_{r.ct}$: in the throat of the nozzle 1000-1300°K for heat-resistant steel, 700-900°K for standard construction steels and 500-700°K for walls of copper or its alloys; at the outlet of the nozzle (depending upon the expansion ratio of the nozzle) 400-700°K for steel walls and 300-600°K for copper. In the combustion chamber and at the entrance into the nozzle $T_{r.ct}$ is 20-40% lower than the temperature of the walls in the throat.

If there are no preliminary considerations about the character of the distribution of $T_{r.ct}$ along the length (data of similar constructions, etc.), then in the first approximation the distribution of intermediate values of $T_{r.ct}$ can be considered linear. However, if values of $T_{r.ct}$ for similar designs of a ZhRD are known, it is more expedient than for the first approximation to take these values.

4. We determine the distribution of radiant heat flows q_R along the length of the chamber and nozzle (see section 4.8).

5. We determine the total specific heat flow into walls of the chamber of the engine (section 4.1):

$$q_1 = q_2 + q_3.$$

6. We check the sufficiency of flow rate of the coolant for the removal of heat proceeding into walls of the chamber of the engine. With the steady state of cooling, all heat entering into walls of the chamber of the engine goes for heating the coolant. The equation of heat balance

$$\sum q_i \Delta F_i = c_{cp} G_{Ox} (T_{out} - T_{in}) \quad (4.220)$$

where $q_{\Sigma 1}$ and ΔF_1 — total heat flow and surface area of the wall of the i -th section of the chamber of the engine; G_{Ox} — flow rate of the coolant; T_{in} and T_{out} — temperatures of input and output of the coolant; c_{cp} — average heat capacity of the coolant taken at a temperature of

$$T_{cp} = \frac{T_{in} + T_{out}}{2}.$$

From equality (4.220) we determine

$$T_{out} = \frac{\sum q_i \Delta F_i}{c_{cp} G_{Ox}} + T_{in}. \quad (4.221)$$

The temperature of the input of the coolant T_{in} is considered equal to the greatest possible ambient temperature at which operation of the ZhRD (for example, $+90^\circ\text{C}$) is assumed. The adequacy of the quantity of coolant is determined by the condition $T_{out} \leq T_g$, where T_g — boiling point of the coolant at the outlet pressure from the coolant passage. If T_{out} is greater than T_g , then it is necessary either to cool by two components according to the diagram of Fig. 4.4 or to decrease the total heat flow into the wall q_2 by means of amplification of the internal cooling.

7. We determine heating of the coolant and average temperature of the coolant on every section. With the known temperature of the entrance of the coolant the heating of it is determined from the equation of heat balance on section

$$q_{2i} \Delta F_i = c_1 G_{\text{cool}} (T_{\text{cool},i} - T_{\text{cool},i-1}) \quad (4.222)$$

where c_1 - average heat capacity of the coolant on the i -th section. Hence

$$T_{\text{cool},i} = \frac{q_{2i} \Delta F_i}{c_1 G_{\text{cool}}} + T_{\text{cool},i-1} \quad (4.223)$$

The temperature of the coolant on section $T_{\text{K} 1}$ is defined as an average:

$$T_{\text{K} 1} = \frac{T_{\text{cool},i-1} + T_{\text{cool},i}}{2} \quad (4.224)$$

8. We determine the coefficient of heat transfer from the wall to the liquid on each section. (The order of the determination of the coefficient of heat transfer α_{K} , $\alpha_{\text{K},p}$, or $\alpha_{\text{K},\text{TP}}$ for different forms of the coolant passage is given in sections 4.9 and 4.11.)

9. We determine the temperature of the liquid wall for each section. According to equation (4.191)

$$T_{\text{L},i} = \frac{q_{2i}}{\alpha_{\text{K}}} + T_{\text{cool},i} \quad (4.225)$$

where α_{K} - coefficient of heat transfer from the wall to the liquid, which is defined for the given form of coolant passage, i.e., α_{K} , $\alpha_{\text{K},p}$, or $\alpha_{\text{K},\text{TP}}$.

10. We determine the temperature of the gas wall $T_{\text{T},\text{OT}}$.

According to the heat-conduction equation

$$q = \frac{\lambda}{\delta} (T_{\text{L},i} - T_{\text{T},\text{OT}})$$

whence

$$T_{r,cr} = \frac{q_{cr} \delta_{cr}}{\lambda} + T_{m,cr} \quad (4.226)$$

where δ_{cr} - thickness of the internal wall of the combustion chamber and nozzle; λ - thermal conduction of the material of the wall at the average temperature of the wall

$$T_{cp} = \frac{T_{1,cr} + T_{2,cr}}{2}$$

Values of thermal conduction for different metals are shown in Fig. 4.41.

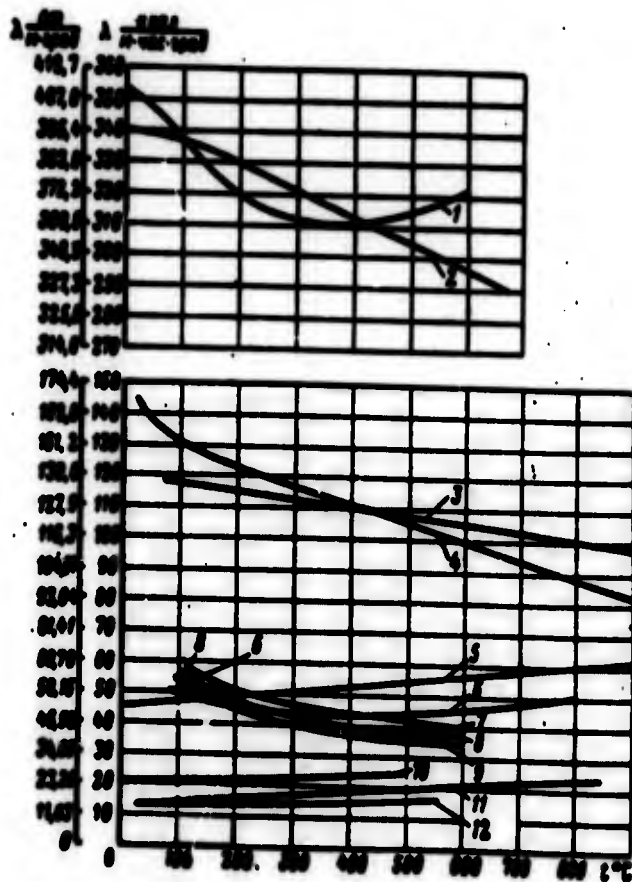


Fig. 4.41. Thermal conduction of metals: 1 - silver, 99.9%; 2 - copper, 99.9%; 3 - molybdenum; 4 - tungsten; 5 - niobium; 6 - nickel; 7, 8, 9 - construction steel; 10, 11 - stainless steels; 12 - titanium.

11. We check the coincidence of the assigned temperature of the gas wall with $T_{r.ct}$ obtained according to formula (4.226).

If the divergence of values $T_{r.ct}$ is more than 5%, we assign the new distribution $T_{r.ct}$ intermediate between that assigned in the first approximation and the one obtained (but closest to the latter), and the calculation starting from No. 3 is conducted again. If value $T_{r.ct}$ on some section exceeds the maximum permissible for a given material, it is necessary either to decrease the thickness of the wall or to improve heat removal from the wall to the liquid. If this is impossible, it is necessary to decrease the heat flows q_{Σ} owing to the intensification of internal cooling.

Example of the calculation of cooling

Produce a checking calculation of the cooling of the chamber of an engine operating on components (80% HNO_3 + 20% N_2O_4) and Tonka 250.

Given: pressure in the combustion chamber $p_2 = 65 \text{ kgf/cm}^2$ (6.37 MN/m^2); temperature in the combustion chamber $T_2 = 3070^\circ\text{K}$; flow rates of components $G_{\Sigma} = 48 \text{ kg/s}$; $v = \frac{G_{\Sigma}}{\rho} = \frac{48}{10.65} = 4.5$ m/s; diameter of the combustion chamber $D_K = 240 \text{ mm}$; throat diameter $D_{xp} = 122 \text{ mm}$; diameter of outlet section $D_3 = 439 \text{ mm}$; length of the cylindrical part of the combustion chamber $L_K = 276 \text{ mm}$.

The contour of the combustion chamber and profiled nozzle is shown in Fig. 4.42. The external cooling is by fuel; at the internal wall of the chamber of the engine by the corresponding location of injectors on the head a boundary layer is created with the relationship of component $\nu_{CT} = 1.943$; the thickness of the boundary layer is equal to the spacing between injectors $H = 15 \text{ mm}$. The coolant passage is made with corrugations; the number of ribs of the corrugation - z_u ; it is variable in length and on the sections is accepted as the following:

No. of section	1	2	3, 4, 5, 6	7, 8, 9	10, 11, 12	13, 14
Number of ribs of the corrugation δ_c	200	200	200	200	500	600

The height of the clearance of the coolant passage $\delta_{oxл}$ and thickness of the inner shell δ_{CT} and corrugations b are constant and equal to $\delta_{oxл} = 3$ mm, $\delta_{CT} = 1$ mm, and $b = 0.4$ mm.

The inner shell is made of stainless steel and the corrugations — from construction steel.

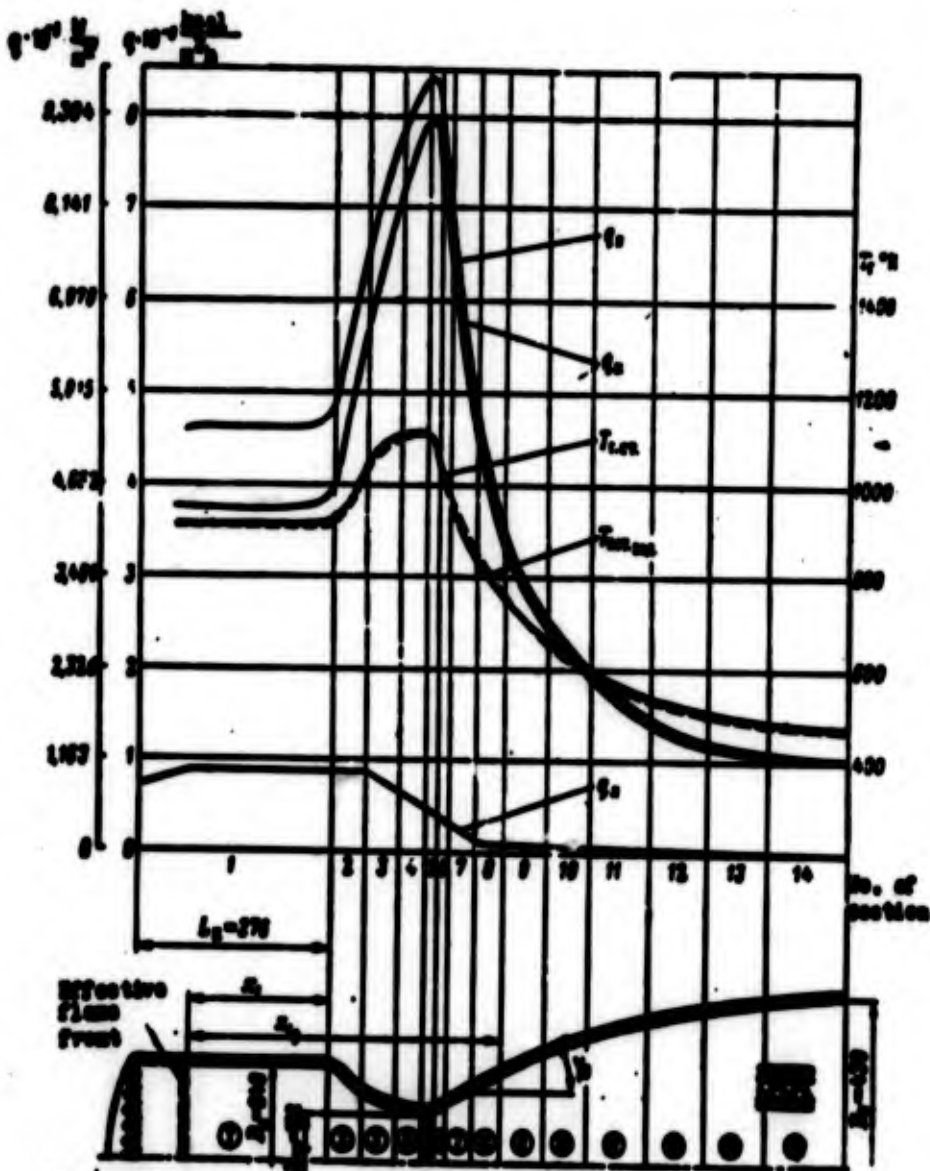


Fig. 4.42. Example of the calculation of cooling.

From the thermodynamic calculation the partial pressures necessary for calculation of q_H are also known: $P_{H_2O} = 22.4 \text{ kgf/cm}^2$ (2.2 MN/m^2); $P_{CO_2} = 7.7 \text{ kgf/cm}^2$ (0.75 MN/m^2).

Solution. The calculation of cooling is produced in the order stated above; all data of the calculation are given in Table 4.4.

1. We divide the combustion chamber and nozzle in length into 14 sections, as was shown on Fig. 4.42.

For simplification of the calculation we will not separate into separate sections the places of the joint of corrugations. From the drawing of contour we determine for each section the necessary (for further calculation) mean values of the internal diameter D , the cosine of the angle of inclination of contour $\cos \gamma$, the distance from the effective flame front s_1 , and the length of the section along the axis Δx_1 , and we calculate the dimensionless values \bar{D} and $\bar{\Delta x}_1$ (lines 1-6, Table 4.4).

2. We assign the temperature of the gas wall $T_{r,GT} = 700^\circ\text{K}$ constant in length, and in the order discussed in section 4.6 we determine for each section the values of convection heat flow q_{K700} (lines 7-17). The values necessary with calculation T_{sp00} , R_H , $c_{p,sp,cp}$ and $\bar{\mu}_{sp00}$ for our fuel when $\nu_{GT} = 1.943$ are determined from graphs of Fig. 4.16:

$$T_{sp00} = 1800^\circ\text{K}, \text{ where } T_{sp00} = \frac{T_{fl}}{T_{sp00}} = 0.222$$

$$R_H = 0.1 \text{ kgf/cm}^2 \cdot \text{deg} \text{ (see 4.16-16)}$$

$$c_{p,sp,cp} = 0.21 \text{ kcal/kg} \cdot \text{deg} \text{ (see 4.16-16)}$$

$$\bar{\mu}_{sp00} = 10^{-4} \text{ kgf} \cdot \text{cm}^2 \text{ (see 4.16-16)}$$

We calculate value Re_{00} from formula (4.159): $Re_{00} = 4.94 \cdot 10^6$ (if for some fuel there are no auxiliary values the shown can be calculated in the order given in 4.6).

3. We assign the distribution $T_{r,OT}$ in length, and according to formulas of conversion we determine the real values of convection heat flow q_{gr} (lines 18-20). A change in q_{gr} in length of the chamber and nozzle is shown in Fig. 4.42.

4. We determine the radiant heat flows q_{gr} . We find $q_{gr,K}$ in the combustion chamber, neglecting the boundary layer

Since $L = \frac{1}{2} - \frac{20}{20} = 1.18$, the length of the path of the ray will be equal to $1.18 \cdot 2 = 2.36$.

Then

$$\begin{aligned} \epsilon_{gr,K} &= 2.4 \cdot 0.12 = 0.288 \\ \epsilon_{gr,K} &= 7.7 \cdot 0.12 = 0.924 \end{aligned}$$

We find the degree of blackness of the gas in the combustion chamber ϵ_p . According to Fig. 4.21 when $T_2 = 3070^\circ\text{K}$ and $p_{H_2O} = 3.5$, the degree of blackness of H_2O when $p_2 = 1$ will be

$$\epsilon_{H_2O} = 0.187$$

Determining from the graph on Fig. 4.22 the exponent

$$n = 1 + 0.2 \cdot p_{H_2O} = 1.07$$

According to formula (4.187) or the graphs of Fig. 4.23 we find ϵ_{H_2O} - degree of blackness of H_2O with the parameters of operation of the chamber:

$$\epsilon_{H_2O} = 1 - (1 - 0.187)^{1.07} = 1 - 0.817 = 0.183$$

The degree of blackness of CO_2 according to the graph of Fig. 4.24 when $T_2 = 3070^\circ\text{K}$ is equal $\epsilon_{CO_2} = 0.0525$.

Knowing ϵ_{H_2O} and ϵ_{CO_2} according to formula (4.186) we find the degree of blackness of products of combustion in the chamber:

$$\epsilon = \epsilon_{H_2O} + \epsilon_{CO_2} - \epsilon_{H_2O} \epsilon_{CO_2} = 0.671 + 0.0225 - 0.671 \cdot 0.0225 = 0.689$$

Considering the degree of blackness of the wall $\epsilon_{GT} = 0.8$, by formula (4.188) determine the effective degree of blackness of the wall:

$$\epsilon_{\text{eff}} = \epsilon_{GT} + (1 - \epsilon_{GT})(1 - \epsilon) = 0.8 + (1 - 0.8)(1 - 0.689) = 0.82$$

Since walls of the chamber have external cooling, we will disregard the second term in formula (4.184) and determine the magnitude of radiant heat flow in the combustion chamber $q_{R, \Sigma}$ according to (4.185):

$$q_{R, \Sigma} = \epsilon_{\text{eff}} \sigma T_{\text{ch}}^4 = 0.82 \cdot 0.689 \cdot 4.9 \left(\frac{2000}{100} \right)^4 = 1.9 \cdot 10^5 \text{ kcal/m}^2 \cdot \text{h} \quad (2.2 \cdot 10^5 \text{ W/m}^2)$$

We determine the value of radiant heat flow in the combustion chamber taking into account the boundary layer $q_{R, \Sigma, \text{CT}}$. The coefficient φ , considering the decrease in intensity of radiation according to formula (4.190) is equal to

$$\varphi = \frac{2 - \frac{2.1}{2.1}}{2.1} = \frac{2 - 1}{2.1} = \frac{1}{2.1} = \frac{2.1 - 1}{2.1} = 0.73$$

Then according to expression (4.189)

$$q_{R, \Sigma, \text{CT}} = \varphi q_{R, \Sigma} = 0.73 \cdot 1.9 \cdot 10^5 = 0.73 \cdot 1.9 \cdot 10^5 = 0.14 \cdot 10^6 \text{ kcal/m}^2 \cdot \text{h} \quad (0.16 \cdot 10^6 \text{ W/m}^2)$$

We determine the distribution q_R along the length of the combustion chamber: near the head

$$q_{R, \text{head}} = q_{R, \Sigma, \text{CT}} = 0.14 \cdot 10^6 = 0.14 \cdot 10^6 = 0.14 \cdot 10^6 \text{ kcal/m}^2 \cdot \text{h} \quad (0.16 \cdot 10^6 \text{ W/m}^2)$$

in the throat

$$q_{R, \text{throat}} = 0.14 q_{R, \text{head}} = 0.14 \cdot 0.14 \cdot 10^6 = 0.02 \cdot 10^6 \text{ kcal/m}^2 \cdot \text{h} \quad (0.02 \cdot 10^6 \text{ W/m}^2)$$

in the section where $\bar{D} = 2.5$

$$q_{\text{max}} = 0.02 \cdot 10^6 = 0.02 \cdot 0.05 \cdot 10^6 = 0.017 \cdot 10^6 \text{ kcal/m}^2 \cdot \text{h} \quad (0.002 \cdot 10^6 \text{ W/m}^2)$$

Tracing the graph of distribution q_{Σ} along the length of the chamber of the engine (see Fig. 4.42), we determine the value of q_{Σ} for every section (line 21).

5. We determine the total heat flows

$$q_0 = q_1 + q_2$$

Values q_{Σ} are given in line 22. The change in q_{Σ} along the length of the chamber and nozzle is shown on Fig. 4.42.

6. We check the adequacy of the quantity of the coolant. We consider the temperature of the input equal to $+50^{\circ}\text{C}$ (323°K). Then according formula 4.221 the temperature of the coolant outflow

$$T_{\text{out}} = \frac{20 \cdot 10^6 \cdot 0.017}{0.02 \cdot 10^6} + T_{\text{in}} = \frac{0.017 \cdot 0.02}{0.02 \cdot 10^6} + 50 = 107^{\circ}\text{C} (380^{\circ}\text{K})$$

i.e., $T_{\text{max}} < T_0$.

7. We determine heating of the coolant and average temperature of it on each section (line 23-27).

8. We determine the coefficient of heat transfer from the wall to the liquid, taking into account ribbing $\alpha_{\Sigma,p}$ (lines 28-40). The complex $Z\beta$ and the coefficient of thermal conduction of corrugations λ_p were determined on the assumption that the temperature of the liquid wall is constant and equal to 200°C (473°K). Such an assumption does not considerably affect the value $Z\beta$ and ξ and, respectively, α_{Σ} and $\alpha_{\Sigma,p}$, since in the region of the change in $T_{\Sigma,0T}$ (line 42), $Pr_{\Sigma,0T}$ and all the more so β , proportional to $(Pr_{\Sigma,0T})^{-0.25}$, and also ξ , proportional to $(\lambda_p)^{-0.5}$, are changed very insignificantly. Thus, according to the auxiliary graphs of Fig. 4.25 or formulas (4.195) and (4.196) $Z\beta = \text{const} = 0.044$, and according to the graph of Fig. 4.41 $\lambda_p = 60 \text{ kcal/m h} \cdot \text{deg}$ on all the sections. In the given

example the impairment of value η_p , owing to the increase in thermal resistance at places of soldering the corrugation, is not considered.

9. We determine the temperature of the liquid wall by formula (4.223) (lines 41-42).

10. We determine the temperature of the gas wall obtained under the assigned conditions of cooling (lines 43-46).

11. A comparison of the obtained $T_{r,CT}$ (line 46) and assigned (line 18) shows that the divergence between them does not exceed 5%, and therefore we consider the calculation final.

4.13. Certain Special Cases of Cooling ZhRD

We will examine the special features of radiation cooling of a ZhRD, cooling by low-boiling components, and cooling of a ZhRD having a nozzle with a central body.

Radiation Cooling

Above in section 4.2, radiation cooling is examined as one of the methods of cooling a ZhRD. Such cooling can be expedient for a ZhRD with a large nozzle expansion ratio and a prolonged operating time (for a comparatively short time of operation ablative cooling is more rational). Radiation cooling can be applied in those engines which are set on the external surface of the vehicle. The basic problem in the calculation of radiation cooling is the determination of the value of the equilibrium temperature of the wall, $T_{CT,p}$.

Determination of $T_{CT,p}$ during radiation cooling

In the general case the following balance of heat fluxes occurs during radiation cooling (Fig. 4.43):

$$q_s + q_a = q_{a,s} + q_{a,p} \quad (4.227)$$

where q and q_R are convection and radiant fluxes in the wall of the engine chamber; $q_{K.H}$ and $q_{\Pi.H}$ are convection and radiant fluxes into the environment.

Equation (4.227) is also the fundamental equation for determination of the equilibrium temperature of the wall $T_{CT.P}$.

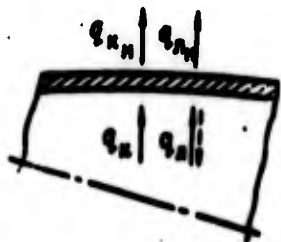


Fig. 4.43. For calculation of radiation cooling.

The values of heat fluxes entering into it are determined as follows. The convection heat fluxes from the gases to the wall and from the wall into the environment are equal, respectively,

$$q_K = \alpha_r (T_{sp00} - T_{CT.P}); \quad (4.228)$$

$$q_{K.H} = \alpha_H (T_{CT.P} - T_H), \quad (4.229)$$

where T_{sp00} — just as in preceding calculations, is determined from equation (4.27) with a component ratio ν_{CT} in the near-wall layer (if there is one) or in the flow core.

The coefficients of convective heat transfer from the gases to the wall and from the wall into the environment, α_r and α_H , are determined by the known formulas of heat transfer, taken in reference to the given conditions of heat exchange.

In the particular case, when values of q_R at some given $T_{\Gamma.CT}$ on a certain section of the nozzle are already known from calculations of cooling of ZhRD, it is possible to determine α_r by the formula

$$\alpha_r = \frac{q_R}{T_{sp00} - T_{CT.P}}. \quad (4.230)$$

During further calculations in the first approximation it is possible to consider α_r to be independent of the wall temperature.

During engine operation in vacuum conditions, obviously, α_H and, accordingly, $q_{K.H}$ are equal to zero.

The magnitude of the radiant heat flux q_R is determined by equation (4.184) or approximately by equations (4.182) and (4.183) with replacement of T_R by the thermodynamic temperature $T_{H.C}$ of the combustion products in the flow core and of $T_{r.ct}$ by the equilibrium temperature $T_{ct.p}$. Here q_R can be directed both from the gas to the wall and vice versa.

The value of the radiant heat flux into the environment is determined by the equation

$$q_{e.e} = \epsilon_{CT} \sigma \left(\frac{T_{ct.p}}{100} \right)^4. \quad (4.231)$$

where ϵ_{CT} is the degree of blackness of the wall material; $T_{ct.p}$ is the external equilibrium wall temperature.

With a sufficient degree of accuracy it is possible to consider

$$T_{ct.p} = T_{cr.p} = T_{r.ct}$$

Substituting the expanded expressions for heat flux in equation (4.227) and solving it, we shall determine the values of equilibrium wall temperature $T_{ct.p}$ for different sections of the nozzle. If the greatest wall temperature permissible for the given material is known, it is possible to find the section, starting from which the nozzle unit can be made without special cooling.

Example of calculation of equilibrium wall temperature

Determine the equilibrium temperature of the wall of the nozzle of an ZhrD made from chrome-nickel alloy. The parameters of the ZhrD which determine the heat exchange in a given section are as follows.

Given: nozzle diameter $D = 0.5$ mm; effective stagnation temperature in the near-wall layer $T_{s,00} = 1800^\circ\text{K}$; coefficient of heat transfer $\alpha_p = 250$ kcal/m²·h·deg (291 W/m²·deg); $\alpha_n = 0$ (heat transfer in vacuum). The thermodynamic temperature of the flow core $T_{n,0} = 1000^\circ\text{K}$; partial pressures of H₂O and CO₂ are

$$p_{H_2O} = 0.05 \text{ kg/m}^2 (7.25 \text{ mmHg});$$

$$p_{CO_2} = 0.05 \text{ kg/m}^2 (7.25 \text{ mmHg}).$$

Solution. Let us express the values of the heat fluxes entering into equation (4.227) through the equilibrium temperature of the wall $T_{OT,p}$, for which we will determine $\epsilon_{OT,p}$ and ϵ_p entering into expression (4.184). The length of the path of a ray will be determined as for a cylindrical shell of infinite length:

$$l = 0.5D = 0.25 \text{ m} = 0.45 \text{ m};$$

$$(\alpha_{H_2O})_0 = 0.05 \cdot 0.45 = 0.0225;$$

$$(\alpha_{CO_2})_0 = 0.05 \cdot 0.45 = 0.0225.$$

We will determine ϵ_{H_2O} and ϵ_{CO_2} . From the graphs in Figs. 4.21 and 4.22 at $T_{n,0} = 1000^\circ\text{K}$

$$\epsilon_{H_2O} = 0.04; \quad \alpha = 1 + \alpha_{H_2O} / \alpha_{CO_2} = 1.$$

Then

$$\epsilon_{CO_2} = 1 - (1 - \epsilon_{H_2O})^\alpha = 1 - (1 - 0.04) = 0.04.$$

From the graph in Fig. 4.24 $\epsilon_{CO_2} = 0.055$.

We determine ϵ_p by formula (4.186):

$$\epsilon_p = \epsilon_{H_2O} + \epsilon_{CO_2} - \epsilon_{H_2O}\epsilon_{CO_2} = 0.04 + 0.055 - 0.04 \cdot 0.055 = 0.131.$$

Considering that there is soot on the internal wall, its degree of blackness is taken as $\epsilon_{OT} = 0.8$.

Then by formula (4.186)

$$\epsilon_{\text{eff}} = \epsilon_w (1 + (1 - \epsilon_w)(1 - \epsilon_s)) = 0.9(1 + (1 - 0.9)(1 - 0.12)) = 0.94.$$

The radiant heat flux from the combustion products to the wall will be determined according to equation (4.184), considering $\epsilon_T = \Lambda_T$:

$$q_r = \epsilon_{\text{eff}} \sigma \left[\left(\frac{T_{\text{cp}}}{100} \right)^4 - \left(\frac{T_{\text{st}}}{100} \right)^4 \right] = 0.94 \sigma \left[\left(\frac{1800}{100} \right)^4 - \left(\frac{T_{\text{st}}}{100} \right)^4 \right]. \quad (4.232)$$

The sign of q_R (i.e., the direction of heat flow) will depend on the relationship between $T_{\text{H.C}}$ and $T_{\text{OT.P}}$.

The convective heat flux is

$$q_c = \alpha (T_{\text{H.C}} - T_{\text{OT.P}}) = 20(1800 - T_{\text{OT.P}}). \quad (4.233)$$

We will determine the radiant heat flux from the external wall into the environment.

According to Table 4.3 the degree of blackness of the external wall is

$$\epsilon_w = 0.12.$$

Considering $T_{\text{OT.P}}$ to be identical over the thickness of the wall, we find $q_{R.H}$ by equation (4.231):

$$q_{R.H} = \epsilon_w \sigma \left(\frac{T_{\text{OT.P}}}{100} \right)^4 = 0.12 \cdot 1.9 \left(\frac{T_{\text{OT.P}}}{100} \right)^4 = 2.28 \left(\frac{T_{\text{OT.P}}}{100} \right)^4. \quad (4.234)$$

Placing the expressions for q_R , q_c , and $q_{R.H}$ in the equation of balance (4.227), we will obtain

$$2.28 \left(\frac{T_{\text{OT.P}}}{100} \right)^4 = 20(1800 - T_{\text{OT.P}}) + 0.94 \sigma \left[\left(\frac{1800}{100} \right)^4 - \left(\frac{T_{\text{OT.P}}}{100} \right)^4 \right].$$

or

$$0.28 \cdot 10^{-4} \left(\frac{T_{\text{OT.P}}}{100} \right)^4 = 1 - 0.94 \sigma \left(\frac{T_{\text{OT.P}}}{100} \right)^4.$$

It is most convenient to solve the obtained equation graphically. Constructing the dependence of the right and left parts of the equation on $\left(\frac{T_{\text{ст.р.}}}{100}\right)$, we will find the unknown value of the equilibrium temperature of the wall (Fig. 4.44):

$$T_{\text{ст.р.}} = 1315^{\circ}\text{K.}$$

For appraisal of the magnitudes of the heat fluxes we find $q_{\text{г}}$, $q_{\text{к}}$, and $q_{\text{г.к}}$. From equations (4.232), (4.233), and (4.234)

$$q_{\text{г}} = 0.200 \left[\left(\frac{1000}{100} \right)^4 - \left(\frac{1315}{100} \right)^4 \right] = -0.11 \cdot 10^6 \text{ kcal/m}^2\text{h} \\ (-0.126 \cdot 10^6 \text{ W/m}^2)$$

[minus sign indicates reverse direction of flow (from wall to gases)]

$$q_{\text{к}} = 200(1000 - 1315) = 1.21 \cdot 10^6 \text{ kcal/m}^2\text{h} (1.41 \cdot 10^6 \text{ W/m}^2);$$

$$q_{\text{г.к}} = 3.67 \left(\frac{1315}{100} \right)^4 = 1.1 \cdot 10^6 \text{ kcal/m}^2\text{h} (1.26 \cdot 10^6 \text{ W/m}^2).$$

Comparing the obtained results, we see that in this case the value of $q_{\text{г}}$ is very small as compared with $q_{\text{к}}$ and $q_{\text{г.к}}$ and is equal to approximately 10% of the radiant heat flow into the environment.

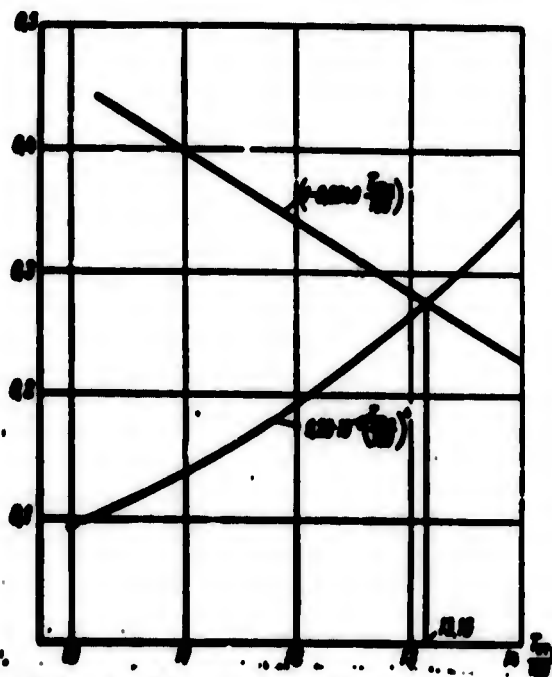


Fig. 4.44. For the example of determination of equilibrium wall temperature $T_{\text{ст.р.}}$.

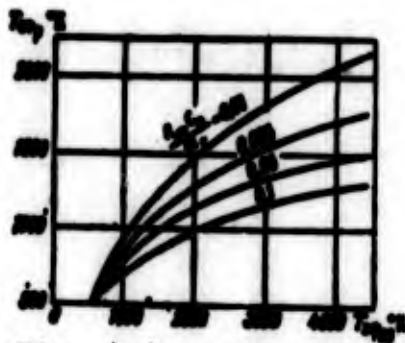


Fig. 4.45. Dependence of equilibrium wall temperature on $T_{\infty} \phi_{00}$.

Frequently during radiation cooling the fraction of q_{π} can be even smaller. Therefore during rough calculations of radiation cooling it is possible to disregard radiant heat transfer from combustion products to the wall. If it is also possible to disregard convection into the environment (during operation of ZhRD in vacuum or in a very rarefied medium), then equation (4.227) is simplified and at $T_{r,cr} = T_{cr,p} = T_{cr,p}$ in expanded form, taking into account expressions (4.228) and (4.231), has the form

$$\epsilon_{cr,p} (T_{\infty} \phi_{00} - T_{cr,p}) = \epsilon_{cr,p} c_0 \left(\frac{T_{cr,p}}{100} \right)^4. \quad (4.235)$$

By solving this equation, using $\frac{T_{cr,p}}{T_{\infty} \phi_{00}}$ as a parameter, it is possible to construct the graphic dependence of $T_{cr,p}$ on $T_{\infty} \phi_{00}$; this allows immediate estimation of the expected value of $T_{cr,p}$ (in the absence q_{π} and $q_{k,h}$) (Fig. 4.45).

Analyzing the values entering into formula (4.227) and the graphs in Fig. 4.45, we see that $T_{cr,p}$ also depends to a considerable extent on the degree of blackness of the wall, $\epsilon_{cr,p}$. The equilibrium temperature of the wall is inversely proportional to the magnitude of $\epsilon_{cr,p}$. Therefore during radiation cooling it is better to leave the external radiating surface, since degree of blackness of a rough surface is greater than that of a polished one. In certain cases it is even expedient to create special grooves on the radiating surface, increasing the apparent degree of blackness of the surface by 50-100% [86].

External Cooling by Low-Boiling Components

During operation of a ZhRD on low-boiling components (for example, $O_2 + H_2$ or $F_2 + H_2$) it is impossible to organize external cooling of the chamber walls by the liquid component alone, in view of the very low boiling points of both the fuel and the oxidizer. The coolant, upon entering the coolant passage, is quickly turned into vapor and further external cooling of the chamber is then produced by cold gas (vapor). The problem of reliable cooling of the chamber walls of the engine is severely complicated by the following factors.

During the transition of the coolant from the liquid into the gaseous state the coefficient of heat transfer from the wall to the gas is less than the α_x of the liquid coolant.

The specific volume of the gaseous coolant is considerably greater than that of the liquid, and is strongly increased with a rise in temperature (by two-three times). Therefore it is sometimes necessary to make the cross section area of the coolant passage variable in length so that in every section of the duct the speed of the cooling gas will ensure a value of α_x corresponding to the arriving heat flux.

The complexity of solving the problem is aggravated also by the fact that under the conditions which obtain in a ZhRD the cooling of the chamber walls by a low-boiling component occurs in the near-critical and supercritical regions of parameters of state of the coolant. Moreover, in the near-critical region a sharp change occurs in the physical properties of the coolant, rendering a strong influence on heat exchange. Thus, for example, the heat capacity of hydrogen in the near-critical region is increased by 5-10 times.

In comparison with other low-boiling components hydrogen has the best cooling properties, since it has high values of heat capacity (approximately 3 times greater than that for water and four times greater than that for oxygen).

Possible regions of state of hydrogen
during its use as a coolant for
a ZhRD

In the general case the curve of phase equilibrium $p_s = f(T)$ has the form depicted on Fig. 4.46.

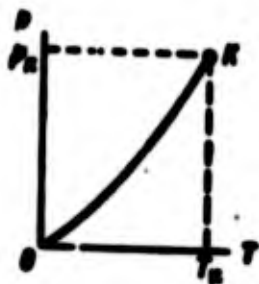


Fig. 4.46. Curve of phase equilibrium.

The curve of phase equilibrium, OK , has finite length and terminates at critical point K , corresponding for every given substance to the fully defined values of temperature T_K and pressure p_K .

At values of pressure and temperature higher than critical the substance is in the region of supercritical parameters of state. In this region it is no longer permissible to talk about the phase transition of a substance, since the substance does not have a liquid and gaseous phase boundary and there is no fundamental distinction between liquid and gas. Although it is difficult to visualize distinctly such a medium, lacking boundaries, it is acceptable to consider that a substance in this region constitutes a conglomerate of groups of molecules with different density. Depending upon the values of pressure and temperature, the substance is in a state closer to gaseous or closer to the liquid. If hydrogen is examined from the point of view of its use as a coolant for ZhRD, the diagram which characterizes the state of hydrogen (Fig. 4.47) can be somewhat tentatively divided into the following five regions:

1. Region of boiling.
2. Region of the near-critical state.
3. Region of state of hydrogen at a pressure considerably exceeding the critical ($\gg 2.8 \text{ kgf/cm}^2$) and at a comparatively low

temperature (\sim up to 150°K).

4. Region of state of hydrogen at supercritical pressure and high temperature (above 150°K).

5. Region of gaseous hydrogen at subcritical pressure.

At present there are very few recommendations on the calculation of heat transfer to hydrogen in the boiling, near-critical, and supercritical states. For approximate calculations it is possible to use the schemes proposed in works [92] and [97] for determination of $\alpha_{\text{ж}}$ for different hydrogen states.

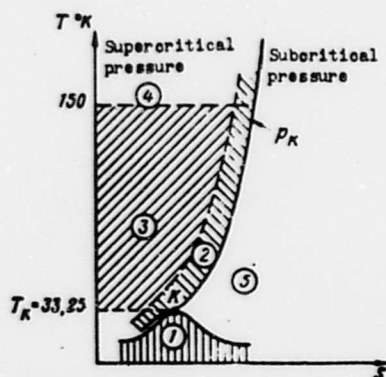


Fig. 4.47. Regions of state of hydrogen.

During calculation of cooling by hydrogen for determination of $\alpha_{\text{ж}}$ in the first approximation it is possible to use formula (4.192).

Order of calculation of cooling by a low-boiling component

The calculation of cooling by low-boiling components is conducted by the method of successive approximations. For this the combustion chamber and nozzle should be separated along their length into 15-20 sections and every section should be calculated consecutively. It is possible to propose the following order for the calculations.

1. Find the distribution of temperature of the gas wall [sic] $T_{r,OT}$ over the length of the engine chamber and use the methods outlined above to determine the distribution of q_H , q_G , and q_Z along the length.

2. Knowing q_Z and $T_{r,OT}$, and also the thermal conductivity λ and thickness δ_{OT} of the internal wall, determine the temperature of the liquid wall by formula (4.225):

$$T_{in} = T_{OT} - \frac{q_Z \delta_{OT}}{\lambda}.$$

Where the value of λ is taken for average temperature of the wall equal to

$$\frac{T_{in} + T_{OT}}{2}.$$

3. Determine the value of α_H necessary for removal of the total heat flux. By formula (4.191)

$$\alpha_H = \frac{q_H}{T_{in} - T_H}. \quad (4.236)$$

Take the value of T_H as average for each section:

$$T_H = \frac{T_{in} + T_{OT}}{2}.$$

[HX = inlet; HX = outlet/outflow]

4. Determine coolant preheating ΔT_{cool} and the temperature of coolant outflow on each section. According to formula (4.222)

$$\Delta T_{cool} = \frac{q_H \Delta F_1}{c_{p1} \rho_{cool}}. \quad (4.237)$$

where ΔF_1 - heat exchange surface area on a given section; c_{p1} - heat capacity at mean values of pressure and temperature on a given section.

Knowing ΔT_{cool} , find

$$T_{cool} = T_{in} + \Delta T_{cool}$$

5. Find the coolant pressure $P_{OXR,EX}$ on the inlet into the first section.

6. From the formulas for calculation of α_M determine the speed of coolant w_{OXR} which ensures a value of α_M equal to that obtained by expression (4.236). Mean values of coolant temperature and pressure on a given section are used in the calculations.

7. Knowing coolant speed w_{OXR} , determine the dimensions of the flow section of the coolant passage:

$$f_{OXR} = \frac{G_{OXR}}{\rho_{OXR} w_{OXR}} \quad (4.238)$$

where the value of ρ_{OXR} is taken with average parameters of state on a given section.

Since the diameter of the coolant passage over the circumference of the cross section of the engine chamber is known, the determination of f_{OXR} usually reduces to determination of the height of the coolant passage δ_{OXR} .

8. Determine the loss of pressure Δp_1 on a given section and the pressure of the coolant on the outlet of the section. The quantity Δp_1 is made up of local losses (Δp_M), losses on friction (Δp_{TP}), and also losses of pressure as a result of acceleration of gas on a given section (Δp_W):

$$\Delta p_1 = \Delta p_M + \Delta p_{TP} + \Delta p_W \quad (4.239)$$

The order of determination of Δp_M , Δp_{TP} , and Δp_W is given below, in section 6.6. It is necessary to note that the magnitude of friction losses during motion of hydrogen along the passage (Δp_{TP}) is comparatively small, due to the low viscosity of hydrogen.

Knowing Δp_1 , determine coolant pressure on the outlet of the section:

$$P_{OXR,EX} = P_{OXR,IN} - \Delta p_1 \quad (4.240)$$

9. Conducting consecutive calculations for all sections, analyze the acceptability of the obtained results and if necessary correct or repeat the calculation. If the values of $f_{\text{охл}}$ (or $\delta_{\text{охл}}$) obtained on separate sections difficult to fulfill in practice, the assigned value of $T_{\text{г.ст}}$ is corrected and the calculation is repeated.

Knowing the pressure loss over the length of the entire duct ($\Sigma \Delta p_1$), determine the pressure $P_{\text{охл.вх}}$ of the component at the combustion chamber inlet (Fig. 4.48). If the obtained value of $P_{\text{охл.вх}}$ differs from the given value, the calculation is repeated with a new value of coolant pressure $P_{\text{охл.вх}}$ on the inlet.

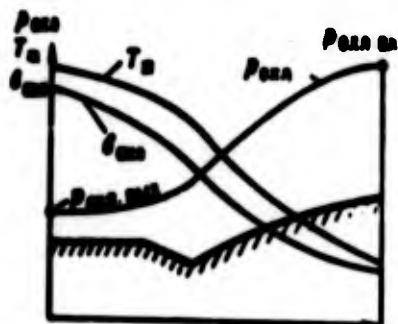


Fig. 4.48. Change in $P_{\text{охл}}$, $T_{\text{ж}}$, and height of coolant passage tube during cooling by hydrogen.

As can be seen, the calculation of cooling by low-boiling components is considerably complicated not only by difficulties connected with determination of $\alpha_{\text{ж}}$ for different states of the coolant, but also by the fact that, in contrast to cooling by dropping liquids, the calculations must take into account the compressibility of the component and the influence of pressure losses along the length of the duct on the process of heat exchange.

Figure 4.48 shows typical graphs of the change in coolant pressure and temperature and also in the area of the passage section (height of channel $\delta_{\text{охл}}$) along the length of duct during cooling of a can-type [tubular] chamber by hydrogen.

Heat Exchange in Nozzles with a Center Body

One of basic difficulties in using nozzles with a center body in ZhRD is the complexity of organizing the cooling of such a nozzle.

These complexities are caused in the first place by the fact that, in contrast to the usual ZhRD with a Laval nozzle, the critical section and combustion chamber of an engine with a nozzle with a center body have annular form.

Due to this shape the perimeter of the critical section and combustion chamber is sharply increased. Elementary calculations show that for a nozzle with a center body the perimeter of critical section (place of the most intense heat exchange) is increased by 5-10 times. Furthermore, on one side of the critical section there is usually a sharp edge, the cooling of which is in itself a complicated problem.

The surface of an annular combustion chamber is also considerably larger than the surface of a chamber of the usual shape, which leads to an increase in the total quantity of heat output on the section of the combustion chamber.

The large perimeter of the critical section of the annular shape severely hampers the creation of a reliable near-wall layer for internal cooling. The area occupied by the near-wall layer in the critical section grows in proportion to the perimeter of the section and this leads to its obstruction. Especially strong obstruction occurs with large diameters of the center body, when the annular critical section resembles a narrow slot. In this case in the section in general no place is left for a reliable protective near-wall layer.

Cooling of an engine with a nozzle with a center body is additionally hampered by the fact that such engines have two independent coolant passages (see Fig. 2.21) — over the contour of the center body and over the external contour. Depending upon the type of nozzle, one of these ducts ensures cooling of the chamber ahead of the critical part and the second provides cooling of both the chamber and the transcritical part of the nozzle. This presence of two coolant passages strongly complicates input and the subsequent "separation" of coolant along the passage.

Calculation of cooling of nozzles with a center body.

Calculation of cooling for nozzles with a center body can be conducted in the same order as that for the usual nozzles. We will note only certain peculiarities in using the calculation formulas obtained above for determination of q_k .

During calculation of cooling of round nozzles we selected the critical throat diameter D_{kp} as the characteristic dimension, which in this case is impossible because the critical section is annular. However, we can select as characteristic some other dimension of a nozzle with a center body — for example, the usually given value of the small diameter d of a toroid or annular chamber (Fig. 4.49).

Effective
flame front



Fig. 4.49. For calculation of cooling of a nozzle with a center body.

Then in the expressions for calculation of z_T the dimensionless length of the section \bar{x} and diameter of the center body \bar{D} will equal

$$\bar{x} = \frac{x}{d}; \quad \bar{D} = \frac{D}{d}. \quad (4.241)$$

Since the usual gas-dynamic relationships which determine β and p/\bar{p}_{00} as $f(\bar{D})$ are inapplicable for a nozzle with a center body, formula (4.146) also is inapplicable and calculation of z_T must be conducted by formula (4.141) (with constant $T_{r,0T}$).

$$z_T = \frac{q_{k0}}{c_p \rho_0 \bar{w}} \int_0^{\bar{x}} \beta \frac{p}{\bar{p}_{00}} \bar{D}^2 d\bar{x}.$$

where $\beta = \frac{p}{\bar{p}_{00}}$; \bar{w} is the speed of the flow "core" near the chamber wall, i.e., flow rate along the rarefaction wave incident to a given

point of the contour; p is the pressure near the contour at the given point; b_T^2 and a_T are determined by equations (4.127) and (4.129).

We will obtain the expression for Re_{00} (4.159), replacing D_{kp} with the new characteristic dimension d :

$$Re_{00} = \frac{1.107 \cdot 10^{10} \bar{d} \bar{p}_{00}}{F_{00} \bar{v} \sqrt{R_a \bar{T}_{00}}} \quad (4.242)$$

The formula for determining q_K is obtained from formula (4.160), after substitution of the values of \bar{v}_∞ and w from expressions (4.155) and (4.161) and calculation of the influence of the Pr number by formula (4.172) in a form analogous to equality (4.173):

$$q_K = 450 \cdot 10^6 \frac{\beta p_c p_{00} \bar{v}_{00} (1 - \bar{T}_{i,cr})}{\delta_T^2 \bar{v} \sqrt{R_a \bar{T}_{00}}}, \quad (4.243)$$

where p is the static pressure near the contour at the given point.

Footnotes

¹Rules and methods of averaging are analyzed in detail in works [94], [137].

²The obtaining of equations of the turbulent boundary layer can be found in detail in works [18], [28], [94].

³The derivation of integral equations, their solution, and an analysis and obtaining of dependences for determining q_K are conducted on the basis of works of V. M. Iyevlev [77], [78].

⁴See work [25].

⁵It must be noted that due to the accepted assumptions expression (4.207) gives oversized values of η_p . Furthermore, with the calculation for η_p for the coolant passage with soldered corrugations values of η_p are obtained even more oversized, since the additional thermal resistance at soldering places of corrugations to the wall is not considered.

⁶A detailed analysis of the effect of the geometry of ribbing on η_p is given in the work of V. S. Zarubin [76].

Table 4.4.

Name of value and dimension	Designation and formula	Number of section of cooling duct													
		1	2	3	4	5	6	7	8	9	10	11	12	13	14
1 Internal mean diameter of chamber cross section, m	D	0.23	0.26	0.35	0.48	0.72	0.97	1.64	2.20	3.22	4.62	6.36	8.54	11.17	14.25
2 Cosine of angle of inclination of contour	$\frac{D}{D_0}$	1.00	1.07	1.23	1.65	1.00	1.12	1.34	1.66	2.06	2.68	3.41	4.33	5.36	6.53
3 Dimensionless value of mean diameter	$\cos \alpha$	1.00	0.77	0.58	0.36	1.00	0.89	0.84	0.80	0.80	0.81	0.82	0.83	0.84	0.85
4 Distance along the axis from the effective flame front, m	A_0	0.207	0.23	0.29	0.37	0.52	0.67	0.85	1.13	1.54	2.01	2.55	3.15	3.82	4.56
5 Length of section, r	$A_0 A_1 \dots A_{14}$	0.207	0.66	0.66	0.64	0.63	0.61	0.59	0.58	0.57	0.56	0.55	0.54	0.53	0.52
6 Dimensionless length of section	A_1, A_2, \dots, A_{14}	2.28	0.37	0.37	0.32	0.32	0.33	0.33	0.32	0.32	0.32	0.32	0.32	0.32	0.32
7 Function $f(\bar{r})$	$f(\bar{r}) = 1 + 10^{-5} \bar{r}^2 / D^2$	0.02	0.17	0.19	0.12	0.13	0.14	0.16	0.18	0.20	0.22	0.24	0.26	0.28	0.30
8	$f(\bar{r})^2$	0.002	0.34	0.37	0.17	0.17	0.17	0.17	0.17	0.17	0.17	0.17	0.17	0.17	0.17
9	$f(\bar{r})^3$	—	0.011	0.012	0.011	0.011	0.011	0.011	0.011	0.011	0.011	0.011	0.011	0.011	0.011
10	$\sum_{i=1}^{14} \frac{f(\bar{r}_i)^2}{D_i^2}$	—	0.013	0.126	0.180	0.202	0.208	0.208	0.207	0.206	0.205	0.204	0.203	0.202	0.201
11	$\frac{0.102 \sum_{i=1}^{14} f(\bar{r}_i)^2}{D_i^2} + 10^5$	0.107	0.360	0.330	0.278	0.302	0.308	0.308	0.307	0.306	0.305	0.304	0.303	0.302	0.301
12	$\frac{1}{\exp(\bar{r})}$	3.1	8.09	8.15	9.5	9.5	8.15	5.37	3.23	2.06	1.26	0.80	0.50	0.30	0.18
13	Mean value of $f(\bar{r})$	7.07	7.03	6.30	4.207	4.205	4.216	4.072	3.866	3.712	3.586	3.486	3.404	3.332	3.270
14	\bar{r}	12.24	13.3	13.9	13.8	14.0	13.86	13.58	13.2	12.8	12.5	12.35	12.25	12.18	12.1
15	\bar{r}^2	152	176	186	193	195	192	184	174	164	154	145	137	130	124

Table 4.4. (Cont'd).

16	$\frac{10 \cdot 10^3}{1000} \cdot \frac{1000}{1000} \cdot \frac{1000}{1000}$	0.609	0.075	0.128	0.143	0.175	0.118	0.077	0.041	0.085	3.077	0.015	0.009	0.009	0.000	By formula (4.144) or auxiliary graphs (Appendix 1)
17	Convective heat flow at T_{ccr} + const = 700 K in kcal/m ² ·h	0.800	0.0475	0.136	0.150	0.181	0.119	0.078	0.039	0.079	3.700	0.019	0.010	0.010	0.000	By formula (4.173)
18	Assigned temperature of gas wall in K	300	300	300	300	300	300	300	300	300	300	300	300	300	300	By formula (4.180) or auxiliary graphs (Fig. 4.15)
19	Complex S	0.18	0.036	0.090	0.075	0.078	0.078	0.078	0.078	0.078	0.078	0.078	0.078	0.078	0.078	By formula (4.181)
20	Actual convective heat flow at assigned T_{ccr} in kcal/m ² ·h	0.770	0.070	0.140	0.140	0.140	0.140	0.140	0.140	0.140	0.140	0.140	0.140	0.140	0.140	q_{ccr} - by formula (4.189); distribution of q_{ccr} is determined as described in Section 4.3
21	Radiant heat flows in kcal/m ² ·h	0.800	0.030	0.030	0.030	0.030	0.030	0.030	0.030	0.030	0.030	0.030	0.030	0.030	0.030	According to sketch of the reactor
22	Total heat flow kcal/m ² ·h	4.270	0.075	0.200	0.200	0.200	0.200	0.200	0.200	0.200	0.200	0.200	0.200	0.200	0.200	$\frac{10 \cdot 10^3}{1000} \cdot \frac{1000}{1000} \cdot \frac{1000}{1000}$
23	Area of wall on the section, m ²	0.700	0.000	0.000	0.000	0.000	0.000	0.000	0.000	0.000	0.000	0.000	0.000	0.000	0.000	T_{ccr} and T_{ccr} are determined according to formula (4.224). Temperature of coolant at its entrance the cooling system is 334.4°C
24	Heat loss from the wall	0.700	0.000	0.000	0.000	0.000	0.000	0.000	0.000	0.000	0.000	0.000	0.000	0.000	0.000	See Fig. 4.28
25	Heat loss from the wall	0.700	0.000	0.000	0.000	0.000	0.000	0.000	0.000	0.000	0.000	0.000	0.000	0.000	0.000	See formula (4.221)
26	Temperature of coolant on the section	0.8	11.8	18.2	7.8	3.2	3.1	2.6	0.8	0.2	0.7	0.3	0.3	0.3	0.3	
27	Temperature of coolant on the section	0.8	11.8	18.2	7.8	3.2	3.1	2.6	0.8	0.2	0.7	0.3	0.3	0.3	0.3	
28	Number of convective ribs on the section	0.8	11.8	18.2	7.8	3.2	3.1	2.6	0.8	0.2	0.7	0.3	0.3	0.3	0.3	
29	Number of convective ribs on the section	0.8	11.8	18.2	7.8	3.2	3.1	2.6	0.8	0.2	0.7	0.3	0.3	0.3	0.3	
30	Temperature of coolant on the section	0.8	11.8	18.2	7.8	3.2	3.1	2.6	0.8	0.2	0.7	0.3	0.3	0.3	0.3	

Table 4.4. (Cont'd).

31	Equivalent diameter of active section, m	$d_e = \frac{2d_o^2}{d_o + d_i}$	2.10·10 ⁻⁴	2.2·10 ⁻⁴	2.3·10 ⁻⁴	2.4·10 ⁻⁴	2.5·10 ⁻⁴	2.6·10 ⁻⁴	2.7·10 ⁻⁴	2.8·10 ⁻⁴	2.9·10 ⁻⁴	3.0·10 ⁻⁴	3.1·10 ⁻⁴	3.2·10 ⁻⁴	3.3·10 ⁻⁴	3.4·10 ⁻⁴	3.5·10 ⁻⁴	3.6·10 ⁻⁴	3.7·10 ⁻⁴	3.8·10 ⁻⁴	3.9·10 ⁻⁴	4.0·10 ⁻⁴	By formula (4.200)	
32	Area of active section of cooling system, m ²	$F_a = \pi d_e l_{act}$	0.294	0.295	0.296	0.297	0.298	0.299	0.300	0.301	0.302	0.303	0.304	0.305	0.306	0.307	0.308	0.309	0.310	0.311	0.312	0.313	By formula (4.199)	
33	Area of active section of cooling system, m ²	$(\frac{d_o}{d_i})^2 F_a$	18.0·10 ⁻⁴	18.1·10 ⁻⁴	18.2·10 ⁻⁴	18.3·10 ⁻⁴	18.4·10 ⁻⁴	18.5·10 ⁻⁴	18.6·10 ⁻⁴	18.7·10 ⁻⁴	18.8·10 ⁻⁴	18.9·10 ⁻⁴	19.0·10 ⁻⁴	19.1·10 ⁻⁴	19.2·10 ⁻⁴	19.3·10 ⁻⁴	19.4·10 ⁻⁴	19.5·10 ⁻⁴	19.6·10 ⁻⁴	19.7·10 ⁻⁴	19.8·10 ⁻⁴	19.9·10 ⁻⁴	By formula (4.204)	
34	Coefficient of heat transfer from wall to fluid, taking ribbing into account, kcal/m ² ·h·deg	$\alpha_w = \frac{1}{\frac{1}{\alpha_{w0}} + \frac{d_o}{2\lambda r} + \frac{d_o}{2\lambda r} + \frac{1}{\alpha_{w1}}}$	1120	1120	1120	1120	1120	1120	1120	1120	1120	1120	1120	1120	1120	1120	1120	1120	1120	1120	1120	1120	By formula (4.205)	
35	Coefficient of heat exchange from wall to fluid, taking ribbing into account, kcal/m ² ·h·deg	$\alpha_{w0} = \frac{1}{\frac{1}{\alpha_{w0}} + \frac{d_o}{2\lambda r} + \frac{d_o}{2\lambda r} + \frac{1}{\alpha_{w1}}}$	2.9	2.9	2.9	2.9	2.9	2.9	2.9	2.9	2.9	2.9	2.9	2.9	2.9	2.9	2.9	2.9	2.9	2.9	2.9	2.9	By formula (4.206)	
36	Factor	$\beta = \frac{d_o - d_i}{d_o + d_i}$	0.5	0.5	0.5	0.5	0.5	0.5	0.5	0.5	0.5	0.5	0.5	0.5	0.5	0.5	0.5	0.5	0.5	0.5	0.5	0.5	By formula (4.207)	
37	Coefficient of heat exchange from wall to fluid, taking ribbing into account, kcal/m ² ·h·deg	$\alpha_{w1} = \frac{1}{\frac{1}{\alpha_{w1}} + \frac{d_o}{2\lambda r} + \frac{d_o}{2\lambda r} + \frac{1}{\alpha_{w2}}}$	1.02	1.02	1.02	1.02	1.02	1.02	1.02	1.02	1.02	1.02	1.02	1.02	1.02	1.02	1.02	1.02	1.02	1.02	1.02	1.02	By formula (4.208)	
38	Temperature of liquid wall, °C	$t_{w0} = \frac{t_{f0} + t_{w1}}{2}$	6.8	6.8	6.8	6.8	6.8	6.8	6.8	6.8	6.8	6.8	6.8	6.8	6.8	6.8	6.8	6.8	6.8	6.8	6.8	6.8	By formula (4.209)	
39	Mean temperature of wall, °C	$t_{w0} = \frac{t_{f0} + t_{w1}}{2}$	7.4	7.4	7.4	7.4	7.4	7.4	7.4	7.4	7.4	7.4	7.4	7.4	7.4	7.4	7.4	7.4	7.4	7.4	7.4	7.4	By formula (4.210)	
40	Heat conductance of wall at mean temperature, kcal/m ² ·h·deg	$\frac{1}{R_w} = \frac{1}{\frac{d_o}{\lambda}}$	0.1	0.1	0.1	0.1	0.1	0.1	0.1	0.1	0.1	0.1	0.1	0.1	0.1	0.1	0.1	0.1	0.1	0.1	0.1	0.1	By formula (4.211)	
41	Temperature of gas wall, °C	$t_{w0} = \frac{t_{f0} + t_{w1}}{2}$	8.7	8.7	8.7	8.7	8.7	8.7	8.7	8.7	8.7	8.7	8.7	8.7	8.7	8.7	8.7	8.7	8.7	8.7	8.7	8.7	8.7	By formula (4.212)